ULTRASOUND CLINICS

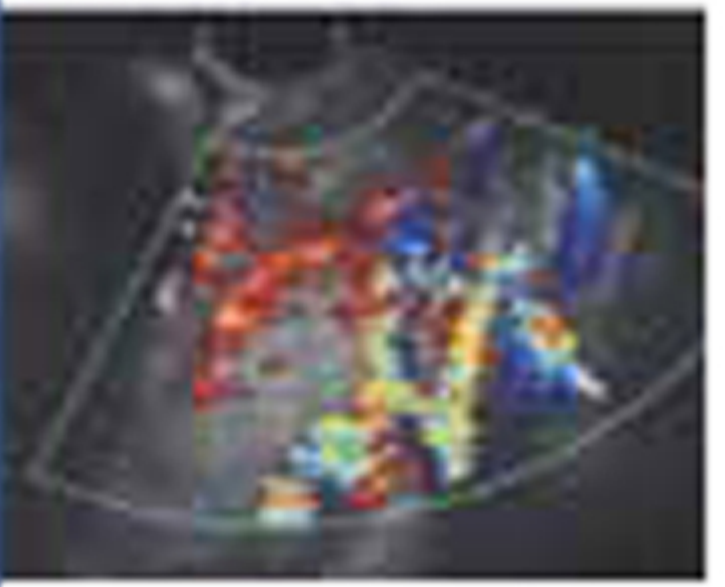

ELSEVIER SAUNDERS

ULTRASOUND CLINICS

Ultrasound Clin 2 (2007) xi

Preface

Vikram Dogra, MD

Shweta Bhatt, MD

Guest Editors

Vikram Dogra, MD
University of Rochester School of Medicine
Department of Imaging Sciences
601 Elmwood Avenue, Box 648
Rochester, NY 14642

E-mail address:
Vikram_Dogra@URMC.Rochester.Edu

Shweta Bhatt, MD
University of Rochester School of Medicine
Department of Imaging Sciences
601 Elmwood Avenue, Box 648
Rochester, NY 14642

E-mail address:
Shweta_Bhatt@URMC.Rochester.Edu

Ultrasound Clinics is now entering its second year as a publication devoted to medical ultrasound. This quarterly journal is a welcome addition to the demand for more knowledge of ultrasound imaging involving every aspect of sonography. Upcoming issues will be dedicated to advances and new developments in ultrasound technology pertaining to obstetrics and gynecology, abdominal, vascular, emergency, genitourinary disease, and cardiac imaging.

Today, due to ongoing advances in modern imaging systems, practicing radiologists have a wide array of diagnostic tools at their fingertips. Ultrasound techniques have improved with new materials and faster computer processing. High-resolution real-time grayscale imaging, tissue harmonic evaluation, and color and power Doppler analysis are now readily available. As a consequence of these improvements, more ultrasound examinations are being performed, leading to the demand for more knowledge of medical ultrasound. *Ultrasound Clinics* aims to fill that demand by providing the most recent and relevant information.

The topics in this issue have been chosen with particular attention to genitourinary ultrasound. We assembled a group of leading radiologists to provide new insight into key ultrasound techniques and concepts that will benefit readers who are new to the practice of ultrasound as well as practicing imaging specialists and clinicians.

I am honored to be the Guest Editor of this issue of *Ultrasound Clinics* along with Shweta Bhatt, MD, and wish to express my sincere thanks for her assistance. We wish to thank Barton Dudlick and our outstanding contributors for their amazing work and their cooperation.

1556-858X/07/$ – see front matter
doi:10.1016/j.cult.2007.05.001
ultrasound.theclinics.com

ELSEVIER SAUNDERS

ULTRASOUND CLINICS

Ultrasound Clin 2 (2007) 1–16

Sonography of Urolithiasis and Hydronephrosis

Edward P. Lin, MD, Shweta Bhatt, MD, Vikram S. Dogra, MD, Deborah J. Rubens, MD*

Urolithiasis, the presence of renal calculi within the urinary tract, is the most common cause of extrarenal obstructive uropathy. Obstructive uropathy can be defined as an interruption of normal urine flow at some point along the urinary tract from the renal tubule to the urethra. Obstruction results in an increase in pressure within the urinary tract, causing structural and physiologic changes. Hydronephrosis refers to the structural change, describing a dilatation of the calyces and renal pelvis. Hydroureter, or ureteral dilatation, sometimes accompanies hydronephrosis. The physiologic changes that result from obstruction of urine flow are referred to as obstructive nephropathy. Without intervention, obstructive nephropathy eventually leads to an irreversible loss of renal function.

The causes of obstructive uropathy are diverse. It is classified according to location, duration, and degree of obstruction. Obstructive uropathy may be congenital or acquired, which may be further divided into upper and lower urinary tract and intra- or extrarenal causes. Obstruction may be unilateral or bilateral. The duration of obstruction may be described as acute (hours to days), subacute (days to weeks), and chronic (months to years). The obstruction may be partial or complete.

Following a review of normal anatomy and sonographic technique, this article focuses on urolithiasis as a disease process, its findings on ultrasound, and its effects on the kidney and the collecting system. The authors discuss the physiologic changes that accompany hydronephrosis following obstruction of the collecting system and the important causes to consider when presented with hydronephrosis.

Sonographic technique and anatomy

The kidneys are imaged with the patient placed in the supine and lateral decubitus positions. A 3- to 7-MHz transducer is selected, with higher

Department of Imaging Sciences, University of Rochester School of Medicine, 601 Elmwood Avenue, Box 648, Rochester, NY 14642, USA
* Corresponding author.
E-mail address: deborah_rubens@urmc.rochester.edu (D.J. Rubens).

1556-858X/07/$ – see front matter
doi:10.1016/j.cult.2007.01.007
ultrasound.theclinics.com

frequencies used in children and thinner patients. A breath-hold during maximum inspiration allows better visualization of the kidneys by displacing the kidneys inferiorly by approximately 2.5 cm.

The right kidney is best visualized by placing the transducer in the right lateral subcostal margin in the anterior axillary line during deep inspiration. If bowel gas obscures the right kidney, the transducer can be placed laterally in the mid or posterior axillary line.

Because the left kidney is located in a more superior position, it is often more difficult to visualize. The left kidney is also frequently obscured by the stomach and small bowel, whereas imaging of the right kidney is benefited by the liver, which acts as an acoustic window. To improve visualization of the left kidney, the patient is placed in the right lateral decubitus position and the transducer is positioned in the left posterior axillary line or left costovertebral angle.

Routine images include long-axis and transverse views of the upper pole, mid-kidney and lower pole. The sonographer should record renal length in the long axis. A normal kidney length is approximately 11 to12 cm [1]. Kidneys are generally within 2 cm of each other in length. Normal width is approximately 4 to 5 cm.

The renal cortex should be evaluated for echogenicity, contour, and thickness. A normal right and left renal cortex demonstrates equal or less echogenicity than the liver and spleen, respectively (Fig. 1). Occasionally the left kidney displays a prominent masslike protrusion in the mid-kidney, known as a Dromedary hump, which is a result of the spleen impressing on the left kidney as it develops. The hump exhibits normal renal parenchyma. The kidneys should also be assessed for atrophy, scarring, calcifications, hydronephrosis, and masses.

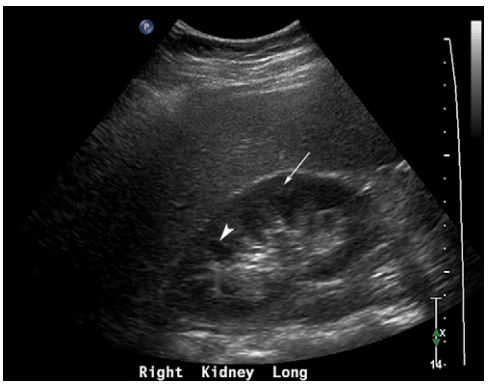

Fig. 1. Longitudinal gray-scale image of a normal kidney. Note that the echogenicity of the renal cortex (*arrow*) is less than the adjacent liver parenchyma, but more than the renal medulla, also referred to as the pyramids (*arrowhead*). The renal sinus is the hyperechoic region centrally.

The renal medulla consists of small, rounded structures adjacent to the renal sinus. The medulla contains the pyramids, which are hypoechoic to the renal cortex (see Fig. 1). The renal sinus is more centrally located and appears echogenic secondary to fatty tissue and interwoven connective tissue (see Fig. 1). The renal sinus contains the major branches of the renal artery and vein, the collecting system, and lymphatics. Fatty tissue is interspersed throughout this potential space.

When hydronephrosis is present, the affected collecting system should always be compared with the contralateral kidney. Knowledge of whether hydronephrosis is unilateral or bilateral helps narrow the differential and localize the level of obstruction if present. In cases in which the finding of hydronephrosis is uncertain, the kidney size can be compared with prior studies if available. Secondary findings, such as perinephric fluid, may also suggest an obstructive cause when hydronephrosis is identified. The presence and extent of hydroureter should be followed distally as far as possible, in an attempt to determine a cause. In addition, postvoid images and a change in patient position, such as a prone or decubitus position, are important to exclude the possibility of a false-positive finding. The collecting system may occasionally appear dilated if the bladder is full, or if the renal pelvis or ureter is compressed when the patient lies in a certain position.

Color Doppler evaluation of the renal arteries may be challenging and requires an understanding of the normal vascular anatomy and waveforms. The color gain, pulse repetition frequency, and wall filter should be optimized within a normal segment of the renal artery. A low wall filter and pulse repetition frequency should be used. Pulsed Doppler examination should be performed with a sample angle of less than 60 degrees, because angles greater than 60 degrees may overestimate velocities.

A complete renal vascular study includes obtaining samples from the ostium, proximal, mid, and distal portions of the main renal arteries, and at least three segmental branches of the mid-kidney, upper, and lower pole interlobar or arcuate arteries using a volume size of approximately 2 to 5 cm^3. Resistive indices (RI) are then determined from these waveforms.

Epidemiology and natural history of urolithiasis

Urolithiasis occurs across all geographic, cultural, and ethnic groups [2]. The lifetime risk is less than 2% to 5% in Asia, 8% to 15% in the West,

and as high as 20% in Saudi Arabia [3]. Incidence is less than 0.5% in the United States and Europe. Stamatelou and colleagues [4] found the prevalence of kidney stone disease to be increasing from 3.2% in the mid-1970s to 5.2% in the mid-1990s in the United States, possibly secondary to dietary factors.

In general, urolithiasis is more common in men than women [2]. Kidney stone disease tends to recur, with relapse rates as high as 50% within 10 years and 75% within 20 years [5]. Once chronic, the likelihood of recurrence increases and the interval between episodes shortens [6]. Risk factors of recurrent disease include younger age at onset, family history of stones, associated urinary tract infection, and systemic disease that promotes stone formation, such as hyperparathyroidism [2].

Acute obstructive urolithiasis initially causes mild discomfort and progresses to extreme pain within 30 to 60 minutes. If the stone obstructs the ureteropelvic junction, pain localizes to the flank [7]. As the stone travels distally, the pain migrates inferiorly and anteriorly, often radiating to the groin [7]. Stones traveling down the right ureter may present with symptoms similar to appendicitis. A stone lodged in the ureterovesicular junction results in dysuria and urinary frequency, sometimes mimicking urinary tract infections [8]. Associated symptoms include fever, nausea, and vomiting.

Stones less than 5 mm in diameter will most likely pass [8]. Stones 5 to 7 mm have an approximately 50% chance of passing [8]. Stones greater than 7 mm will most likely require urologic intervention [8].

Pathophysiology of stone formation

Stone formation depends on the solubility product of a solution. Solubility is defined as the number of grams of solute in one liter of a saturated solution (g/L). The solubility product describes the equilibrium between an ion crystal and its ions in solution. Greater solubility products therefore allow for a higher capacity of a solution to dissolve particles before becoming saturated.

Kidney stones are ionic crystals, composed of anions and cations. Because urine contains many different ions, it is considered a polyionic solution. Polyionic solutions create strong electrical forces of attraction and repulsion. These forces increase the solubility product of the solution, resulting in a supersaturated solution. At some point, the supersaturability of urine is exceeded, and crystallization, which may be referred to as primary nucleation, occurs [7,8]. A nidus within the solution provides a scaffold on which crystallization may proceed at a lower solubility. This process is known as secondary nucleation [7]. Factors such as hydration status, ion concentration, presence of a nidus, or stone inhibitor, such as citrate or magnesium, greatly affect the rate of crystallization and stone formation [8].

Systemic conditions, such as hyperparathyroidism, increase the concentration of urine calcium, promoting stone formation. Cellular debris secondary to infection or the presence of Randall plaques (lesions composed of various crystal and organic compounds, which arise in the loops of Henle within the renal papillae and eventually extend into the uroepithelium) function as a nidus and allow crystallization to occur at lower solubilities [9,10]. Randall plaques are found in all patients who have calcium oxalate stones [10].

Sonographic detection of uroliths

Recommendations for the imaging of obstructive uropathy have changed rapidly over the past 2 decades. Intravenous urography and ultrasound have been largely replaced by noncontrast CT in the mid 1990s [11,12]. Several studies have compared ultrasound with noncontrast CT in detecting renal calculi. Sensitivities for ultrasound ranged from 19% to 93%, with specificities greater than 90% [13–17]. Sensitivities and specificities for noncontrast CT have consistently been reported to be greater than 90% [13–16]. Although noncontrast CT has evolved into the modality of choice, ultrasound still plays a role in the initial work-up of renal failure and in patients who have obstructive uropathy when radiation should be minimized, such as in the pediatric population and pregnant women.

Identifying renal calculi by ultrasound depends primarily on the size and location of the stone. The composition of renal calculi, hydration status, presence of hydronephrosis, renal and vascular disease, and choice of transducer frequency and focus, are secondary factors that may affect the sensitivity of detection. The use of color Doppler may aid in the detection of small stones and obstruction.

Composition of renal calculi

The chemical constitution of uroliths is diverse and often mixed. Calcium-containing, or calcareous, stones are the most common type, accounting for 60% to 80% of all uroliths, followed by uric acid stones, which account for 5% to 10% [1,18]. Calcareous stones primarily include variations of calcium oxalate and calcium phosphate [2]. Most of these stones are calcium oxalate predominant [8]. These stones are typically uniform in density and are easily detected on plain films and noncontrast CT. Uric acid stones form in acidic urine and may be found in various disorders, such as hyperuricosuria

secondary to a lack of the enzyme uricase, gout, and Lesch-Nyhan syndrome [19]. Uric acid stones are not easily identified on plain films, but may be visualized on noncontrast CT, depending on the concentration of calcium [8].

Still less common compositions include magnesium ammonium phosphate (struvite) and cystine stones. Struvite stones are rarely pure in composition, and are more often triple phosphate (calcium-magnesium-ammonium phosphate), which allow these stones to be detected on plain films and CT because of the presence of calcium. They form in alkaline urine, often in association with urinary tract infections, such as *Proteus mirabilis*, *Serratia*, and *Mycoplasma*. Seventy percent of staghorn calculi are struvite in composition [19].

Cystine calculi are an uncommon form of urolithiasis secondary to an autosomal recessive defect in tubular reabsorption of the amino acid cystine. The result is an excess in urinary cystine and the formation of cystine stones that are often ground glass in appearance [19]. These stones demonstrate less attenuation than calcareous stones, with an attenuation on noncontrast CT of 405 to 1180 Hounsfield Units (HU) in vitro and approximately 250 HU in vivo [20,21]. Uric acid stones exhibit the lowest attenuation (193–540 HU in vitro, 136–304 in vivo) [20,21]. Stone size and calcium content affect the attenuation in vivo, however, and the range of different stone compositions may overlap [21].

Radiolucent stones contain no calcium. Examples include pure urates and matrix stones composed of mucoprotein and mucopolysaccharides. Hereditary xanthinuria or the use of allopurinol may result in radiolucent xanthine stones. Indinavir stones are also radiolucent, and are associated with protease inhibitor drugs used in HIV therapy [22].

Although the chemical composition greatly influences whether stones are visualized on radiographic studies, it plays a less significant role in ultrasound. King and colleagues [23] found that chemical composition does not affect acoustic shadowing. The composition, however, does affect the reflective nature of the stone, which influences the presence of the color Doppler twinkling artifact.

Color Doppler twinkling artifact

When detection of renal calculi is limited by beam-attenuating tissue, such as renal sinus fat and bowel, or by size and lack of acoustic shadowing, color Doppler twinkling artifacts may improve sensitivity. The physical basis of twinkling artifact is complex. Twinkling artifacts arise when a sonographic beam interacts with a strongly reflecting crystalline or irregular surface [24]. On arriving at the interface, the beam undergoes a phase shift, resulting in an increase in pulse duration. When multiple incidental beams generate various Doppler shifts that are received by the transducer, the result is a rapidly changing mixture of red and blue colors [24]. The presence of the artifact therefore depends on the composition of the stone, with most irregular crystalline surfaces being capable of generating this artifact (Fig. 2) [25].

Lee and colleagues [26] found that 83% of 36 stones in their study exhibited twinkling artifacts. They also found in a phantom study that twinkling artifacts might depend on the location of the focal zone. Focal zones placed distal to the stone increase the artifactual color signal produced by the stone [26].

Twinkling artifact, however, may not be as specific for renal calculi. Other bright reflectors include calcified renal vessels, prominent papillae, milk of calcium cysts (Fig. 3) [27], renal cortical calcifications, calcified tumors (such as renal cell carcinoma), and calcified foreign bodies. Calcifications within normal sinus structures may also give rise to acoustic shadows.

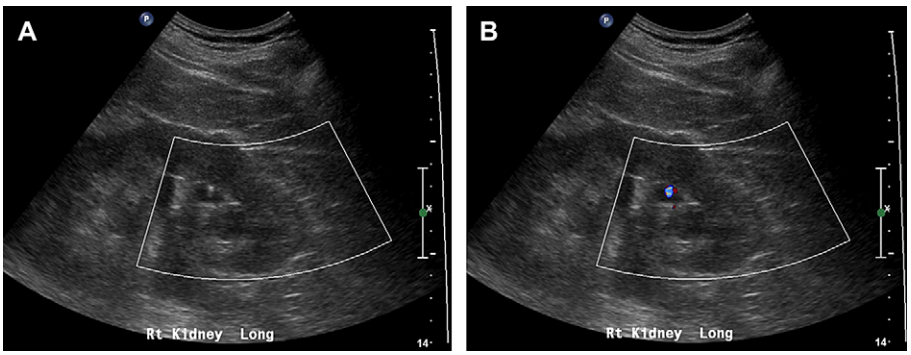

Fig. 2. Longitudinal gray-scale image (*A*) of the right kidney reveals a small echogenic focus, which does not exhibit acoustic shadowing, within a mildly dilated calyx. Twinkling artifact is shown within the echogenic focus on color Doppler image (*B*), confirming a non-obstructing stone.

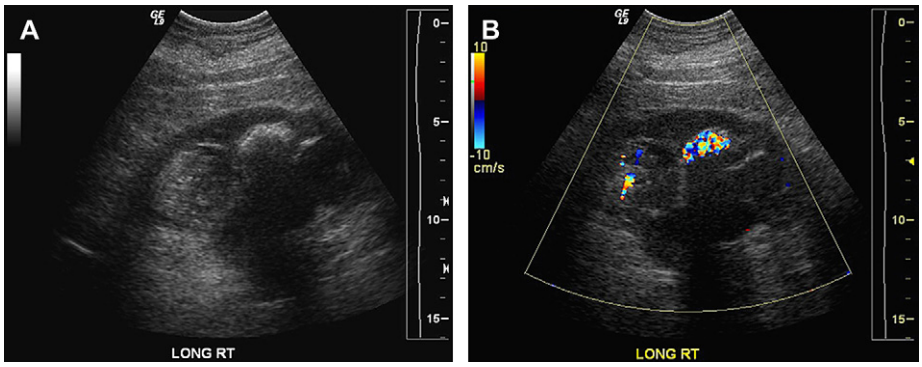

Fig. 3. Longitudinal gray-scale (*A*) and color Doppler (*B*) images of the right kidney demonstrate a milk of calcium cyst with twinkling artifact.

Knowledge of the normal vascular anatomy and the appearance of renal vessels may avoid confusion. For instance, the division of segmental arteries into interlobular arteries appears as regularly spaced, tiny echogenic foci at the periphery of the renal sinus [28]. In addition, because of the vascularity of the kidney, normal vessels may also appear as tiny echogenic foci within the parenchyma.

Calcifications of the papillae may appear prominent particularly when mild calyceal dilatation is present. These calcifications occur in the Anderson-Carr progression of early medullary nephrocalcinosis [29], papillary necrosis (Fig. 4), medullary sponge kidneys, and cytomegalovirus or *Candida albicans* infection [28].

Cortical calcifications are less often confused with renal calculi because of their more peripheral location. These calcifications arise in various diseases, including acute tubular necrosis, chronic glomerulonephritis, Alport syndrome, oxalosis, chronic hypercalcemia secondary to neoplasm, and tuberculosis.

Size

Ultrasound may detect with relative confidence stones greater than or equal to 5 mm [17]. Size alone remains the most important factor in the detection of acoustic shadowing [23]. Smaller stones may not exhibit acoustic shadowing, making a definitive diagnosis more difficult. Fowler and colleagues [13] demonstrated a sensitivity of 13% with stones of 3 mm or less. The average size of calculi depicted on CT but not on ultrasound was 3.3 mm $\pm$ 0.6 mm. Other studies have reported similar lengths of 5 to 7 mm as the minimum size that can be reliably detected on ultrasound [30,31].

Location

There are three areas of ureteric narrowing: just distal to the ureteral pelvic junction (Fig. 5) (UPJ), the lower third where the ureter crosses the iliac vessels, and the ureterovesical junction (UVJ) (Fig. 6). Of the three locations, the UVJ most commonly

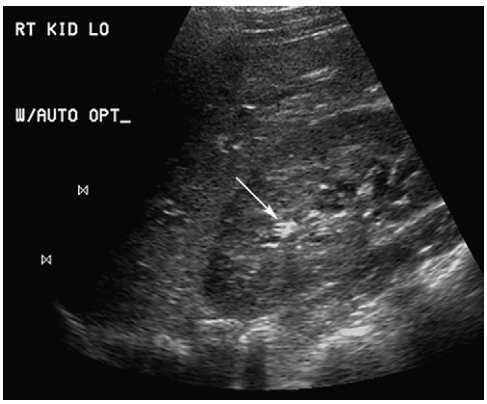

Fig. 4. Longitudinal gray-scale image of the right kidney demonstrates echogenic foci in the region of the papilla (*arrow*) in the upper pole, secondary to papillary necrosis, which can mimic renal calculi.

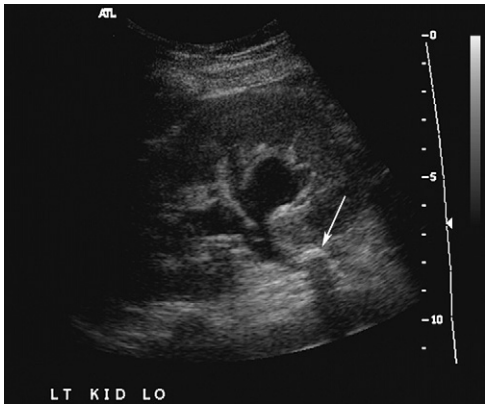

Fig. 5. Longitudinal gray-scale image of the left kidney demonstrates stone in the left UPJ (*arrow*) with acoustic shadowing, and mild hydronephrosis of the left kidney.

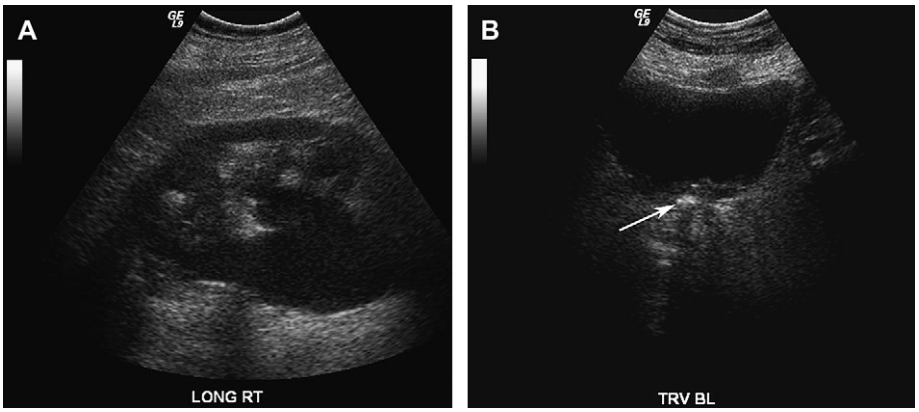

Fig. 6. Longitudinal gray-scale image of the right kidney (*A*) demonstrates moderate hydronephrosis and a dilated extrarenal pelvis. A hyperechoic focus (*arrow*) with posterior acoustic shadowing is detected on a transverse gray-scale image of the bladder (*B*), representing a stone within the right UVJ.

obstructs or slows the passage of kidney stones, affecting approximately 75% to 80% of all stones (see Fig. 6) [32]. Distal ureteral calculi are also more symptomatic than proximal stones.

A major disadvantage of ultrasound in detecting ureteral calculi, compared with CT, is its inability to follow the entire course of the ureter secondary to overlying bowel gas. Proximal stones are often more easily detectable on transabdominal ultrasound than mid or distal ureteral stones (see Fig. 5). UVJ calculi should be easily visualized with a fully distended bladder [33]. Mid-ureter stones are the most difficult to visualize by ultrasound [33]. A dilated ureter may sometimes assist in localizing calculi by allowing the sonographer to follow the path of the ureter distally. Transvaginal and transperineal ultrasound have also been found to improve the sensitivity for detecting distal ureteral calculi [34–36].

Technical factors

Several technical factors have been investigated regarding their ability to detect small renal calculi, particularly within the renal sinus. King and colleagues [23] have emphasized the importance of optimizing scanning parameters to produce an acoustic shadow. Reducing the distance between the transducer and the area of interest and placing the stone within the focal zone improves the image resolution and ability to detect an acoustic shadow. A transducer frequency should therefore have a focal zone 2 to 3 cm greater than the depth of the kidney cortex, preferably 5 MHz or greater, and the focal zone should be placed at the depth of the suspected stone or slightly deeper [37]. In addition, King and colleagues [23] found that increasing the power improves the contrast between the shadow and surrounding tissue.

Aside from scanning parameters, Chau and Chan [30] concluded in a small study that a fluid challenge (ingestion of approximately 1800 mL of water) improves the detection of small calculi by distending the collecting system. This distention provides additional contrast in areas that may be difficult to assess, such as the renal sinus. This technique prolongs the length of the examination, however.

Hydronephrosis

Hydronephrosis describes the dilatation of the renal pelvis and calyces but does not attribute the cause of dilatation. It is derived from Greek, with *hydor* meaning "water," *nephros* meaning "kidney," and the suffix *-osis* meaning "condition" [38].

Grading of hydronephrosis in adults is most commonly categorized into mild, moderate, and severe. Mild hydronephrosis corresponds to blunting of the caliceal fornices and enlargement of the calices (Fig. 7A) [39]. The papillae, however, are still easily visualized. Moderate hydronephrosis refers to rounding of the calices with obliteration of the papillae (Fig. 7B) [39]. Severe hydronephrosis indicates ballooning of the calices without or with parenchymal thinning (Fig. 8) [39]. The grade of obstruction, however, does not correlate with the grade of hydronephrosis. A patient who has complete obstruction may only demonstrate mild hydronephrosis.

Causes of hydronephrosis

The causes of hydronephrosis are diverse. Hydronephrosis can be grouped into obstructive and nonobstructive causes (Box 1).

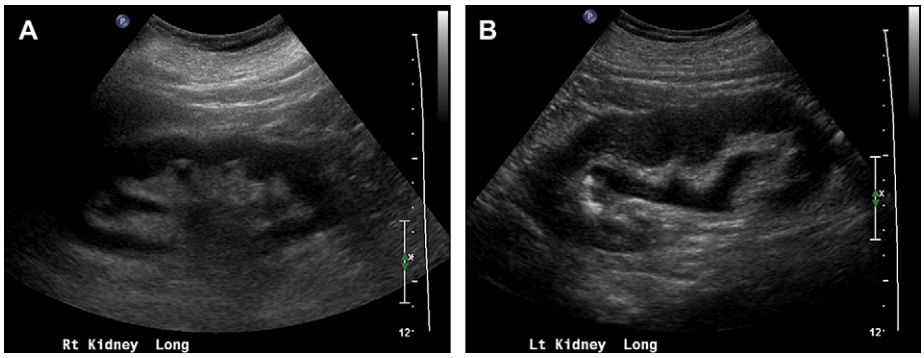

Fig. 7. Longitudinal gray-scale images of a patient who has bladder carcinoma demonstrating mild hydronephrosis in the right kidney (*A*) and moderate hydronephrosis in the left kidney (*B*).

Congenital nonobstructive causes include primarily vesicoureteral reflux, which is an abnormal retrograde flow of urine from the bladder into the ureter and proximal collecting system. Acquired nonobstructive causes of hydronephrosis include acute pyelonephritis and increased urine flow states, such as in aggressive intravenous hydration, diuretic use, and less common conditions, such as diabetes insipidus.

Obstructive causes of hydronephrosis may also be congenital or acquired. Examples of congenital causes of obstructive uropathy include posterior urethral valves (Fig. 9), UPJ obstruction (Fig. 10), ureteroceles (Fig. 11), and spina bifida. Posterior urethral valves occur in males and are best depicted by a voiding cystourethrogram. UPJ obstruction is the most common cause of hydronephrosis in infancy and early childhood, and affects males more often than females. Abnormal smooth muscle architecture is believed to cause an abnormal ureteral peristalsis, leading to functional obstruction. Anatomic obstruction at the UPJ from fibrous bands or vessels may exhibit findings similar to UPJ obstruction. A duplicated collecting system may also cause obstruction of the upper pole moiety. The Weigert Meyer rule states that the upper moiety inserts inferiorly and medially to the lower pole moiety, and is more likely to cause obstructive hydronephrosis [40]. When the upper pole moiety is dilated, it exerts a mass effect on the lower pole, displacing the lower pole moiety inferiorly and laterally, a finding known as the drooping lily sign [40].

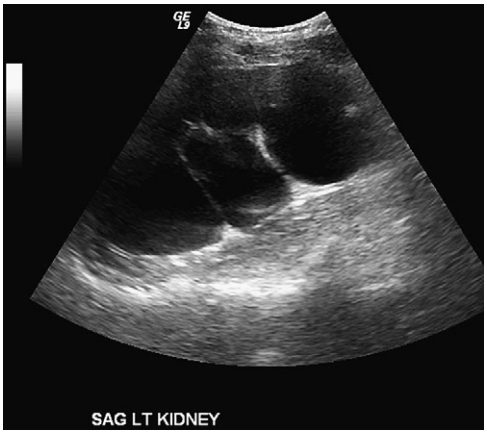

Fig. 8. Longitudinal gray-scale image of a patient who has severe hydronephrosis of the right kidney.

Acquired causes of obstructive hydronephrosis may be further divided into intrinsic (obstruction from within the urinary tract) or extrinsic (obstruction as a result of external compression) causes. Aside from intrarenal crystal precipitation from hyperuricosuria and drugs such as acyclovir, precipitation of Bence Jones proteins secondary to multiple myeloma, and tumor lysis secondary to chemotherapy, most causes of intrinsic and extrinsic obstruction are extrarenal. Urolithiasis is the most common cause of extrarenal obstruction.

Important intrinsic causes include neoplasms, such as transitional cell (Fig. 12) carcinoma of the bladder, ureter or renal pelvis, renal cell carcinoma, and metastatic disease, primarily breast cancer or melanoma. Ureteral and urethral strictures secondary to infection, trauma, or sequela of radiation therapy for cervical (Fig. 13) and pelvic tumors may be evident from the patient's history. *Schistosomiasis haematobium* is a significant problem in third world countries, affecting nearly 100 million people. Intramural deposits of ova lead to inflammatory changes of the distal ureteral and bladder wall, resulting in fibrosis and stricture. In addition, functional causes of obstruction may result from neurologic disorders, such as neurogenic bladder, which may lead to outflow obstruction and vesicoureteral reflux, diabetes mellitus, and anticholinergic drugs.

The most common extrinsic cause of obstruction in females is pregnancy (Fig. 14), followed by cervical cancer. Up to 90% of pregnant women have some degree of hydronephrosis in the third trimester [41]. The gravid uterus compresses the ureters

Box 1: Causes of hydronephrosis

Nonobstructive
Congenital
- Vesicoureteral reflux

Acquired
- Acute pyelonephritis
- High urine outflow

Obstructive
Congenital
- Ureteropelvic junction obstruction (most common)
- Prune-belly syndrome
- Ureterocele
- Bladder diverticula
- Posterior urethral valves
- Myelodysplasia

Acquired
- Intrinsic
  - Intrarenal: Tubular precipitation
    - Bence Jones proteins
    - Uric acid
    - Medications: acyclovir, methotrexate, sulfonamides
  - Extrarenal
    - Intraluminal ureteral obstruction
      - Urolithiasis
      - Blood clot
      - Fungus ball
      - Papillary necrosis
    - Neoplastic
      - Genitourinary
      - Transitional cell carcinoma
      - Renal cell carcinoma
      - Squamous cell carcinoma
    - Metastatic disease
    - Inflammatory
      - *Schistosomiasis haematobium*
      - Tuberculosis
      - Gonococcal and non-gonococcal urethritis
    - Other
      - Radiation therapy
      - Surgery or trauma
    - Functional
      - Neurogenic bladder
      - Diabetes mellitus
      - Multiple sclerosis
      - Spinal cord injury
      - Anticholinergic drugs
- Extrinsic
  - Neoplastic
    - Gynecologic
      - Benign and malignant uterine tumors
      - Benign and malignant ovarian tumors
      - Cervical carcinoma
    - Genitourinary
      - Benign prostate hypertrophy
      - Prostate adenocarcinoma
      - Gastrointestinal
      - Colorectal carcinoma
    - Lymphoma
    - Sarcomas
    - Metastatic disease
  - Inflammatory
    - Inflammatory bowel disease
    - Appendicitis
    - Diverticulitis
    - Pelvic inflammatory disease
    - Tubo-ovarian abscess
  - Vascular
    - Inflammatory abdominal aortic aneurysm
    - Ovarian vein thrombophlebitis
    - Retrocaval ureter
  - Other
    - Pregnancy
    - Retroperitoneal fibrosis
    - Pelvic lipomatosis
    - Radiation therapy

against the pelvic brim [42]. The right ureter is often more affected than the left ureter, because of an engorged right uterine vein [43]. Ureteral dilatation manifests in weeks 6 through 10, and does not resolve until 4 to 6 weeks postpartum [44]. Occasionally, dilatation may be seen in the first trimester, and is possibly attributable to the influences of progesterone, which causes smooth muscle relaxation.

Urolithiasis related to pregnancy is uncommon, affecting 1 in 1500 pregnancies [41]. Stones are more likely to be found in the ureter compared with the kidney (see **Fig. 14**) and affect the left and right sides equally [41]. Patients usually present in the second or third trimesters. Diagnosis is usually difficult, and ultrasound remains a primary imaging modality because of concerns for radiation exposure to the fetus. Sensitivity in detecting stones may be improved with the use of a transvaginal approach [34]. In addition, placing the patient in a decubitus position may help to relieve the hydronephrosis on the contralateral side, possibly differentiating between physiologic and stone-related hydronephrosis.

The most common extrinsic cause of obstruction in older males is benign prostatic hypertrophy, resulting in symptomatic obstruction in 50% to 75% of males over age 50 years and hydronephrosis in 10%. The second most common extrinsic cause is prostate adenocarcinoma, which directly obstructs the bladder outlet or ureters or metastasizes to lymph nodes. If it directly invades the ureter, it may cause intrinsic obstruction.

Other important causes of extrinsic obstruction include pelvic malignancies with direct extension,

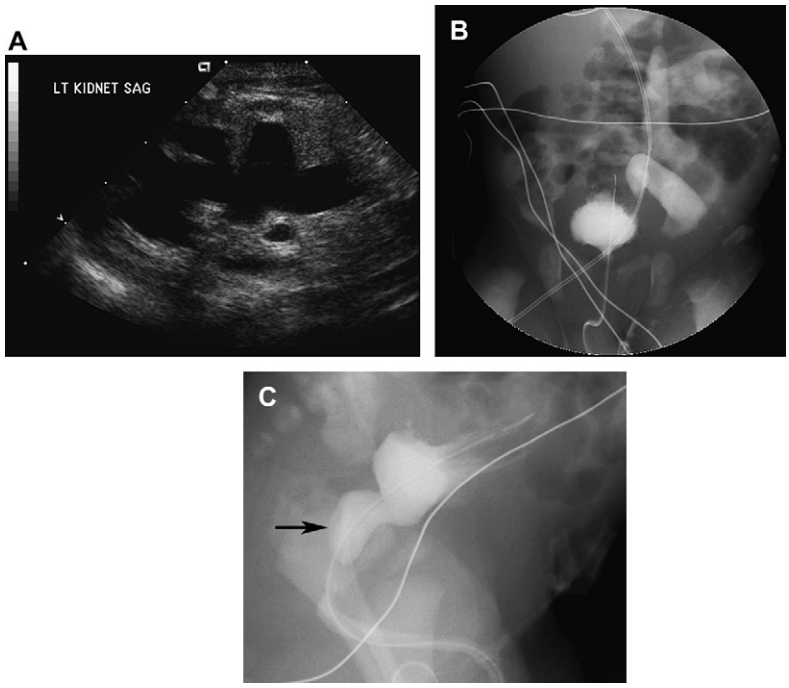

Fig. 9. Longitudinal gray-scale image of the left kidney in a 2-year-old boy who has a posterior urethral valve demonstrating moderate to severe hydronephrosis of the left kidney (*A*). Anteroposterior (*B*) and lateral (*C*) views of a voiding cystourethrogram demonstrate dilatation of the posterior urethra (*arrow*) and reflux of contrast into a dilated and tortuous left ureter.

such as endometrial, ovarian, and colorectal carcinoma and metastatic disease to lymph nodes, which may compress the ureters. Other causes, such as inflammatory changes in the vicinity of the ureters secondary to diverticulitis, appendicitis, inflammatory bowel disease, and pelvic inflammatory disease, may result in transient hydronephrosis. If fibrosis ensues, chronic hydronephrosis may develop.

Retroperitoneal fibrosis is an uncommon cause of unilateral and bilateral hydronephrosis. The incidence is 0.1 per 100,000, affecting men three times more than women [45]. The causes of retroperitoneal fibrosis are diverse, and include idiopathic, drug-related, malignancy, surgical, and inflammatory causes [45]. Retroperitoneal fibrosis was originally diagnosed by IVP, which demonstrates medial deviation of the ureters bilaterally and proximal hydroureteronephrosis. CT and MR have now become imaging modalities of choice, demonstrating a rind of tissue surrounding the vessels. Diagnosis is difficult to make by ultrasound

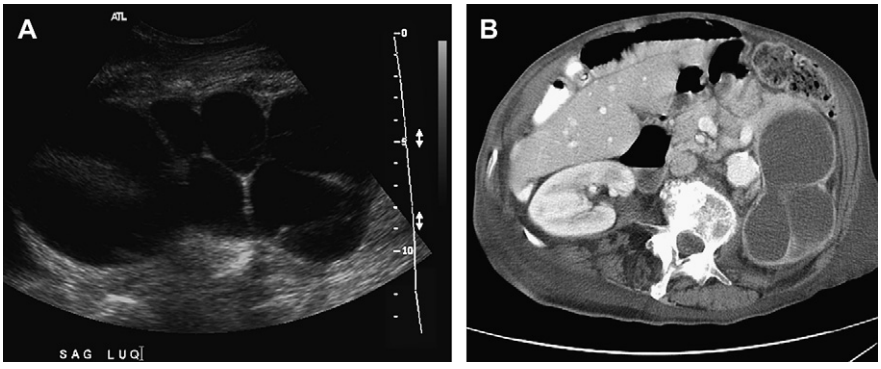

Fig. 10. Longitudinal gray-scale (*A*) and postcontrast axial CT through the level of the mid-abdomen (*B*), in a patient who has longstanding left UPJ obstruction, demonstrating severe hydronephrosis of the left kidney with no hydroureter, thinning of the renal cortex, and a normal right kidney.

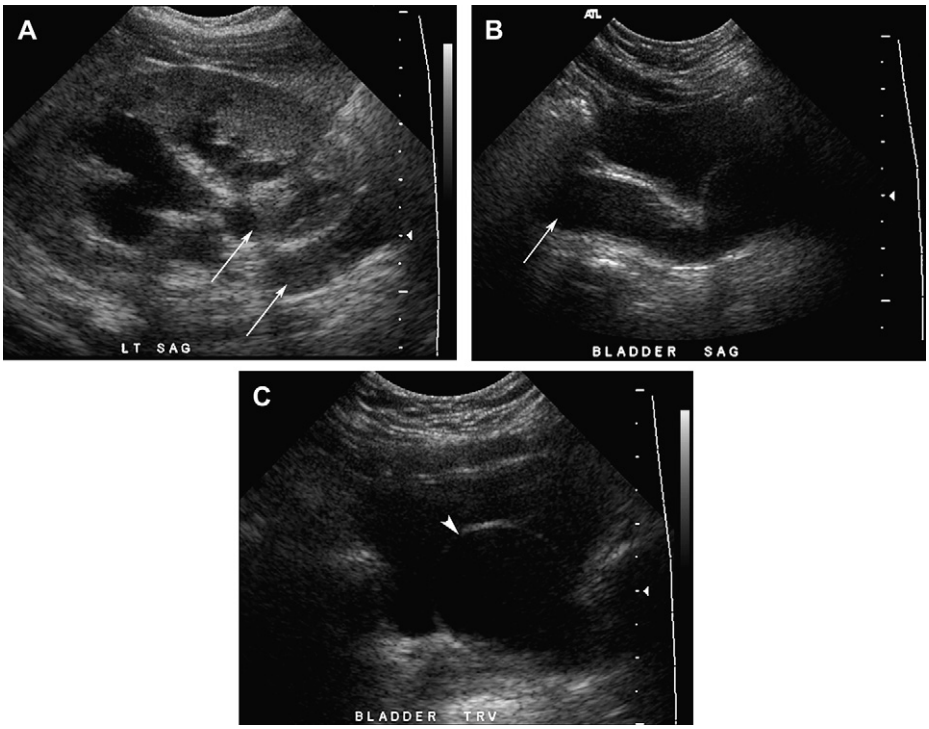

Fig. 11. Longitudinal gray-scale image (*A*) in a patient who has a duplicated collecting system demonstrates moderate to severe hydronephrosis of the upper pole of the left kidney and mild hydronephrosis of the lower pole. There are two dilated proximal ureters (*arrows*). Two transverse images (*B* and *C*) of the bladder reveal a dilated upper pole ureter (*arrow*) obstructed by a ureterocele (*arrowhead*).

alone, but ultrasound may demonstrate hydronephrosis and iso- or hypoechoic mass engulfing the aorta and ureters [45].

Finally, pelvic lipomatosis is another cause of bilateral hydronephrosis, although the collecting system is sometimes unaffected. It is an idiopathic disease associated with cystitis glandularis, characterized by the proliferation of mature unencapsulated fat within the retroperitoneal pelvic space. It classically elevates and deforms the bladder into the shape of a pear or gourd and at times causes severe bilateral hydronephrosis. In contrast to retroperitoneal fibrosis, which affects the proximal to mid ureters, pelvic lipomatosis displaces the distal ureters medially.

The causes of hydronephrosis are extensive. When confronted with hydronephrosis on ultrasound, the patient's age, sex, presenting symptoms, and medical history should help narrow the differential considerably. In most cases, additional imaging with CT or MR should provide a working diagnosis.

Physiologic effects of hydronephrosis

The acute physiologic effects of hydronephrosis on the kidney have been described in three phases. The first phase occurs 1 to 1.5 hours following ureteral obstruction. Intraureteral pressures and renal blood flow increase secondary to afferent arterial vasodilation, a process believed to be mediated by prostaglandins and possibly nitric oxide [46–49]. These prostaglandins also cause a diuresis that further increases renal pelvic pressure.

The second phase occurs between 1.5 to 5 hours following obstruction. Efferent arteriole vasoconstriction is believed to cause a decrease in renal perfusion and an increase in intraureteral pressures secondary to an increased glomerular filtration rate [46,48].

From 6 to 18 hours the third phase ensues, characterized by vasoconstriction of the afferent arteriole. Many factors are believed to contribute, including angiotensin II, thromboxane A2, antidiuretic hormone, and endothelin [50]. The result is a decrease in renal perfusion, glomerular filtration, and intraureteral pressure [46–48]. An increase in the venous and lymphatic reabsorption of urine contributes to the decrease in intraureteral pressures.

Imaging in the work-up of patients who have renal colic captures a snapshot of a dynamic physiologic process. Because obstructive hydronephrosis secondary to ureteral calculi undergoes a series of

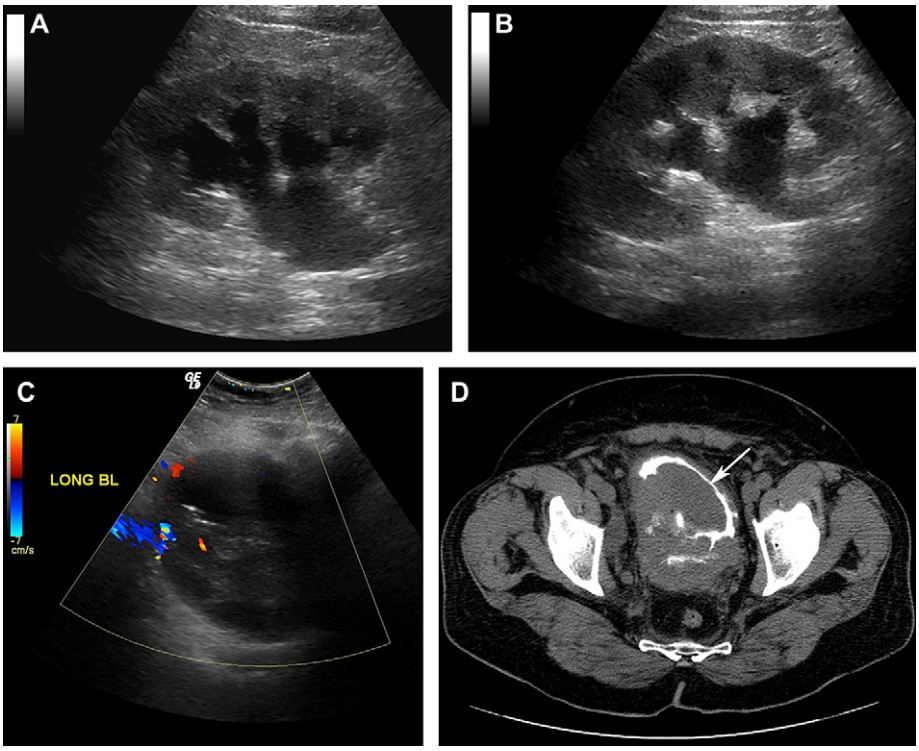

Fig. 12. Longitudinal gray-scale images in a patient who has transitional cell carcinoma demonstrating moderate bilateral hydronephrosis (*A* and *B*) and a large bladder mass that exhibits vascularity on color Doppler evaluation (*C*). Delayed postcontrast axial CT through the level of the bladder (*D*) confirming large mass outlined by contrast within the bladder.

physiologic changes, a normal ultrasound does not exclude the presence of obstruction. Patients are typically not imaged during the first several hours after the onset of symptoms. In addition, imaging may be performed after the kidney has compensated by increasing venous and lymphatic reabsorption. In cases in which the calices have ruptured, pressure within the ureters and renal pelvis has been relieved and the collecting system may appear normal.

Mimics of hydronephrosis

Many conditions may confound a diagnosis of obstructive hydronephrosis. False-positives include: (1) patients who have received significant

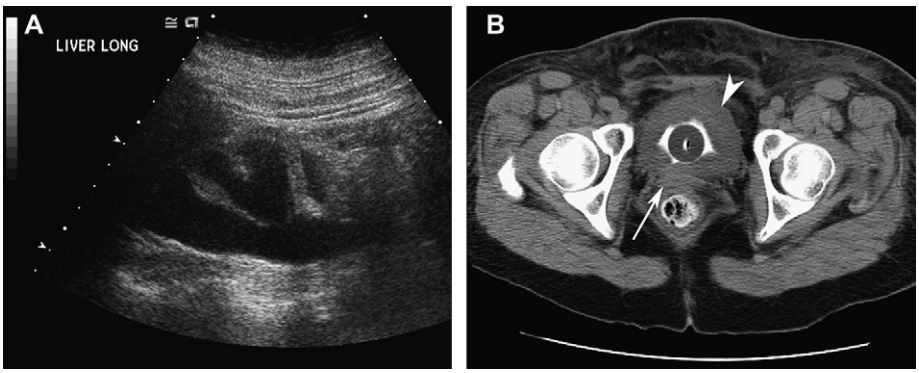

Fig. 13. Longitudinal gray-scale image (*A*) of a patient with a history of radiation therapy of the pelvis for cervical cancer, revealing severe chronic hydronephrosis of the right kidney with parenchymal thinning of the cortex. Postcontrast axial CT at the level of the bladder (*B*) demonstrates a thick-walled bladder (*arrowhead*) and fibrosed irregularly shaped cervix (*arrow*) secondary to radiation sequela.

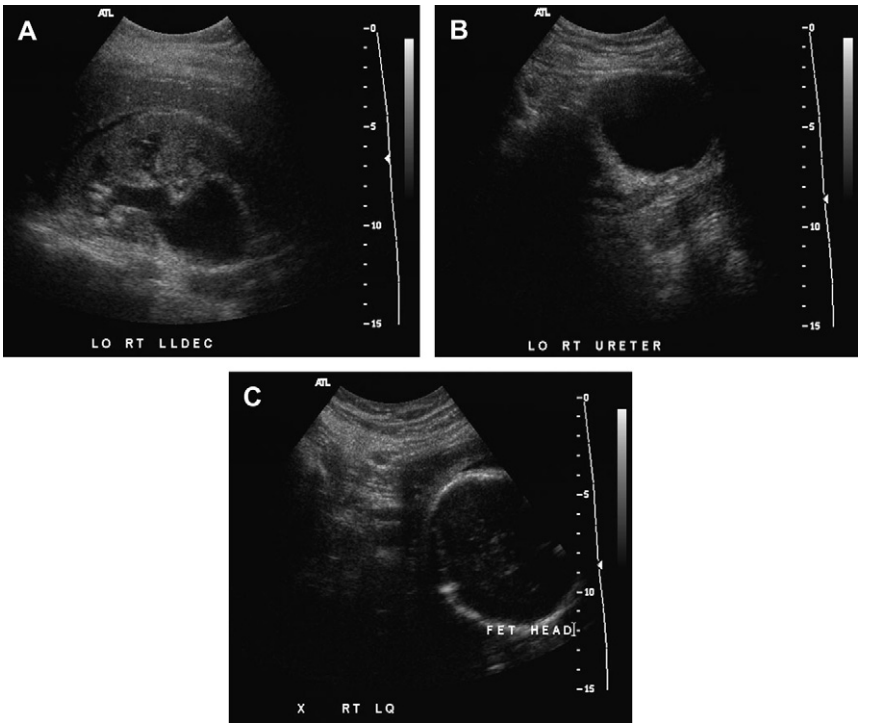

Fig. 14. Longitudinal gray-scale image of the right kidney (*A*) demonstrates mild hydronephrosis, dilated renal pelvis, and perinephric fluid. Transverse image of the right UVJ (*B*) reveals a stone with acoustic shadowing. The examination also reveals a previously unknown intrauterine pregnancy, which contributes to the hydronephrosis (*C*).

intravenous fluids or who are under conditions of diuresis, (2) prior urinary tract infections or obstruction, which may result in a distended collecting system, (3) dilated calices secondary to other conditions, such as papillary necrosis and reflux nephropathy, and (4) centralized fluid collections not connected to the collecting system, such as peripelvic cysts, distended renal veins, and renal artery aneurysms.

Renal sinus cysts, such as peripelvic cysts, may mimic the appearance of hydronephrosis (Fig. 15) [51]. Peripelvic cysts are benign extraparenchymal cysts, believed to be lymphatic in origin [52], arising from the renal sinus. Peripelvic cysts do not connect with the collecting system, a finding which may be difficult to appreciate by ultrasound. Excretory urography or contrast-enhanced CT should easily differentiate between peripelvic cysts, which often compress the collecting system, and hydronephrosis, which distends it.

Vascular lesions, such as aneurysms or arteriovenous fistulas (AVF), can involve the renal sinus and appear as a hypoechoic mass on gray-scale imaging [52]. These lesions are readily identified by the color Doppler imaging, which reveals the presence of flow. Fluid collections, such as urinomas and hematomas, may present with a similar appearance as renal sinus cysts on ultrasound. Urinomas typically result from forniceal rupture secondary to outflow obstruction, and exhibit perinephric low attenuation fluid on noncontrast CT [52]. Contrast-enhanced CT demonstrates extravasation of contrast outside the collecting system. Hematomas are usually related to a history of trauma, such as lithotripsy, or anticoagulation.

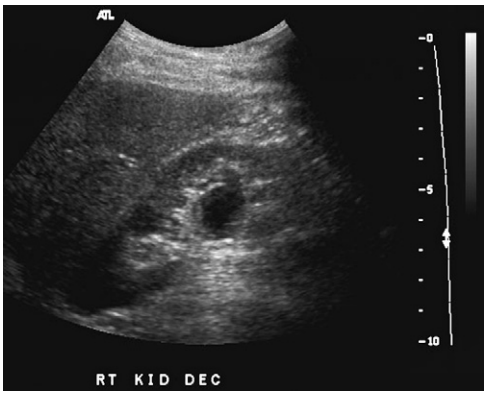

Fig. 15. Longitudinal gray-scale image of the right kidney demonstrating a peripelvic cyst, mimicking the appearance of hydronephrosis.

In this setting, noncontrast CT reveals high attenuation fluid, ranging from 30 to 50 HU.

Hypoechoic malignancies, such as lymphoma (Fig. 16), may infrequently mimic the appearance of hydronephrosis. Lymphoma involving the renal sinus is typically non-Hodgkin lymphoma and is one of the most common manifestations of retroperitoneal lymphoma [53]. It presents as a bulky retroperitoneal mass that is contiguous with the renal sinus. The mass usually engulfs rather than displaces or occludes vessels and surrounding structures. Ultrasound usually depicts a homogenous, hypoechoic mass (see Fig. 16).

Ureteric jets on color Doppler evaluation

Ureteral jets are streams of urine exiting the ureteral orifices in the bladder, detected by color Doppler ultrasound as streams of color. Normal humans exhibit 1 to 12 jets/min on either side [54]. After a fluid challenge of up to one liter, ureteral jets may be used in the detection of high-grade obstruction, which often demonstrates persistent absence or infrequent ureteral jet on one side [54]. Continuous flow may also suggest partial obstruction at the ureteral vesical junction. Ureteral jets are insensitive in the detection of partial low-grade obstruction, however, and may be absent even in patients who do not have obstruction [54]. The presence or absence of ureteral jets does not correspond to the degree of hydronephrosis and should be used, at best, as an adjunct during ultrasound evaluation of obstruction.

Role of resistive indices in hydronephrosis

Since the late 1980s, several studies have investigated the potential of the Doppler RI ([peak systolic velocity − end diastolic velocity]/peak systolic velocity) as a measure of changes in renal blood flow [55]. In an attempt to provide a more specific adjunct to gray-scale sonography in the diagnosis of acute obstructive hydronephrosis, the findings from these studies were often contradictory and discouraging.

Normal renal arterial flow exhibits a low resistance waveform with flow maintained throughout diastole. RI in a normal kidney has been reported to be approximately 0.60 ± 0.01 in a series of 58 patients [56], 0.64 ± 0.05 in a series of 21 patients [57], and 0.62 ± 0.04 in a series of 28 patients [58]. An RI of 0.7 is now considered to be the upper limits of normal [59].

RIs have been found to be elevated in disorders of native kidneys other than obstructive nephropathy, such as acute tubular necrosis, acute pyelonephritis, tubular-interstitial disease, glomerulopathies, vasculitides, and subcapsular fluid collections [60–62]. Normal RIs are also slightly higher in neonates and infants [63] and increase with decreases in heart rate [64].

Initial studies investigating the potential role of RIs in the evaluation of obstructive hydronephrosis reported sensitivities as high as 92% and specificities of up to 88% when using a threshold of 0.70 [65,66]. These results were found to precede pelvicaliceal dilation. An RI difference greater than 0.1 between an affected and unaffected kidney was found only in patients who had true obstructive nephropathy and was more specific than the criteria of an RI of 0.7 for obstructive hydronephrosis [67,68]. Although many other studies produced encouraging results [67,69–71], several investigations also reported sensitivities as low as 44% [72–74]. These conflicting results have led to a decrease in use of RIs as a reliable indicator of acute obstruction.

Studies have also suggested a role of RIs in the evaluation of ureteric colic in pregnancy. Normal pregnant women who do not have significant renal disease demonstrate normal and symmetric RIs

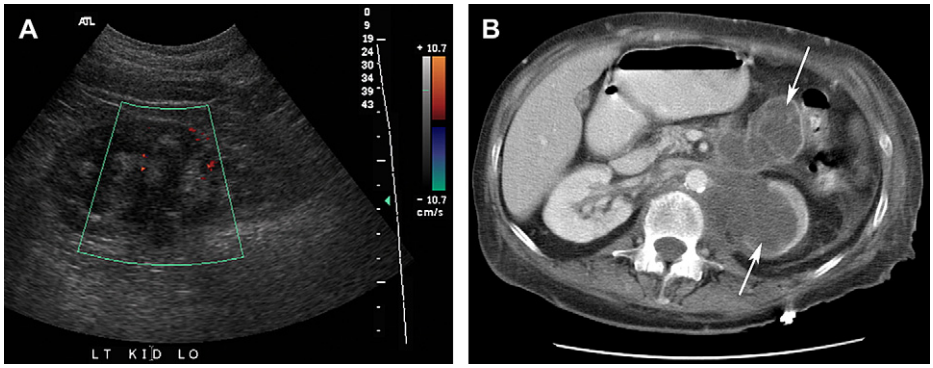

Fig. 16. Longitudinal color Doppler image of the left kidney (*A*) demonstrates a hypoechoic region in the renal sinus with the appearance of mild hydronephrosis. Postcontrast axial CT image through the left kidney (*B*) reveals large retroperitoneal mass (*arrows*) contiguous with the left renal sinus, representing lymphoma.

throughout pregnancy [75]. When an RI difference between kidneys greater than 0.1 is encountered, functionally significant obstruction is likely and an attempt should be made to identify a ureteral stone. The absence of a ureteral jet may also reinforce a clinical suspicion for a ureteral stone. These findings should be confirmed with the patient in the contralateral decubitus position, which relieves the pressure of the gravid uterus on the ureter [76].

Several reasons have been proposed to explain the variability in results of past studies. These include the exclusion of patients who had partial obstruction in earlier studies that supported the use of RIs, the vasodilatory effects of nonsteroidal anti-inflammatory medications (NSAIDs) used for pain control, and potential vasoconstrictive properties of contrast used in intravenous pyelograms [59]. In addition, RIs are not significant during the first several hours and peak within the first 48 hours, after which they remain elevated but to a lesser degree [72]. If a fornix ruptures, the RI may even normalize. The timing of the examination relative to the onset of obstruction affects the sensitivity of RIs.

Current perspectives of RIs have begun to realize the complex relationship between RIs and arterial parameters, such as vascular resistance, vascular compliance, and heart rate. In vitro studies have examined these parameters, concluding that although the RI depends on vascular resistance and compliance, it may, in certain instances, become independent of vascular resistance, such as when compliance is zero [77]. Another ex vivo study has demonstrated a linear relationship between pulse pressure index, or driving pulse pressures, and RI [78]. The vascular changes that occur during obstructive nephropathy are therefore complex, and RIs do not necessarily reflect these changes directly. If the relationship is better understood it may be possible to use the RI as a means of evaluating functional, as opposed to anatomic, dysfunction.

Summary

Urolithiasis, the most common cause of acquired extrarenal obstructive uropathy, is a common disease encountered in the emergency room. In the presence of ureteral calculi, initial imaging, such as ultrasound, often reveals hydronephrosis, which characterizes the anatomic changes resulting from the obstruction. Because the differential for hydronephrosis is broad, an attempt to narrow the differential should be undertaken, taking into account the patient's age, sex, symptoms, and pertinent medical history.

Ultrasound is significantly less sensitive than noncontrast CT in detecting stones, but may be useful in patients in whom radiation exposure should be minimized. Methods of optimizing detection include following dilated ureters as far distally as feasible, focusing on the three primary regions of ureteral narrowing, using color Doppler to identify twinkling artifacts where acoustic shadowing is not present, optimizing scanning parameters to detect acoustic shadowing, and potentially using transvaginal ultrasound in female adolescents and pregnant women, particularly when gynecologic disease enters the clinical differential.

Effort should be made to distinguish between obstructive uropathy and nephropathy, the latter signifying functional dysfunction of the kidney secondary to outflow obstruction. Because the grade of hydronephrosis does not necessarily correlate with the degree of obstruction, using the RI as a means of quantifying functional impairment may be important in guiding medical and interventional therapy. Our understanding of how the RI relates to vascular parameters, such as vascular resistance, vascular compliance, and driving pulse pressures, is incomplete. Further studies need to elucidate how these factors change in this dynamic pathophysiologic process, particularly when medications, presence of significant atherosclerotic disease, medical renal disease, and use of contrast invariably affect these vascular parameters. Because ultrasound is a noninvasive, economical, and accessible imaging modality, refining the RI as a tool for assessing functional impairment would be of great usefulness in the management of kidney stones.

References

[1] Madsen KM, Tisher CC. Anatomy of the kidney. In: Brenner BM, Rector F, editors. The kidney. 7th edition. Philadelphia: Saunders; 2002. p. 4.
[2] Moe OW. Kidney stones: pathophysiology and medical management. Lancet 2006;367:333–44.
[3] Pak CY. Kidney stones. Lancet 1998;351: 1797–801.
[4] Stamatelou KK, Francis ME, Jones CA, et al. Time trends in reported prevalence of kidney stones in the United States: 1976–1994. Kidney Int 2003; 63:1817–23.
[5] Trinchieri A, Ostini F, Nespoli R, et al. A prospective study of recurrence rate and risk factors for recurrence after a first renal stone. J Urol 1999; 162:27–30.
[6] Strauss AL, Coe FL, Deutsch L, et al. Factors that predict relapse of calcium nephrolithiasis during treatment: a prospective study. Am J Med 1982; 72:17–24.
[7] Srivastava T, Alon US. Urolithiasis in children. Adolesc Med Clin 2005;16(1):87–109.
[8] Coe FL, Evan A, Worcester E. Kidney stone disease. J Clin Invest 2005;115:2598–608.
[9] Randall A. The origin and growth of renal calculi. Ann Surg 1937;105:1009–27.

[10] Evan AP, Lingeman JE, Coe FL, et al. Randall's plaque of patients with nephrolithiasis begins in basement membranes of thin loops of Henle. J Clin Invest 2003;115:607–16.
[11] Smith RC, Rosenfeld AT, Choe KA, et al. Acute flank pain: comparison of non-contrast enhanced CT and intravenous urography. Radiology 1995;194:789–94.
[12] Smith RC, McCarthy S, Rosenfield AT. Diagnosis of acute flank pain: value of unenhanced helical CT. AJR Am J Roentgenol 1996;166:97–101.
[13] Fowler KA, Locken JA, Joshua HD, et al. US for detecting renal calculi with nonenhanced CT as a reference standard. Radiology 2002;222:109–13.
[14] Sheafor DH, Hertzberg BS, Freed KS, et al. Nonenhanced helical CT and US in the emergency evaluation of patients with renal colic: prospective comparison. Radiology 2000;217:792–7.
[15] Yilmaz S, Sindel T, Arslan G, et al. Renal colic: comparison of spiral CT, US and IVU in the detection of ureteral calculi. Eur Radiol 1998;8:212–7.
[16] Patlas M, Farkas A, Fisher D, et al. Ultrasound vs CT for the detection of ureteric stones in patients with renal colic. Br J Radiol 2001;74:901–4.
[17] Middleton WD, Dodds WJ, Lawson TL, et al. Renal calculi: sensitivity for detection with US. Radiology 1988;167:239–44.
[18] Spirnak JP, Resnick M, Banner MP. Calculus disease of the urinary tract, general considerations. In: Pollack HM, editor. Clinical urography. An atlas and textbook of urologic imaging. Philadelphia: WB Saunders; 1990. p. 1752–8.
[19] Dunnick RN, Sandler CM, Newhouse JH, et al. Nephrocalcinosis and nephrolithiasis. In: Dunnick RN, Sandler CM, Newhouse JH, et al, editors. Textbook of uroradiology. 3rd edition. Philadelphia: Lippincott Williams and Wilkins; 2001. p. 178–94.
[20] Newhouse JH, Prien EL, Amis ES Jr, et al. Computed tomography analysis of urinary calculi. AJR Am J Roentgenol 1984;142:545–8.
[21] Motley G, Dalrymple N, Keesling C, et al. Hounsfield unit density in the determination of urinary stone composition. Urology 2001;58: 170–3.
[22] Kohan A, Armenakas N, Fracchia J. Indinavir urolithiasis: an emerging cause of renal colic in patients with human immunodeficiency virus. J Urol 1999;161:1765–8.
[23] King W, Kimme-Smith C, Winter J. Renal stone shadowing: an investigation of contributing factors. Radiology 1985;154:191–6.
[24] Rahmouni A, Bargoin R, Herment A, et al. Color Doppler twinkling artifact in hyperechoic regions. Radiology 1996;199:269–71.
[25] Chelfouh N, Grenier N, Higueret D, et al. Characterization of urinary calculi: in vitro study of "twinkling artifact" revealed by color-flow sonography. AJR Am J Roentgenol 1998;171: 1055–60.
[26] Lee YJ, Seung HK, Jeong YC, et al. Color and power Doppler twinkling artifacts from urinary stones: clinical observations and phantom studies. AJR Am J Roentgenol 2001;176:1441–5.
[27] Melekos MD, Kosti PN, Karakovitis IE, et al. Milk of calcium cysts masquerading as renal calculi. Eur J Radiol 1998;28:62–6.
[28] Durr-e-Sabih, Khan AN, Craig M, et al. Sonographic mimics of renal calculi. J Ultrasound Med 2004;23:1361–7.
[29] Patriguin H, Robitaille P. Renal calcium deposition in children: sonographic demonstration of the Anderson-Carr progression. AJR Am J Roentgenol 1986;146:1253–6.
[30] Chau WK, Chan SC. Improved sonographic visualization by fluid challenge method of renal lithiasis in the non-dilated collecting system: experience in seven cases. Clin Imaging 1997; 21:276–83.
[31] Juul N, Holm-Bentzen M, Rygaard H, et al. Ultrasonographic diagnosis of renal stones. Scand J Urol Nephrol 1987;21:135–7.
[32] Rous SN. A review of 171 consecutive patients with urinary lithiasis. J Urol 1981;126:376–9.
[33] Erwin BC, Carroll BA, Sommer FG. Renal colic: the role of ultrasound in initial evaluation. Radiology 1984;152:147–50.
[34] Laing FC, Benson CB, DIsalvo DN, et al. Distal ureteric calculi: detection with vaginal US. Radiology 1994;192:545–8.
[35] Hertzberg BS, Kliewer MA, Paulson EK, et al. Distal ureteral calculi: detection with transperineal sonography. AJR Am J Roentgenol 1994;164: 1151–3.
[36] Lerner RM, Rubens D. Distal ureteral calculi: diagnosis by transrectal sonography. AJR Am J Roentgenol 1986;147(6):1189–91.
[37] Kimme-Smith C, Perrella RR, Kaveggia LP, et al. Detection of renal stones with real-time sonography: effect of transducer and scanning parameters. AJR Am J Roentgenol 1991;157: 975–80.
[38] Gillenwater JY. Pathophysiology of urinary tract obstruction. In: Walsh PC, Retik AB, Vaughan ED Jr, et al, editors. Walsh Campbell's urology. 8th edition. Philadelphia: Saunders; 2002. p. 412–5.
[39] Brenner BM, Levine SA. Urinary tract obstruction. In: Brenner BM, Rector F, editors. The kidney. 7th edition. Philadelphia: Saunders; 2002. p. 1867–74.
[40] Callahan MJ. The drooping lily sign. Radiology 2001;219:226–8.
[41] McAleer SJ, Loughlin KR. Nephrolithiasis and pregnancy. Curr Opin Urol 2004;14:123–7.
[42] Gorton E, Whitfield H. Renal calculi in pregnancy. Br J Urol 1997;80:4–9.
[43] Biyani C, Joyce A. Urolithiasis in pregnancy. I: pathophysiology, fetal considerations and diagnosis. BJU Int 2002;89:811–8.
[44] Swanson S, Heilman R, Eversman W. Urinary tract stones in pregnancy. Surg Clin North Am 1995;75:123–42.
[45] Vaglio A, Salvarani C, Buzio C. Retroperitoneal fibrosis. Lancet 2006;367:241–51.

[46] Vaughan ED Jr, Sorenson EJ, Gillenwater JY. The renal hemodynamic response to chronic unilateral complete ureteral occlusion. Invest Urol 1970;8:78–90.
[47] Vaughan ED Jr, Shenasky JH II, Gillenwater JY. Mechanism of acute hemodynamic response to ureteral occlusion. Invest Urol 1971;9:109–18.
[48] Moody TE, Vaughan ED Jr, Gillenwater JY. Relationship between renal blood flow and ureteral pressure during 18 hours of total unilateral uretheral occlusion. Implications for changing sites of increased renal resistance. Invest Urol 1975; 13:246–51.
[49] Lanzone JA, Gulmi FA, Chou S, et al. Renal hemodynamics in acute unilateral ureteral obstruction: contribution of endothelium-derived relaxing factor. J Urol 1995;153:2055–9.
[50] Reyes AA, Klahr S. Renal function after release of ureteral obstruction: role of endothelin and the renal artery endothelium. Kidney Int 1992;42: 632–8.
[51] Cronan JJ, Amis ES Jr, Yoder IC, et al. Peripelvic cysts: an impostor of sonographic hydronephrosis. J Ultrasound Med 1982;1(6):229–36.
[52] Rha SE, Byun JY, Jung SE, et al. The renal sinus: Pathologic spectrum and multimodality imaging approach. Radiographics 2004;24:S117–31.
[53] Urban BA, Fishman EK. Renal lymphoma; CT patterns with emphasis on helical CT. Radiographics 2000;20:197–212.
[54] Burge HJ, Middleton WD, McClennan BL, et al. Ureteral jets in healthy subjects and in patients with unilateral ureteral calculi: comparison with colour Doppler US. Radiology 1991;180:437–42.
[55] Shokeir AA, Provoost AP, Nijman RJ. Resistive index in obstructive uropathy. BJU Int 1997;80: 195–200.
[56] Keogan M, Kliewer M, Hertzberg B, et al. Renal resistive indexes: variability in Doppler US measurement in a healthy population. Radiology 1996;199:165–9.
[57] Norris C, Pfeiffer J, Rittgers S, et al. Noninvasive evaluation of renal artery stenosis and renovascular resistance: experimental and clinical studies. J Vasc Surg 1984;1:192–201.
[58] Kim S, Kim W, Choi B, et al. Duplex sonography of the native kidney: resistive index vs serum creatine. J Ultrasound Med 1990;9:S25.
[59] Tublin ME, Bude RO, Platt JF. The resistive index in Renal Doppler Sonography: where do we stand? AJR Am J Roentgenol 2002;180:885–92.
[60] Platt JF, Ellis JH, Rubin JM, et al. Intrarenal arterial Doppler sonography in patients with nonobstructive renal disease: correlation of resistive index with biopsy findings. AJR Am J Roentgenol 1990;154:1223–7.
[61] Mostbeck GH, Kain R, Mallek R, et al. Duplex Doppler sonography in renal parenchymal disease. Histopathologic correlation. J Ultrasound Med 1991;10:189–94.
[62] Platt JF, Rubin JM, Ellis JH. Acute renal failure: possible role of duplex Doppler US in distinction between acute prerenal failure and acute tubular necrosis. Radiology 1991;179:419–23.
[63] Bude RO, DiPietro MA, Platt JF, et al. Age dependency of the renal resistive index in healthy children. Radiology 1992;184:469–73.
[64] Mostbeck GH, Gossinger HD, Mallek R, et al. Effect of heart rate on Doppler measurements of resistive index in renal arteries. Radiology 1990;175:511–3.
[65] Platt J, Rubin J, Ellis J, et al. Duplex Doppler US of the kidney; differentiation of obstructive from nonobstructive dilatation. Radiology 1989;171: 515–7.
[66] Platt J, Rubin J, Ellis J. Distinction between obstructive and nonobstructive pyelocaliectasis duplex Doppler sonography. AJR Am J Roentgenol 1989;153:997–1000.
[67] Rodgers PM, Bates JA, Irving HC. Intrarenal Doppler ultrasound studies in normal and acutely obstructed kidneys. Br J Radiol 1992; 65:207–12.
[68] Platt JF, Rubin JM, Ellis JH. Acute renal obstruction: evaluation with intrarenal duplex Doppler and conventional US. Radiology 1993;186:685–8.
[69] Gottlieb R, Luhmann K, Oates R. Duplex ultrasound evaluation of normal native kidneys with urinary tract obstruction. J Ultrasound Med 1989;8:609–11.
[70] Brkljacic B, Drinkovic I, Sbajar-Matovianovic M, et al. Intrarenal duplex Doppler sonographic evaluation of unilateral native kidney obstruction. J Ultrasound Med 1994;13:197–204.
[71] Shokeir AA, Abdulmaaboud M. Resistive index in renal colic: a prospective study. BJU Int 1999;83: 378–82.
[72] Chen J, Pu Y, Liu S, et al. Renal hemodynamics in patients with obstructive uropathy evaluated by duplex Doppler sonography. J Urol 1993; 159:18–21.
[73] Tublin M, Dodd G, Verdile V. Acute renal colic: diagnosis with duplex Doppler US. Radiology 1994;193:697–701.
[74] Deyoe L, Cronan J, Breslaw B, et al. New techniques of ultrasound and color Doppler in the prospective evaluation of acute renal obstruction: do they replace intravenous urogram? Abdom Imaging 1995;20:58–63.
[75] Nazarian GK, Platt JF, Rubin JM, et al. Renal duplex Doppler sonography in asymptomatic women during pregnancy. J Ultrasound Med 1993;12:441–4.
[76] Wachsberg RH. Unilateral absence of ureteral jets in the third trimester of pregnancy: pitfall in color Doppler US diagnosis of urinary obstruction. Radiology 1998;209:279–81.
[77] Bude RO, Rubin JM. Relationship between the resistive index and vascular compliance and resistance. Radiology 1999;211:411–7.
[78] Tublin ME, Tessler FN, Murphy ME. Correlation between renal vascular resistance, pulse pressure and the resistive index in isolated perfused rabbit kidneys. Radiology 1999;213:258–64.

ELSEVIER SAUNDERS

ULTRASOUND CLINICS

Ultrasound Clin 2 (2007) 17–26

Sonography of the Urinary Bladder

Sarah E. McAchran, MD[a], David M. Hartke, MD[b], Dean A. Nakamoto, MD[c], Martin I. Resnick, MD[b,*]

Bladder ultrasound (US) is noninvasive, readily accessible, and easy to use. It has been extensively investigated as a possible substitution for some of the more common invasive modalities used to evaluate the bladder, namely cystoscopy and cystography. In fact, the US machine has become as integral a part of the urologist's office as the cystoscope. Modern US machines are compact, portable, and easily brought to the bedside, clinic, or operating room. Images are created in real time and interpretation and diagnosis occur as the images are created. For these reasons, and because US is noninvasive and without harmful side effects, US has been liberally adopted by urologists for its diagnostic and procedural capabilities. Its broad range of applications includes determination of the presence and volume of postvoid residual urine, assessment of suspected bladder stones, diverticula, and other lesions, evaluation of the bladder neck for hypermobility in women suspected of stress incontinence, and assessment of pediatric patients who have posterior urethral valves, ureteroceles, and, more recently, vesicoureteral reflux.

Embryology

Bladder development is a two-stage process beginning with the terminal end of the primitive gut, the embryonic cloaca (Fig. 1). The cloaca is divided into an anterior and posterior portion by the urorectal septum. The anterior portion forms the primitive bladder and the posterior portion forms the anorectal canal. The mesonephric ducts insert into the anterior portion of the cloaca, dividing it into a superior portion, the primitive bladder, and an inferior portion, the urogenital sinus. As the mesonephric ducts are incorporated into the bladder they maintain separate openings near the lower portion, giving rise to the ureteral orifices. The upper portion of the cloaca or primitive bladder is

[a] Department of Urology, Glickman Urological Institute, 9500 Euclid Avenue/A100, Cleveland, OH 44195, USA
[b] Department of Urology, Case School of Medicine, 11100 Euclid Avenue, Cleveland, OH 44106-5046, USA
[c] Department of Radiology, Case School of Medicine, 11100 Euclid Avenue, Cleveland, OH 44106-5056, USA
* Corresponding author.
E-mail address: martin.resnick@case.edu (M.I. Resnick).

1556-858X/07/$ – see front matter
doi:10.1016/j.cult.2007.01.010
ultrasound.theclinics.com

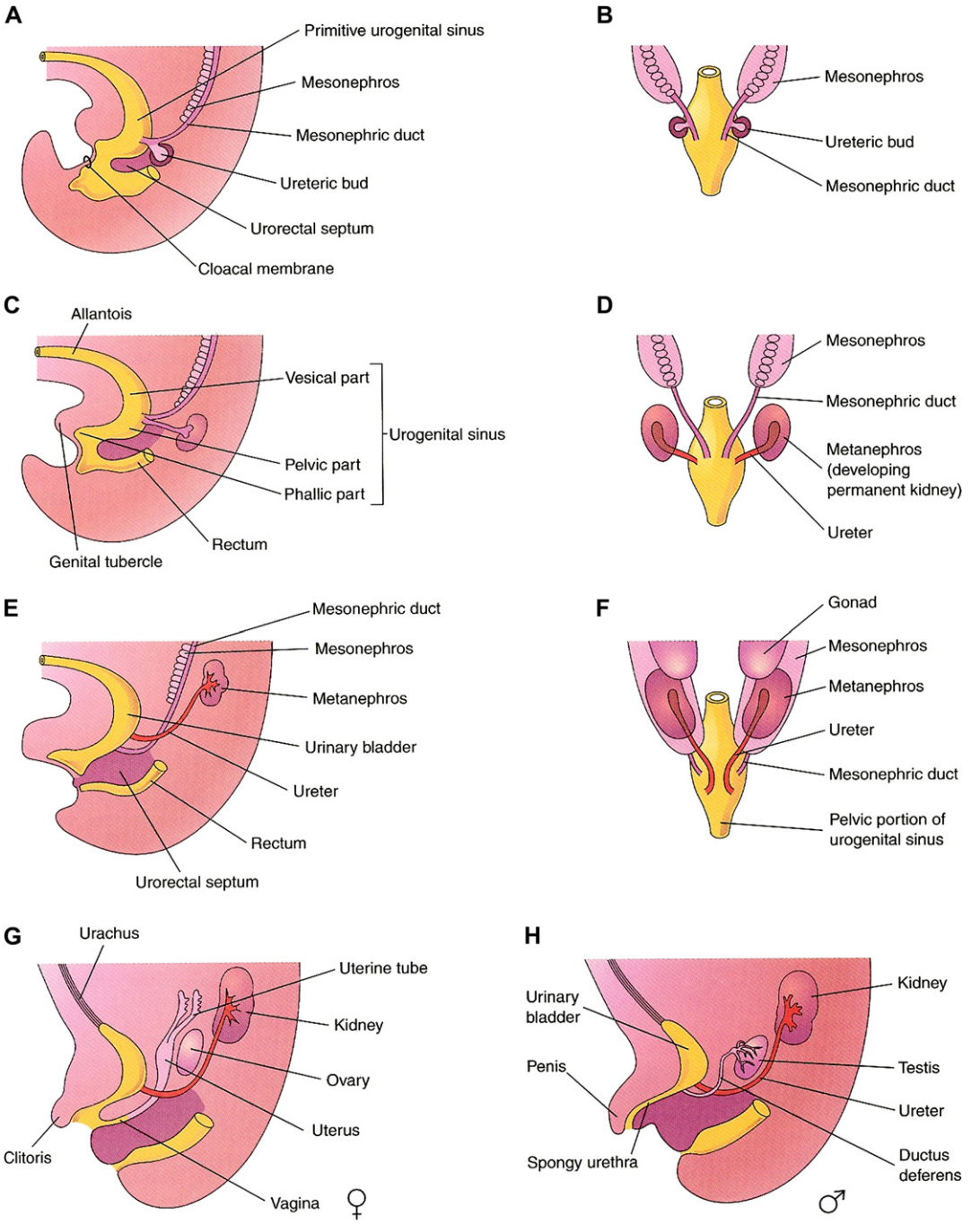

Fig. 1. Urogenital embryology. Division of the cloaca into the urogenital sinus and rectum and development of the urinary bladder, urethra, and urachus. (*A*) Lateral view of the caudal half of a 5-week embryo. (*B*, *D*, *F*) Dorsal views. (*C*, *E*, *G*, *H*) Lateral views. The stages shown in *G* and *H* are reached by the 12th week. (*From* Moore KL, Persaud TVN. The developing human: clinically oriented embryology. 6th edition. Philadelphia: WB Saunders; 1998. p. 303–47; with permission.)

continuous with the allantois. The urachus is the superior connection with the allantois, which degenerates into a cordlike structure called the median umbilical ligament in the adult.

At birth, the neonatal bladder occupies a much more superior location in the pelvis than the adult bladder. With maturation, the bladder assumes a lower position within the true pelvis.

Sonographic technique

Bladder ultrasonography can be performed through a transabdominal, transrectal, transvaginal, or transurethral approach. The transabdominal approach is used most commonly. For most adults a 3.5-MHz probe provides appropriate images. A 2.0-MHz probe is necessary for use on the very obese patient, however; this longer wavelength sacrifices resolution to provide better depth of penetration. Conversely, for the very thin patient a 5.0-MHz probe may penetrate deep enough to image the bladder and provide excellent resolution.

Transabdominal scanning

When empty, the bladder lies behind the pubic symphysis and is difficult to find with US. US should be performed with the bladder full. The average adult bladder holds about 500 mL comfortably, and patients should be instructed to drink 8 to 16 ounces of fluid before their study [1]. With the patient supine, the appropriate transducer is placed 1 cm superior to the pubic symphysis and angled caudally. The bladder should be scanned in real time in longitudinal and transverse orientations. To image the anterior basal portions of the bladder, the transducer must be angled behind the symphysis pubis; in some patients body habitus precludes adequate visualization of this region.

Several factors may complicate transabdominal imaging. For instance, the postsurgical patient may have incisions and dressings in the suprapubic region that hamper adequate probe placement. Alternatively, patients who have an indwelling catheter or those who have had recent bladder instrumentation may have air at the dome of the bladder, limiting through-transmission of the US beam.

Transrectal scanning

Transrectal US is primarily used to image the prostate; however, it may be used to image the bladder also. With the patient in either the lateral decubitus or dorsal lithotomy position, the well-lubricated transrectal probe is guided into the rectum above the anal verge and a thorough sonographic examination of the bladder is performed. Biplane, multiplane, and end-fire endorectal probes with a frequency range from 6 to 8 MHz are used to image the bladder, prostate, and adjacent structures, including the seminal vesicles and urethra. Longitudinal movement provides an infinite number of serial sections of the bladder, and the rotational movement (depending on the probe type) provides sonotomograms of it. For best results, an enema can be administered before transrectal scanning; however, it is not absolutely necessary. A catheter can be inserted into the bladder so that the bladder may be readily distended for the study. The balloon from an indwelling transurethral catheter provides a useful landmark to identify the bladder neck.

Transurethral scanning

Although evidence suggests that transurethral scanning may be the best method for the evaluation of bladder tumors, this approach requires the placement of a resectoscope sheath and must be performed with either a local or general anesthetic. These requirements significantly limit its clinical applications. The 3.5- to 7.0-MHz transducer fits within a standard 24-French resectoscope sheath. When further information is desired during cystoscopy, the optics can be removed from the sheath and replaced with the transurethral scanner. With the bladder distended, dynamic scans are obtained at different angles, positions, and degrees of inflation to view all surfaces of the bladder. Transurethral imaging provides superior resolution of the bladder wall, enabling a more precise staging of bladder tumors than other methods of ultrasonography.

Transvaginal scanning

The same probes used for transrectal scanning may be placed inside the vagina to scan the bladder and urethra. The main application of this mode of scanning today is for urodynamic applications and for the evaluation of urethral pathology.

Normal anatomy

The anatomic structures adjacent to the bladder vary according to the sex of the patient. The adult bladder sits in the bony true pelvis. The dome, apex, superior, lateral, and posterior one third of the bladder are covered by peritoneum. The symphysis pubis abuts the anterior aspect of the bladder in both sexes and blocks the through-transmission of the US waves. In the female pelvis, the bladder is immediately anterior to the uterus; the rectovesical pouch, therefore, lies between the uterus and the rectum. In the male, the rectovesical pouch lies posterior to the bladder as do the fluid-filled seminal vesicles. Medial to the seminal vesicles, the tubular-shaped vas deferens can be imaged. The base of the male bladder sits atop the prostate. As mentioned, the prostate is generally better imaged transrectally.

The bladder should appear as a sonolucent structure with sharply demarcated walls. Typically, the bladder is seen as a spherical structure and the interface between the fluid medium and the bladder wall is distinct. The bladder wall normally appears as a symmetric, smooth, gently curved surface. The sonographic appearance of the bladder wall

varies with the frequency of the US probe used. The separate layers of the bladder wall are only discernible when a high-frequency probe is used in children and some young adults. When discernible, the echogenic mucosa is seen abutting the more sonolucent muscle layers (Fig. 2) [1]. With the typical 3.5-MHz transabdominal transducer, the bladder wall appears as a single echogenic layer.

When viewed transabdominally, the bladder shows some variability in shape depending on the amount of fluid present, intrapelvic pressure variations, patient position, and the position of the probe. The seminal vesicles and prostate can be imaged transabdominally but not as precisely as with a transrectal probe. Longitudinal scans reveal a tapering of the bladder anteriorly with an orientation toward the umbilicus. Sometimes the flow of urine into the bladder can be seen on routine US. A ureteral jet of urine can be seen as an intermittent echogenic focus emerging from the ureteral orifice [2,3]. Ureteral jets are more easily observed with color flow Doppler (Fig. 3) [1]. When inserted, the balloon of a Foley catheter serves as a useful landmark to identify the bladder neck (Fig. 4).

Measurement of bladder wall thickness

Elevated intravesical pressures because of bladder outlet obstruction or neurogenic changes to the bladder may ultimately result in pathologic bladder wall thickening. If bladder wall thickness could be reliably and reproducibly measured using US, this could be assessed at regular office visits. If the bladder wall thickness becomes abnormal or worsens, further evaluation and treatment can be undertaken. Because measurement of bladder wall thickness varies depending on the degree of bladder distention, the area of the bladder measured, and transducer frequency, great care must be taken when interpreting these measurements (Fig. 5). As

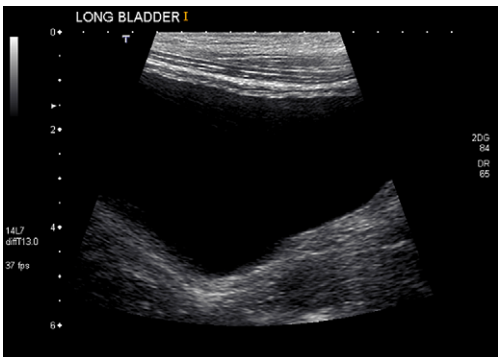

Fig. 2. High-frequency ultrasound of a normal bladder in a thin patient. The bladder is lined by echogenic mucosa and layers of detrusor muscle.

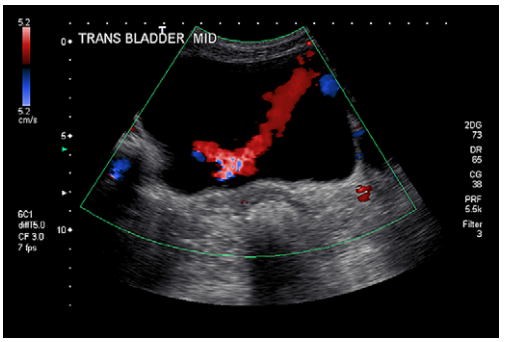

Fig. 3. Bilateral crossing ureteral jets are well visualized using color Doppler ultrasonography.

a general guideline for adults, the normal full bladder wall is about 3 mm and the normal empty bladder wall is about 5 mm [1]. A recent study of bladder wall thickness in 150 normal children from newborn to 13 years old demonstrated that normal thickness increases slightly with age [4]. The authors found that at a bladder fullness of 10% of expected bladder capacity the average bladder wall thickness was 2.0 mm. This thickness decreased to 1.5 mm once the bladder exceeded 50% of expected bladder capacity. Yamazaki and colleagues [5] found that mean bladder wall thickness, measured at a bladder volume greater than 10 mL, was significantly greater in males than in females at 1.63 mm versus 1.38 mm, respectively.

Residual urine volume

Measurement of residual urine to evaluate for urinary retention or voiding efficiency is perhaps the most common application of bladder US. US provides a rapid, noninvasive means to estimate residual urine volume without the risk for infection or the discomfort associated with urethral catheterization. Minimizing the risk for infection is particularly important in the ICU and inpatient settings in which urinary tract infection is the most common nosocomial infection and the risk increases with repeated catheterizations [6]. Similarly, several recent articles have advocated performing bladder US in neonates and young children to evaluate bladder fullness and eliminate unfruitful, painful catheterizations [7,8]. Using the standard gray-scale, real-time scanner the bladder is imaged transversely and longitudinally. Measurements are taken of the width, height, and length. The formula for calculating the volume of an ellipsoid has been found to be the most accurate for estimating bladder volume: volume = 0.52 × length × width × height [9]. This calculation is performed automatically by most current US machines.

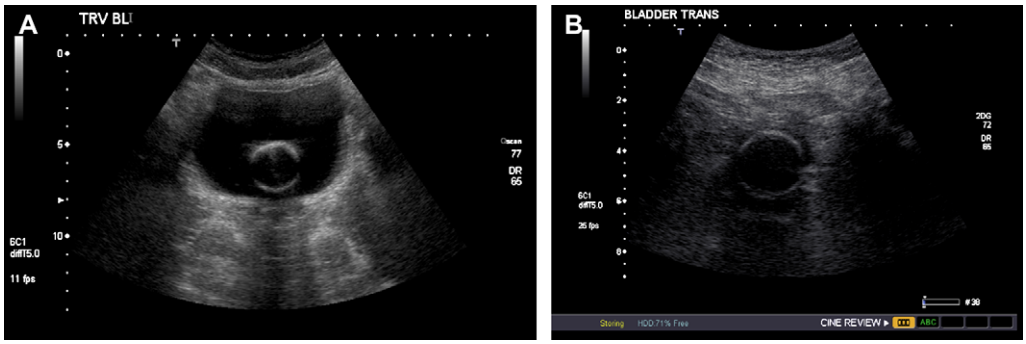

Fig. 4. A Foley catheter is demonstrated as an echogenic circle with an anechoic interior in a moderately filled bladder (*A*). A Foley catheter balloon is inflated in a decompressed bladder (*B*).

Newer devices or bladder scanners are small and portable, fitting easily into the palm of the hand, and specifically designed for automated bladder volume determinations by minimally trained personnel. The transducer is placed in the normal position for bladder US until the bladder shadow appears in the cross-hairs of the sighting display. After activating the scanner, multiple spatially interlocked ultrasonic images are generated at fixed angles to each other. A volumetric model of the whole bladder is constructed. Bladder volume is determined by a three-dimensional integration process rather than by a fixed geometric formula. Scanned volumes have been shown to have an overall accuracy of 94% for volumes 100 mL or greater [10]. Scanned volume underestimates the true bladder volume by an average of 10 mL in men and 20 mL in women.

Numerous studies have evaluated the accuracy of US-determined bladder volumes with standard machines and handheld bladder scan units compared with catheter-determined volumes [9,11–13]. In general standard machines are more accurate than handheld machines; however, given their portability and point-and-shoot ease of use, handheld scanners do have a place in clinical practice. For clinical purposes it is seldom necessary to know the precise amount of residual urine. It is more important to know whether residual urine is present, and, if present, if it is significant [14]. One notable exception in which precision is of the utmost importance is in determining bladder volumes in neonates. US-determined volumes are more accurate at volumes greater than 100 mL and have error ranges in the 20 to 50 mL range. The normal neonatal bladder capacity is about 60 mL. A study of 10 neonatal patients who had neurogenic bladders compared automated bladder scan volumes to catheterized volumes and, as expected, found a low correlation [15].

Congenital abnormalities

Most congenital anomalies are diagnosed during the neonatal period. Megaureter, or ureteral diameter greater than 1.0 cm, can be detected on bladder US as a dilated structure immediately posterior to the bladder [16]. The normal ureter is not detectable on this view. Any suspected midline omphalovesical abnormalities in children or adults should be evaluated with US [17]. Urachal remnants, vesical duplication anomalies, and in cases of

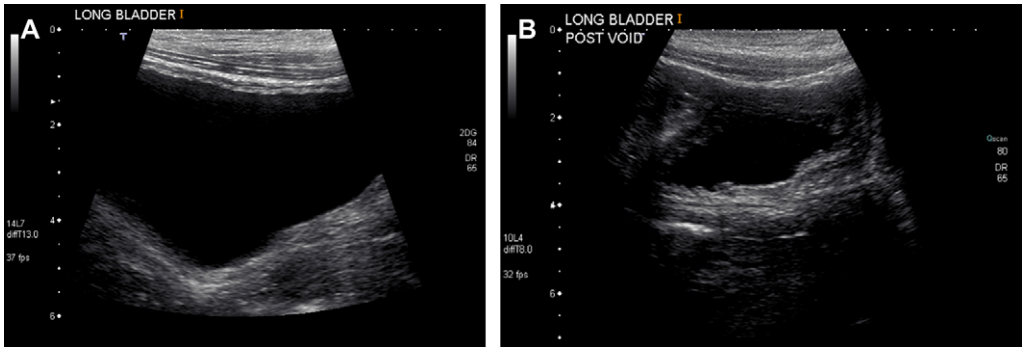

Fig. 5. The normal bladder wall appears thinner in a filled state (*A*) compared with the postvoid state (*B*).

a solid mass, urachal carcinoma, can be detected [18]. Ultrasonographically, the urachal cyst occupies an extraperitoneal location and is in the expected line of the median umbilical ligament. Uninfected, it is a sonolucent, oval-shaped cyst (Fig. 6). The vesicourachal diverticulum appears as a saclike midline projection from the superior aspect of the bladder. Today, bladder exstrophy is generally detected on routine prenatal US and specific findings have been described [19].

Ureteroceles are easily detected with transabdominal bladder sonography. Ureteroceles have a fixed base with an anechoic center and thin echogenic wall (Fig. 7). Their sonolucent center and the easily-identifiable thin wall help to differentiate ureteroceles from bladder tumors, which are also fixed to the bladder wall. Occasionally, a stone may form within a ureterocele and is easily detected as an echogenic focus with posterior shadowing.

Acquired abnormalities

Bladder diverticula

One of the sequelae of bladder outlet obstruction, a thickened bladder wall, has already been discussed. Bladder diverticula represent a second sequela of this process. They are seen most often in men who have chronic bladder outlet obstruction attributable to benign prostatic hyperplasia. Rarely, they are a congenital anomaly. Diverticula greater than 2 cm appear as sonolucent masses adjacent to the bladder wall, which is often thickened (Fig. 8). If the opening of the diverticulum cannot be identified then the differential diagnosis would include cystic masses extrinsic to the bladder, such as ovarian cysts, hematomas, or lymphoceles [1]. Occasionally the diverticulum may harbor calculi, blood clots, and neoplasms, which appear as an echogenic focus. Postvoiding scans are helpful because often the diverticula do not empty and occasionally increase in size. Cystography can confirm the diagnosis.

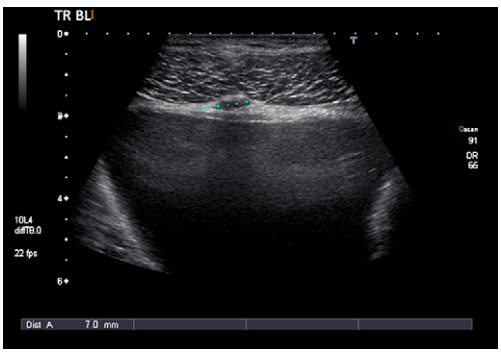

Fig. 6. A urachal cyst (marked, *A*) is an oval-shaped, midline, sonolucent structure just anterior to the bladder.

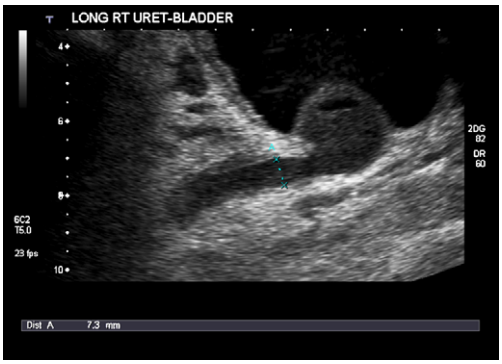

Fig. 7. An ureterocele is demonstrated as an echogenic ring protruding into the bladder. A dilated ureter (marked, *A*) is well visualized because of obstruction caused by the ureterocele.

Calculi, clots, and other debris

The same stones and blood clots that can be found in a diverticulum can be found in the bladder or distal ureter also. Bladder stones should move with changes in patient position and appear hyperechoic with acoustic shadowing (Fig. 9). Blood clots are typically viewed as masses of increased echogenicity mobile within the bladder. The mobility of blood clots often distinguishes them from fixed neoplasms; however, clots can be adherent also. When there is a large amount of clot in the bladder it may be imaged as a medium echogenic focus that layers dependently.

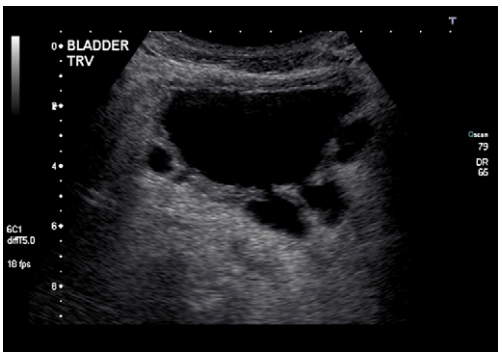

Fig. 8. Several bladder diverticula are visualized as sonolucent structures adjacent to the bladder. They represent out-pouchings of bladder mucosa between hypertrophied bundles of detrusor muscle. The bladder wall is diffusely thickened, but the diverticula are devoid of muscle.

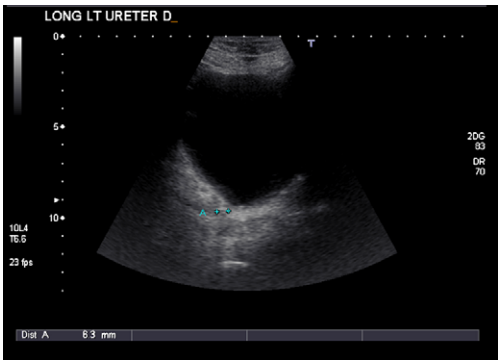

Fig. 9. An echogenic calculus (marked, *A*) is well visualized at the ureterovesical junction with a line of posterior acoustic shadowing. The shadowing occurs as a result of the inability of ultrasound to penetrate beyond the dense calculus.

Cystitis

US does not typically play a role in the evaluation of patients who have acute bacterial cystitis; however, if performed, the most common finding is a diffusely thickened bladder wall. Several authors have suggested serial bladder US as a way of monitoring progression or resolution of certain bladder pathologies. Cartoni and colleagues [20] used US to follow hemorrhagic cystitis secondary to bone marrow transplantation. Dittrich and Doehring [21] reported using US to follow urinary schistosomiasis.

Masses

Superficial transitional cell carcinoma appears as a polypoid, echogenic, or hyperechoic projection from the bladder wall (Fig. 10) [1]. Bladder disorders that can mimic malignancy on US include cystitis, bladder trabeculae, blood clots, stones, ureteroceles, and a prominent prostatic median lobe. Ultimately, cystoscopy and biopsy are needed to differentiate between these lesions.

Factors that affect the accuracy of transabdominal US in evaluating the bladder for malignancy include body habitus, bladder distention, and size and location of the tumor [1]. The dome and anterior bladder are difficult to evaluate with transabdominal US. The size of the tumors is also important, with studies noting diagnostic accuracy of only 38% for tumors smaller than 5 mm, 82% for tumors 5 to 10 mm, and 100% for tumors greater than 10 mm [22]. Transabdominal US is not accurate in staging superficial versus deeply invasive tumors (Fig. 11). In situ lesions cannot be detected and transabdominal US cannot distinguish Ta from T1 lesions or T1 from T2 lesions [23]. If the tumor has invaded beyond the bladder wall or involves the perivesical or retroperitoneal lymph nodes, transabdominal US can stage these lesions with an accuracy approaching 100% [24].

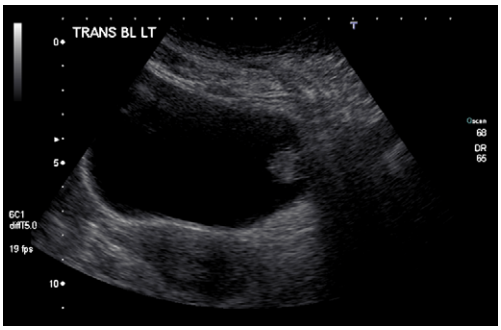

Fig. 10. An echogenic mass projects from the left bladder wall and represents a superficial papillary transitional cell carcinoma.

Extrinsic masses

Disorders of structures adjacent to the bladder may deform it and cause distortion and fixation the bladder wall. Cervical, colon, and prostate cancer may extend locally into the bladder muscle. Although an intraluminal mass may not be present, the involved wall is fixed and difficult to differentiate from the primary tumor mass. Benign perivesical processes may also distort the bladder (Fig. 12). These include müllerian duct remnants, abscesses, hematomas, urinary extravasation, uterine fibroids, and ovarian cysts. US is also helpful in differentiating a distended bladder from another type of pelvic mass [25].

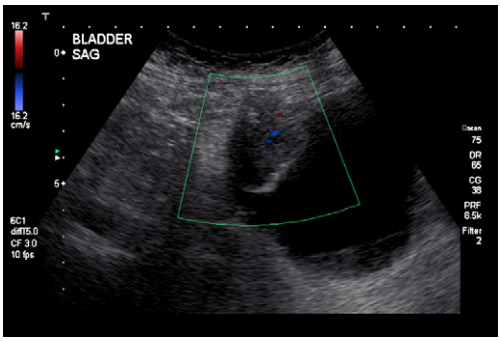

Fig. 11. A sessile mass at the right lateral bladder wall that was later confirmed to be muscle-invasive transitional cell carcinoma. Color Doppler ultrasonography helps differentiate the mass as perfused tissue from echogenic clot, which would not demonstrate blood-flow.

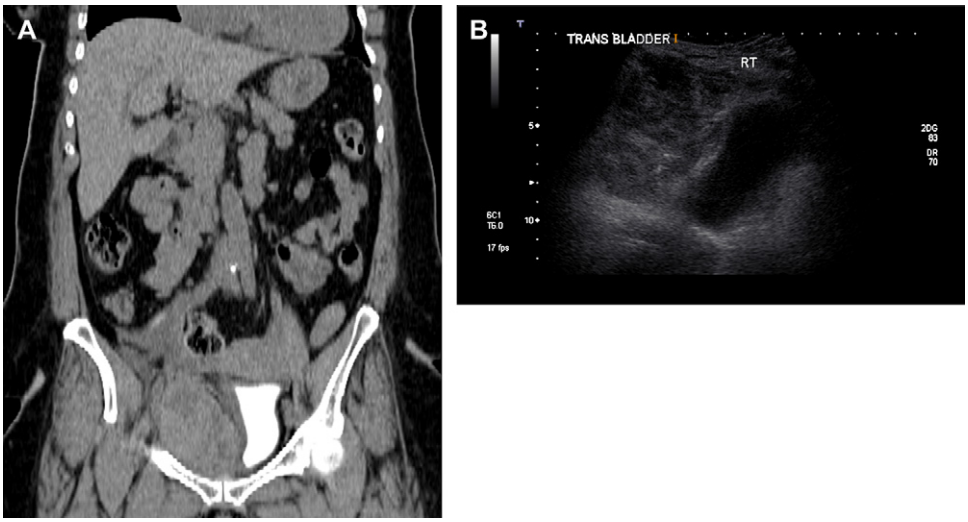

Fig. 12. A large hematoma in the right hemipelvis displaces an otherwise normal bladder laterally. This is demonstrated on a coronal CT with the bladder filled with contrast (*A*) and also on ultrasound (*B*) as an echogenic hematoma displacing a sonolucent bladder.

Suprapubic aspiration

Suprapubic placement of a needle into the bladder may be required to obtain a sterile urine specimen or as the first step in the placement of a percutaneous cystostomy tube. The position of the distended bladder is determined and the needle can be directed into the bladder with US guidance. This technique is particularly helpful in children and obese patients, in whom the distended bladder may be more difficult to percuss.

The retained Foley

Failure of a Foley catheter balloon to deflate is a rare complication of urinary catheterization. When initial techniques for removal fail, US can be used to image the balloon and guide its safe puncture. Transabdominal US is used to locate the balloon within the full bladder. A small-gauge spinal needle can then be advanced percutaneously by way of a suprapubic approach, under US guidance. The balloon is punctured under direct monitor view. On removal, the balloon must be examined to ensure that it was removed intact [26].

Urodynamics

Real-time US can be combined with standard urodynamics in the evaluation of voiding disorders and has been proposed as a radiation-free alternative to fluoroscopy. Furthermore, US can provide useful information regarding the anatomy of the bladder base, pelvic floor, and urethra [27]. The bladder neck and proximal urethra are best seen by transrectal, transvaginal, and transperineal probe placement. For transrectal scanning a high-frequency (7 to 10 MHz) linear array probe is preferred. Patients may be studied in the left lateral decubitus, dorsal lithotomy, or standing positions. Once the probe is inserted the face of the transducer is directed anteriorly toward the urethra. Transvaginal scanning is performed similarly. Transperineal scanning uses a 3.5- to 5.0-MHz probe placed on the perineum. On transverse section three distinct layers of the urethra may be seen: an outer hyperechoic layer representing the rhabdosphincter, a central hyperechoic layer representing smooth muscle and connective tissue, and an innermost hypoechoic layer corresponding to the urethral lumen.

Transvaginal US been used to evaluate the mid-urethra and urethral sphincter in cases of incontinence and urinary retention [28,29]. Ultrasonographic measurement of the urethral angle has been proposed for more accurate evaluation of urethral hypermobility [30–32]. Transperineal color Doppler US has been used to measure urine velocity in the prostatic urethra of men who have bladder outlet obstruction [33,34]. Most of these applications are still in the experimental phase, and the widespread clinical applicability of US in this field remains to be determined.

New frontiers

Most new research in applications of bladder US has been in the pediatrics realm, in which limiting exposure to ionizing radiation is particularly important. It is estimated that as much as 25% of the radiation that has the potential to produce genetic alterations is received by the pediatric

population during imaging of the urinary system, especially with voiding cystourethrography (VCUG) [35,36]. Over the last decade, several studies have evaluated the application of contrast-enhanced US to the evaluation of vesicoureteral reflux (VUR) [37–40]. These injectable agents are a fluid suspension containing small particles measuring 1 to 5 μm that increase the backscattered US signals and thus result in better image contrast [41]. Berrocal and colleagues [39] used a sonographic echo enhancer made of a galactose suspension to perform voiding cystosonography on 216 pediatric patients aged 3 days to 18 years. The results were compared with standard VCUG performed at the same sitting. Ten milliliters of contrast solution was instilled with normal saline to a volume equal to the patient's estimated bladder capacity by age. VUR was diagnosed at cystosonography when microbubbles appeared in the ureter or renal pelvis. It was graded by using the classification of Atala and colleagues [40]: grade 1, echo contrast in only the ureter; grade 2, echo contrast in the pelvicaliceal system with no dilatation; grade 3, mild to moderate dilatation of the pelvicaliceal system; grade 4, moderate to severe dilatation of the pelvicaliceal system; and grade 5, gross dilatation of the pelvicaliceal system with total or partial atrophy. The comparison of cystosonography with VCUG showed that both techniques were concordant for the presences or absence of VUR and for the grade of VUR in 83.7% of renal units. There was concordance in the detection of VUR but not in the grade of VUR in 3.8% of the units. Cystosonography tended to depict a higher grade of VUR than did VCUG when both tests demonstrated VUR. Because treatment recommendations for VUR are based on grades determined by fluoroscopic VCUG, the upgrading inherent to cystosonography may have significant clinical impact; this needs to be further evaluated before its incorporation into routine use.

One of the inherent benefits to VCUG is its ability to provide anatomic evaluation of the urethra during the voiding phase of the scan. Using transperineal US applied to the labia in females or penoscrotal junction in males as part of a contrast-enhanced voiding US of the bladder, Berrocal and colleagues [37] were able to evaluate the urethra of 146 pediatric patients. Sensitivity and specificity for detecting urethral abnormalities, such as posterior urethral valves or urethral strictures, were 100% when compared with VCUG.

Summary

Ultrasonography of the bladder and using the bladder as an acoustic window are diagnostic tools adaptable to various clinical settings. Because bladder US noninvasive and does not require ionizing radiation, the range of its clinical usefulness will continue to be investigated and broadened.

References

[1] Cochlin DL, Dubbins PA, Goldberg BB, et al. Urogenital US: a text atlas. Philadelphia: JB Lippincott Co; 1994.
[2] Kremer H, Dobrinski W, Mikyska M, et al. Ultrasonic in vivo and in vitro studies on the nature of the ureteral jet phenomenon. Radiology 1982; 142(1):175–7.
[3] Dubbins PA, Kurtz AB, Darby J, et al. Ureteric jet effect: the echographic appearance of urine entering the bladder. A means of identifying the bladder trigone and assessing ureteral function. Radiology 1981;140(2):513–5.
[4] Muller L, Jacobsson B, Marild S, et al. Detrusor thickness in healthy children assessed by a standardized US method. J Urol 2001;166(6): 2364–7.
[5] Yamazaki Y, Yago R, Toma H. Sonographic characteristics of the urinary tract in healthy neonates. J Urol 2001;166(3):1054–7.
[6] Habib FA, McKenney MG. Surgeon-performed US in the ICU setting. Surg Clin North Am 2004;84(4):1151–79, vii.
[7] Chen L, Hsiao AL, Moore CL, et al. Utility of bedside bladder US before urethral catheterization in young children. Pediatrics 2005;115(1): 108–11.
[8] Milling TJ Jr, Van Amerongen R, Melville L, et al. Use of ultrasonography to identify infants for whom urinary catheterization will be unsuccessful because of insufficient urine volume: validation of the urinary bladder index. Ann Emerg Med 2005;45(5):510–3.
[9] Roehrborn CG, Peters PC. Can transabdominal US estimation of postvoiding residual (PVR) replace catheterization? Urology 1988;31(5): 445–9.
[10] Marks LS, Dorey FJ, Macairan ML, et al. Three-dimensional US device for rapid determination of bladder volume. Urology 1997;50(3):341–8.
[11] Dudley NJ, Kirkland M, Lovett J, et al. Clinical agreement between automated and calculated US measurements of bladder volume. Br J Radiol 2003;76(911):832–4.
[12] Coombes GM, Millard RJ. The accuracy of portable US scanning in the measurement of residual urine volume. J Urol 1994;152(6 Pt 1):2083–5.
[13] Cardenas DD, Kelly E, Krieger JN, et al. Residual urine volumes in patients with spinal cord injury: measurement with a portable US instrument. Arch Phys Med Rehabil 1988;69(7): 514–6.
[14] Djavan B, Roehrborn CG. Bladder ultrasonography. Semin Urol 1994;12(4):306–19.
[15] Wyneski HK, McMahon DR, Androulakakis V, et al. Automated bladder scan urine volumes

are not reliable in complex neonatal cases. J Urol 2005;174(4 Pt 2):1661–2 [discussion: 1662].
[16] Vinstein AL. Neonatal radiologic casebook. J Perinatol 1988;8(4):374–5.
[17] Avni EF, Matos C, Diard F, et al. Midline omphalovesical anomalies in children: contribution of US imaging. Urol Radiol 1988;10(4):189–94.
[18] Cacciarelli AA, Kass EJ, Yang SS. Urachal remnants: sonographic demonstration in children. Radiology 1990;174(2):473–5.
[19] Jaffe R, Schoenfeld A, Ovadia J. Sonographic findings in the prenatal diagnosis of bladder exstrophy. Am J Obstet Gynecol 1990;162(3): 675–8.
[20] Cartoni C, Arcese W, Avvisati G, et al. Role of ultrasonography in the diagnosis and follow-up of hemorrhagic cystitis after bone marrow transplantation. Bone Marrow Transplant 1993; 12(5):463–7.
[21] Dittrich M, Doehring E. Ultrasonographical aspects of urinary schistosomiasis: assessment of morphological lesions in the upper and lower urinary tract. Pediatr Radiol 1986;16(3):225–30.
[22] Malone PR. Transabdominal US surveillance for bladder cancer. Urol Clin North Am 1989;16(4): 823–7.
[23] Vallancien G, Veillon B, Charton M, et al. Can transabdominal ultrasonography of the bladder replace cystoscopy in the followup of superficial bladder tumors? J Urol 1986;136(1):32–4.
[24] Singer D, Itzchak Y, Fischelovitch Y. Ultrasonographic assessment of bladder tumors. II. Clinical staging. J Urol 1981;126(1):34–6.
[25] Lee TG, Reed TA. Ultrasonic diagnosis of the bladder as a symptomatic pelvic mass. J Urol 1977;117(3):283–4.
[26] Daneshmand S, Youssefzadeh D, Skinner EC. Review of techniques to remove a Foley catheter when the balloon does not deflate. Urology 2002;59(1):127–9.
[27] Kuo HC. Transrectal sonographic investigation of urethral and paraurethral structures in women with stress urinary incontinence. J Ultrasound Med 1998;17(5):311–20.
[28] Kondo Y, Homma Y, Takahashi S, et al. Transvaginal US of urethral sphincter at the mid urethra in continent and incontinent women. J Urol 2001;165(1):149–52.
[29] Wiseman OJ, Swinn MJ, Brady CM, et al. Maximum urethral closure pressure and sphincter volume in women with urinary retention. J Urol 2002;167(3):1348–51 [discussion: 1351].
[30] Bergman A, McKenzie CJ, Richmond J, et al. Transrectal US versus cystography in the evaluation of anatomical stress urinary incontinence. Br J Urol 1988;62(3):228–34.
[31] Pregazzi R, Sartore A, Bortoli P, et al. Perineal US evaluation of urethral angle and bladder neck mobility in women with stress urinary incontinence. BJOG 2002;109(7):821–7.
[32] Reddy AP, DeLancey JO, Zwica LM, et al. On-screen vector-based US assessment of vesical neck movement. Am J Obstet Gynecol 2001; 185(1):65–70.
[33] Ozawa H, Kumon H, Yokoyama T, et al. Development of noninvasive velocity flow video urodynamics using Doppler sonography. Part I: experimental urethra. J Urol 1998;160(5): 1787–91.
[34] Ozawa H, Kumon H, Yokoyama T, et al. Development of noninvasive velocity flow video urodynamics using Doppler sonography. Part II: clinical application in bladder outlet obstruction. J Urol 1998;160(5):1792–6.
[35] Cleveland RH, Constantinou C, Blickman JG, et al. Voiding cystourethrography in children: value of digital fluoroscopy in reducing radiation dose. AJR Am J Roentgenol 1992;158(1): 137–42.
[36] Gonzalez L, Vano E, Ruiz MJ. Radiation doses to paediatric patients undergoing micturating cystourethrography examinations and potential reduction by radiation protection optimization. Br J Radiol 1995;68(807):291–5.
[37] Berrocal T, Gaya F, Arjonilla A. Vesicoureteral reflux: can the urethra be adequately assessed by using contrast-enhanced voiding US of the bladder? Radiology 2005;234(1):235–41.
[38] Valentini AL, De Gaetano AM, Minordi LM, et al. Contrast-enhanced voiding US for grading of reflux in adult patients prior to antireflux ureteral implantation. Radiology 2004;233(1):35–9.
[39] Berrocal T, Gaya F, Arjonilla A, et al. Vesicoureteral reflux: diagnosis and grading with echo-enhanced cystosonography versus voiding cystourethrography. Radiology 2001;221(2): 359–65.
[40] Atala A, Wible JH, Share JC, et al. Sonography with sonicated albumin in the detection of vesicoureteral reflux. J Urol 1993;150(2 Pt 2): 756–8.
[41] Deng C. Contrast agents for US imaging. In: Dogra V, Rubens D, editors. US secrets. Philadelphia: Hanley & Belfus; 2004. p. 23–9.

ELSEVIER SAUNDERS

ULTRASOUND CLINICS

Ultrasound Clin 2 (2007) 27–44

Ultrasound Evaluation of Testicular Neoplasms

Ercan Kocakoc, MD[a], Shweta Bhatt, MD[b], Vikram S. Dogra, MD[b,*]

The development of digital sonographic equipment and new high-frequency broadband transducers improves the quality of ultrasound imaging, particularly in superficial tissues, such as those of the testis. Sonography may be the preferred imaging technique for evaluation of testis anatomy and pathologies because its improved spatial resolution allows evaluation of normal and pathologic structures, and increased color Doppler sensitivity for low flows allows full evaluation of testicular vascularity. Ultrasound (US) with a high-frequency transducer and the use of gray-scale, pulsed, color, and power Doppler modes has become the imaging modality of choice for evaluating testicular anatomy and disease states affecting the testes [1].

US with a high-frequency transducer helps to image and better characterize the testicular anatomy and flow and, in many circumstances, allows for a more specific diagnosis. One of the most important roles of sonography is to differentiate the solid from cystic nature of lesions and intratesticular lesions from extratesticular lesions; although most of the intratesticular solid lesions are malignant, most of the extratesticular lesions are benign regardless of solid or cystic nature. High-resolution, real-time US is accurate for distinguishing intratesticular from extratesticular lesions [2] and its accuracy approaches nearly 100%. High-frequency sonography can help identify certain benign intratesticular lesions, resulting in testis-sparing surgery [1].

Although testicular neoplasms are a rare, constituting about 1% of all malignant neoplasms in men, it is the most common malignancy in young men and boys 15 to 34 years of age [3]. Most tumors are discovered on physical examination as painless or slightly painful enlargement of the testis or as a nodular abnormality with an irregular surface [4]. Physical examination alone is not reliable to differentiate intratesticular lesions from extratesticular lesions. To detect small masses or subtle changes in the testis may also be difficult even by

[a] Department of Radiology, Faculty of Medicine, Firat University, 23119 Elazig, Turkey
[b] Department of Radiology, University of Rochester School of Medicine and Dentistry, 601 Elmwood Avenue, Box 648, Rochester, NY 14642, USA
* Corresponding author.
E-mail address: vikram_dogra@urmc.rochester.edu (V.S. Dogra).

1556-858X/07/$ – see front matter
doi:10.1016/j.cult.2007.01.006
ultrasound.theclinics.com

careful physical examination. Moreover, it is not possible to predict the nature of the lesion by physical examination. For these reasons, high-resolution US is used as the primary imaging modality for evaluation of the symptomatic or suspected testicular lesions.

The aim of this article is to familiarize the reader with the sonographic appearances of the most common and some of the least common testicular tumors and tumor-like lesions. Some other lesions that may mimic neoplasms are also reviewed. In addition, ultrasound examination technique and normal anatomy of the testis are mentioned briefly.

Ultrasound technique

Scrotal sonography is performed with the patient lying in a supine position and the scrotum supported by a towel placed between the thighs and the penis placed on the abdomen and covered with a towel [1,5,6]. Scrotal US should be performed with the highest frequency linear array transducer that gives adequate penetration (7–14 MHz). To avoid cremasteric muscle contraction that causes erroneous skin thickening, the temperature of the examination room and ultrasonic acoustic gel should be warm. Examination is usually performed with the transducer in direct contact with the skin, but if necessary a stand-off pad can be used for assessment of superficial lesions [1]. Copious amounts of gel should be applied to the skin to allow adequate contact and transducer movement over the scrotal skin without causing patient discomfort.

The testes are examined in at least two planes, along the longitudinal and transverse axes, and multiple static images are obtained in each plane. The size, echogenicity, and vascularity of each testis and epididymis are compared with those on the opposite side. If the patient is evaluated for an acute scrotum, the asymptomatic side should be examined initially to set the gray-scale and color Doppler gains to allow comparison with the affected side. Color Doppler and spectral Doppler parameters are optimized to demonstrate low-flow velocities and blood flow in the testis and surrounding scrotal structures [1,5]. Power Doppler US may also be used to demonstrate intratesticular flow, especially in patients who have an acute scrotum. In power Doppler US technique, the color map displays the integrated power of the color signal to depict the presence of blood flow instead of its mean Doppler frequency shifts. It provides higher sensitivity to low blood flow than color Doppler technique and its signal is independent of the Doppler angle [7]. Three-dimensional (3-D) color or power Doppler is used alternatively to display vascular patterns of lesions. Transverse images with portions of each testis on the same image should be recorded in gray-scale and color Doppler for comparison purposes. The structures within the scrotal sac are examined to detect extratesticular masses or other abnormalities [1].

A significant problem with using high-frequency transducer during scrotal examination is the limited field of view (FOV) [8]. To overcome this limitation, an extended FOV imaging or panoramic imaging technique has been designed [9]. In this technique, multiple images are acquired from many transducer positions during the lateral movement of the transducer over the area of interest [8,9]. The proper relative positions of the multiple images are determined in the scanner by comparison of image data features in the regions of overlap between successive images. The images are registered with respect to each other, and the registered image data are accumulated in a large image buffer and then combined to form the complete, large FOV image [9]. This technique permits visualization of large anatomic segments as a panoramic image and it clearly shows the exact location of the lesion and its relationship with the surrounding structures [8].

Because patient history is important for accurate diagnosis, obtaining a patient history and performing a physical examination before the US procedure (to detect a small palpable mass and directly examine it) is an essential part of a complete examination [6]. In patients who have small palpable masses, scans should include the area of clinical concern. A finger should be placed beneath the nodule and the transducer should be placed directly over the nodule for scanning, or a finger can be placed on the nodule and the transducer opposite to confirm imaging of the lesion [1].

Sonographic anatomy of the testis

The scrotum is separated by a midline septum (the median raphe), with each half of the scrotum containing a testis, the epididymis, and scrotal portion of the spermatic cord. The normal scrotal wall thickness is 2 to 8 mm depending on cremasteric muscle contraction [10]. The normal adult testes are symmetric, roughly ovoid structures with medium-level echoes and measure about $5 \times 3 \times 2$ cm [1]. Echogenicity of the testis is low to medium in neonates and infants and the echogenicity progressively increases from 8 years of age to puberty with the development of germ cell elements [11,12]. The tunica albuginea is the fibrous sheath that covers the testicle. The tunica albuginea appears as a thin echogenic line around the testis sonographically, and is covered on the inside by

the tunica vaginalis that consists of visceral and parietal layers normally separated by a few milliliters (2–3 mL) of fluid (Fig. 1). The parietal and visceral layers of the tunica join at the posterolateral aspect of the testis, where the tunica attaches to the scrotal wall. The tunica vaginalis covers the testis and epididymis except for a small posterior area [1,5]. The tunica albuginea projects into the interior of the testis to form the incomplete septum, the mediastinum testis [1,13]. Sonographically, the mediastinum testis is an echogenic band of variable thickness that extends across the testis in the craniocaudal direction. It may resemble a testicular lesion, if imaged at an angle [5]. From the mediastinum, numerous fibrous septa extend into the testis dividing it into 250 to 400 lobules, each of which contains one to three seminiferous tubules supporting the Sertoli cells and spermatocytes that give rise to sperm [1]. Spermatogenesis occurs within the seminiferous tubules. Each seminiferous tubule is approximately 30 to 80 cm long; thus, the total estimated length of all seminiferous tubules is 300 to 980 m [3]. The seminiferous tubules open by way of the tubuli recti into dilated spaces called the rete testis within the mediastinum. The normal rete testis can be identified at high-frequency US in 18% of patients as a hypoechoic area with a striated configuration adjacent to the mediastinum testis (Fig. 2) [1]. The rete testis, a network of epithelium-lined spaces embedded in the fibrous stroma of the mediastinum, drains into the epididymis through 10 to 15 efferent ductules. The epididymis, a tubular structure consisting of a head, body, and tail, is located superior to and is contiguous with the posterior aspect of the testis. The normal epididymis is best evaluated in a longitudinal view. It is homogenous, well-defined, and its echogenicity is variable. The head of the epididymis is a pyramidal

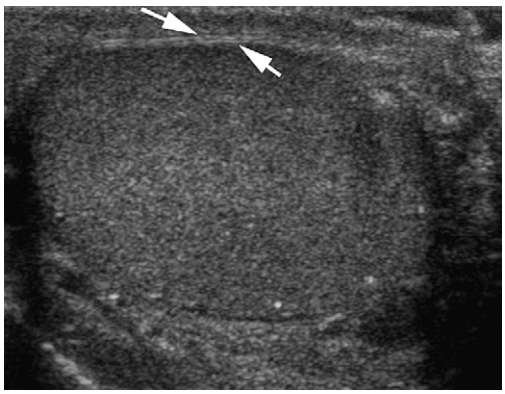

Fig. 1. Normal testis. Longitudinal gray-scale sonogram of the right testis shows homogenous medium-level echogenicity. Tunica albuginea covering the testis can be seen anteriorly (*arrows*).

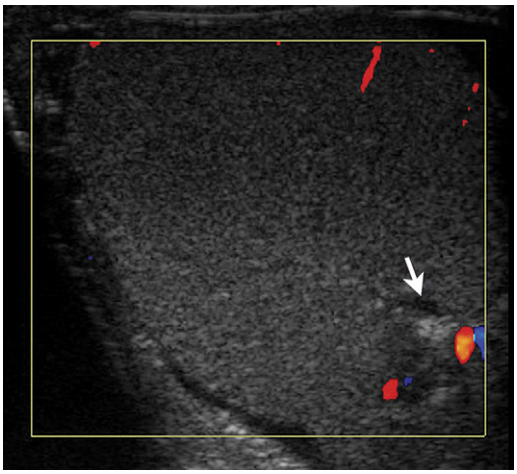

Fig. 2. Normal rete testis. Transverse oblique color flow Doppler sonogram of the testis reveals tubular hypoechoic, avascular area (*arrow*) consistent with normal rete testis at the posterior end of the right testis.

structure 5 to 12 mm in maximum length and mostly isoechoic to the testis, and its echotexture may be coarser than that of the testicle [1,14]. The head of the epididymis is composed of 8 to 12 efferent ducts converging into a single larger duct in the body and tail. This single duct becomes the vas deferens and continues in the spermatic cord [1]. The narrow body of the epididymis (2–4 mm in diameter), when normal, is usually indistinguishable from the surrounding peritesticular tissue. The tail of the epididymis is about 2 to 5 mm in diameter and can be seen as a curved structure at the inferior pole of the testis [1].

There are four testicular appendages: the appendix testis (hydatid of Morgagni), the appendix epididymis, the vas aberrans, and the paradidymis. They are remnants of the mesonephric and paramesonephric ducts [1,15]. The appendix testis and the appendix epididymis are usually seen on scrotal US. The appendix testis is a small ovoid structure attached to the upper pole of the testis in the groove between the testis and the epididymis (Fig. 3); it is normally hidden by the head of epididymis, making it nearly impossible to differentiate in normal examinations unless it is surrounded by fluid [1,16]. The appendix testis has been identified in 92% of testes unilaterally and 69% bilaterally in postmortem studies [17]. The appendix epididymis is the same size and echogenicity as the appendix testis but is often pedunculated, attached to the head of the epididymis, and is encountered unilaterally in 34% and bilaterally in 12% of postmortem series [1,5,11]. The presence of a minimal amount of fluid facilitates visualization on sonography.

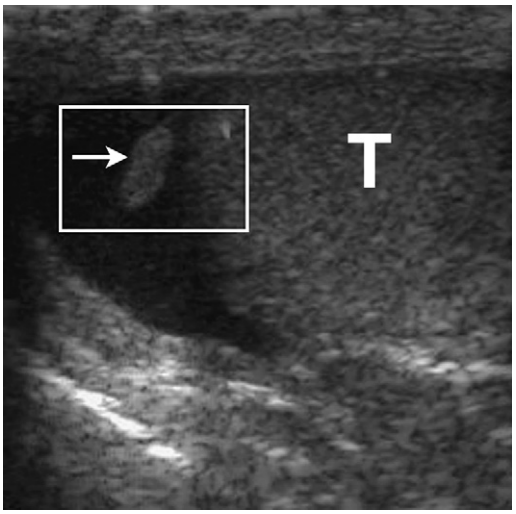

Fig. 3. Appendix of testis. Longitudinal gray-scale sonogram of the superior pole of the testis demonstrates an isoechoic structure (*arrow*) arising from the superior pole of the testis (*T*), suggestive of appendix of testis. Presence of hydrocele permits its easy identification.

The paradidymis is normally not identified sonographically, but it may swell and distend, forming a cyst-like structure that can be seen sonographically and should not be confused with an epididymal cyst [13].

The right and left testicular arteries arise from the abdominal aorta and supply the testis and epididymis. They enter the spermatic cord at the deep inguinal ring and continue along the posterior surface of the testis, penetrating the tunica albuginea and forming the capsular arteries, coursing through the tunica vasculosa located beneath the tunica albuginea [1]. Centripetal branches arising from the capsular arteries carry blood toward the mediastinum, dividing to form the recurrent rami that carry blood away from the mediastinum into the testis [1]. A transmediastinal artery branch of the testicular artery occurs in approximately one half of normal testes [18]. It courses through the mediastinum to supply the capsular arteries and is usually accompanied by a large vein [1,5]. The deferential artery, a branch of the superior vesicle artery, and the cremasteric artery, a branch of the inferior epigastric artery, supply the epididymis, vas deferens, and peritesticular tissue (Fig. 4) [19]. Branches of the pudendal artery supply the scrotal wall [20]. The spectral waveform of the intratesticular arteries characteristically has a low-resistance pattern, with a mean resistive index of 0.62 (range, 0.48–0.75) [12,21]. This observation is not true for a testicular volume of less than 4 cm^3, as is often found in prepubertal boys, when diastolic arterial flow may not be detectable [22]. Color Doppler US can demonstrate blood flow in a normal epididymis. The resistive index of a normal epididymis ranges from 0.46 to 0.68 [23].

The testicular veins exit from the mediastinum and drain into the pampiniform plexus, which also receives venous drainage from the epididymis and scrotal wall. These vessels join together, pass through the inguinal canal, and form single testicular veins, which drain the vena cava on the right side and the left renal vein on the left side [13].

Malignant testicular neoplasms

Testicular cancer accounts for about 1% of all cancers in men and is the most common malignancy among 15- to 34-year-olds [3]. It was estimated that 7200 new cases of testicular cancer were diagnosed in the United States in the year 2001 [24]. Testicular cancer is 4.5 times more common in white men than in black men [25]. There are some positive associations with testicular carcinoma: prior testicular tumor, positive family history, cryptorchidism, infertility, and intersex syndromes (gonadal dysgenesis, true hermaphroditism, and pseudohermaphroditism) [3]. Patients who have cryptorchidism have 2.5 to 8 times more risk for developing a testicular cancer [26]. Testicular microlithiasis is another risk factor for developing testicular cancer and a recent study showed a 21.6-fold increased relative risk for carcinoma in patients who have testicular microlithiasis [27]. These issues are discussed later in this article.

The peak prevalence of testicular tumors occurs in the 20- to 35-year-old age group. The other peaks occur in infancy and greater than age 50 [28]. Each peak corresponds to specific tumor types [28] which are shown in **Box 1**.

Although the most common symptom of testicular cancer is a lump or painless swelling of the testis, it can present with pain because of associated hemorrhage or infection [1]. Testicular tumors are prone to hemorrhage, which can obscure the primary mass [28]. Disproportionate testicular hemorrhage following minor scrotal trauma should prompt the examiner to consider the diagnosis of an underlying tumor [28]. Ten percent of patients who have testicular cancer present with acute symptoms, such as fever and pain (usually diagnosed as epididymo-orchitis), whereas 10% are detected following trauma and 10% are detected after presenting with complaints related to metastatic disease [1,20,29]. Seminomas and testicular lymphomas may cause orchitis secondary to obstruction of the seminiferous tubules [1,28]. Some patients may have normal or small testes at

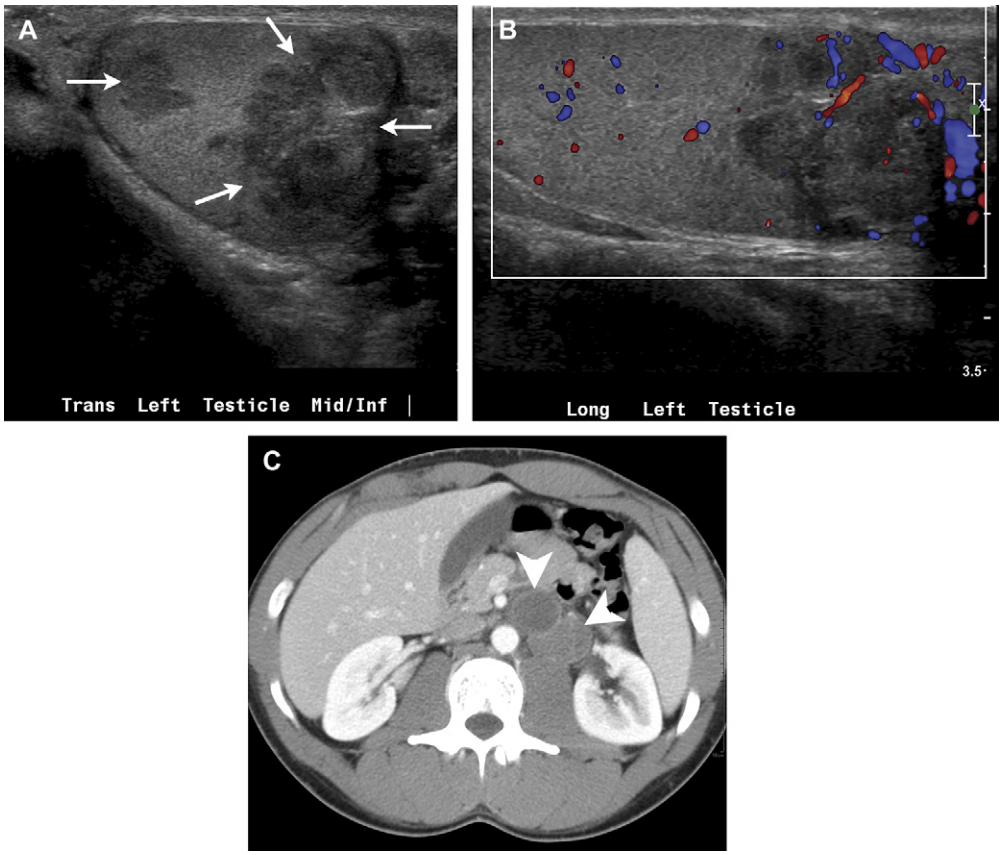

Fig. 4. Mixed germ cell tumor of testis with retroperitoneal adenopathy. Transverse gray-scale (*A*) and corresponding longitudinal color flow Doppler (*B*) sonograms of the left testis demonstrate two predominantly hypoechoic lesions (*arrows*) with mild internal vascularity. Corresponding contrast-enhanced CT of the abdomen (*C*) at the level of the renal hilum demonstrates two retroperitoneal lymph nodes (*arrowheads*) at the renal hilum on the ipsilateral side.

presentation because of tumor regression, necrosis, and scarring (so-called "burned-out" germ cell tumors) [30]. This subgroup of patients, along with those who have an aggressive histologic tumor type, may present with metastases [31]. A small portion of patients who have hormonally active tumors may present with endocrine abnormalities, such as gynecomastia [3].

Box 1: Most commonly encountered tumor types according to specific age peaks

Infancy
Embryonal carcinoma
Teratoma

Ages 20 to 35
Seminoma
Embryonal carcinoma
Teratoma
Teratocarcinoma

Greater than age 50
Lymphoma
Metastases
Spermatocytic seminomas

Gray-scale US is almost 100% accurate for detecting testicular tumors [32,33]. The main role of US examination is to distinguish intratesticular from extratesticular lesions, because most extratesticular masses are benign and intratesticular masses are more likely to be malignant [28]. US does not provide the histologic and morphologic diagnosis [1]. The most common mimics of malignancy are hematomas, orchitis, abscesses, infarction, and granuloma [1]. It is thus important to know patients' clinical histories and correlate their US findings for the diagnosis and to avoid unnecessary intervention [1]. Sometimes a follow-up US may be required to rule out a tumor or for exact diagnosis.

Color Doppler and power Doppler US may demonstrate increased vascularity in the malignant tumors and help to better define testicular involvement [34]. It may be difficult to demonstrate

increased blood flow in small tumors (<2 cm), and the presence of hypervascularity is not specific for a diagnosis of malignancy [1]. In addition, there is no strong correlation between tumor type or histologic stage and Doppler findings [28]. Color Doppler may be useful in the pediatric population, in whom tumors may be subtle by gray-scale US but tend to be hypervascular by color Doppler imaging [35].

Malignant testicular tumors are divided into two main groups: germ cell tumors and non–germ cell tumors. The classifications of the most common testicular neoplasms are listed in Box 2.

Germ cell tumors

Some 90% to 95% of testicular neoplasms have germ cell origins arising from spermatogenic cells. They are almost always malignant. Non–germ cell tumors of the testis arise from the sex cords (Sertoli cells) and stroma (Leydig cells), which are malignant in only 10% of cases [3,30]. Germ cell tumors can be subdivided into two groups: seminomatous and nonseminomatous tumors. This distinction is important for treatment and prognosis [1].

Metastatic spread of germ cell tumors is by way of either lymphatic or hematogenous routes. Except for choriocarcinoma, which has early hematogenous spread, most of the germ cell tumors spread first by way of the lymphatics rather than hematogenously [30]. Direct extension through the tunica albuginea with the scrotal skin involvement is a rare and late finding [3].

Testicular lymphatic drainage follows the testicular veins [30]. Although the interaortocaval chain at the second lumbar vertebral body is the first-echelon node for the right testis, the left paraaortic nodes, in an area bounded by the renal vein, aorta, ureter, and inferior mesenteric artery, are the first-echelon nodes for the left testis [30,36,37]. Some crossover of lymphatic involvement can occur following the normal drainage pattern to the cisterna chyli and thoracic duct [30]. Tumor can spread from the thoracic duct to the left supraclavicular nodes and then to the lungs. Left-to-right crossover is rare [30,36,37]. If the tumor volume increases, the common, internal, and external iliac nodes may be involved. Tumor within the epididymis can spread directly to the external iliac nodes. Direct spread to the inguinal nodes is seen in patients who have skin involvement [30].

Hematogenous metastases can occur in the late phase of germ cell tumors, except for choriocarcinoma. The most common metastases of germ cell tumors are lung, liver, brain, and bone [38]. Brain metastases are predominantly common with choriocarcinoma [3]. Germ cell tumor metastases may have different histologic characteristics than those of the primary testicular lesion; this indicates the totipotential nature of the germ cells [3].

Some tumor markers are important for the diagnosis, staging, prognosis, and follow-up of germ cell tumors. In the presence of a palpable testicular mass, an elevated serum level of tumor markers increases confidence of diagnosis. Many tumor markers have been identified for use with testicular neoplasms, but only α-fetoprotein (AFP) and β-human chorionic gonadotropin (β-HCG) have demonstrated clinical usefulness [28]. AFP is a glycoprotein and synthesized in the fetal liver, yolk sac, gastrointestinal tract, and occasionally the placenta [28]. AFP is not elevated in pure seminomas and is elevated in yolk sac tumors and mixed germ cell tumors with yolk sac elements [30]. Other causes of AFP elevation include hepatocellular carcinoma, some gastrointestinal malignancies, hepatitis, and regenerating hepatic necrosis [39]. HCG is also a glycoprotein produced by the syncytiotrophoblasts of the placenta, and its level is elevated in tumors containing syncytiotrophoblasts (seminomas or choriocarcinoma) [30]. The β-HCG is markedly elevated in choriocarcinoma because of the larger number of syncytiotrophoblasts [28].

Numerous staging systems are present for testicular tumors. In clinical practice, patients are often classified as having low-stage or advanced-stage disease [37]. If the tumor is limited to the testis,

Box 2: Classification of the most commonly encountered testicular neoplasms

Germ cell tumors
Seminomatous germ cell tumors (seminoma)
Nonseminomatous germ cell tumors
- Embryonal carcinoma
- Yolk sac tumor (Endodermal sinus tumors)
- Teratoma
- Choriocarcinoma
- Mixed germ cell tumors
  - Embryonal carcinoma plus teratoma (teratocarcinoma)
  - Choriocarcinoma and other cell types
- Regressed or burned-out germ cell tumors

Sex cord–stromal tumors
Leydig cell tumor
Sertoli cell tumor
Gonadoblastoma
Granulosa cell tumor
Theca cell tumor

Lymphoma
Leukemia
Metastases
Tumor-like lesions

epididymis, or spermatic cord and mild to moderate adenopathy is present, the patient has a low-stage disease. If the tumors invade the scrotal wall and significant retroperitoneal adenopathy or visceral metastases are present, the patient has an advanced-stage disease [37]. A different simple form of staging based on clinicopathologic findings proposed by Catalona states: if the tumor is confined to the testis, stage I; if subdiaphragmatic lymph node metastases are present, stage II; if hematogenous or supradiaphragmatic lymph node metastases are present, stage III [28,40].

Seminomatous tumors (seminoma)

Seminoma is the most common pure germ cell tumor and accounts for 40% to 50% of all germ cell tumors [1,28]. Thirty percent of mixed germ cell tumors contain foci of seminoma [28]. Seminomas occur most often in the fourth and fifth decades of life with an average patient age of 40.5 years, and almost never occur in infants [1,41]. Approximately 15% of patients who have seminoma have a history of cryptorchidism. It is the most common germ cell tumor associated with cryptorchid testis [1,28]. Seminomas are also commonly found in patients who have testicular microlithiasis [1,27]. The right testis is more commonly affected [28]. About 75% of patients present with the disease limited to the testis, whereas 20% have retroperitoneal adenopathy and 5% have extranodal metastases [3,30].

The AFP level is always normal in patients who have pure seminomas [1,28,42]. If a patient has elevated AFP with seminoma histology, the tumor is treated as nonseminomatous [1]. Serum β-HCG levels are also normal unless syncytiotrophoblasts are present, which constitutes about 7% of cases [28]. A different study showed that 83% of patients who have seminomas have elevated β-HCG levels [43]. Seminomas are responsive to radiation therapy and chemotherapy, and have the best prognosis among the germ cell tumors, with reported cure rates of 95% to 100% for all stages [26,28].

There are three pathologic subtypes of seminomas: typical (classic) seminomas (85% of the total cases), anaplastic (5%–10%), and spermatocytic (4%–6%). Spermatocytic seminomas occur usually in men in their 60s and 70s, associated with an excellent prognosis [1]. Spermatocytic seminoma is bilateral more often than classic seminoma and metastases are practically nonexistent [44]. All subtypes of seminomas produce bulky masses, usually involving more than 50% replacement of the entire testicle [28]. The entire testis is replaced by the tumor in more than half the cases [1].

Seminomas may present as small, well-defined lesions to large masses almost replacing the entire testicle (Fig. 5) [30]. On gray-scale US examination, seminomas classically appear as a homogenous hypoechoic mass, which corresponds to the smooth uniform appearance of the gross specimen [1]. The vast majority (85%) of pure seminomas are strongly hypoechoic and 70% of cases have a predominantly homogenous texture without dense echogenic foci [4]. Ten percent of seminomas present with small cystic areas [4], which corresponded to the dilated rete testis caused by tumor-related occlusion and liquefaction necrosis [45]. A diffuse texture change may also be seen secondary to seminomatous infiltration [46]. Larger tumors may be heterogeneous. Lobulated or multinodular seminomas can also occur, but these nodules are usually in continuity with one another and true multifocal nodules are rarely seen [30]. Seminomas are mostly confined by the tunica albuginea and rarely extend to peritesticular structures [1]. Gross invasion of the spermatic cord or tunica albuginea should prompt consideration of another tumor type, particularly lymphoma [28].

Color or power Doppler US can be used to demonstrate vascularity of tumors. A previous color Doppler study showed increased vascularity in 95% of primary testicular tumors larger than 1.6 cm in diameter and hypovascularity in 86% of those smaller than 1.6 cm in diameter [34]. Although there is no correlation between vascularity and type or histologic stage of tumors, color Doppler US and power Doppler US in particular are useful tools for demonstrating vascularity of lesions. 3-D power Doppler US is an excellent alternative

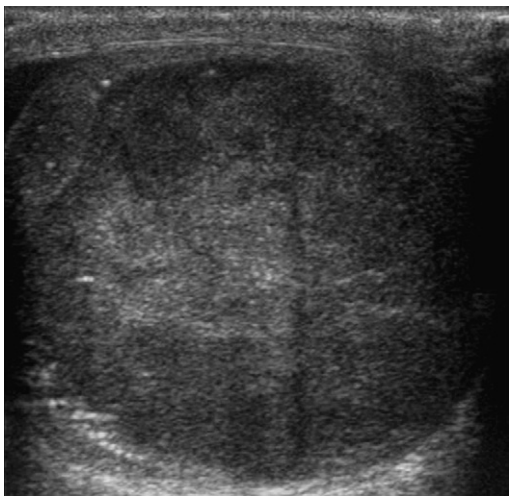

Fig. 5. A 21-year-old male who has surgically confirmed testicular seminoma. Longitudinal gray-scale sonogram of the testis shows an enlarged heterogenous hypoechoic testis, consistent with a large tumor replacing the entire testicle.

technique for displaying the vascularity of lesions (Fig. 6).

Nonseminomatous tumors

Nonseminomatous germ cell tumors (NSGCTs) occur most often in men in their 30s. Multiple histologic patterns are seen in 40% to 60% of these cases [28]. The ultrasonographic and macroscopic appearance of tumors with a multihistologic pattern depends on the proportions of each component [1]. Sonographically, they may have a heterogeneous echotexture (71%), irregular or ill-defined margins (45%), and cystic components (61%) [4]. Echogenic foci represent areas of hemorrhage, calcification, or fibrosis [1]. A true cyst with an epithelial lining suggests a teratoma component; otherwise, the cysts usually represent a dilated rete testis or an area of necrosis [4].

Embryonal carcinoma

Embryonal carcinoma occurs in a younger population than seminoma, usually between 25 and 35 years [30]. They are the most common (approximately 87%) component of mixed germ cell tumors and are usually associated with teratomas (teratocarcinoma) [3,28]. It is the second most common histologic type of testicular tumor after seminoma [3,30]. Embryonal carcinomas are more aggressive than seminomas and usually smaller than seminomas at the time of presentation. They do not cause enlargement of the scrotum [1,30]. The AFP and β-HCG levels are elevated in 60% and 70% of patients, respectively [28]. Unlike seminomas, invasion of the tunica albuginea and extension into the epididymis can occur in approximately 20% of cases, causing contour distortion of the testis [26,28]. On US examination, embryonal carcinomas are predominantly hypoechoic lesions with poorly defined margins and a heterogeneous echotexture (Fig. 7) [1,47]. Twenty percent of embryonal carcinomas and 89% of teratocarcinomas have cystic components [1].

Yolk sac tumor (endodermal sinus tumors)

These tumors account for 80% of childhood testicular neoplasms [48]. They occur most often in children less than 2 years of age and exclusively produce AFP (more than 90% of cases) [3,11,41]. Pure yolk sac tumors are rare in adults and the presence of any yolk sac tumor element in an adult mixed tumor indicates a poor prognosis [1,28,30]. The US appearances of yolk sac tumor are nonspecific; they are usually inhomogeneous and may contain echogenic foci secondary to hemorrhage, or hypoechoic areas attributable to necrosis [1,11].

Teratoma

Teratoma is the second most common testicular neoplasm in children, occurring in children less than 4 years of age [1,11,30]. They are classified as mature or immature forms. Pure teratomas are rare (2% to 3% of testicular neoplasms) in adults, but teratomatous components occur in more than 50% of all adult cases of mixed germ cell tumors [3,28]. Serum AFP level is elevated in 38% of patients and the β-HCG level is elevated in 25% of cases [28]. Metastases can be observed in one third of patients who have teratoma at the initial

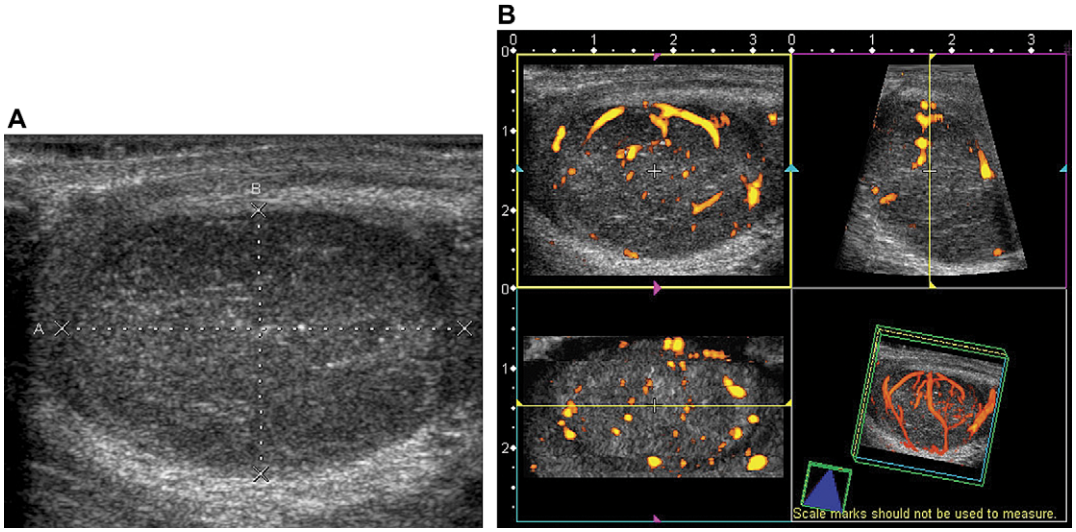

Fig. 6. Surgically confirmed testicular seminoma. Longitudinal gray-scale sonogram (*A*) shows a hypoechoic, slightly heterogenous solid mass that involves the entire testis. (*B*) Corresponding power Doppler and 3-D power Doppler sonogram reveals increased vascularity of the lesion.

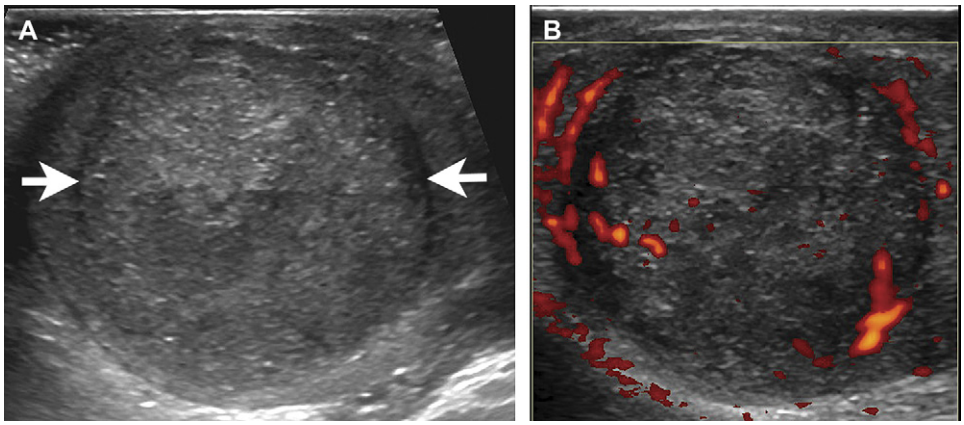

Fig. 7. Surgically confirmed embryonal carcinoma with tumor necrosis. Longitudinal gray-scale (*A*) and corresponding power Doppler (*B*) sonograms of the right testis demonstrate a heterogeneous, predominantly hypoechoic mass (*arrows*) involving the testis.

presentation [28]. Mature teratomas in children are usually benign, even if they are histologically immature, but may undergo malignant transformation in adults and can metastasize, irrespective of histologic characteristics [1,28,30]. Teratomas contain all three germ cell layers: endoderm, mesoderm, and ectoderm [1,3]. At gray-scale US, teratomas tend to be very large and markedly inhomogeneous masses. Cystic components are more common than other NSGCTs and may appear anechoic or complex depending on the cyst contents (Fig. 8) [29,30]. Echogenic foci may or may not shadow, representing calcification, cartilage, immature bone, and fibrosis [1,30]. A diffuse parenchymal texture change with broad bands of dense echogenic foci associated with an acoustic shadow may also be seen with teratomas [46].

Choriocarcinoma

Choriocarcinoma is a highly malignant rare testicular tumor. Although its pure form is seen in less than 1% of patients, it is seen as microscopic foci in 16% of mixed germ cell tumors [1,30]. Its peak incidence is in the third to fourth decade of life. The β-HCG level is always elevated because of the presence of a large number of syncytiotrophoblasts that may cause associated gynecomastia [28,30]. Choriocarcinoma has the worst prognosis of any of the germ cell tumors, with death usually occurring within 1 year of diagnosis [30]. Microscopic vascular invasion and early hematogenous metastasis are common [1]. The primary tumor and metastases are usually hemorrhagic [30]. Sonographically, choriocarcinomas are heterogeneous and show extensive hemorrhagic necrosis in the

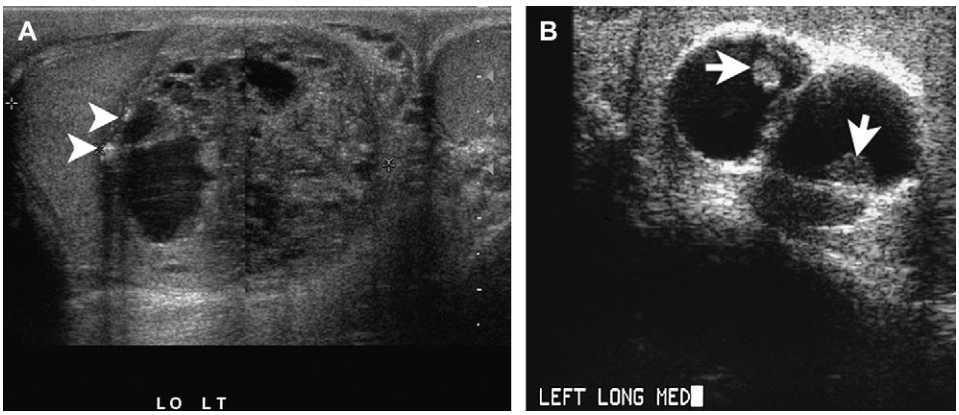

Fig. 8. Teratoma (immature and mature). Longitudinal gray-scale sonogram (*A*) of the left testis demonstrates a large heterogeneous mass with multiple cystic components and areas of calcification (*arrowheads*). It was surgically confirmed to be an immature testicular teratoma. Longitudinal gray-scale sonogram (*B*) of the left testis demonstrates a large septate cystic lesion with two solid nodules (*arrows*) within; surgically confirmed to be a mature cystic testicular teratoma.

central portion of the tumor with a mixed cystic and solid appearance [1,28]. Testicular enlargement is seen because of associated hemorrhage rather than because of the tumor itself [28].

Mixed germ cell tumor

These tumors contain more than one germ cell component. They constitute about 40% to 60% of all germ cell tumors [28,30]. Any combination of cell type can be observed. Embryonal carcinoma is the most common component and the most common combination is teratoma and embryonal carcinoma (teratocarcinoma) [28,30]. This tumor is usually the largest of all testicular tumors [28]. Patients who have mixed germ cell tumors present at an average age of 30 years [3]. Tumors may contain foci of calcification, hemorrhage, or cysts, and sonographic appearances depend on the dominant component (Fig. 9) [28].

Regressed germ cell (burned-out) tumors

These tumors occur secondary to rapid tumor growth and result in the tumor outstripping its blood supply, with subsequent tumor regression [1]. In this rare entity, the patient may present with widespread metastases, mostly attributable to teratocarcinoma or choriocarcinoma, even though the primary tumor has involuted [30]. Histologic evaluation reveals presence of fibrosis and scar tissue with no tumor cells [1,49]. At US, these primary tumors have a variable appearance. They are usually small and can be hypoechoic, hyperechoic, or an area of calcification [1,30]. In a recent study, burned-out tumors were reported to present as an area of calcification 5 mm in diameter or as microlithiasis in an atrophic testis, and poorly circumscribed hypoechoic and hyperechoic areas, the latter being more frequent [50].

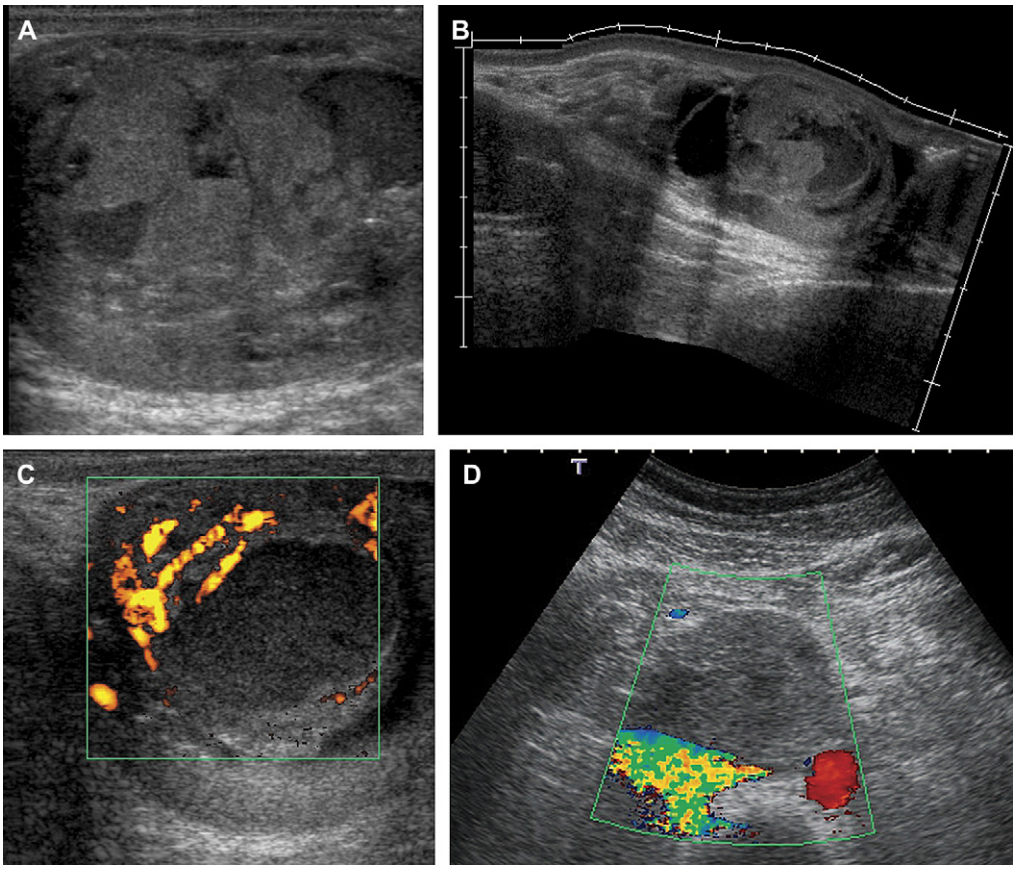

Fig. 9. Mixed germ cell tumor of the testis. Longitudinal gray-scale sonogram (*A*) and extended field of view image (*B*) of testis reveal a large heterogeneous mass with some cystic necrotic areas, pathologically confirmed to be a mixed germ cell tumor (mature teratoma plus yolk sac tumor). Corresponding power Doppler sonogram (*C*) shows marked vascularity within the solid areas of the lesion. Transverse color flow Doppler sonogram of the abdomen (*D*) in the same patient revealed hypoechoic lymphadenopathy anterior to the aorta and inferior vena cava.

Sex cord–stromal tumors

Most non–germ cell tumors are sex cord–stromal tumors, representing 4% of all testicular tumors [1,30]. The prevalence is higher in the pediatric age group. Non–germ cell tumors constitute 10% to 30% of all testicular neoplasms [48]. These tumors are usually benign (more than 90% of the cases), but even tumors without aggressive histologic features may metastasize [3]. They are typically small and are usually discovered incidentally. Their US appearances are not specific, but they may appear as well-defined hypoechoic masses [1]. Types of sex cord–stromal tumors include Leydig cell tumors and Sertoli cell tumors, among others.

Leydig cell tumor

These tumors are usually seen in boys older than 4 years, or in men between the ages of 20 and 50 [28]. They constitute about 3% of all testicular tumors and are the most common type of sex cord–stromal tumors [1,3,51]. Secretion of androgens or estrogens by the tumor leads to endocrinopathy in about 30% of patients, which includes gynecomastia (most common), precocious puberty, and decreased libido [3,30]. This tumor can present as small nodules or large masses up to 10 cm. About 10% of cases have bilateral tumors [28]. Histologically, a rectangular eosinophilic cytoplasmic inclusion, the Reinke crystal, is characteristic and present in 33% of cases [28]. Approximately 10% of Leydig cell tumors are malignant, and patients who have malignant tumors are likely to be older, with symptoms of shorter duration and an absence of endocrine manifestations [1,51]. Malignant tumors are usually larger and may spread beyond the testis with an infiltrative margin [52]. In a recent US study, Leydig cell tumors were mostly observed as small tumors less than 1 cm, with a homogeneous hypoechoic appearance without discernible calcification (Fig. 10) [51]. In addition, the prominent peripheral and circumferential blood flow and the lack of internal vascularity are reported in Leydig cell tumors by color and power Doppler US [51]. A hyperechoic Leydig cell tumor with a prominent feeding artery has been reported, but this is an unusual feature for this tumor [53]. Leydig cell tumors may also be associated with Klinefelter syndrome, and an intrinsic Doppler signal may be observed in these cases [51].

Sertoli cell tumor

Sertoli cell tumors are rare and constitute less than 1% of testicular tumors [30]. There are three histologic types of Sertoli cell tumors: Sertoli cell tumor not otherwise specified, sclerosing Sertoli cell tumor, and large cell calcifying Sertoli cell tumor [1,29]. The large cell calcifying type is mostly seen in children and manifests as multiple and bilateral masses with large calcifications [30,54]. It is unusual to have sufficient hormonal production to induce clinically apparent endocrinologic changes [28]. Malignant lesions (less than 10% of cases) are more likely associated with gynecomastia [55]. At US, Sertoli cell tumors are typically seen as unilateral, small, hypoechoic, well-defined masses [28,30].

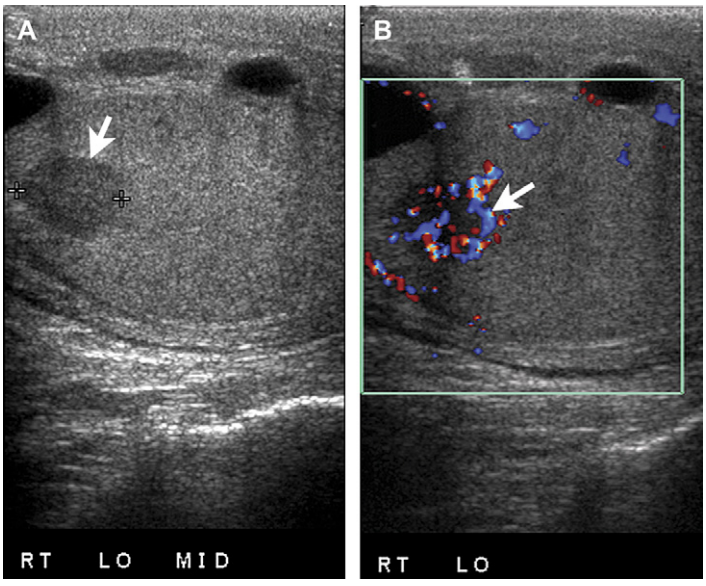

Fig. 10. Surgically confirmed Leydig cell tumor. Longitudinal gray-scale (*A*) and color flow Doppler (*B*) sonograms of the right testis demonstrate presence of a well-defined hypoechoic lesion (*arrow*) with abundant circumferential vascularity.

Other sex cord–stromal tumors

These tumors are rare and include granulosa cell tumors (juvenile and adult), fibroma-thecomas, and mixed sex cord–stromal tumors [1,30]. Granulosa cell tumors can appear as a hypoechoic mass with few internal echoes. The juvenile type has been described as having a "Swiss cheese" sonographic appearance with solid and cystic areas [56]. Gonadoblastoma contains both sex cord–stromal elements and germ cells; it is almost always seen in patients who have dysgenic gonads and an intersex syndrome. Eighty percent are phenotypically female [1,3].

Lymphoma

Lymphoma accounts for 5% of all testicular tumors and is the most common bilateral testicular tumor, but testicular lymphoma occurs in less than 1% of patients who have lymphoma [57]. They occur in older people and are the most common testicular neoplasms in men more than 60 years of age, accounting for 50% of cases [30,57,58]. The most common type of lymphoma involving the testis is diffuse large B-cell lymphoma [1,28,59]. Bilateral tumors are seen in 38% of patients, but metachronous lesions are more common than synchronous [3]. Testicular lymphoma is locally aggressive and can typically infiltrate the epididymis, spermatic cord, or scrotal skin [59,60]. At US, normal homogeneous testis is replaced focally or diffusely with hypoechoic vascular lymphomatous tissue and usually demonstrates increased intralesional blood flow regardless of tumor size (Fig. 11) [61]. Homogeneous hypoechoic testis, multifocal hypoechoic lesions of various sizes, and striated hypoechoic bands with parallel hyperechoic lines radiating peripherally from the mediastinum testis have also been described [1,59]. Lymphomatous involvement of the epididymis can cause it to become enlarged and hypoechoic; however, the testicular component is usually more extensive than the epididymal component [59]. Testicular lymphoma carries a worse prognosis than its nodal counterpart, with a 5-year survival rate of about 12% and a median survival time of less than 12 months [57].

Leukemia

Primary leukemia of the testis is rare. Testes may be a sanctuary organ for hematologic malignancies, such as leukemia and lymphoma [61]. The blood–testis barrier prevents the accumulation of chemotherapeutic drugs within the testes [61,62]. Leukemic infiltration to the testis has been found at autopsy in 40% to 65% of patients who have acute leukemia and in 20% to 35% of patients who have chronic leukemia [1,29]. Leukemic involvement of the testis is clinically apparent in approximately 8% of children who have acute lymphocytic leukemia but is rare in adults [29,61,62]. Because chemotherapy does not completely eliminate leukemic tumor cells from the testes, any patient who has a testicular mass found during the course of leukemia should undergo cytologic or histologic evaluation [1]. Leukemia diffusely infiltrates the testis and may produce an enlarged hypoechoic testis (Fig. 12) [34]. Unilateral testicular enlargement with normal echogenicity can also be seen

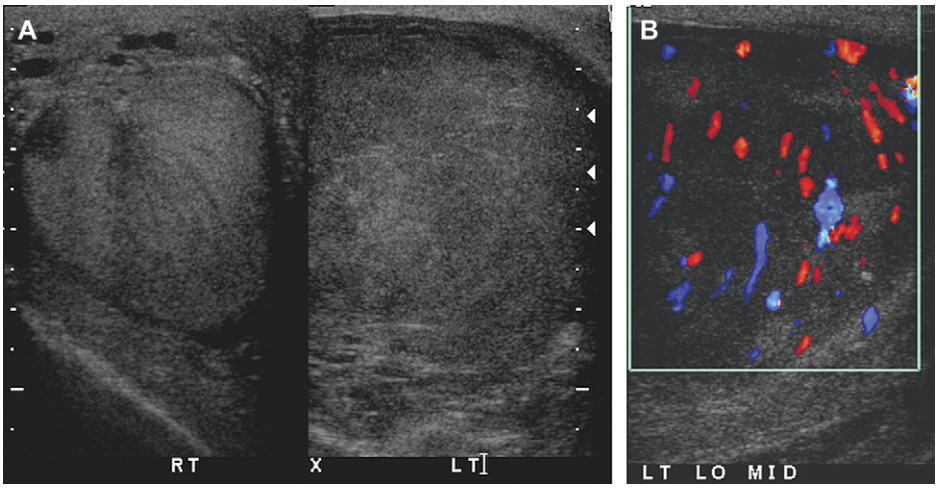

Fig. 11. A 67-year old male who has surgically confirmed B-cell lymphoma of testis. Transverse gray-scale sonograms (*A*) of the right and left testis show an enlarged hypoechoic left testis and a normal right testis. Corresponding color flow Doppler sonogram (*B*) of the left testis shows increased vascularity, consistent with lymphomatous infiltration of the left testis.

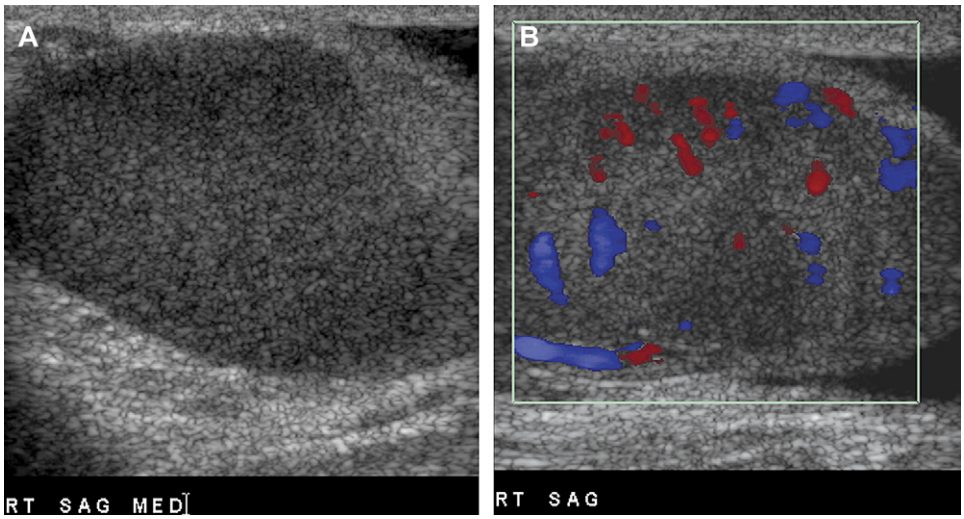

Fig. 12. Leukemic infiltration of testis. Longitudinal gray-scale (*A*) and color flow Doppler (*B*) sonograms of the testis demonstrate a hypoechoic testis with increased vascularity; pathologically confirmed to be diffuse leukemic infiltration of the testis in this patient with known history of leukemia.

and color Doppler with increased vascularity is helpful to demonstrate leukemic infiltration [35].

Metastases and other rare tumors

Testicular metastases are rare (with an incidence of 0.68%); the most common primary tumors to metastasize to testis are prostate (35%), lung (19%), malignant melanoma (9%), colon (9%), and kidney (7%) [29,63]. Many other tumors may rarely metastasize to the testis, such as neuroblastoma. Their sonographic appearances are nonspecific, and differentiating other primary testicular tumors is difficult [64]. Plasmacytoma of the testes also has been reported [29]; 2% of multiple myelomas may involve the testis. Plasmacytomas appear as heterogeneous hypoechoic masses that show marked hypervascularity in power Doppler mode [65]. Carcinoid tumor is an extremely rare tumor of the testis and accounts for less than 1% of all testicular neoplasms. At US, carcinoids appear as solid, well-defined, hypoechoic, hypervascular intratesticular masses, and may contain dense calcification [66]. Primary adenocarcinoma of the rete testis is a rare, highly malignant tumor originating in the mediastinum of the testis. US may reveal nonspecific multiple hypoechoic lesions in the testis [67]. Primary osteosarcoma of the testis also has been reported as a large, heavily calcified testicular mass [68]. Another rare testicular tumor is leiomyoma; its sonographic appearance has been reported as a predominantly hypoechoic lesion with areas of hyperechogenicity and moderate vascularity on color Doppler sonography [69].

Testicular microlithiasis

Testicular microlithiasis is an uncommon condition, occurring in 0.6% of patients referred for scrotal sonography [70]. At US, testicular microlithiasis appears as multiple small nonshadowing hyperechogenic foci measuring 1 to 3 mm in diameter [1,71]. They occur within the testicular parenchyma and are randomly scattered; five or more foci per transducer field in one testis is an accepted diagnostic criterion for testicular microlithiasis (**Fig. 13**) [1,27,71] Several associations have been reported with this entity, including Klinefelter's syndrome, cryptorchidism, Down's syndrome, male pseudohermaphroditism, pulmonary alveolar microlithiasis, previous radiotherapy, subfertility states, and, most importantly, testicular carcinoma [1,27,30]. Testicular microlithiasis is usually a bilateral condition, except in cases of cryptorchidism [1,27,28,72]. Testicular microlithiasis has been associated with testicular neoplasia in 18% to 75% of cases [72], with the largest series reporting a frequency of 40% [28]. A recent study showed a 21.6-fold increased relative risk for carcinoma in patients who have testicular microlithiasis [27]. Because of these high associations and risks, annual US follow-up is recommended for at least several years after the diagnosis [27,72].

Undescended testis with seminoma

Cryptorchidism is defined as complete or partial failure of the intra-abdominal testes to descend into the scrotal sac [1]. Cryptorchidism is present in about 6% of full-term neonates and 0.8% of

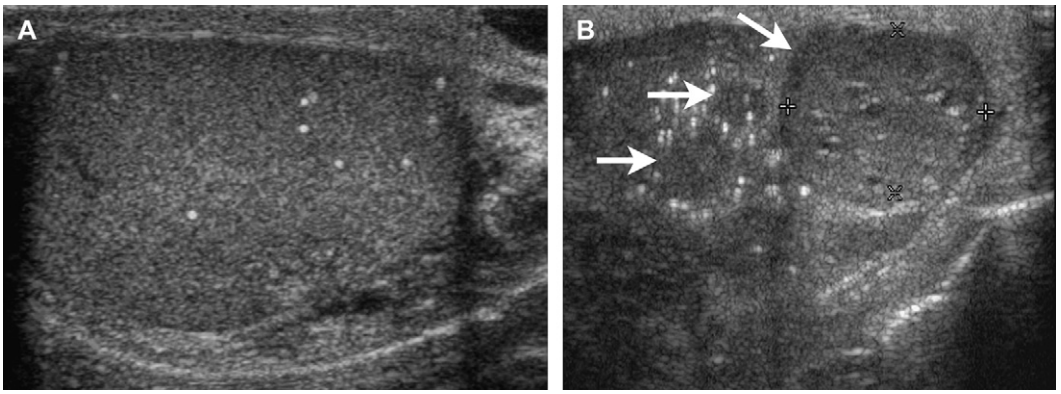

Fig. 13. Testicular microlithiasis. Longitudinal gray-scale sonogram (*A*) of the right testis shows multiple punctate echogenic foci consistent with microlithiasis. (*B*) Longitudinal gray-scale sonogram of the right testis in another patient reveals testicular microlithiasis with multiple hypoechoic masses (*arrows*); surgically confirmed to be testicular seminomas.

infants at age 1 year. It can be bilateral in 10% of patients [48,73]. An undescended testis appears hypoechoic with US, and a mediastinum testis should be identified for confident diagnosis [73]. Undescended testis is a risk factor (2.5- to 8-fold) for the development of a seminoma (Fig. 14) [26,73]. Although the overall incidence of cryptorchidism is low (<1%), a history of undescended testis is present in 3.5% to 14.5% of patients who have testicular tumors [3]. Risk for testicular carcinoma is not limited to the undescended testis only, but extends to the contralateral testis, even if it is normally descended [3,73]. Cryptorchidopexy does not alter the risk for developing a carcinoma [73].

The risk for carcinoma increases with the degree of ectopy, with a patient who has an intra-abdominal testis being at highest risk. Most of these tumors are seminomas [3]. Demonstration of a testicular vein draining into the left renal vein or inferior vena cava originating from a pelvic mass can help diagnosis of the testicular origin of a pelvic mass [74].

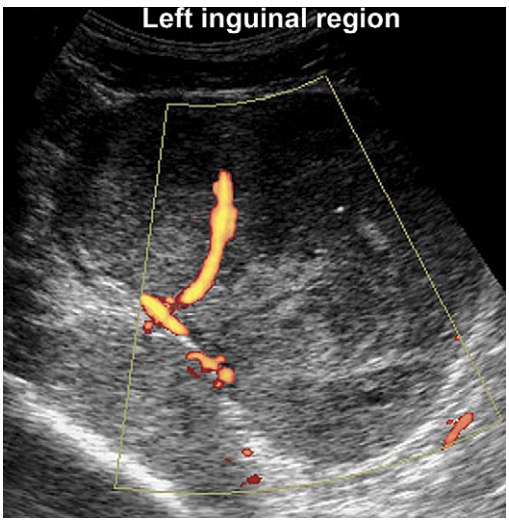

Fig. 14. Surgically confirmed seminoma in an undescended testis. Transverse power Doppler sonogram of the inguinal region shows a well-defined, heterogenous, predominantly hypoechoic solid mass with some peripheral vascularity, consistent with a tumor within a cryptorchid testis.

Benign tumors and tumor-like lesions

Epidermoid cyst of the testis is a benign tumor composed of pure ectodermal elements that can only be differentiated from teratoma by histologic examination [1,28]. They constitute 1% of testicular tumors with a peak incidence in the second to fourth decades of life [1,28,30]. At US, they appear as well-circumscribed cystic masses with a few low-level internal echoes or as a solid-appearing 1- to 3-cm mass with a hyperechoic rim. Concentric hypoechoic and hyperechoic rings or an "onion-skin" appearance has been described as characteristic, but not pathognomonic, of epidermoid cysts [1,28,30,75]. Color or pulsed Doppler US demonstrates no flow within the cyst [1,75].

Many nonneoplastic conditions, such as orchitis, hemorrhage, scar tissue attributable to prior biopsy, and ischemia or infarction, may appear as a testicular mass and mimic testicular neoplasms (Figs. 15 and 16). Focal orchitis appears as an ill-defined hypoechoic lesion with increased vascularity (Fig. 17) [1]. Hematoma appears avascular at color Doppler US [1]. Their clinical history is important for correct diagnosis; most of them present with an acute

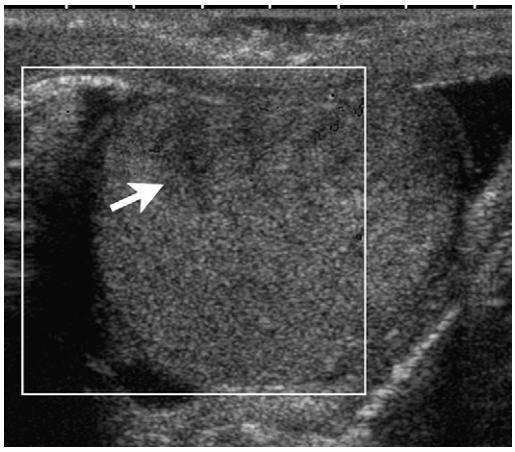

Fig. 15. Testicular infarct. Transverse color Doppler sonogram shows an avascular hypoechoic lesion (*arrow*), surgically confirmed to be a focal infarct.

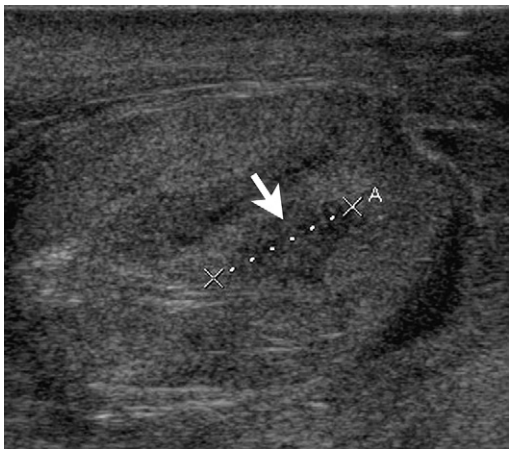

Fig. 17. Focal orchitis. Longitudinal oblique gray-scale sonogram of the left testis shows heterogeneous-appearing testis with a focal hypoechoic area (*arrow*) consistent with focal orchitis (clinically proven as nonspecific epididymoorchitis).

scrotum. Sometimes follow-up US is required to differentiate tumoral lesions from other lesions.

Granulomatous orchitis mimics testicular tumors; many pathogens, such as tuberculosis, syphilis, fungi, and parasites, may cause a granulomatous orchitis [30]. They tend to involve the epididymis more commonly than the testis, and an isolated testicular mass is unusual [30]. Gray-scale US demonstrates an irregular hypoechoic infiltration of the testis, with increased blood flow at the periphery of the lesion but no flow into the lesion (Fig. 18). It cannot be reliably distinguished from malignancy and a final diagnosis can only be confirmed with specimens from orchiectomy [1,76].

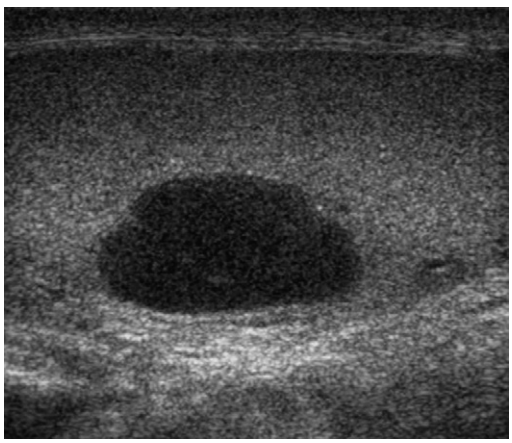

Fig. 16. Testicular hematoma. Longitudinal gray-scale sonogram reveals a well-defined hypoechoic lesion consistent with a testicular hematoma in a patient having a history of testicular trauma about 10 days previously. Follow-up sonogram showed decrease in size (not shown).

Testicular adrenal rest tissue occurs in up to 29% of patients who have congenital adrenal hyperplasia [77]. Sonography usually reveals bilateral testicular masses located close to the mediastinum with posterior acoustic shadowing [78]. Color Doppler shows no flow within the lesion [78].

Sarcoidosis may involve the testis, but epididymal involvement is more common. Sarcoidosis of the testis is typically multiple small, bilateral, hypoechoic masses [28,30,79]. It is more common in African Americans than other racial groups [3].

Tubular ectasia of rete testis is a benign condition resulting in partial or complete obstruction of the efferent ducts, usually seen in men older than 55 years [1]. They are located in or adjacent to the mediastinum testis and are composed of a series of dilated tubules. Gray-scale US reveals fluid-filled tubular structures that are avascular on color or power Doppler US. It is usually bilateral and asymmetric and mostly associated with an ipsilateral spermatocele (Fig. 19).

Tunica albuginea cysts are usually palpable, peripherally located single or multiple anechoic lesions measuring 2 to 5 mm in size [1,80]. These cysts are believed to be mesothelial in origin [1]. They characteristically are located at the upper anterior or lateral aspect of the testicle [75]. They can beunilocular or multilocular and sometimes calcify [1,75].

Simple cysts are detected incidentally in men older than 40 [75]. Their size varies from 2 mm to 2 cm and they are usually solitary. They are located adjacent to the mediastinum testis and may be associated with extratesticular spermatoceles [1,75].

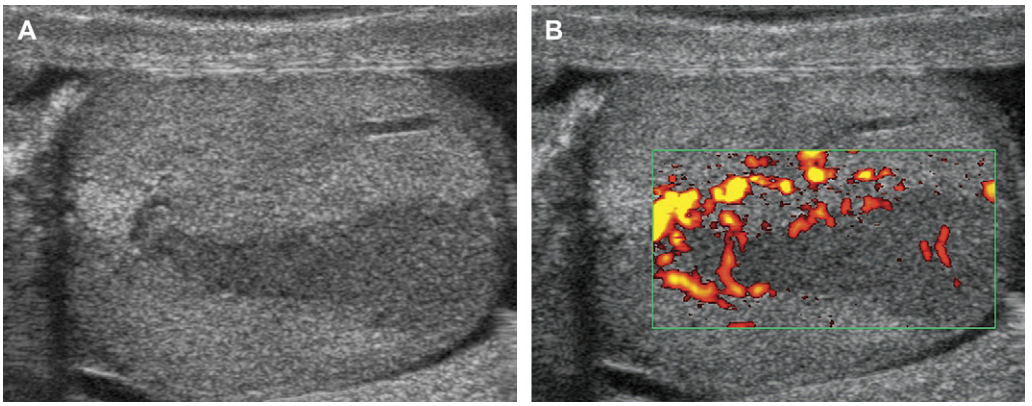

Fig. 18. Granulomatous orchitis. Longitudinal gray-scale (*A*) and corresponding power Doppler (*B*) sonograms of the testis show a wedge-shaped hypoechoic lesion with prominent peripheral and some internal vascularity. Patient underwent orchiectomy because of the concern for a malignancy, and it was confirmed to be granulomatous orchitis.

Careful analysis should be performed to differentiate these cysts from cystic neoplasms, especially teratomas [30]. Presence of any solid components must raise the possibility of malignancy [30,45]. Other intratesticular cystic benign lesions are intratesticular spermatocele, intratesticular abscess, and intratesticular varicocele; the latter has typical tubular anechoic structures of varying size with a venous flow pattern [1]. Intratesticular arteriovenous malformation and hemangioma are other rare intratesticular benign lesions that have characteristic vascular patterns [81,82].

Summary

Sonography is a useful imaging technique for identifying location (intra- or extratesticular) of scrotal masses. Most solid intratesticular lesions are malignant. Sonographic appearance is not reliable for distinguishing benign from malignant testicular lesions, but certain sonographic features may help in the differentiation. The patient's age, race, and clinical history is useful for differential diagnosis and sometimes a follow-up US examination can help rule out many acute conditions mimicking testicular malignancy.

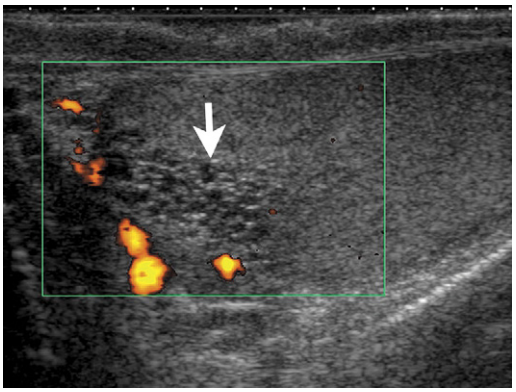

Fig. 19. Tubular ectasia of the rete testis. Longitudinal power Doppler sonogram of the testis reveals multiple avascular hypoechoic channels (*arrow*) on the posterior aspect of the testis, consistent with tubular ectasia of the rete testis.

References

[1] Dogra VS, Gottlieb RH, Oka M, et al. Sonography of the scrotum. Radiology 2003;227(1):18–36.
[2] Frates MC, Benson CB, DiSalvo DN, et al. Solid extratesticular masses evaluated with sonography: pathologic correlation. Radiology 1997; 204(1):43–6.
[3] Ulbright TM, Amin MB, Young RH. Tumors of the testis, adnexa, spermatic cord, and scrotum. In: Kumar V, Cotran RS, Robbins SL, editors. Atlas of tumor pathology, fasc 25, ser 3. Washington, DC: Armed Forces Institute of Pathology; 1999. p. 1–290.
[4] Schwerk WB, Schwerk WN, Rodeck G. Testicular tumors: prospective analysis of real-time US patterns and abdominal staging. Radiology 1987; 164(2):369–74.
[5] Dogra V, Bhatt S. Acute painful scrotum. Radiol Clin North Am 2004;42(2):349–63.
[6] Woodward PJ, Schwab CM, Sesterhenn IA. From the archives of the AFIP: extratesticular scrotal masses: radiologic-pathologic correlation. Radiographics 2003;23(1):215–40.
[7] Rubin JM, Bude RO, Carson PL, et al. Power Doppler US: a potentially useful alternative to mean frequency-based color Doppler US. Radiology 1994;190(3):853–6.
[8] Secil M, Kefi A, Gulbahar F, et al. Sonographic features of spermatic cord leiomyosarcoma. J Ultrasound Med 2004;23(7):973–6.
[9] Hangiandreou NJ. AAPM/RSNA physics tutorial for residents. Topics in US: B-mode US: basic

concepts and new technology. Radiographics 2003;23(4):1019–33.
[10] Hricak H, Filly RA. Sonography of the scrotum. Invest Radiol 1983;18(2):112–21.
[11] Aso C, Enriquez G, Fite M, et al. Gray-scale and color Doppler sonography of scrotal disorders in children: an update. Radiographics 2005; 25(5):1197–214.
[12] Siegel MJ. The acute scrotum. Radiol Clin North Am 1997;35(4):959–76.
[13] Sudakoff GS, Quiroz F, Karcaaltincaba M, et al. Scrotal ultrasonography with emphasis on the extratesticular space: anatomy, embryology, and pathology. Ultrasound Q 2002;18(4):255–73.
[14] Bree RL, Hoang DT. Scrotal ultrasound. Radiol Clin North Am 1996;34(6):1183–205.
[15] Sellars ME, Sidhu PS. Ultrasound appearances of the testicular appendages: pictorial review. Eur Radiol 2003;13(1):127–35.
[16] Blaivas M, Brannam L. Testicular ultrasound. Emerg Med Clin North Am 2004;22(3):723–48.
[17] Rolnick D, Kawanoue S, Szanto P, et al. Anatomical incidence of testicular appendages. J Urol 1968;100(6):755–6.
[18] Middleton WD, Bell MW. Analysis of intratesticular arterial anatomy with emphasis on transmediastinal arteries. Radiology 1993;189(1): 157–60.
[19] Siegel BA, editor. Diagnostic ultrasonography test and syllabus (second series). Reston (VA): American College of Radiology; 1994. p. 148–9.
[20] Tumeh SS, Benson CB, Richie JP. Acute diseases of the scrotum. Semin Ultrasound CT MR 1991; 12(2):115–30.
[21] Middleton WD, Thorne DA, Melson GL. Color Doppler ultrasound of the normal testis. AJR Am J Roentgenol 1989;152(2):293–7.
[22] Paltiel HJ, Rupich RC, Babcock DS. Maturational changes in arterial impedance of the normal testis in boys: Doppler sonographic study. AJR Am J Roentgenol 1994;163(5):1189–93.
[23] Keener TS, Winter TC, Nghiem HV, et al. Normal adult epididymis: evaluation with color Doppler US. Radiology 1997;202(3):712–4.
[24] Greenlee RT, Hill-Harmon MB, Murray T, et al. Cancer statistics, 2001. CA Cancer J Clin 2001; 51(1):15–36.
[25] Moul JW, Schanne FJ, Thompson IM, et al. Testicular cancer in blacks. A multicenter experience. Cancer 1994;73(2):388–93.
[26] Heiken JP. Tumors of the testis and testicular adnexa. In: Pollack HM, McClennan BL, editors. Clinical urography. Philadelphia: Saunders; 2000. p. 1716–41.
[27] Cast JE, Nelson WM, Early AS, et al. Testicular microlithiasis: prevalence and tumor risk in a population referred for scrotal sonography. AJR Am J Roentgenol 2000;175(6):1703–6.
[28] Geraghty MJ, Lee FT Jr, Bernsten SA, et al. Sonography of testicular tumors and tumor-like conditions: a radiologic-pathologic correlation. Crit Rev Diagn Imaging 1998;39(1):1–63.
[29] Richie JP, et al. Neoplasms of the testis. In: Walch PC, Retik AB, Vaughan ED, editors. Campbell's urology. 7th edition. Philadelphia: Saunders; 1998. p. 2411–52.
[30] Woodward PJ, Sohaey R, O'Donoghue MJ, et al. From the archives of the AFIP: tumors and tumorlike lesions of the testis: radiologic-pathologic correlation. Radiographics 2002;22(1):189–216.
[31] Glazer HS, Lee JK, Melson GL, et al. Sonographic detection of occult testicular neoplasms. AJR Am J Roentgenol 1982;138(4):673–5.
[32] Rifkin MD, Kurtz AB, Pasto ME, et al. Diagnostic capabilities of high-resolution scrotal ultrasonography: prospective evaluation. J Ultrasound Med 1985;4(1):13–9.
[33] Guthrie JA, Fowler RC. Ultrasound diagnosis of testicular tumours presenting as epididymal disease. Clin Radiol 1992;46(6):397–400.
[34] Horstman WG, Melson GL, Middleton WD, et al. Testicular tumors: findings with color Doppler US. Radiology 1992;185(3):733–7.
[35] Luker GD, Siegel MJ. Pediatric testicular tumors: evaluation with gray-scale and color Doppler US. Radiology 1994;191(2):561–4.
[36] Donohue JP, Zachary JM, Maynard BR. Distribution of nodal metastases in nonseminomatous testis cancer. J Urol 1982;128(2):315–20.
[37] Weiss RM, George NJR, O'Reilly PH. Comprehensive urology. London: Mosby; 2001. p. 425–49.
[38] Bredael JJ, Vugrin D, Whitmore WF Jr. Autopsy findings in 154 patients with germ cell tumors of the testis. Cancer 1982;50(3):548–51.
[39] Mostofi FK, Sesterhenn IA. Pathology of germ cell tumors of testes. Prog Clin Biol Res 1985; 203:1–34.
[40] Catalona WJ. Current management of testicular tumors. Surg Clin North Am 1982;62(6):1119–27.
[41] Cotran RS, Kumar P, Collins T. The male genital tract. In: Kumar V, Cotran RS, Robbins SL, editors. Robbins pathologic basis of disease. 6th edition. Philadelphia: Saunders; 1999. p. 1011–34.
[42] Javadpour N. Current status of tumor markers in testicular cancer. A practical review. Eur Urol 1992;21(Suppl 1):34–6.
[43] Hoshi S, Suzuki K, Ishidoya S, et al. Significance of simultaneous determination of serum human chorionic gonadotropin (hCG) and hCG-beta in testicular tumor patients. Int J Urol 2000;7(6): 218–23.
[44] Gorecki T, Kaszuba B, Ostrowska M, et al. Giant spermatocytic seminoma with massive hemorrhage into accompanying hydrocele: case report. Int Urol Nephrol 2005;37(3):529–31.
[45] Hamm B, Fobbe F, Loy V. Testicular cysts: differentiation with US and clinical findings. Radiology 1988;168(1):19–23.
[46] Grantham JG, Charboneau JW, James EM, et al. Testicular neoplasms: 29 tumors studied by high-resolution US. Radiology 1985;157(3):775–80.
[47] Ulbright TM, Roth LM. Testicular and paratesticular tumors. In: Sternberg SS, editor. Diagnostic

surgical pathology. 3rd edition. Philadelphia: Saunders; 1999. p. 1973–2033.
[48] Frush DP, Sheldon CA. Diagnostic imaging for pediatric scrotal disorders. Radiographics 1998; 18(4):969–85.
[49] Comiter CV, Renshaw AA, Benson CB, et al. Burned-out primary testicular cancer: sonographic and pathological characteristics. J Urol 1996;156(1):85–8.
[50] Tasu JP, Faye N, Eschwege P, et al. Imaging of burned-out testis tumor: five new cases and review of the literature. J Ultrasound Med 2003; 22(5):515–21.
[51] Maizlin ZV, Belenky A, Kunichezky M, et al. Leydig cell tumors of the testis: gray-scale and color Doppler sonographic appearance. J Ultrasound Med 2004;23(7):959–64.
[52] Kim I, Young RH, Scully RE. Leydig cell tumors of the testis. A clinicopathological analysis of 40 cases and review of the literature. Am J Surg Pathol 1985;9(3):177–92.
[53] Ricci ZJ, Stein MW, Koenigsberg M, et al. Unusual sonographic appearance of a Leydig cell tumor of the testis. Pediatr Radiol 2004; 34(2):177–8.
[54] Gierke CL, King BF, Bostwick DG, et al. Large-cell calcifying Sertoli cell tumor of the testis: appearance at sonography. AJR Am J Roentgenol 1994; 163(2):373–5.
[55] Dilworth JP, Farrow GM, Oesterling JE. Nongerm cell tumors of testis. Urology 1991;37(5): 399–417.
[56] Gaylis FD, August C, Yeldandi A, et al. Granulosa cell tumor of the adult testis: ultrastructural and ultrasonographic characteristics. J Urol 1989; 141(1):126–7.
[57] Doll DC, Weiss RB. Malignant lymphoma of the testis. Am J Med 1986;81(3):515–24.
[58] Nonomura N, Aozasa K, Ueda T, et al. Malignant lymphoma of the testis: histological and immunohistological study of 28 cases. J Urol 1989; 141(6):1368–71.
[59] Zicherman JM, Weissman D, Gribbin C, et al. Best cases from the AFIP: primary diffuse large B-cell lymphoma of the epididymis and testis. Radiographics 2005;25(1):243–8.
[60] Shahab N, Doll DC. Testicular lymphoma. Semin Oncol 1999;26(3):259–69.
[61] Mazzu D, Jeffrey RB Jr, Ralls PW. Lymphoma and leukemia involving the testicles: findings on gray-scale and color Doppler sonography. AJR Am J Roentgenol 1995;164(3):645–7.
[62] Golan G, Lebensart PD, Lossos IS. Ultrasound diagnosis and follow-up of testicular monocytic leukemia. J Clin Ultrasound 1997;25(8):453–5.
[63] Garcia-Gonzalez R, Pinto J, Val-Bernal JF. Testicular metastases from solid tumors: an autopsy study. Ann Diagn Pathol 2000;4(2):59–64.
[64] Casola G, Scheible W, Leopold GR. Neuroblastoma metastatic to the testis: ultrasonographic screening as an aid to clinical staging. Radiology 1984;151(2):475–6.
[65] Bude RO. Testicular plasmacytoma: appearance on gray-scale and power Doppler sonography. J Clin Ultrasound 1999;27(6):345–6.
[66] Park SB, Kim JK, Cho KS. Imaging findings of a primary bilateral testicular carcinoid tumor associated with carcinoid syndrome. J Ultrasound Med 2006;25(3):413–6.
[67] Perimenis P, Athanasopoulos A, Speakman M. Primary adenocarcinoma of the rete testis. Int Urol Nephrol 2003;35(3):373–4.
[68] Tazi H, Karmouni T, Ouali M, et al. Osteosarcoma of the testis. Int J Urol 2006;13(3):323–4.
[69] Thomas J, Rifkin M, Nazeer T. Intratesticular leiomyoma of the body of the testis. J Ultrasound Med 1998;17(12):785–7.
[70] Hobarth K, Susani M, Szabo N, et al. Incidence of testicular microlithiasis. Urology 1992;40(5): 464–7.
[71] Backus ML, Mack LA, Middleton WD, et al. Testicular microlithiasis: imaging appearances and pathologic correlation. Radiology 1994;192(3): 781–5.
[72] Ganem JP, Workman KR, Shaban SF. Testicular microlithiasis is associated with testicular pathology. Urology 1999;53(1):209–13.
[73] Woodward PJ. Case 70: seminoma in an undescended testis. Radiology 2004;231(2):388–92.
[74] Karcaaltincaba M, Kaya D, Ozkan OS, et al. Preoperative multidetector computed tomography diagnosis of a seminoma originating from an undescended testis by "testicular vascular pedicle" sign. J Comput Assist Tomogr 2006; in press.
[75] Dogra VS, Gottlieb RH, Rubens DJ, et al. Benign intratesticular cystic lesions: US features. Radiographics 2001;21(Spec No):S273–81.
[76] Pekindil G, Huseyin Atakan I, Kaya E, et al. Bilateral synchronous granulomatous orchitis: gray-scale and colour Doppler sonographic findings. Eur J Radiol 1999;31(3):201–3.
[77] Proto G, Di Donna A, Grimaldi F, et al. Bilateral testicular adrenal rest tissue in congenital adrenal hyperplasia: US and MR features. J Endocrinol Invest 2001;24(7):529–31.
[78] Dogra V, Nathan J, Bhatt S. Sonographic appearance of testicular adrenal rest tissue in congenital adrenal hyperplasia. J Ultrasound Med 2004; 23(7):979–81.
[79] Burke BJ, Parker SH, Hopper KD, et al. The ultrasonographic appearance of coexistent epididymal and testicular sarcoidosis. J Clin Ultrasound 1990; 18(6):522–6.
[80] Martinez-Berganza MT, Sarria L, Cozcolluela R, et al. Cysts of the tunica albuginea: sonographic appearance. AJR Am J Roentgenol 1998;170(1): 183–5.
[81] Kutlu R, Alkan A, Soylu A, et al. Intratesticular arteriovenous malformation: color Doppler sonographic findings. J Ultrasound Med 2003; 22(3):295–8.
[82] Ricci Z, Koenigsberg M, Whitney K. Sonography of an arteriovenous-type hemangioma of the testis. AJR Am J Roentgenol 2000;174(6):1581–2.

ELSEVIER SAUNDERS

ULTRASOUND CLINICS

Ultrasound Clin 2 (2007) 45–56

Sonograhic Evaluation of Scrotal and Penile Trauma

Shweta Bhatt, MD[a], Hamad Ghazale, MS, RDMS[b], Vikram S. Dogra, MD[a,*]

Scrotal and penile trauma is relatively uncommon, and imaging is frequently performed to assess the vascular integrity and severity of injury. The commonest scrotal injury is sports related, followed by motor vehicle accidents, accounting for about 17% of injuries. Physical examination is adequate in evaluating superficial injuries, but ultrasound plays a significant role in evaluating the morphologic changes to the testis and penis. Color flow Doppler assesses the organ blood perfusion and localizes the vascular disruption, if any. Scrotal trauma can result in testicular rupture, fracture, dislocation, torsion, and hematocele. The major cause of penile injury is sex-related activity that results in penile fracture. This article discusses the role of sonography in scrotal and penile trauma and emphasizes the role of color and power Doppler and gray-scale imaging.

Scrotal trauma: causes and mechanism

Three percent to 10% of trauma patients have associated genitourinary tract injuries, with male genitalia being particularly involved with associated pelvic injuries. The mobility and elasticity of the scrotum and its contents and the laxity of skin protect it from being injured in most cases of trauma. Nevertheless, scrotal contents can be injured when the scrotum is squeezed between the thighs or compressed against the pubic rami or by objects moving at high velocities [1,2]. Ultrasound can help in identifying the extent and type of injury so that testes can be salvaged with an early exploration.

Sports-related injuries are the leading cause of injuries to the scrotum. These injuries commonly include football injuries, hockey stick injuries, or falls during sports-related activities. Motor vehicle accidents are the second most common cause of scrotal injuries and are usually associated with coexistent abdominal or, more commonly, pelvic injuries. Direct assault to the scrotum is also one of the causes of scrotal injury. Gunshot wounds to the scrotum are on the rise, consistent with the increasing incidence of violence. These wounds are the predominant (and practically the only) type of penetrating injury to the scrotum. Other rare causes include genital self-mutilation and animal

[a] University of Rochester School of Medicine, Department of Imaging Sciences, 601 Elmwood Ave., Box 648, Rochester, NY 14642, USA
[b] Diagnostic Medical Sonography Program, Rochester Institute of Technology, 153 Lomb Memorial Drive, Rochester, NY 14623, USA
* Corresponding author.
E-mail address: vikram_dogra@urmc.rochester.edu (V.S. Dogra).

1556-858X/07/$ – see front matter
doi:10.1016/j.cult.2007.01.003
ultrasound.theclinics.com

bites. Constricting bands placed on the penis to prolong erection may at times result in injury to scrotal contents [3].

Sonographic features

In the past, ultrasound was considered unreliable to assess scrotal injury [4]; however, with current improvements in ultrasound technology and the availability of higher-frequency transducers, this imaging modality now provides a means of assessing the blood perfusion and the degree of injury to the testis and scrotal contents. Penetrating trauma to the scrotum is most often managed by exploration; however, not all patients who have scrotal injury require surgical exploration. Ultrasound helps in triaging such patients for surgical versus nonsurgical management. Ultrasound, with an excellent sensitivity and specificity for testicular evaluation, usually serves as a useful adjunct to physical examination for confirming clinical suspicion [5]; however, under no circumstances should a normal-looking sonogram preclude an exploration in the presence of a grossly abnormal physical examination.

Sonographic appearances of scrotal trauma can be broadly classified into intratesticular and extratesticular findings. A summary of sonographic findings in testicular trauma is presented in Box 1. The American Association for the Surgery of Trauma grading scale of scrotal injury is presented in Table 1.

Intratesticular

Contour abnormality

The testis is bound externally by tunica albuginea (TA), which helps to maintain its shape and integrity [6]. TA is predominantly made of fibrous tissue and is very difficult to rupture. TA requires a very high force, as much as 50 kg of pressure, for its rupture to occur [3,7]. TA appears as two bright echogenic lines on high-frequency transducer sonography. The disruption in the continuity of these bright lines identifies TA rupture (testicular rupture). This disruption in TA results in extrusion of testicular contents, appearing as a contour abnormality [6]. Disruption of tunica vasculosa is an indirect sign of TA rupture. Extrusion of testicular contents through the ruptured tunica can be sometimes seen as a focal bulge at the site of tunica rupture. Trauma resulting in rupture of TA also results in intratesticular injury, seen as altered echotexture of the testis. The presence of heterogeneous echotexture and contour abnormality is considered very specific for testicular rupture (Fig. 1), and the patient should be taken for surgical exploration at the earliest opportunity [5,8]. There is a 50% chance of a testicular rupture in cases of blunt scrotal trauma (unilateral in most cases; bilateral in about 1.5% cases) (Fig. 2) [9].

Testicular rupture may also be rarely associated with epididymal ruptures, which may at times be difficult to detect sonographically.

Box 1: Sonographic findings in testicular trauma

Contour abnormality of the testis
Disruption of the tunica albuginea (evidenced by interruption of tunica vasculosa)
Direct visualization of an intratesticular fracture line
Extratesticular hematocele
Intra- or extratesticular hematoma
Heterogeneous appearance of the testis
Hyperemia of the epididymis

Note that any of these findings may be seen in isolation or in any combination.

From Dogra V, Bhatt S. Acute painful scrotum. Radiol Clin North Am 2004;42(2):360; with permission.

Table 1: Organ injury scale for scrotal injury

AAST grade	Scrotal injury	AIS-90 score
I	Contusion	1
II	Laceration <25% of scrotal diameter	1
III	Laceration = 25% of scrotal diameter	2
IV	Avulsion <50%	2
V	Avulsion = 50%	2

Abbreviations: AAST, American Association for the Surgery of Trauma; AIS, Abbreviated Injury Scale.
From Moore EE, Malangoni MA, Cogbill TH, et al. Organ injury scaling VII: cervical vascular, peripheral vascular, adrenal, penis, testis, and scrotum. J Trauma 1996;41:523; with permission.

Testicular fracture line

Fracture lines are identified on ultrasound by the presence of a relatively linear hypoechoic area through the testicular parenchyma with absent vascularity (Fig. 3). Actual fracture lines through the testicle are seen in less than 20% of cases [10,11]. They may or may not be associated with testicular rupture, and the TA may be intact around the testis.

Intratesticular hematoma

Intratesticular hematoma is a relatively common finding in blunt testicular trauma. These hematomas may be single or multiple, depending on the

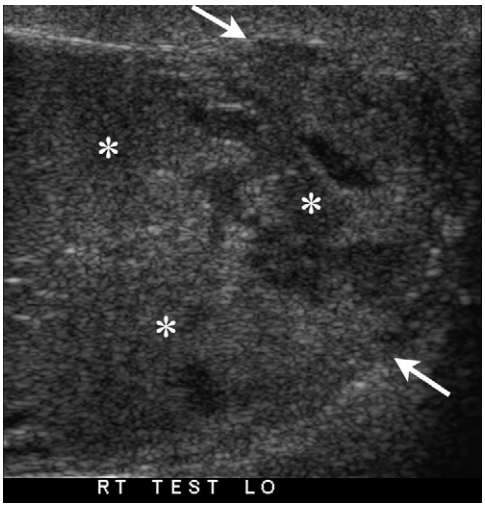

Fig. 1. Contour abnormality. Longitudinal gray-scale sonogram demonstrates a TA tear in the lower pole of the testis, giving rise to a contour abnormality (*arrows*). Heterogeneous intratesticular echotexture (*asterisks*) secondary to trauma is also seen.

nature of injury. Large hematomas are usually associated with testicular ruptures and may sometimes be the only finding with an intact TA. Ultrasound can help exclude other findings such as tunica rupture and prevent unnecessary exploration because most patients who have a small intratesticular hematoma are usually managed conservatively with ice packs, nonsteroidal anti-inflammatory drugs, and urologic and sonographic follow-up. Close follow-up of these patients is mandatory because 40% of testicular hematomas result in testicular infection or necrosis, which often requires orchiectomy [7].

Sonographic appearance of intratesticular hematomas varies with the size and duration of the hematoma. Acute hematomas may present as focal echogenic areas with absent vascularity, which later become organized and retracted to appear as septated or anechoic collections (Fig. 4) within the testis on ultrasound. Large hematomas involving the entire testis may give a heterogeneous appearance to the entire testicle. Color flow Doppler ultrasound evaluation in these patients helps in assessing the potential viability of the testis. Testicular hematomas may be associated with an extratesticular hematocele and scrotal wall injuries.

About 10% to 15% of testicular tumors present for the first time after an episode of scrotal trauma [7]. Therefore, it is important to follow any intratesticular abnormality seen on sonogram after trauma to its complete resolution, particularly if the testis is not explored, so that these tumors are not missed.

Testicular torsion

Trauma-induced testicular torsion is a well-recognized entity, the incidence being 4% to 8% in most studies reporting on testicular torsion [12]. Trauma can result in testicular torsion by stimulating forceful contraction of the cremasteric muscles. Gray-scale and color flow Doppler evaluations are very helpful in demonstrating the morphologic alterations caused by trauma and in excluding testicular torsion [13]. Sonographic features of post-traumatic testicular torsion are similar to spontaneous torsion (Fig. 5) [6]. Early exploration in these patients may be helpful [14].

Dislocation

Testicular dislocation is a very rare event after testicular trauma and its diagnosis on ultrasound is even rarer. It may be easily missed unless the

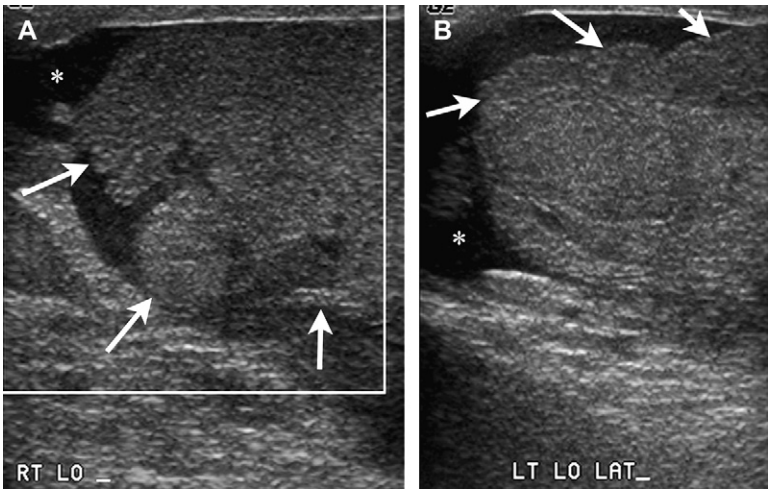

Fig. 2. Bilateral testicular rupture. Longitudinal gray-scale images of the right (*A*) and left (*B*) testes demonstrate complete disruption of TA (*arrows*) with accompanying hematocele (*asterisk*).

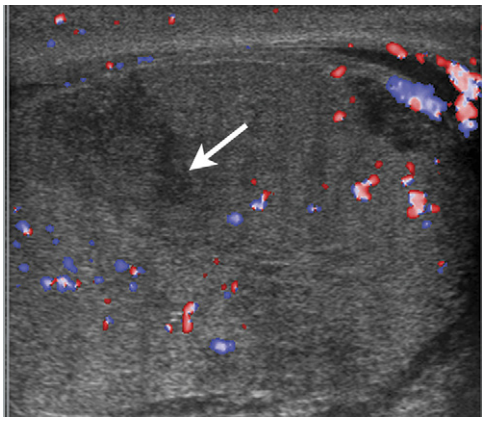

Fig. 3. Testicular fracture line. Color flow Doppler of the testis demonstrates a linear, hypoechoic, and avascular area (*arrow*) across the testicular parenchyma.

sonographer/radiologist is aware of its existence. It is often a delayed diagnosis because it lies low on the list of clinical suspicion in a polytrauma patient for whom the main emphasis of imaging is on identifying major organ damage.

Testicular dislocation is usually unilateral and rarely bilateral [15]. The mechanism involved in dislocation of testis is usually related to sudden force and is particularly common in motorcyclists secondary to deceleration straddle injuries [16,17]. Dislocated testis can be found anywhere along the radius described by the spermatic cord, the center of which is located in the external inguinal ring. The superficial inguinal area is the commonest site of dislocation, other less common sites include the perineum, retrovesical [18], and even acetabular areas [19]. A mechanism involving preloading of the cremaster muscle as the source of dislocation has also been postulated [20].

Dislocated testis can be diagnosed clinically by palpation of an empty and ecchymotic hemiscrotum and an associated ipsilateral inguinal mass [21]. High-frequency transducer sonography helps to exclude intratesticular injuries, and color flow Doppler examination confirms the viability of the testis. If the testis is viable, a manual reduction of the dislocated testis is usually performed; if this is unsuccessful, then immediate surgical reduction and fixation should be performed [22].

Extratesticular

Traumatic epididymitis

The exact incidence of epididymal injury in scrotal trauma is not known, but according to unpublished data of the authors, it was seen in 18 of 63 patients who had scrotal trauma. Enlargement and hyperemia of epididymis have been described secondary to scrotal trauma [23,24]. This presentation is called traumatic epididymitis [25]. Following trauma, epididymis may reveal the presence of small contusions or hematomas within, resulting in its enlargement and inflammatory response (Fig. 6). Color flow Doppler evaluation reveals absence of blood flow within these hematomas or contusion, with surrounding reactive hyperemia. Presence of these changes should not be interpreted as infectious epididymitis; correlation with relevant history is important. Trauma to the epididymis may be associated with hematoceles.

Epididymal fracture

Epididymal fractures or ruptures are difficult to detect on ultrasound. They are usually diagnosed only on scrotal exploration performed for associated testicular injuries. Isolated epididymal injuries are rare. Ruptured epididymis should be considered when the epididymis cannot be well identified

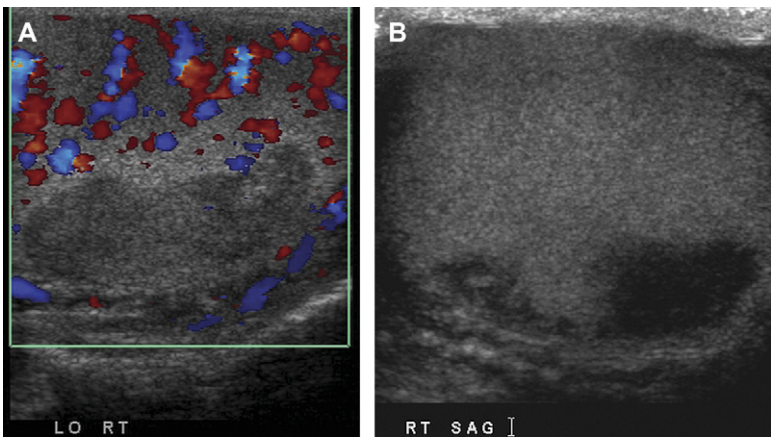

Fig. 4. Intratesticular hematoma. Color flow Doppler image (*A*) of the testis reveals a hypoechoic, avascular region within the testis. Follow-up ultrasound (*B*) after 1 week shows evolving changes in the intratesticular hematoma.

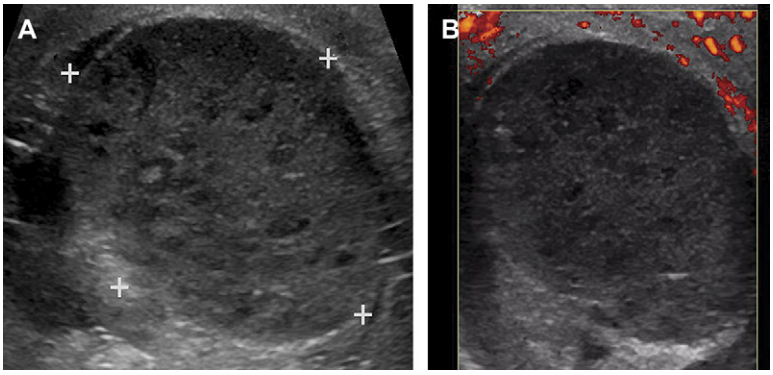

Fig. 5. Testicular torsion. This patient is status post trauma. Gray-scale sonogram (*A*) demonstrates a predominantly hypoechoic testis with areas of variable echogenicity. Corresponding power Doppler image (*B*) reveals complete absence of intratesticular blood flow. On subsequent surgical exploration, patient was found to have a 900° twist, with complete infarction of the testis.

and has ill-defined margins in the setting of scrotal trauma with associated testicular injuries.

Hematocele

Hematocele is defined as collection of blood in the tunica vaginalis. Ultrasound appearance of a hematocele varies depending on the length of time since the trauma occurred. Acute hematoceles are echogenic, and subacute and chronic hematoceles appear as complex fluid collections with septations and may have fluid-fluid levels or low-level internal echoes (Fig. 7) [6,26]. Hematocele may be secondary to extratesticular or testicular injury, despite lack of definite sonographic evidence of testicular rupture. It is the most common finding in blunt scrotal trauma and was present in 11 of 15 patients in a study by Micallef and colleagues [2]. A large hematocele is an indication for surgical exploration [7].

Spermatic cord hematoma

Spermatic cord injury due to blunt trauma to the scrotum is a rare consequence and is characterized by the onset of severe pain, swelling, or hematoma in the groin area. It results from direct injury to the groin causing bleeding of spermatic vessels. The hematoma is usually enclosed by the spermatic fascia and is typically located superior to the testis (Fig. 8) [27]. Other causes of spermatic cord hematoma include idiopathic, secondary to anticoagulation therapy, or as an extension of a retroperitoneal hemorrhage [28]. Another rare but known cause of trauma-related cord hematoma includes rupture of varicocele secondary to blunt abdominal trauma [29]. Because of the rarity of occurrence of cord hematoma secondary to trauma, its clinical presentation usually results in it being misdiagnosed as a subcutaneous hematoma secondary to bleeding from subcutaneous vessels [27]. Almost all cases reported so far have been diagnosed intraoperatively.

Scrotal wall hematoma

Scrotal wall hematoma is a common associated finding in blunt trauma to the testes. It is seen on ultrasound as a thickened and echogenic scrotal

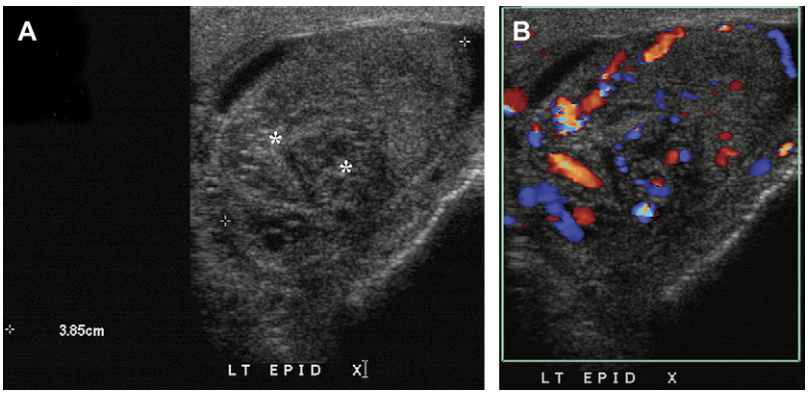

Fig. 6. Traumatic epididymitis. Gray-scale sonogram (*A*) of epididymis in a patient post scrotal trauma reveals enlargement of the epididymis (measuring 3.85 cm) with variable echotexture, secondary to epididymal hematomas (*asterisks*). Corresponding color flow Doppler (*B*) shows absence of blood flow in these hematomas. Patient was managed conservatively.

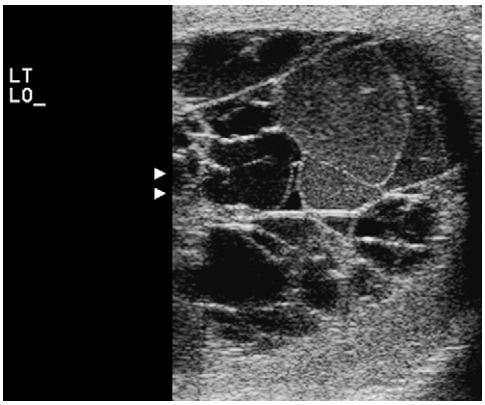

Fig. 7. Hematocele. Gray-scale sonogram demonstrates organizing hematocele. Patient did not have any other associated testicular injury.

wall, with absent or low vascularity. Scrotal wall hematoma is rarely an isolated finding and is commonly associated with an intra- or extratesticular hematoma.

Penetrating trauma

Gunshot wound is the commonest cause of a penetrating injury to the scrotum. It is easy to identify on physical examination by the presence of an entry wound, an exit wound, or both. Sonographic findings characteristic of a penetrating injury can include the presence of air within the scrotum, identified as multiple echogenic foci with reverberation artifact (Fig. 9); a bullet track within the testicular parenchyma, seen as an echo-poor linear avascular area; and sometimes the presence of foreign bodies, seen as bright echogenic foci within the testis or in the extratesticular tissues [30]. Epididymal injuries are also possible but difficult to detect on ultrasound [30]. Associated findings such as hematocele or scrotal wall hematoma may be seen.

Penile trauma

Penile trauma is a relatively uncommon condition. Most cases have a typical clinical history, but because a definitive diagnosis based on clinical findings alone may be difficult, various imaging techniques are used to confirm the diagnosis or to demonstrate the exact location and extent of injury. Sonography is the preferred imaging technique for evaluation of penile trauma patients because of its improved gray-scale resolution and its capability to evaluate penile vascularity [31]. The American Association for the Surgery of Trauma grading scale of penile injury is presented in Table 2.

Sonographic technique

Sonographic examination of the penis is performed with the patient in the supine or lithotomy (frog-leg) position and the penis in the anatomic position, lying on the anterior abdominal wall. No special preparation is required. A high-frequency (7.5–12 MHz) linear array transducer with copious sonographic acoustic gel should be used. Longitudinal and transverse images of the entire length of the penis in gray-scale and color flow Doppler should be obtained [32]. A transperineal approach with elevation of the testicles may be used, if required, to assess the base of the penis. On transverse scans, the two corpora cavernosa are seen as symmetric, homogenous, midlevel echoes, circular structures that are surrounded by an echogenic line representing the TA [32]. During the erectile state, the two corpora cavernosa enlarge and the sinusoids dilate (become anechoic), which may change the echotexture from midlevel, homogeneous to

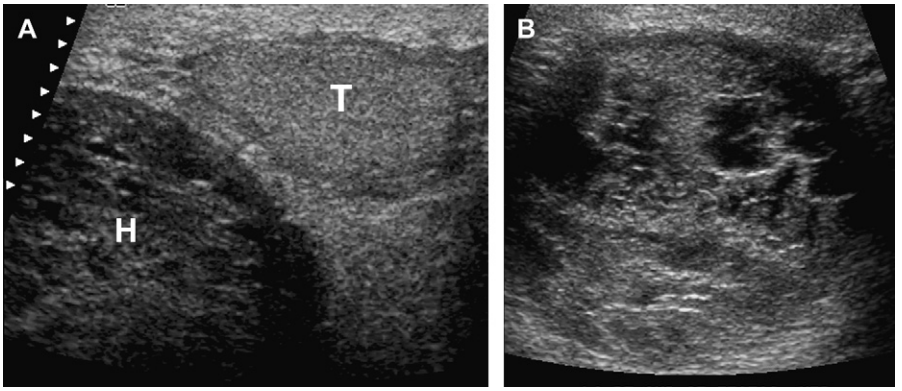

Fig. 8. Spermatic cord hematoma. Gray-scale images (*A*, *B*) reveal a large variable echotexture region (H), superior to right testis. Right testis is displaced inferiorly. Left testis (T) is seen in the image. Patient underwent surgical exploration and was found to have organizing hematoma of the spermatic cord.

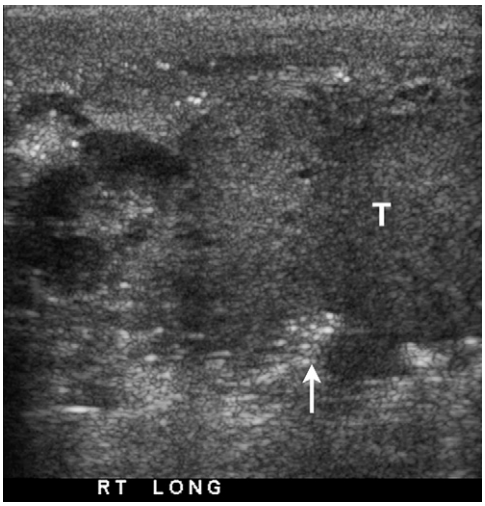

Fig. 9. Testicular penetrating trauma. Patient is status post gunshot to the groin. Gray-scale sonogram reveals a shattered testis (T) with the presence of air in the subcutaneous tissue and testicular parenchyma (*arrow*). Color flow Doppler (not shown) demonstrated complete absence of blood flow. Patient underwent orchiectomy.

low-level, hypoechoic. The two corpora cavernosa are separated by the septum penis, an extension of the TA, which appears as a thin echogenic line. Within each corpus cavernosum, a pulsatile structure with echogenic walls is seen, which represents the cavernosal artery. The cavernosal artery is usually located in the center of the corpus cavernosum or slightly toward the median septum penis. It can be identified on transverse and longitudinal planes and appears as two echogenic dots on a transverse image and as a tubular structure with echogenic walls in a longitudinal plane. In the nonerectile state, the normal diameter of the cavernosal artery ranges from less than 0.3 mm to 1.0 mm (mean, 0.3–0.5 mm) [33].

Table 2: Organ injury scale for penile injury

AAST grade	Penile injury	AIS-90 score
I	Cutaneous laceration or contusion	1
II	Laceration of Buck's fascia (cavernosum) without tissue loss	1
III	Cutaneous avulsion, laceration through glans or meatus, or cavernosal or urethral defect <2 cm	3
IV	Partial penectomy or cavernosal or urethral defect = 2 cm	3
V	Total penectomy	3

Abbreviations: AAST, American Association for the Surgery of Trauma; AIS, Abbreviated Injury Scale.
From Moore EE, Malangoni MA, Cogbill TH, et al. Organ injury scaling VII: cervical vascular, peripheral vascular, adrenal, penis, testis, and scrotum. J Trauma 1996;41:523; with permission.

Penile injury: mechanism

Penile fracture is an uncommon injury caused by the exertion of axial forces on the erect penis, resulting in a tear of the TA, with extrusion of blood subcutaneously [34]. This injury usually occurs during vigorous sexual intercourse when the rigid penis slips out of the vagina and is misdirected against the partner's pubic bone or perineum, resulting in a buckling trauma [35]. Another common cause of penile fracture is self-inflicted. This injury occurs due to sudden downward bending of the erect penis by patients themselves in an attempt to achieve detumescence to avoid embarrassment from their sudden erection [36]. A retrospective study of 56 patients who had penile injuries showed that 28 injuries were sustained during coitus and another 12 during other sexual practices [37]. Other causes of penile fracture include rolling over in bed with an erect penis and direct blunt injury to the penis. Penile injury secondary to a bite during sexual foreplay, resulting in blunt crushing and disruption of the erect corpora cavernosa, has also been reported [38].

One of the reasons for the increased risk of penile fracture during tumescence is the stretching and subsequent thinning of TA during erection: in the flaccid state, it is about 2.4 mm thick; during erection it can be as thin as 0.25 to 0.5 mm [39]. Nonpenetrating injury to the erect penis can produce albuginea tear, intracavernous hematoma, or extra-albugineal hematoma from rupture of the dorsal vessels.

Penile fracture

Penile fractures are urologic emergencies, but not all patients seek medical attention. Delay in presentation because of embarrassment is common. Most patients report hearing a cracking or popping sound associated with a sharp pain, followed by rapid detumescence, swelling, discoloration, and deformity of the penis (eggplant deformity) [31]. Tunica tear usually occurs in only one of the corpora cavernosa (but can occur bilaterally) and in its surrounding TA; however, corpus spongiosal and urethral involvement can also occur. Fractures usually occur in the proximal shaft or midshaft of the penis. Corpus cavernosal ruptures are generally

transverse in orientation and are located in the ventral portion of the corpus cavernosum, adjacent to the urethra [40]. Sonography does not demonstrate direct disruption of the tunica, but it is indirectly inferred by the presence of hematoma at the site of tunica fracture [31]. In one study, ultrasound demonstrated the exact site of rupture in six of seven patients [41]. The integrity of the TA is the most important factor in determining the necessity for surgical intervention. Surgical repair is generally recommended for patients who have a suspected tear of the TA or with urethral injury.

Urethral and spongiosal injury

Penile fracture can occur only when the penis is erect, and the injury results in disruption of the corpora and TA [42]. Of the 180 cases of penile fracture that have been reported in the literature, only 10% have reported accompanying urethral disruption. Of these, only 3 cases were reported to have a complete urethral tear [43]. About 20% of penile fractures are associated with lesions of the corpus spongiosum and urethra. The relatively fixed portion of the urethra between the urogenital diaphragm and the glans is susceptible to injury with penile fracture. Sonourethrography may be useful to demonstrate the continuity of the anterior urethra [44].

Real-time examination of the urethra during instillation of jelly may increase the possibility of detecting extravasations through a ruptured urethral wall [45]. Presence of air in the cavernosal bodies in the absence of external penetrating trauma may be an indirect sign of urethral injury (Fig. 10) [46]. Sonography may be able to demonstrate edema or hematoma of corpus spongiosum following penile trauma [47].

Intracavernosal hematomas

Injury to the subtunical venous plexus or to the smooth muscle trabeculae in the absence of complete tunical disruption can lead to cavernosal hematomas (Fig. 11) [48]. Intracavernosal hematomas are usually bilateral and result from injury to the cavernosal tissue when the base of the penile shaft is crushed against the pelvic bones [46]. Sonographic appearance of a penile hematoma varies with the age of the lesion. Cavernosal damage can cause fibrosis, which appears as an

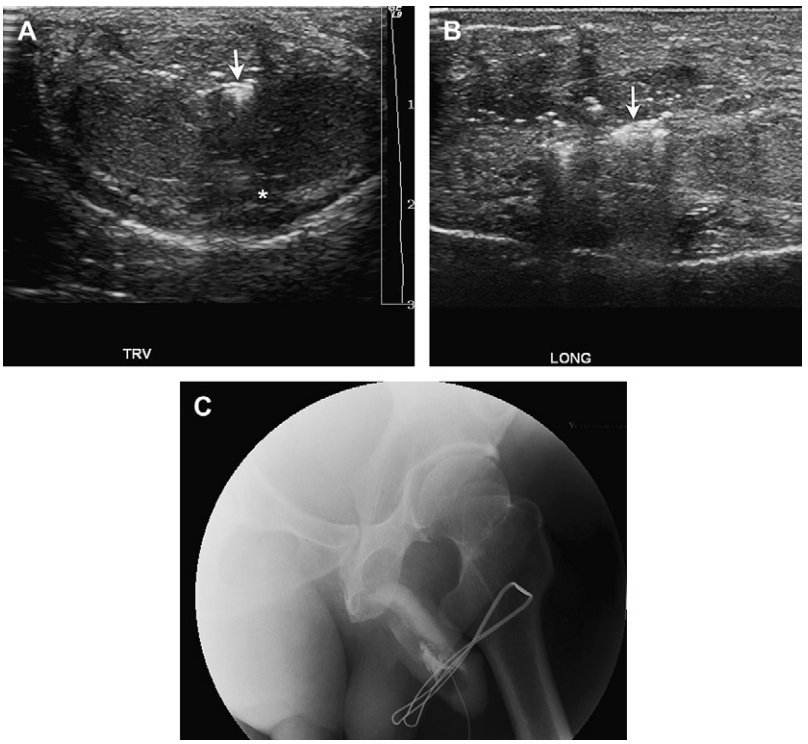

Fig. 10. Penile fracture. Patient heard a popping sound during sexual intercourse followed by immediate detumescence and presented to the hospital immediately for evaluation. Transverse (*A*) and longitudinal (*B*) gray-scale sonogram of the penis reveals air (*arrow*) as evidenced by reverberation artifact in the expected location of anterior urethra. There is also disruption of TA on the left side (*asterisk*). Retrograde urethrogram (*C*) further confirms the rupture of anterior urethra.

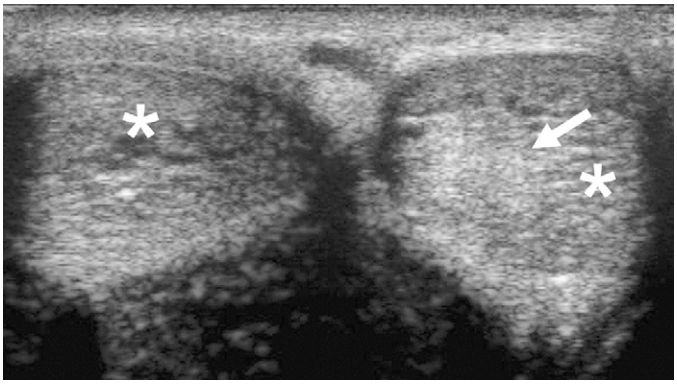

Fig. 11. Intracavernosal hematoma following sexual intercourse. Transverse gray-scale images of both corpora cavernosa (*asterisks*) reveal a hyperechoic area (*arrow*) on the medial aspect of the left corpus cavernosum, suggestive of a cavernosal hematoma. This hematoma resolved on follow-up within 2 weeks. The right corpus is normal. (*From* Bhatt S, Kocakoc E, Rubens DJ, et al. Sonographic evaluation of penile trauma. J Ultrasound Med 2005;24:998; with permission).

ill-defined echogenic scar replacing the erectile tissue. A case of spontaneous cavernosal hemorrhage has been reported [49].

Avulsion of the dorsal penile vessels and thrombosis

Rupture or thrombosis of a superficial vein of the penis can mimic a penile fracture [50], but deformation and immediate detumescence do not occur because of the intact TA. The hematoma secondary to rupture of these veins may be superficial or remain under Buck's fascia, depending on the site of involvement of the penile veins. A high index of clinical suspicion can lead to the diagnosis of rupture of the superficial dorsal vein of the penis, with subsequent conservative management.

Sonography demonstrates a noncompressible dorsal vein, and if ruptured, an associated hematoma can be visualized (Fig. 12) [51].

High-flow priapism

Nonischemic or arterial priapism is a less common form of priapism that presents clinically as a painless erection that typically follows some type of penile or perineal trauma leading to unregulated arterial inflow into the sinusoidal space. The penis is often not maximally rigid in these cases, but intercourse may be possible. High-flow priapism is characterized by formation of a fistula between the cavernosal artery and the lacunae in the corpus cavernosum, known as an arterial-lacunar fistula [32]. This condition is not a urologic emergency, and corporeal aspiration of oxygenated blood is confirmatory for high-flow priapism [31,32,52]. The venous outflow is maintained, thereby preventing complete erection, stasis, and hypoxia [31]. High-flow priapism may present days or even weeks after the original injury [52].

Color duplex Doppler sonography has replaced arteriography as the imaging modality of choice for the diagnosis of priapism because it is sensitive, noninvasive, and has wide availability [52].

In patients who have recent arterial laceration, gray-scale ultrasound reveals an irregular hypoechoic region secondary to tissue injury or distended lacunar spaces in the corpus cavernosum. This irregular area appears with well-circumscribed margins, mimicking a pseudoaneurysm analogous to a capsule formation if the injury has been long-standing [45]. The arteries exhibit normal or increased flow within the cavernosal arteries and an irregular flow from the artery to

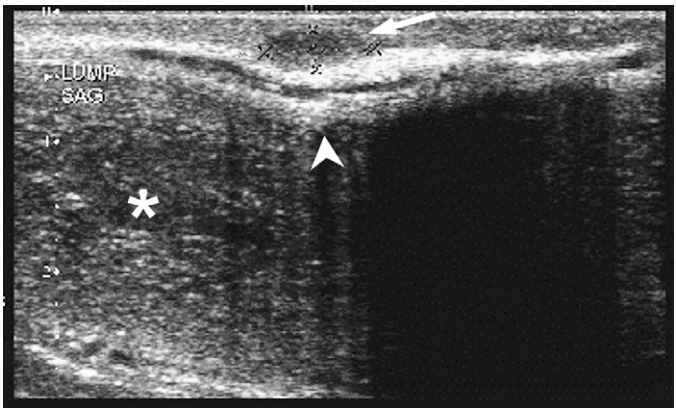

Fig. 12. Penile hematoma due to avulsion of dorsal penile vessels. Longitudinal gray-scale sonogram of the penis reveals a hypoechoic area (*arrow*) anterior to the TA (*arrowhead*) suggestive of a penile hematoma. The corpora cavernosa (*asterisk*) and the TA are intact. (*From* Bhatt S, Kocakoc E, Rubens DJ, et al. Sonographic evaluation of penile trauma. J Ultrasound Med 2005;24:999; with permission).

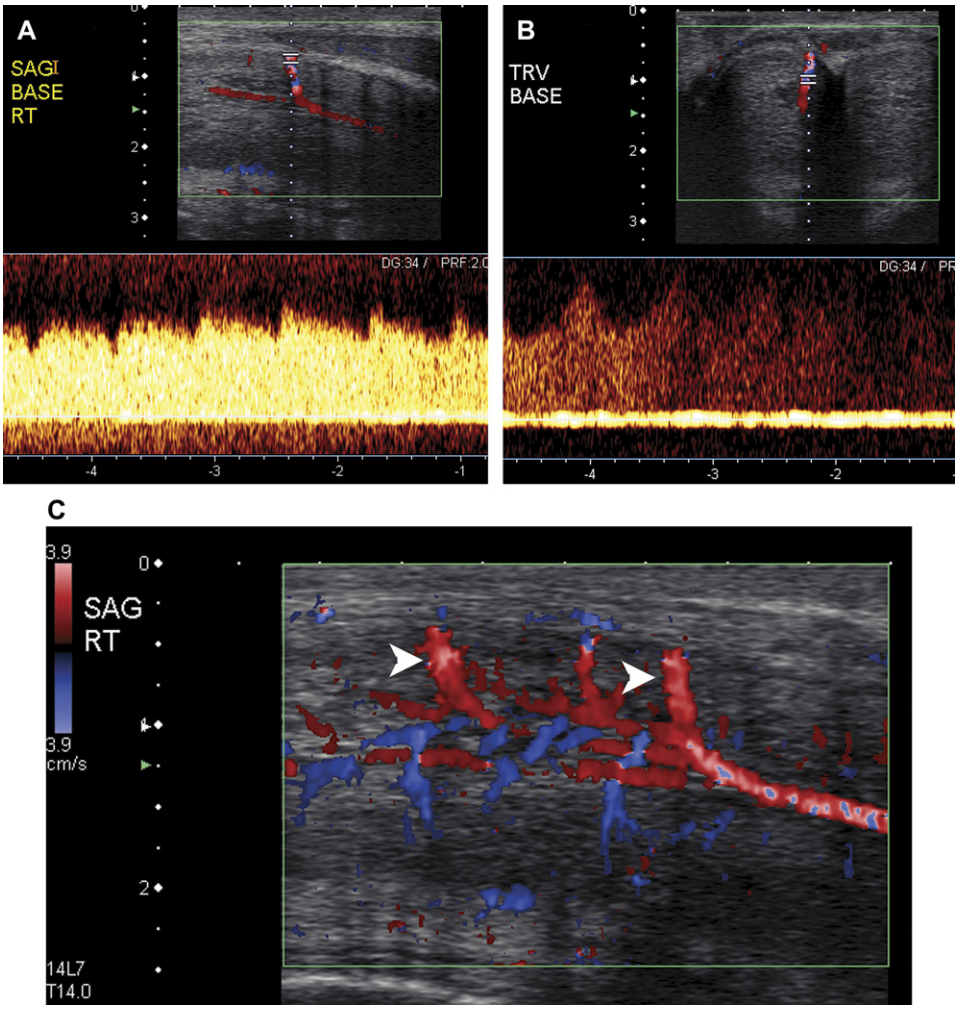

Fig. 13. High-flow priapism. Longitudinal (*A*) and transverse (*B*) color flow Doppler sonograms of base of right corpora cavernosa reveal marked turbulent flow suggestive of cavenosal-lacunar fistula. Longitudinal color flow Doppler image of right corpus cavernosa (*C*) reveals increased vascularity as evidenced by the prominence of helicine vessels (*arrowheads*) consistent with priapism secondary to arterio-lacunar fistula. Patient also gave history of trauma to the perineum in the recent past as a result of horseback riding. Detumescence of penis could be achieved by external pressure at the base of penis/perineum, and release of pressure resulted in tumescence of penis, further confirming the sonographic findings.

the cavernosal body at the site of injury. The arterial-lacunar fistula seen in high-flow priapism essentially bypasses the helicine arteries and appears as a characteristic color blush extending into the cavernosal tissue and as turbulent high-velocity flows on color duplex sonography (Fig. 13) [31]. A second ultrasound manifestation of high-flow priapism is detection of increased cavernosal artery flow without sexual stimulation.

Treatment of high-flow priapism is embolization; it may also be followed up without any intervention [52]. Surgical correction of high-flow priapsim is also possible [53].

Summary

Sonography is an ideal technique for evaluating patients who have scrotal and penile trauma. Sonography can demonstrate the integrity of the TA and the extent and location of a tunical tear in testicular ruptures and penile fractures. Associated vascular injuries can be demonstrated using color or power Doppler techniques.

References

[1] Wessells H, Long L. Penile and genital injuries. Urol Clin North Am 2006;33:117–26, vii.

[2] Micallef M, Ahmad I, Ramesh N, et al. Ultrasound features of blunt testicular injury. Injury 2001;32:23–6.
[3] McAninch JW, Santucci RA. Genitourinary trauma. 8th edition. Philadelphia: Saunders; 2002.
[4] Ugarte R, Spaedy M, Cass AS. Accuracy of ultrasound in diagnosis of rupture after blunt testicular trauma. Urology 1990;36:253–4.
[5] Buckley JC, McAninch JW. Diagnosis and management of testicular ruptures. Urol Clin North Am 2006;33:111–6, vii.
[6] Dogra VS, Gottlieb RH, Oka M, et al. Sonography of the scrotum. Radiology 2003;227:18–36.
[7] Dogra V, Bhatt S. Acute painful scrotum. Radiol Clin North Am 2004;42:349–63.
[8] Buckley JC, McAninch JW. Use of ultrasonography for the diagnosis of testicular injuries in blunt scrotal trauma. J Urol 2006;175: 175–8.
[9] Cass AS, Ferrara L, Wolpert J, et al. Bilateral testicular injury from external trauma. J Urol 1988; 140:1435–6.
[10] Blaivas M, Brannam L. Testicular ultrasound. Emerg Med Clin North Am 2004;22:723–48, ix.
[11] Jeffrey RB, Laing FC, Hricak H, et al. Sonography of testicular trauma. AJR Am J Roentgenol 1983; 141:993–5.
[12] Seng YJ, Moissinac K. Trauma induced testicular torsion: a reminder for the unwary. J Accid Emerg Med 2000;17:381–2.
[13] Horstman WG, Middleton WD, Melson GL, et al. Color Doppler US of the scrotum. Radiographics 1991;11:941–57 [discussion: 958].
[14] Kursh ED. Traumatic torsion of testicle. Urology 1981;17:441–2.
[15] Tsai HN, Wu WJ, Huang SP, et al. Bilateral traumatic testicular dislocation—a case report. Kaohsiung J Med Sci 2002;18:95–8.
[16] Nagarajan VP, Pranikoff K, Imahori SC, et al. Traumatic dislocation of testis. Urology 1983; 22:521–4.
[17] Pollen JJ, Funckes C. Traumatic dislocation of the testes. J Trauma 1982;22:247–9.
[18] O'Brien MF, Collins DA, McElwain JP, et al. Traumatic retrovesical testicular dislocation. J Urol 2004;171:798.
[19] Kochakarn W, Choonhaklai V, Hotrapawanond P, et al. Traumatic testicular dislocation: a review of 36 cases. J Med Assoc Thai 2000;83:208–12.
[20] Feder M, Sacchetti A, Myrick S. Testicular dislocation following minor scrotal trauma. Am J Emerg Med 1991;9:40–2.
[21] Chang KJ, Sheu JW, Chang TH, et al. Traumatic dislocation of the testis. Am J Emerg Med 2003; 21:247–9.
[22] Wu CJ, Tsai WF, Tsai JL, et al. Bilateral traumatic dislocation of testes. J Chin Med Assoc 2004;67: 311–3.
[23] Lupetin AR, King W 3rd, Rich PJ, et al. The traumatized scrotum. Ultrasound evaluation. Radiology 1983;148:203–7.
[24] Martinez-Pineiro L Jr, Cerezo E, Cozar JM, et al. Value of testicular ultrasound in the evaluation of blunt scrotal trauma without haematocele. Br J Urol 1992;69:286–90.
[25] Gordon LM, Stein SM, Ralls PW. Traumatic epididymitis: evaluation with color Doppler sonography. AJR Am J Roentgenol 1996;166:1323–5.
[26] Dogra VS, Bhatt S. Acute scrotal pain: imaging evaluation for a more specific diagnosis. 1st edition. Oak Brook (IL): RSNA; 2006.
[27] Takasu A, Morita K, Kaneko N, et al. Spermatic cord injury associated with blunt trauma. Am J Emerg Med 2005;23:806–7.
[28] McKenney MG, Fietsam R Jr, Glover JL, et al. Spermatic cord hematoma: case report and literature review. Am Surg 1996;62:768–9.
[29] Gordon JN, Aldoroty RA, Stone NN. A spermatic cord hematoma secondary to varicocele rupture from blunt abdominal trauma: a case report and review. J Urol 1993;149:602–3.
[30] Learch TJ, Hansch LP, Ralls PW. Sonography in patients with gunshot wounds of the scrotum: imaging findings and their value. AJR Am J Roentgenol 1995;165:879–83.
[31] Bhatt S, Kocakoc E, Rubens DJ, et al. Sonographic evaluation of penile trauma. J Ultrasound Med 2005;24:993–1000 [quiz: 1001].
[32] Dogra V, Bhatt S. Erectile dysfunction and priapism. 1st edition. Philadelphia: Hanley and Belfus; 2004.
[33] Benson CB, Doubilet PM, Richie JP. Sonography of the male genital tract. AJR Am J Roentgenol 1989;153:705–13.
[34] Cummings JM, Parra RO, Boullier JA. Delayed repair of penile fracture. J Trauma 1998;45:153–4.
[35] Fergany AF, Angermeier KW, Montague DK. Review of Cleveland clinic experience with penile fracture. Urology 1999;54:352–5.
[36] Zargooshi J. Penile fracture in Kermanshah, Iran: report of 172 cases. J Urol 2000;164:364–6.
[37] Pryor JP, Hill JT, Packham DA, et al. Penile injuries with particular reference to injury to the erectile tissue. Br J Urol 1981;53:42–6.
[38] Hinev AI. Re: penile injury. J Urol 2002;167: 1802–3.
[39] Bitsch M, Kromann-Andersen B, Schou J, et al. The elasticity and the tensile strength of tunica albuginea of the corpora cavernosa. J Urol 1990; 143:642–5.
[40] Choi MH, Kim B, Ryu JA, et al. MR imaging of acute penile fracture. Radiographics 2000;20: 1397–405.
[41] Koga S, Saito Y, Arakaki Y, et al. Sonography in fracture of the penis. Br J Urol 1993;72:228–9.
[42] Forman HP, Rosenberg HK, Snyder HM 3rd. Fractured penis: sonographic aid to diagnosis. AJR Am J Roentgenol 1989;153:1009–10.
[43] Tsang T, Demby AM. Penile fracture with urethral injury. J Urol 1992;147:466–8.
[44] Berman LH, Bearcroft PW, Spector S. Ultrasound of the male anterior urethra. Ultrasound Q 2002; 18:123–33.

[45] Doubilet PM, Benson CB, Silverman SG, et al. The penis. Semin Ultrasound CT MR 1991;12: 157–75.
[46] Bertolotto M, Mucelli RP. Nonpenetrating penile traumas: sonographic and Doppler features. AJR Am J Roentgenol 2004;183:1085–9.
[47] Pavlica P, Barozzi L, Menchi I. Imaging of male urethra. Eur Radiol 2003;13:1583–96.
[48] Matteson JR, Nagler HM. Intracavernous penile hematoma. J Urol 2000;164:1647–8.
[49] Haq A, Doble A. Idiopathic corpus cavernosal haemorrhage. Int J Impot Res 2001;13:46.
[50] Bujons Tur A, Rodriguez-Ledesma JM, Cetina Errando A, et al. [Penile hematoma secondary to rupture of the superficial dorsal vein of the penis]. Arch Esp Urol 2004;57:748–51.
[51] Sharma GR. Rupture of the superficial dorsal vein of the penis. Int J Urol 2005;12:1071–3.
[52] Sadeghi-Nejad H, Dogra V, Seftel AD, et al. Priapism. Radiol Clin North Am 2004;42: 427–43.
[53] Shapiro RH, Berger RE. Post-traumatic priapism treated with selective cavernosal artery ligation. Urology 1997;49:638–43.

ELSEVIER SAUNDERS

ULTRASOUND CLINICS

Ultrasound Clin 2 (2007) 57–71

Male Erectile Dysfunction

Hossein Sadeghi-Nejad, MD[a,b,c], Daniel Brison, MD[a], Vikram Dogra, MD[d,*]

Definitions and epidemiology

Erectile dysfunction (ED) is defined as the persistent or repeated inability, for a duration of at least 6 months, to attain or maintain an erection sufficient for satisfactory sexual performance [1]. Although the terms impotence and ED had been used interchangeably for many years, in 1992 a panel at the National Institutes of Health (NIH) Consensus Conference on Impotence recommended that the term erectile dysfunction be used instead of impotence to move away from the inaccuracy and negative connotations of the latter term. The current NIH definition allows a broader definition of ED by deemphasizing intercourse as the only objective parameter of sexual function.

Approximately 18 to 30 million men in the United States are estimated to be affected by ED. Atherosclerotic vascular disease, hypertension, diabetes mellitus, hypercholesterolemia, heart disease, cigarette smoking, and aging are important risk factors that are known to be associated with a higher prevalence of ED. The Massachusetts Male Aging Study (MMAS), a population-based questionnaire survey of 1290 men between the ages of 40 and 70, is considered to be one of the most important epidemiologic studies highlighting ED. The MMAS revealed the presence of ED in 52% of the volunteers. The age-adjusted prevalence of complete ED was 39% in men who had coronary artery disease, 15% in men who had hypertension, and 25% in men who had diabetes [2]. A subsequent

[a] Department of Surgery, Division of Urology, UMDNJ New Jersey Medical School, 20 Prospect Avenue, #711, Hackensack, NJ 07601, USA
[b] NJ Veterans Affairs Hospitals, 20 Prospect Avenue, #711, Hackensack, NJ 07601, USA
[c] Center for Male Reproductive Medicine, Hackensack University Medical Center, Hackensack, 20 Prospect Avenue, #711, Hackensack, NJ 07601, USA
[d] Department of Imaging Sciences, University of Rochester School of Medicine, 601 Elmwood Avenue, Box 648, Rochester, NY 14642, USA
* Corresponding author.
E-mail address: vikram_dogra@urmc.rochester.edu (V. Dogra).

1556-858X/07/$ – see front matter
doi:10.1016/j.cult.2007.01.005
ultrasound.theclinics.com

longitudinal evaluation of the original cohort of men aged between 40 and 69 years suggested that 617,715 new cases of ED are expected to occur in the United States every year and that the number of men affected by ED will increase in a constant manner as the world's population continues to age [3].

Perhaps the most important contribution of the MMAS was the concrete demonstration that ED is an age-dependent pathology. The study showed that the probability of complete and moderate ED increased linearly between the ages of 40 and 70; by age 70, only 32% portrayed themselves as free of ED. Other risk factors, such as cigarette smoking, increased the probability of total ED in men who had treated heart disease, hypertension, or untreated arthritis [2]. Diabetes, heart disease, and hypertension were noted to be important risk factors for ED: men treated for diabetes, heart disease, and hypertension had significantly higher probabilities for ED (28%, 39%, and 15%, respectively) than the sample as a whole (9.6%) after adjusting for age. Yet another significant and more recent epidemiologic study is the National Health Social and Life Survey, a population survey of 1410 men aged 18 to 59 that reported a 31% prevalence of male sexual dysfunction [4]. The three most common male sexual dysfunctions noted in this important study were premature ejaculation (21%), hypogonadism (5%), and ED (5%).

Several other investigations have highlighted the association of aging and ED. A study of the prevalence of ED in Japanese men demonstrated a significant increase in prevalence with aging among 2311 Japanese men between 23 and 79 years of age [5]. Similarly, a comparison of age-related prevalence of ED among 289 Japanese and 2115 American men by Masumori and colleagues [6] indicated an age-related decline in erectile function, sexual libido, and sexual satisfaction: 80% of men aged 70 to 79 years perceived sexual drive once or less during the past month and 71% reported having erections only "a little of the time or less" when sexually stimulated.

Another epidemiologic study from Europe demonstrated an approximately 22% prevalence of ED in Dutch men 50 to 54 years of age, in contrast to an approximately 54% prevalence in men 70 to 78 years old [7]. A sharp age-related increase in the prevalence of ED was also shown by Braun and colleagues [8], who mailed a validated questionnaire on male ED to a sample of 8000 men (30 to 80 years of age) in Germany. Evaluation of the questionnaires from 4489 respondents revealed the overall prevalence of ED to be 19.2%.

To compare the independent effects of aging on ED to the effects of comorbidities typically associated with aging, a group of investigators performed an evaluation of ED in men 65 to 75 years of age in comparison to men older than 75 years of age. The findings indicated that age alone increased the relative risk for sexual dysfunction (relative risk 2.2 for men 65 to 75 years old and 7.9 for those older than 75). In addition, self-reported poor health, diabetes, and bowel or urinary incontinence increased the risk for sexual dysfunction in all age groups. The authors thus demonstrated that aging, along with the comorbidities that are often associated with aging, may independently or synergistically contribute to ED [9].

Sonographic penile anatomy

The penis is composed of the paired corpora cavernosa (erectile bodies) and the corpus spongiosum, the tissue that surrounds the urethra. Ejaculation is facilitated by the rhythmic contractions of the bulbospongiosus muscles surrounding the corpus spongiosum in the bulbar region of the penis. The tunica albuginea is the fibrous tissue surrounding the outer covering of the corpus cavernosum. Pathologic fibrous tissue plaque formation in the subtunical layer (Peyronie's disease) results in decreased elasticity of the tunica albuginea, penile curvature, and venoocclusive ED [10]. Lacunar spaces are specialized, widely-communicating endothelial-lined vascular spaces in the interior of the corpus cavernosum that are surrounded by the trabeculae consisting of connective tissue and corporal smooth muscle.

Penile blood supply is from the internal pudendal artery and its three terminal branches: the bulbourethral, cavernosal, and dorsal penile arteries. Blood vessels and nerves run between the tunica albuginea and the Buck's fascia, a thick, elastic layer that surrounds the tunica albuginea. The accessory pudendal artery is a source of additional blood supply to the corpora cavernosa; this artery may have a critical role in men who have undergone radical pelvic surgery with compromised pudendal arterial blood supply [11]. Within the corpora, the cavernosal artery branches into the helicine arterioles, resistance vessels that open into the lacunar spaces.

Venous blood from the cavernosal sinusoids drains initially into a series of subtunical venules that coalesce into emissary veins. The latter pierce through the tunica albuginea and empty into the deep dorsal vein, directly or by way of the circumflex veins [12]. Extratunical venous drainage occurs by way of the deep dorsal, cavernous/crural, and superficial dorsal veins. Through the emissary and circumflex veins, most of the venous flow from the distal corpora drains into the deep dorsal veins

that empty into Santorini's vesicoprostatic plexus. The cavernosal and crural veins drain the proximal corporal bodies and lead to Santorini's vesicoprostatic plexus and the internal pudendal vein. The superficial dorsal vein drains blood from the pendulous penile skin and glans and communicates with the deep dorsal vein. In each corpus cavernosum, bundles of smooth muscle cells embedded in a matrix of connective tissue and fibroblasts form a series of endothelium-lined blood-filled lacunar spaces [13]. In the flaccid state, the trabecular smooth muscle and the central cavernosal and branching helicine arteries within each cavernosal body are constricted and lacunar venous blood passes unimpeded from the subtunical to the emissary to the extratunical veins.

The pudendal nerve provides the main somatic innervation of the penis. It is composed of efferent fibers that innervate the striated musculature of the perineum and of afferent fibers from the penile and perineal skin [14]. Increased blood flow to the penis is facilitated by sacral parasympathetic stimulation and subsequent dilation of the cavernosal and helicine arteries, eventually resulting in a rigid erection. Concomitant relaxation of the trabecular smooth muscle greatly increases the compliance of the cavernosal bodies and allows the lacunar spaces to expand and accommodate the enhanced blood flow. The subtunical venules become stretched and compressed, thus forming the primary site of venous outflow resistance (the venoocclusive mechanism) during penile erection. The cavernous and crural veins (the deep system) are the main drainage system of the corpora cavernosa and a main source of "leakage" or failure-to-maintain venogenic ED.

Erectile physiology

Erection is a neurovascular event that is governed by the delicate balance between the contractile and relaxation properties of the penile corporal smooth muscle. Normal erectile tissue is composed of trabecular smooth muscle (approximately 50%) and extracellular matrix providing a fibroelastic framework. The corporal smooth muscle is contracted in the flaccid state and relaxed in the erect state. Following sexual stimulation, initially contracted helicine arteriolar smooth muscle undergoes relaxation.

Relaxation of arterial and trabecular smooth muscle results in dilation of the cavernosal and helicine arteries, increased arterial blood inflow across the endothelial cells lining the lacunar spaces, and penile engorgement. Penile rigidity is achieved by increased resistance to the outflow of blood that occurs as the trabecular walls expand against the tunica albuginea and the subtunical venules are compressed (ie, the venoocclusive mechanism) [15,16].

Central mechanism of erection

Erection may occur as a result of local sensory stimulation of the genital organs or by central psychogenic stimuli [14,17]. Most of the critical cerebral regulatory functions for erection occur in the hypothalamus and the limbic system. Sexual drive and psychogenic initiation of erection occur in the medial preoptic area of the brain. The medial preoptic area and the paraventricular nucleus within the hypothalamus are involved in the integration of the visual (occipital area), tactile (thalamus), olfactory (rhinencephalon), and imaginative (limbic system) input; they send neural projections to the thoracolumbar sympathetic and sacral parasympathetic centers of the spinal cord [18]. Activation of the inferior temporal cortex, right insula, right inferior frontal cortex, and left anterior cingulated cortex of the brain by visual evoked sexual arousal has been identified by positron emission tomography [19].

The locus caeruleus and nucleus paragigantocellularis (nPGi) in the brain stem exert an inhibitory effect on sexual arousal, whereas dopamine and oxytocin are believed to play important roles in mediating the pre-erectile response in the medial preoptic area and the paraventricular nucleus respectively [20,21]. Inhibition of serotonin release from the nPGi nerves projecting to sacral segments of the spinal cord may be involved in depression of sexual function by serotonin reuptake inhibitors (SSRIs). It has been suggested that episodes of nocturnal penile tumescence during rapid eye movement (REM) sleep may occur because of suppressed activity of the locus caeruleus and withdrawal of sympathetic input [20,22]. Somatic sensation from genital skin is collected by the pudendal nerve, the afferent limb for reflexogenic erections. The autonomic nerve fibers that arise from the sacral parasympathetic center (S_2–S_4) make up the efferent limb for this reflex, innervating the penile smooth muscle. Control of penile erection is likely to be regulated by synergistic function of the reflexogenic and psychogenic erectile mechanisms [14,17,23–25].

Following sexual stimulation, neuronal-mediated arterial filling is the first event in the corpora cavernosa. This process enables neuronal and endothelial-mediated trabecular smooth muscle relaxation. The subsequent volume change in the corpora cavernosa stretches the subtunical venules, creating venous outflow resistance and increased intracavernosal pressure. Elevation in intracavernosal pressure with continued filling further compresses

the subtunical venules and eventually results in penile rigidity. Axial penile rigidity is defined as the ability of the erect penis to resist buckling from vaginal-mediated axial loads and is affected by intracavernosal pressure, penile tissue mechanical properties, and penile geometry. Neuronal-mediated smooth muscle contraction with restoration of corporal venous drainage results in detumescence.

Peripheral and neurogenic mechanisms of erection

Erectile function in the penis is regulated by autonomic (parasympathetic and sympathetic) and somatic (sensory and motor) pathways. Innervation of the penis is through three sets of peripheral nerves: the sympathetic, parasympathetic, and the pudendal nerves. The main role of the sympathetic system in the regulation of the erectile process is in the initiation and maintenance of arterial and trabecular smooth muscle contraction (the flaccid state). The sympathetic nerves (T10–L2) responsible for detumescence and maintenance of flaccidity project to the corpora, the prostate, and bladder neck by way of the hypogastric nerves. Further detailed description of the role of α-adrenergic receptors in the physiology of penile erection is beyond the scope of this article, but is thoroughly reviewed by Traish and colleagues [26] elsewhere.

The major excitatory input to the penis is provided by the parasympathetic nerves originating from the S2–S4 spinal cord segments. These nerves exit through the sacral foramina and pass forward lateral to the rectum as the pelvic nerve (the efferent pathway) and are joined by the preganglionic parasympathetic nerves originating from S2–S4. The pelvic nerves synapse with postganglionic nonadrenergic, noncholinergic (NANC) nerve fibers in the pelvic plexus and give rise to the cavernous nerve of the penis that innervates the corpora cavernosa.

Stimulation of the pelvic nerves causes a marked increase in flow through the pudendal arteries and entrance of blood into the cavernosal spaces. Penile stimulation in a healthy man causes reflexogenic erections that are primarily controlled by the sacral parasympathetic nerves originating in the spinal cord segments S2–S4. The afferent limb of the erection response is mediated by the dorsal penile nerve (a branch of the pudendal nerve), which transmits sensory impulses to the spinal cord (Table 1).

Nitric oxide (NO) is the primary mediator of NANC parasympathetic input to the penis. NO directly activates guanylate cyclase and is apparently synthesized on demand with little or no storage requirement. Shear stress in the endothelial cell from the increased blood flow activates e-NOS (endothelial nitric oxide synthase), thereby leading to the formation of citrulline (metabolically inactive) and NO from L-arginine and molecular oxygen. Nitric oxide can also be produced by activation of n-NOS (neural nitric oxide synthase) following sexual stimulation. Nitric oxide is a gas and diffuses into the corporal smooth muscle cytosol. The oxygen portion of NO attaches to the heme component of the soluble guanylyl cyclase. This event exposes the active site of the enzyme and leads to conversion of GTP to the second messenger, cGMP (cyclic guanosine monophosphate). The increase in cytosolic cGMP in turn leads to the activation of the cGMP-dependent protein kinase, a lowering of intracellular calcium, and induction of corporal smooth muscle relaxation as previously described. This latter process can only occur if the partial pressure of oxygen in the lacunar spaces is greater than 50 mmHg (ie, after helicine arteriolar dilation and exposure of the lacunar space to systemic arterial blood). During the transition of the penis from the flaccid to the erect state, oxygen tensions change rapidly from venous (?35 mm Hg) to arterial (?100 mm Hg) levels in cavernosal blood. The synthesis of NO is inhibited in low oxygen tension, preventing relaxation of trabecular smooth muscle.

It has been demonstrated that, in addition to guanylate cyclase, NO has other intracellular targets with which it can interact directly and may modulate the contractility of smooth muscle cells independently of the cGMP pathway [27,28]. The levels of cGMP are regulated by phosphodiesterases (PDEs), a superfamily of hydrolytic enzymes that act on cyclic nucleotides and terminate signal transduction. Several PDE subfamilies with different cyclic adenosine monophosphate or cGMP

Table 1: **Neurologic pathways of the erectile and ejaculatory response**

Response	Afferent	Spinal cord	Efferent
Reflexogenic erection	Pudendal nerve	S2–S4 Sacral parasympathetics	Pelvic nerves
Psychogenic erection	Cerebral	Suprasacral	Pelvic nerves
Emission	Pudendal nerve	Lumbosacral	Sympathetic nerves
Ejaculation	Pudendal + pelvic splanchnic nerves	S2–S4	Somatic efferents

specificities and tissue localizations have been identified in mammalian tissues. PDEs hydrolyze cGMP and cyclic adenosine monophosphate; they play a key role in the physiology of erection. Messenger RNA transcripts specific for 14 different human PDE isoenzymes in human corpus cavernosum have been demonstrated in studies using reverse transcriptase–polymerase chain reaction. PDE2, PDE3, PDE4, and PDE5 are the dominant active isoforms in erectile tissue [29].

Current FDA-approved oral medications for treatment of ED are inhibitors of the type 5 phosphodiesterase (PDE5). There are three isoforms of this enzyme in human penile tissue: PDE5A1, PDE5A2, and PDE5A3 [30]. Other neurotransmitters and neuromodulators expressed in penile tissue and associated nerves include vasoactive intestinal polypeptide, calcitonin gene-related peptide, substance P, pituitary adenylate cyclase–activity peptide, adenosine triphosphate, serotonin (5-HT), dopamine, oxytocin, and histamine [31]. The exact function of these molecules in the regulation of normal erectile response has not been conclusively demonstrated. Vasoactive intestinal peptide (VIP) and nitric oxide (NO), both NANC neurotransmitters, are often colocalized in the same nerves in penile tissue. The neurotransmitters norepinephrine, rho-kinase, prostaglandins, and endothelins have vasoconstrictive properties and play a putative role in erectile physiology [32–34].

Cholinergic nerves modulate the activity of NANC nerves through facilitation of NANC relaxation by stimulating the synthesis and release of vasodilatory neurotransmitters including NO. Acetylcholine (Ach) release may thus coordinate the withdrawal of adrenergic input and increase of NANC input by binding to muscarinic receptors on adrenergic and NANC nerves [22]. Decreased synthesis or release of Ach in certain disease states, such as diabetes, may contribute to compromised erectile function [35].

Vascular endothelium is another source of NO synthesis and release. Ach and bradykinin bind their respective membrane receptors and increase intracellular Ca^{2+} within endothelial cells. Shear stress and other physical stimuli also enhance NO production in endothelium as previously described (ie, with trabecular volume expansion secondary to increased blood flow). Endothelium-derived and nerve-derived NO have a similar mode of action.

Prostaglandins are prostanoids produced by the action of cyclooxygenases on arachidonic acid. They may play an important role in the production of extracellular matrix and act locally to exert trophic and tonic effects in an autocrine and paracrine manner. Relaxation and contraction of smooth muscle may occur; however, prostaglandin E1 (PGE) is the only endogenous prostaglandin that seems to elicit relaxation of human trabecular smooth muscle.

Causes of erectile dysfunction

There may be several psychogenic or organic causes for ED (Box 1). A significant proportion of patients may have coexisting factors that affect their sexual performance. Patients who have psychiatric disease may suffer from additional organic impotence that causes considerable secondary anxiety. Intermittent erectile failure in younger patients is frequently caused by psychogenic factors, whereas ED in older men is more likely to involve an organic factor alone or in combination with psychogenic stressors [36]. Damaged or malfunctioning endothelium (endothelial dysfunction) is a common denominator in cardiovascular disease, hypertension, diabetes mellitus, depression, and many other disease states associated with ED [37,38]. Lifestyle issues, including obesity, a sedentary lifestyle, and alcohol and tobacco use, and vasculogenic, neurogenic, endocrinologic, structural (traumatic), and pharmacologic causes may contribute to ED.

Pathophysiology of erectile dysfunction

Decreased concentration of penile elastic fibers associated with aging results in a reduction in elasticity that could contribute to ED in elderly men. Older men have been shown to have a decreased

Box 1: Causes of erectile dysfunction

Organic
Arteriogenic
- Inflammatory: prostatitis, stricture, urethritis
- Mechanical: chordee, phimosis, Peyronie's disease, obesity
- Postoperative: nerve or vascular injury (ie, radical prostatectomy, shunts for priapism)
- Occlusive: atherosclerosis, pelvic injury
- Traumatic: pelvic fracture, urethral rupture
- Endurance: chronic and systemic diseases
- Chemical: alcohol, prescription drugs, marijuana
- Endocrine: testicular failure, pituitary failure (hypogonadotropic hypogonadism), hyperprolactinemia

Neurogenic
- Neuropathy, temporal lobe epilepsy, multiple sclerosis

Nonorganic
Psychogenic

concentration of type III collagen, increased type I collagen, and a decrease of up to 35% in the smooth muscle content of the penis [10]. Additionally, altered collagen content of the penis may result in chronic ischemia and loss of smooth muscle cells [39]. The consequent reduction in the ratio between cavernosal smooth muscle and connective tissue, along with the decreased filling and compliance of vascular spaces, has been associated with increased likelihood of diffuse venous leak and resultant ED [40]. Box 2 demonstrates the various causes and their contributing risk factors.

Evaluation

The ideal evaluation protocol is a biopsychosocial approach that encompasses the complete sequence of male sexual function: hypogonadism, ED, ejaculatory dysfunction, lower urinary tract symptoms, and various psychosocial issues, including depression, relationship factors, partner issues, and social stressors. Evaluation of potential partner issues, both psychologic and physiologic, and understanding these factors as contributors to ED, cannot be overemphasized.

A multidisciplinary approach to the above-mentioned problems, with involvement from the urologist, psychologist, endocrinologist, and psychiatrist, may be best for dealing with ED in an ideal environment. In a real-world setting, however, it is important to assume that, at least for the purposes of the first visit, the evaluation will be performed without input from multiple specialties. A thorough history and physical examination are therefore critical and of paramount importance.

Sexual history

The onset, duration, and circumstances of ED must be elicited. Questions are posed concerning erection quality during intercourse, masturbation, and nocturnal erections. The degree of axial penile rigidity (hardness) can be quantitated by using a 1 to 10 scale. Validated sexual questionnaires, such as the International Index of Erectile Function, may be helpful tools in the evaluation of erectile function [41]. The degree of erection maintenance and spontaneity (effort, concentration, and time) required to achieve an erection relative to previous capabilities must be known. Associated abnormalities (or changes) in ejaculation, libido, or orgasm should also be noted. A psychogenic cause is suggested by sudden onset of impotence or the presence of impotence under some circumstances, but normal erectile function at other times. A gradual deterioration of erectile quality with preservation of libido is more likely to be caused by an organic risk factor.

Box 2: Partial list of medications and drugs that have been associated with erectile dysfunction

Centrally acting agents
Marijuana
Reserpine
Clonidine
Alpha-methyldopa
Tricyclic antidepressants
Phenothiazines
Narcotics
Ethanol

Anticholinergic agents
Antihistamines
Antimuscarinic agents
Tricyclic antidepressants
Phenothiazines

Antiandrogenic agents
Estrogens
Spironolactone
Cyproterone acetate
Disopyramide
Ketoconazole
Cimetidine

Hyperprolactinemic agents
Phenothiazines
Estrogen
Haloperidol
Metoclopramide
Imipramine
Opiates
Reserpine
Alpha-methyldopa

Sympatholytic agents
Alpha blockers
Guanethidine
Reserpine
Clonidine
Bretylium
Beta blockers
Alpha-methyldopa

Agents with other properties or unknown mechanism causing erectile dysfunction
Epsilon-aminocaproic acid
Naproxen
Digoxin
Thiazides

Most patients who have impotence can ejaculate despite poor quality or absent erections.

Medical history

Inquiry is made about the patient's past and present medical problems, including diabetes mellitus, hypertension, smoking, hyperlipidemia, and liver, renal, vascular, neurologic, psychiatric, or endocrine disease. A history of abdominal, pelvic, or perineal

surgery or trauma, including possible bicycle injury, is informative. Use of androgenic steroids and related substances by athletes mandates inquiries about these agents as they are associated with decreases serum testosterone levels and decreased libido.

Psychologic evaluation

A brief psychosocial history is mandatory to gain insight into potential personal, interpersonal, social, and occupational roots of sexual problems. When deemed appropriate, an interview with a psychologist or sex therapist may be helpful to uncover personality disorders or the relation of psychologic factors to ED (ie, performance anxiety causing ED or organic ED leading to anxiety). The expectations of the couple from the planned therapy are assessed.

Physical examination

In addition to a focused examination of the genitalia, the general body habitus and status of secondary sexual characteristics should be assessed. The presence, size, and consistency of the testes are determined by palpation. The presence of small testes may suggest hypogonadism as a cause of ED. Gynecomastia may be present in patients who have androgen deficiency or estrogen excess. Vascular insufficiency is suspected with absent peripheral pulses in the lower extremities. Careful examination of the penis, including evaluation in the stretched and nonstretched positions, is performed to assess adequacy of length, fibrotic plaques in the tunica albuginea (Peyronie's disease), or deformity of the corporal bodies. Pinprick testing of the penile and perineal skin may provide information about the sensory function of the pudendal nerve. Similarly, eliciting the bulbocavernosus reflex provides information about the integrity of the sacral reflexes. A digital rectal examination of the prostate to screen for prostate cancer is wise in men older than 50 (age 40 if African American or with a positive family history of prostate cancer).

Laboratory tests

Hormonal status and evaluation of the integrity of the hypothalamic–pituitary–gonadal axis is performed by checking the serum testosterone, luteinizing hormone (LH), and serum prolactin levels. Standard serum chemistries, complete blood cell count, and lipid profiles may reveal vascular risk factors. The serum prostate specific antigen (PSA) should be ordered in men over the age of 50 (age 40 if African American or with a positive family history of prostate cancer) to screen for possible prostate cancer. A higher incidence of prostate cancer in men who have ED has not been demonstrated. This test is done for routine male screening, therefore, rather than ED-associated prostate cancer screening [42]. Diurnal variations in testosterone levels are seen and one abnormal value may not be reliable. If both LH and testosterone levels are decreased, hypogonadotrophic hypogonadism is suspected and warrants consultation with an endocrinologist. If a low serum testosterone is confirmed, it is mandatory to check serum prolactin levels to rule out the presence of pituitary adenomas.

Specialized diagnostic testing

The introduction of sildenafil in 1998 dramatically changed the need for specialized testing. As a general rule, although these diagnostic modalities help uncover pathophysiologic mechanisms and further confirm the impressions discovered on the initial evaluation, their disadvantages, including cost and associated potential complications, have lead to reduced indications for routine testing.

Nocturnal penile tumescence and rigidity (NPTR) refers to the assessment of changes in penile circumference that occur during REM sleep (eg, Rigiscan, strain gauge and plethysmography). NPTR has been used to distinguish organic from psychogenic ED, but its validity remains controversial. False positive results may occur because sleep disorders and psychologic stress factors can cause abnormal erectile patterns in patients without any organic pathology. Furthermore, the ability of NPTR to evaluate axial rigidity is poor. Although NPTR is still commonly performed by some practitioners, its use should be limited to a general discrimination of organic versus psychogenic ED because of its low sensitivity and specificity [43].

Penile biothesiometry (vibration testing) is a noninvasive diagnostic modality that is used to assess the threshold for vibratory sensation. Biothesiometry is a limited test because it is not neurophysiologic. It measures vibratory thresholds, provides further understanding of the somatosensory pathway, and has proved helpful in the management of patients who have diabetes and ED.

Sonographic technique for evaluation of the penis

Sonographic examination of the penis is performed with the patient in either the supine or lithotomy (frog leg) position with the penis lying on the anterior abdominal wall or supported with towels between the thighs. Because the structures being imaged lie close to the surface of the transducer, high frequency (7–14 MHz) linear array transducers are used to obtain high-resolution images of the penis. A sufficient amount of sonographic acoustic gel should be used on the surface of the penis to obtain good quality images, and excessive compression by

the transducer should be avoided, especially in trauma patients. Examination is performed in transverse and longitudinal planes starting at the level of the glans and moving toward the base of the penis. A transperineal approach may be used if required to assess the base of the penis. The two corpora cavernosa are homogenous in echotexture and are identified as two hypoechoic circular structures. The tunica albuginea is visualized as a linear hyperechoic structure covering the corpora cavernosa. The cavernosal artery is visualized on the central portion of the corpora cavernosa (Fig. 1). The normal cavernosal artery diameter ranges from 0.3 mm to 1.0 mm (mean 0.3–0.5 mm) in the flaccid state. The corpus spongiosum is often compressed and is difficult to visualize optimally from the ventral aspect. Color Doppler examination of the penis should be performed in transverse and longitudinal planes. Peak systolic velocities of the cavernosal arteries should also be recorded. The cavernosal artery velocity in normal healthy volunteers is 10 to 15 cm/s in the flaccid state [44,45].

Duplex Doppler sonograph

Duplex Doppler sonography is highly reliable and is recommended as a first-line test to evaluate penile arterial and venoocclusive function. The diameters of the cavernous arteries are measured before and after intracavernous injection of vasodilator agent. After injecting a vasodilator, spectral waveforms of the cavernosal arteries and their peak systolic velocities are measured at 5-minute intervals for 25 minutes [44,45].

Doppler evaluation technique of erectile dysfunction

After a detailed clinical evaluation, patients should be informed about the examination procedure and its risks. Doppler ultrasound assessment should be performed in a private setting in a quiet room. To obtain better image quality and spectral data, a 7- to 14-MHz linear array transducer is used for penile Doppler examination. Grayscale examination of the penis is performed to exclude Peyronie's disease. On the ventral side, the corpus cavernosum and cavernous arteries within the corpus cavernosum are identified on the transverse or longitudinal images. The diameter of the cavernous artery is measured on both sides, and the spectral Doppler waveform is recorded. A vasoactive agent is used to stimulate penile erection. Injection of the vasoactive substance results in the physiologic response of erection in normal males and helps to separate patients who have neurogenic or psychogenic dysfunction from those who have vascular disturbances. Several vasoactive agents, including papaverine, phentolamine, and prostaglandin E1, alone or in combination, can be used through the intracavernous route [44,46].

Prostaglandin E1 (PGE1) is preferred because of a lower risk for priapism. Prostaglandin results in physiologic erection in 87% of the subjects studied. PGE1 is injected into the distal two thirds of the shaft of penis in one corpus cavernosum, using a small, 27- to 30-gauge needle [44].

PGE1 is the most accurate diagnostic drug with the lowest prolonged erection rate of 0.1%. The total quantity of PGE1 injected is 10 to 20 μg. Some authors prefer to use PGE1 at a dose of 10 μg followed by a further 10-μg dose 15 minutes later if there is a suboptimal clinical response. A total dose of 20 μg PGE1 produces minimal side effects, but stepwise use is likely to reduce the risk for priapism. After intracavernosal injection of prostaglandin E, 96% of the prostaglandin is locally metabolized within 60 minutes. Priapism is seen in 1% and penile fibrotic lesions are seen in 2% of patients. Papaverine use has fallen out of favor because of its high incidence of postinjection fibrosis.

Intracavernous agents can cause numerous complications, such as pain, ecchymosis, penile hematoma, and prolonged erection in up to 7% to 11%

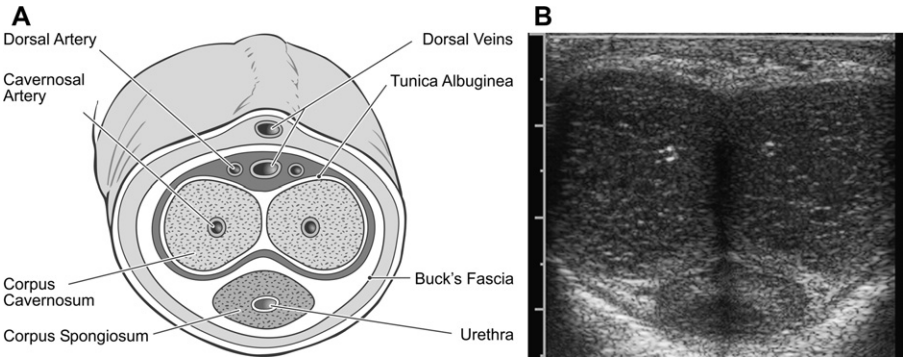

Fig. 1. Diagrammatic representation of penile anatomy in transverse view (*A*) with corresponding gray-scale image (*B*).

of cases [47]. In experienced hands, and for the purposes of diagnostic testing, these adverse events rarely occur or are easily reversible. When an oral vasoactive agent, sildenafil citrate, plus visual sexual stimulation are used alternatively to intracavernosal injection of vasoactive agents for penile Doppler evaluation, similar results to those with PGE1 or papaverine injection can be obtained.

Cavernosal arterial anatomy varies among individuals; hemodynamic parameters differ at various sites of measurement. The peak systolic velocities of the cavernosal arteries should be measured at a constant location, preferably at the junction of the proximal on third and distal two thirds junction of the cavernosal artery.

After injection of vasoactive agents, the cavernous artery diameter is measured and starting at 5 minutes postinjection spectral Doppler waveform in cavernous arteries should be recorded every 5 minutes until 25 minutes elapse. Angle-corrected peak systolic velocity (30° and 60°) of the cavernous artery should be recorded near the proximal third of the penile shaft because the velocities are greatest at this level. The dorsal penile arteries and deep dorsal vein are assessed and peak systolic velocities are then recorded.

Stages of penile erection In the flaccid state there is limited blood supply to the penis. Spectral Doppler waveform of the cavernous artery demonstrates the high resistance wave form. Peak systolic velocities are in the 5 to 15 cm/sec range. In the filling phase there is increased blood flow to the penis by way of the cavernous arteries with characteristic variations in spectral waveforms. The cavernosal arteries dilate and the spectral Doppler waveform is characterized by increasing systolic and diastolic velocities. The helicine arteries also dilate and are seen as tortuous vessels branching from the cavernous arteries that split into several arterioles of smaller size. In the tumescent phase there is progressive decrease in the diastolic velocity and the peak systolic velocity. As a result of venous occlusion, the diastolic flow decreases to zero and then undergoes flow reversal. With maximal rigidity, decreased systolic velocity can be observed. When venous occlusion occurs, the helicine arteries become progressively less visible and disappear with maximum rigidity (rigid phase). During detumescence diastolic flow appears again in the cavernosal arteries and flows are appreciable in the corpus spongiosum, in the circumflex veins, and in the dorsal veins (Fig. 2) [48].

Evaluation of arteriogenic erectile dysfunction

Diagnosis of arterial ED is made based primarily on measurements of diameters of cavernosal arteries and their velocities. The thickness of the cavernous artery wall can be a factor in the assessment of arteriogenic ED (AED). Normal cavernosal arteries have strong, thin walls with strong pulsation, whereas arteries with diffuse atherosclerosis have thick walls with diminished pulsation [49]. Various parameters, such as peak systolic flow velocity, degree of arterial dilatation, and acceleration time, have been suggested, but peak systolic flow velocity is generally accepted to be a more accurate indicator of arterial disease. Because arterial diameter and flow rate change during the various phases of erection, the parameters are measured 5 minutes after injection and measurement of peak systolic velocity is repeated at 5-minute intervals for 25 minutes [44,45]. The average peak systolic velocity after cavernosal injection of vasoactive agents has been found to be 30 to 40 cm/sec in normal volunteers (Fig. 3) [50].

Peak systolic velocities of cavernosal arteries differ and depend on the vasoactive agent used (Table 2). Velocities greater than 25 cm/sec probably are adequate if papaverine is injected; velocities in the 35 to 40 cm/sec range are probably normal if prostaglandins are injected [44]. A peak systolic velocity less than 25 cm/sec in the cavernous artery and dampened waveform are standard diagnostic criteria for arterial insufficiency. The angiographic correlation has shown that a velocity threshold of 25 cm/sec has 92% accuracy in the diagnosis of arterial integrity [51]. When penile angiography is compared with duplex Doppler examination of the same patients, peak systolic velocity less than 25 cm/sec is consistently associated with severe arterial disease [44,51,52].

If patients' peak systolic velocity falls between 25 to 30 cm/sec, diagnosis of AED is suspicious and secondary criteria of arterial disease should be taken into consideration. The secondary diagnostic criteria of arterial insufficiency include failure of cavernous artery dilatation of less than 75%, the presence of focal stenosis, occlusion or retrograde arterial flow, and asymmetry of cavernous peak systolic flow velocities greater than 10 cm/sec. Resistance index (RI) greater than 0.9 is associated with normal results in 90% of patients [44]. Box 3 shows the cavernosal artery peak systolic velocities after prostaglandin injection. The cutoff point for the acceleration time required to discriminate between atherosclerotic and nonatherosclerotic ED have been defined as equal to or greater than 100 milliseconds for atherosclerotic ED [53] (acceleration time is calculated by dividing the peak systolic velocity by the systolic rise time).

It has been reported that spectral Doppler analysis of the cavernous artery in the flaccid penis provides a noninvasive method to assess arterial disease. A cutoff peak systolic velocity value of

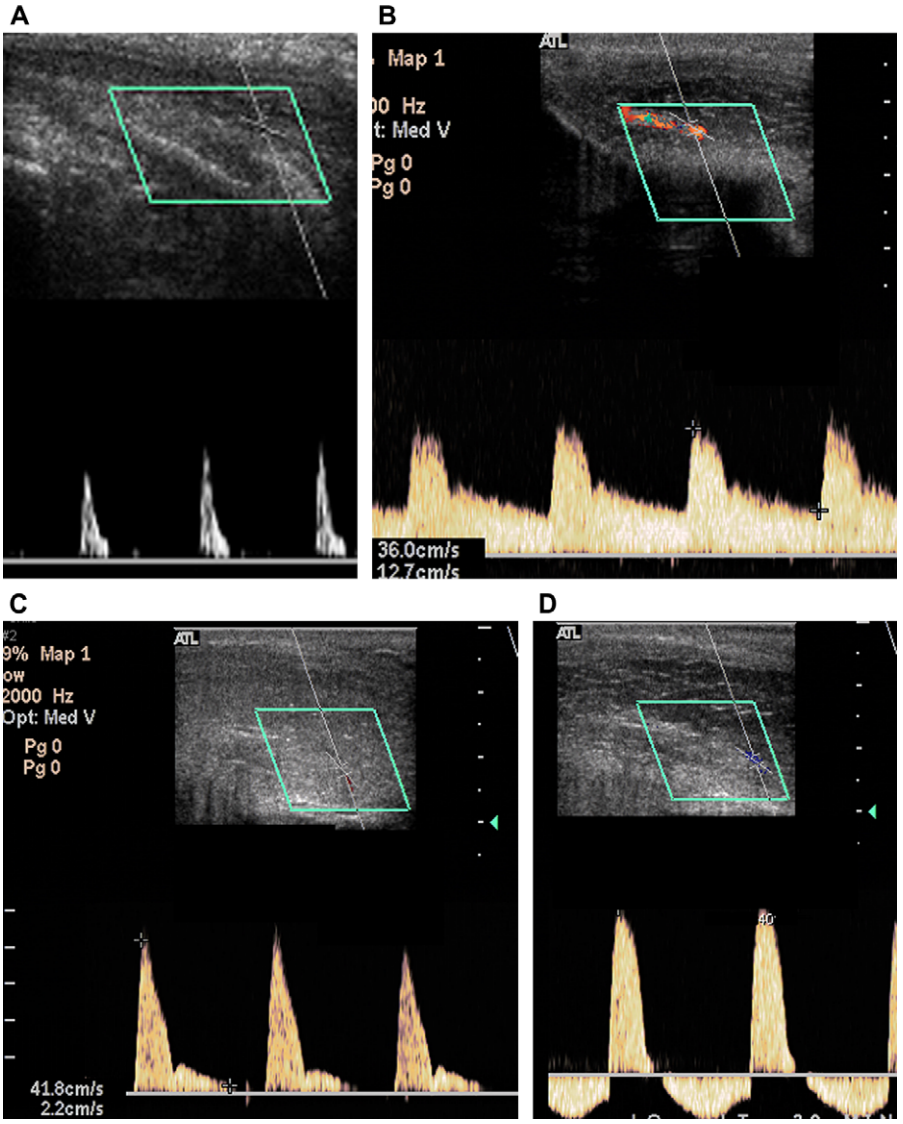

Fig. 2. Stages of penile erection. (*A*) Spectral Doppler tracing demonstrates high resistance flow pattern in flaccid state. (*B*) There is increased diastolic flow in filling phase. (*C*) In tumescent phase there is further increase in the peak systolic velocity with decrease in diastolic blood flow and (*D*) in rigid phase there is reversal of diastolic blood flow, signifying increased resistance to in flow. There may be complete absence of diastolic flow in this stage.

10 cm/sec in the flaccid state in the cavernous artery has been reported to have the best accuracy for predicting arterial insufficiency, with a 96% sensitivity, 92% specificity, and a 93% overall accuracy [54]. The normal velocity criteria have not been definitely established, however, and no data regarding venous abnormalities can be obtained without vasoactive agent injection. If properly performed, duplex Doppler sonography is equal to or may even be superior to pharmacologic arteriography for the diagnosis of arteriogenic impotance.

Evaluation of venous erectile dysfunction

A venous leakage is suspected when there is adequate arterial inflow and erection is obtained but the duration is short and there is persistent antegrade diastolic flow throughout the examination. Using Doppler sonography, diagnosis of venous ED (VED) can be made only if a patient had normal arterial function, (ie, normal peak systolic velocity). An arterial diastolic velocity greater than 5 cm/sec (angle-corrected velocity) throughout all phases of erection constitutes persistent arterial diastolic

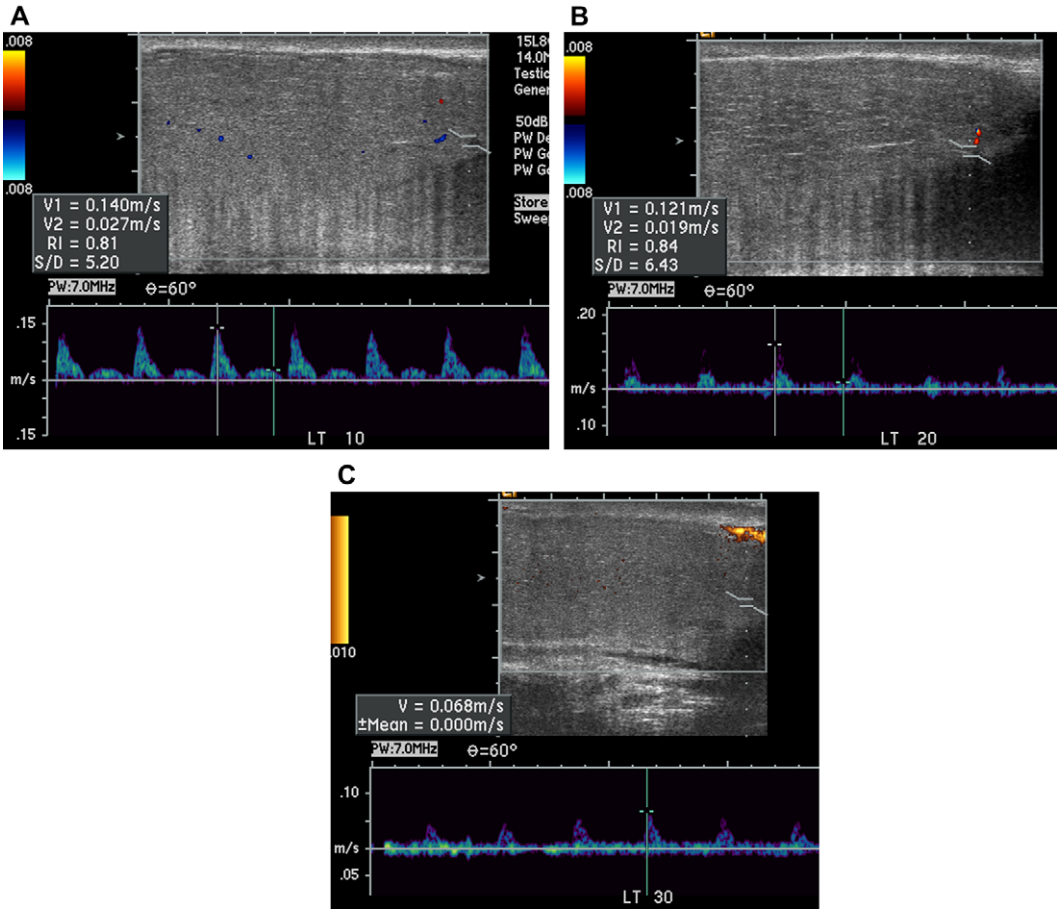

Fig. 3. Arteriogenic erectile dysfunction. The spectral Doppler tracings at (*A*) 10 minutes, (*B*) 20 minutes, and (*C*) 30 minutes post prostaglandin intracavernous injection demonstrate peak systolic velocities in cavernosal artery to be less than 25 cm/s. Similar pattern was observed in the right cavernosal artery.

flow and suggests venous leak (Fig. 4) [44,55]. If a diagnosis of venous leak is made by sonography, further evaluation can be performed by cavernosography and cavernosometry. Persistent blood flow in the dorsal vein also represents venous insufficiency [56]. Demonstration of early blood flow in the dorsal vein has a sensitivity of 80% and specificity 100% on cavernosography for diagnosing VED. RI measurement is also a reliable, noninvasive method for diagnosing venous incompetence. RI is measured at 20 minutes after injection of the vasoactive agent. An RI value of less than 0.75 is associated with venous leakage in 95% of patients, whereas an RI value greater than 0.9 is associated with normal results in 90% of patients. As the pulsatility index reflects the presence of retrograde diastolic flow below the baseline, some authors prefer the pulsatility index to assess venous incompetence

Table 2: **Commonly used drugs with doses for penile Doppler evaluation**

Drug	Dose
Papaverine	30–60 mg
Phentolamine	0.25–1.25 mg[a]
Prostaglandin E1 (alprostadil)	10–20 μg
10 mg papaverine + 0.4 mg phentolamine + 10 μg prostaglandin E1/mL	0.5–1 mL
Sildenafil citrate (oral)	50 mg[b]

[a] This drug may be used with papaverine or prostaglandin E1.
[b] This drug is used with visual sexual stimulation.

Box 3: **Cavernosal artery peak systolic velocities after prostaglandin injection**

Normal range 25–40 cm
25–30 cm/s, borderline
Peak systolic velocities <25 cm/s suggest arterial disease.

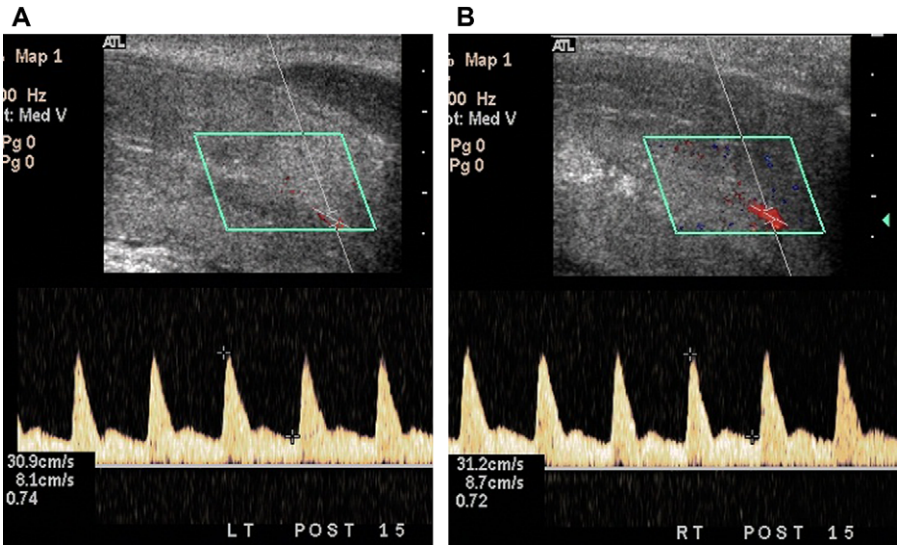

Fig. 4. Venous leak. The peak systolic velocities in cavernosal arteries are greater than 30 cm/s, but there is persistence of diastolic blood flow (>5 cm/s). Same pattern was seen at 25 minutes interval post prostaglandin injection.

and a pulsatility index value less than 4 is used to predict venous incompetence [57].

Occasionally, a suboptimal response to PGE1 injection may be seen and presents as continued forward flow in the diastole because of inadequate venous occlusion, especially in young patients. In this instance, a 2-mg intracavernosal phentolamine, a selective α-adrenergic receptor antagonist, can be injected. Phentolamine blocks the increased sympathetic neuronal activity, thereby producing smooth muscle relaxation that often occurs in the anxious patient during penile ultrasound examination. After phentolamine injection, many patients, especially in this younger age group, exhibit statistically significant increases in grade of erection and peak systolic velocity and a decrease in end diastolic velocity. The use of intracavernosal phentolamine is therefore recommended for ultrasound assessment of venous incompetence, especially in young patients. Alternatively, a rubber band can also be placed at the base of the penis to occlude the dorsal vein and peak systolic velocities in the dorsal vein will then show a decrease and the patient will have a longer period of erection; this is an indirect sign of VED. Deep dorsal vein velocities are summarized in Box 4.

Evaluation of mixed (indeterminate) erectile dysfunction

The diagnosis of mixed arterial and venous ED cannot be made using duplex Doppler sonography because venous competence cannot be assessed in a patient who has arterial insufficiency. In patients who have impaired arterial flow, because the cavernosal sinusoids may never fill to the point of occluding small emissary veins draining the corpora cavernosa, the Doppler findings of venous incompetence, persistent cavernosal arterial diastolic flow, and flow in the dorsal vein may be seen even if the veins are intrinsically normal. When arterial inflow is abnormal with poor erectile response and there is antegrade diastolic flow throughout the examination, it is considered an indeterminate result (Fig. 5).

Other forms of vascular testing include intracavernosal injection testing and studies of the penile brachial index (rarely performed). The incidence of suspected vascular pathology by such vascular testing has ranged from 33% to 87% [58,59]. Selective internal pudendal arteriography is a more invasive test that is indicated if arteriogenic ED is suspected in a candidate for microvascular arterial bypass surgery. Arteriography is usually performed with intravascular and intracavernosal vasodilators with patient sedation to optimize visualization of the cavernosal vessels.

Cavernosometry is the most sensitive test to detect venoocclusive disease, although it is not commonly performed because it is a more invasive test. This test is performed by placing two needles into the corpora. One needle measures cavernosal

Box 4: **Deep dorsal vein velocities**

Normal: <3 cm/s
Moderately increased: 10–20 cm/s
Markedly increased: >20 cm/s

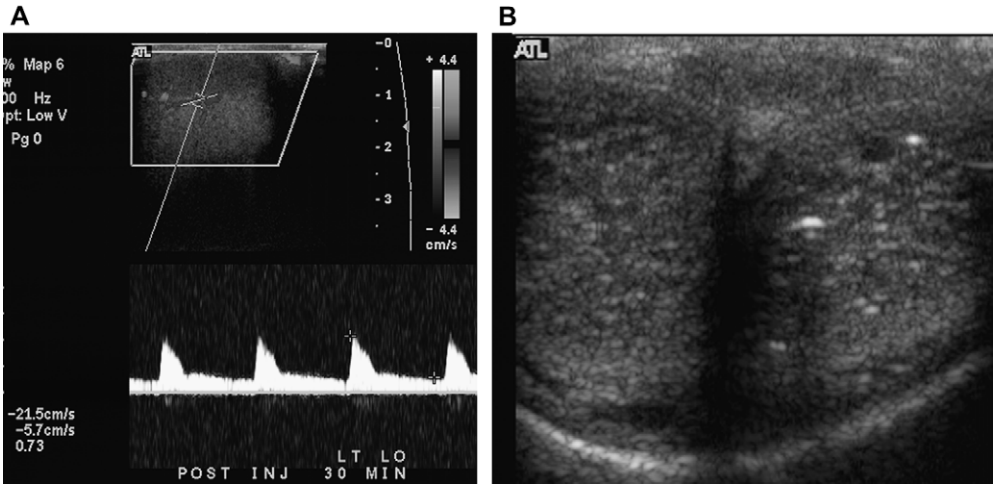

Fig. 5. Mixed erectile dysfunction. The peak systolic velocity at 30 minutes post prostaglandin injection is less than 25 cm/s and there is persistence of diastolic flow (>5 cm/s).

pressure while the other injects heparinized saline generating increasing intercavernosal pressures.

A pharmacologic erection is attained using an injected erectogenic agent (Box 5). Saline is infused into the corpora to pressures of 30, 60, 90, 120, and 150 mm Hg. The flow rate required to maintain these pressures is recorded. The flow of saline needed to maintain a pressure of 150 mm Hg is called the "flow to maintain." A flow of greater than 3 mL/minute represents venoocclusive disease. Pressure decay refers to the decrease in pressure from 150 mm Hg after infusion of saline is terminated. Decline greater than or equal to 45 mm Hg in 30 seconds is another indicator of venoocclusive disease.

An additional indicator of venoocclusive disease is the inability to achieve intracavernosal pressures equal to the mean arterial pressure using peak saline inflow.

Cavernosography is usually performed synchronously with cavernosometry. Radiographic contrast dye is infused into the corpora. Oblique and AP images are taken in an effort to visualize and localize venous leakage. A normal test shows minimal or no venous drainage. In patients who have Peyronie's disease (penile curvature secondary to plaques) and those who have a history of penile fracture, cavernosography reveals focal site-specific abnormalities [60].

***Box 5:* Complications of intracavernosal pharmacotherapy for erectile dysfunction**

Local hematoma
Pain at injection site
Penile induration
Priapism

References

[1] NIH Consensus Conference. Impotence. NIH Consensus Development Panel on Impotence. JAMA 1993;270(1):83–90.
[2] Feldman HA, Goldstein I, Hatzichristou DG, et al. Impotence and its medical and psychosocial correlates: results of the Massachusetts male aging study. J Urol 1994;151(1):54–61.
[3] Johannes CB, Araujo AB, Feldman HA, et al. Incidence of erectile dysfunction in men 40 to 69 years old: longitudinal results from the Massachusetts male aging study. J Urol 2000;163(2):460–3.
[4] Laumann EO, Paik A, Rosen RC. Sexual dysfunction in the United States: prevalence and predictors. JAMA 1999;281(6):537–44.
[5] Marumo K, Nakashima J, Murai M. Age-related prevalence of erectile dysfunction in Japan: assessment by the International Index of Erectile Function. Int J Urol 2001;8(2):53–9.
[6] Masumori N, Tsukamoto T, Kumamoto Y, et al. Decline of sexual function with age in Japanese men compared with American men—results of two community-based studies. Urology 1999; 54(2):335–44 [discussion: 344–5].
[7] Blanker MH, Bosch JL, Groeneveld FP, et al. Erectile and ejaculatory dysfunction in a community-based sample of men 50 to 78 years old: prevalence, concern, and relation to sexual activity. Urology 2001;57(4):763–8.
[8] Braun M, Wassmer G, Klotz T, et al. Epidemiology of erectile dysfunction: results of the 'Cologne Male Survey'. Int J Impot Res 2000;12(6):305–11.
[9] Mulligan T, Retchin SM, Chinchilli VM, et al. The role of aging and chronic disease in sexual dysfunction. J Am Geriatr Soc 1988;36(6):520–4.

[10] Akkus E, Carrier S, Baba K, et al. Structural alterations in the tunica albuginea of the penis: impact of Peyronie's disease, ageing and impotence. Br J Urol 1997;79(1):47–53.
[11] Breza J, Aboseif SR, Orvis BR, et al. Detailed anatomy of penile neurovascular structures: surgical significance. J Urol 1989;141(2):437–43.
[12] Puech-Leao P, Reis JM, Glina S, et al. Leakage through the crural edge of corpus cavernosum. Diagnosis and treatment. Eur Urol 1987;13(3): 163–5.
[13] Goldstein AM, Meehan JP, Zakhary R, et al. New observations on microarchitecture of corpora cavernosa in man and possible relationship to mechanism of erection. Urology 1982;20(3):259–66.
[14] de Groat WC, Steers WD. Neuroanatomy and neurophysiology of penile erection. In: Tanagho EA, Lue TF, McClure RD, editors. Contemporary management of impotence and infertility. Baltimore (MD): Williams & Wilkins; 1988. p. 3–27.
[15] Blanco R, Saenz de Tejada I, Goldstein I, et al. Cholinergic neurotransmission in human corpus cavernosum. II. Acetylcholine synthesis. Am J Physiol 1988;254(3 Pt 2):H468–72.
[16] Ignarro LJ, Bush PA, Buga GM, et al. Nitric oxide and cyclic GMP formation upon electrical field stimulation cause relaxation of corpus cavernosum smooth muscle. Biochem Biophys Res Commun 1990;170(2):843–50.
[17] Weiss HD. The physiology of human penile erection. Ann Intern Med 1972;76(5):793–9.
[18] Giuliano F, Bernabe J, Brown K, et al. Erectile response to hypothalamic stimulation in rats: role of peripheral nerves. Am J Physiol 1997; 273(6 Pt 2):R1990–7.
[19] Stoleru S, Gregoire MC, Gerard D, et al. Neuroanatomical correlates of visually evoked sexual arousal in human males. Arch Sex Behav 1999; 28(1):1–21.
[20] Giuliano F, Rampin O. Central neural regulation of penile erection. Neurosci Biobehav Rev 2000; 24(5):517–33.
[21] Marson L, McKenna KE. The identification of a brainstem site controlling spinal sexual reflexes in male rats. Brain Res 1990;515(1–2):303–8.
[22] Saenz de Tejada I, Kim NN, Goldstein I, et al. Regulation of pre-synaptic alpha adrenergic activity in the corpus cavernosum. Int J Impot Res 2000;12(Suppl 1):S20–5.
[23] Maclean PD, Dua S, Denniston RH. Cerebral localization for scratching and seminal discharge. Arch Neurol 1963;9:485–97.
[24] Saper CB, Loewy AD, Swanson LW, et al. Direct hypothalamo-autonomic connections. Brain Res 1976;117(2):305–12.
[25] Swanson LW, Sawchenko PE. Hypothalamic integration: organization of the paraventricular and supraoptic nuclei. Annu Rev Neurosci 1983;6:269–324.
[26] Traish AM, Kim NN, Goldstein I, et al. Alpha-adrenergic receptors in the penis: identification, characterization, and physiological function. J Androl 1999;20(6):671–82.
[27] Gupta S, Moreland RB, Munarriz R, et al. Possible role of Na(+)-K(+)-ATPase in the regulation of human corpus cavernosum smooth muscle contractility by nitric oxide. Br J Pharmacol 1995;116(4):2201–6.
[28] Stamler JS. Redox signaling: nitrosylation and related target interactions of nitric oxide. Cell 1994;78(6):931–6.
[29] Uckert S, Kuthe A, Stief CG, et al. Phosphodiesterase isoenzymes as pharmacological targets in the treatment of male erectile dysfunction. World J Urol 2001;19(1):14–22.
[30] Lin CS, Lau A, Tu R, et al. Expression of three isoforms of cGMP-binding cGMP-specific phosphodiesterase (PDE5) in human penile cavernosum. Biochem Biophys Res Commun 2000; 268(2):628–35.
[31] Garcia-Reboll L, Mulhall JP, Goldstein I. Drugs for the treatment of impotence. Drugs Aging 1997;11(2):140–51.
[32] Andersson KE. Erectile physiological and pathophysiological pathways involved in erectile dysfunction. J Urol 2003;170(2 Pt 2):S6–13 [discussion: S13–4].
[33] Mills TM, Chitaley K, Lewis RW. Vasoconstrictors in erectile physiology. Int J Impot Res 2001; 13(Suppl 5):S29–34.
[34] Wang H, Eto M, Steers WD, et al. RhoA-mediated Ca2+ sensitization in erectile function. J Biol Chem 2002;277(34):30614–21.
[35] Blanco R, Saenz de Tejada I, Goldstein I, et al. Dysfunctional penile cholinergic nerves in diabetic impotent men. J Urol 1990;144(2 Pt 1): 278–80.
[36] Lue TF. Erectile dysfunction. N Engl J Med 2000; 342(24):1802–13.
[37] Araujo AB, Durante R, Feldman HA, et al. The relationship between depressive symptoms and male erectile dysfunction: cross-sectional results from the Massachusetts Male Aging Study. Psychosom Med 1998;60(4):458–65.
[38] Shabsigh R, Klein LT, Seidman S, et al. Increased incidence of depressive symptoms in men with erectile dysfunction. Urology 1998;52(5): 848–52.
[39] Lin JS, Lin YM, Chow NH, et al. Novel image analysis of corpus cavernous tissue in impotent men. Urology 2000;55(2):252–6.
[40] Vanegas JP, Raviv G, Kiss R, et al. [Intra-cavernous collagen analysis in impotence]. Acta Urol Belg 1996;64(1):7–10 [in French].
[41] Rowland DL, Greenleaf W, Mas M, et al. Penile and finger sensory thresholds in young, aging, and diabetic males. Arch Sex Behav 1989;18(1): 1–12.
[42] Lerner SE, Melman A, Christ GJ. A review of erectile dysfunction: new insights and more questions. J Urol 1993;149(5 Pt 2):1246–55.
[43] Ansong KS, Punwaney RB. An assessment of the clinical relevance of serum testosterone level

determination in the evaluation of men with low sexual drive. J Urol 1999;162(3 Pt 1):719–21.
[44] Dogra V, Bhatt S. Erectile dysfunction and priapism. In: Dogra V, Rubens D, editors. Ultrasound secrets. 1st edition. Philadelphia: Hanley & Belfus; 2004. p. 420–4.
[45] Golijanin D, Singer E, Davis R, et al. Doppler evaluation of erectile dysfunction—part 1. Int J Impot Res 2007;19(1):37–42.
[46] Moemen MN, Hamed HA, Kamel II, et al. Clinical and sonographic assessment of the side effects of intracavernous injection of vasoactive substances. Int J Impot Res 2004;16:143–5.
[47] Doubilet PM, Benson CB, Silverman SG, et al. The penis. Semin Ultrasound CT MR 1991;12: 157–75.
[48] Benson CB, Doubilet PM, Vickers MA Jr. Sonography of the penis. Ultrasound Q 1991;9: 89–109.
[49] Rao DS, Donatucci CF. Vasculogenic impotence. Arterial and venous surgery. Urol Clin North Am 2001;28:309–19.
[50] Schwartz AN, Wang KY, Mark LA, et al. Evaluation of normal erectile function with color flow Doppler sonography. AJR Am J Roentgenol 1989;153:1155–60.
[51] Golijanin D, Singer E, Davis R, et al. Doppler evaluation of erectile dysfunction—part 2. Int J Impot Res 2007;19(1):43–8.
[52] Lue TF, Mueller SC, Jow YR, et al. Functional evaluation of penile arteries with duplex ultrasound in vasodilator-induced erection. Urol Clin North Am 1989;16:799–807.
[53] Speel TG, van Langen H, Wijkstra H, et al. Penile duplex pharmaco-ultrasonography revisited: revalidation of the parameters of the cavernous arterial response. J Urol 2003;169:216–20.
[54] Roy C, Saussine C, Tuchmann C, et al. Duplex Doppler sonography of the flaccid penis: potential role in the evaluation of impotence. J Clin Ultrasound 2000;28:290–4.
[55] Quam JP, King BF, James EM, et al. Duplex and color Doppler sonographic evaluation of vasculogenic impotence. AJR Am J Roentgenol 1989; 153:1141–7.
[56] Benson CB, Vickers MA. Sexual impotence caused by vascular disease: diagnosis with duplex sonography. AJR Am J Roentgenol 1989; 153:1149–53.
[57] Fitzgerald SW, Erickson SJ, Foley WD, et al. Color Doppler ultrasound in the evaluation of erectile dysfunction: prediction of venous incompetence. Radiology 1990;177(P):129.
[58] Holmes S. Treatment of male sexual dysfunction. Br Med Bull 2000;56(3):798–808.
[59] Morales A, Heaton JP. Hormonal erectile dysfunction. Evaluation and management. Urol Clin North Am 2001;28(2):279–88.
[60] Rhoden EL, Teloken C, Sogari PR, et al. The relationship of serum testosterone to erectile function in normal aging men. J Urol 2002;167(4): 1745–8.

ELSEVIER SAUNDERS

ULTRASOUND CLINICS

Ultrasound Clin 2 (2007) 73–88

Sonographic Evaluation of the Renal Transplant

Jill E. Langer, MD*, Lisa P. Jones, MD, PhD

Renal transplantation has become the preferred method of treating end-stage renal disease. Improvements in surgical technique, histocompatibility matching, and immunosuppressive regimens in conjunction with close clinical and imaging graft surveillance have extended the average life expectancy to 7 to 10 years for a cadaveric kidney and 15 to 20 years for a living related donor kidney [1]. Over the past few decades, gray-scale sonography in combination with spectral, color, and power Doppler techniques has become the primary imaging examinations for the evaluation of renal transplants [1–6]. Sonography is relatively inexpensive, nonnephrotoxic, and can be performed at the bedside allowing rapid diagnosis of complications that threaten graft viability. Color and spectral Doppler examination of the transplant provides an excellent noninvasive method to assess immediate and delayed vascular complications. Sonography also plays a key role in guiding percutaneous interventional diagnostic and therapeutic procedures.

Surgical technique

The transplanted kidney is typically placed extraperitoneally into either the right or left iliac fossa, depending on the need for simultaneous pancreatic transplantation, prior surgery, or preference of the surgeon [2,3]. An anatomic right kidney is transplanted into the recipient's left iliac fossa and vice versa [4]. The kidney's orientation within the iliac fossa is variable depending on the surgical technique and the patient's body habitus. If both iliac fossae have had previous surgery, an intraperitoneal approach to the iliac vessels may be used [3].

Cadaveric renal transplants are typically harvested with an intact main renal artery and an attached portion of the aorta. The aortic segment is trimmed into an oval patch (a Carrel patch) and attached by way of an end-to-side anastomosis to the anterior aspect of recipient's external iliac artery. Slight deviations from this technique, usually because of space constraints in the pelvis, may cause the transplant main renal artery to be tortuous or kinked. When a living related donor kidney is transplanted, only the main renal artery is harvested and anastomosed end-to-side to the recipient's external iliac artery, or less commonly, end-to-end to the recipient's internal iliac artery [1,4]. Transplantation of a kidney with multiple renal arteries, a condition that is present in 18% to 30% of the population and

Department of Radiology, Hospital of the University of Pennsylvania, University of Pennsylvania Medical Center, 3400 Spruce Street, Philadelphia, PA 19104, USA
* Corresponding author.
E-mail address: jill.langer@uphs.upenn.edu (J.E. Langer).

1556-858X/07/$ – see front matter
doi:10.1016/j.cult.2007.01.012
ultrasound.theclinics.com

is bilateral in 15%, poses some technical difficulties for the surgeon [7]. When more than one main artery is noted in a cadaveric kidney, the renal arteries are sutured to a common Carrel patch (Fig. 1). Living donor kidneys with multiple renal arteries were previously not considered candidates for transplantation. Extracorporeal microsurgical techniques and bench reconstruction of multiple arteries into a common stem have enabled successful transplantation of these kidneys without additional risk for complication, however [7]. The donor renal vein is always connected by way of an end-to-side anastomosis of the recipient's external iliac vein [2,4].

The current preferred method of reestablishing continuity of the urinary tract is the creation of a ureteroneocystostomy. The ureterovesical anastomosis is formed by attaching the distal end of the donor ureter to the dome of the bladder. Less commonly, a ureteroureterostomy (an end-to-end anastomosis of the donor ureter to the recipient ureter) or a pyeloureterostomy (a connection of the donor renal pelvis to the recipient ureter) may be performed [2,4].

Sonographic technique

The renal transplant is usually relatively superficial in location and easily imaged by sonography (Fig. 2). The sonographic evaluation may be more difficult in obese patients or if the transplant is displaced by an adjacent collection. A wide-angle, deeply focused general abdominal probe should be used for gray-scale imaging of the transplant, the urinary bladder, the operative bed including the superficial tissues, the transplant artery and vein, the external iliac vessels, and their anastomoses. Color Doppler sonography and spectral Doppler sonography are then performed of the extrarenal vessels, their anastomoses, and the intrarenal vessels as described later. A higher-frequency probe can be used to evaluate the anatomic detail of the transplant and the parenchymal vascularity using color and possibly power Doppler examinations.

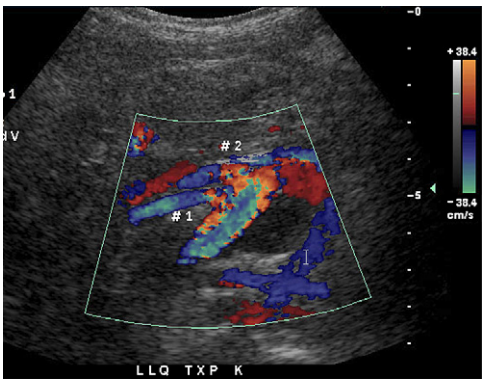

Fig. 1. Two donor renal arteries. Color Doppler image demonstrating two donor renal arteries that were anastomosed to the recipient's external iliac artery by way of Carrel patch of donor aorta.

The graft is usually best visualized from an anterolateral approach with the patient in a supine or decubitus position with the side of the transplant elevated. On gray scale, the transplant kidney appears similar to the native kidney, although the morphology is better delineated secondary to the use of a higher-frequency transducer (see Fig. 2A). The renal pyramids typically appear hypoechoic and easily distinguished from the renal cortex. Absence of corticomedullary differentiation may be a normal finding, however [6]. The renal pelvis may be identified but should not be distended; typically the calyces are collapsed.

The size of the kidney should be assessed by measuring the length and width of the transplant in orthogonal planes and then calculating the volume using the formula for a prolate ellipse. A slightly more accurate estimation of the renal transplant volume can be performed if necessary. This estimate is obtained by multiplying the maximum transverse cross-sectional area (MCA) by the renal length. The MCA is obtained by electronically tracing around the kidney at the widest width on a transverse image and using the calculated area within the tracing. The dimensions should be compared with previous measurements because volumetric changes may reflect an underlying pathologic condition, such as rejection [8]. The renal transplant volume is larger compared with the volume at the time of harvesting, even in the absence of underlying graft dysfunction, possibly related to compensatory hypertrophy [9].

Assessment of the transplant vasculature

Doppler ultrasound (US) has proved to be an excellent noninvasive screening modality to assess the transplant's vasculature (see Fig. 2B–E) [5]. The success depends on the ability to directly visualize the renal vessels and their anastomoses, however. Color and spectral analysis should be performed of the ipsilateral external iliac artery both proximal and distal to the anastomosis, the transplant main renal artery (or arteries) at the anastomosis and in the mid portion of the vessel, the transplant main renal vein, and the interlobar arteries within the upper, mid, and lower pole of the transplant. Color Doppler examination should be performed of each vascular segment to assess patency of the vessels and to detect any focal area of color aliasing, which would indicate a focal stenotic segment. The spectral parameters most commonly assessed include peak

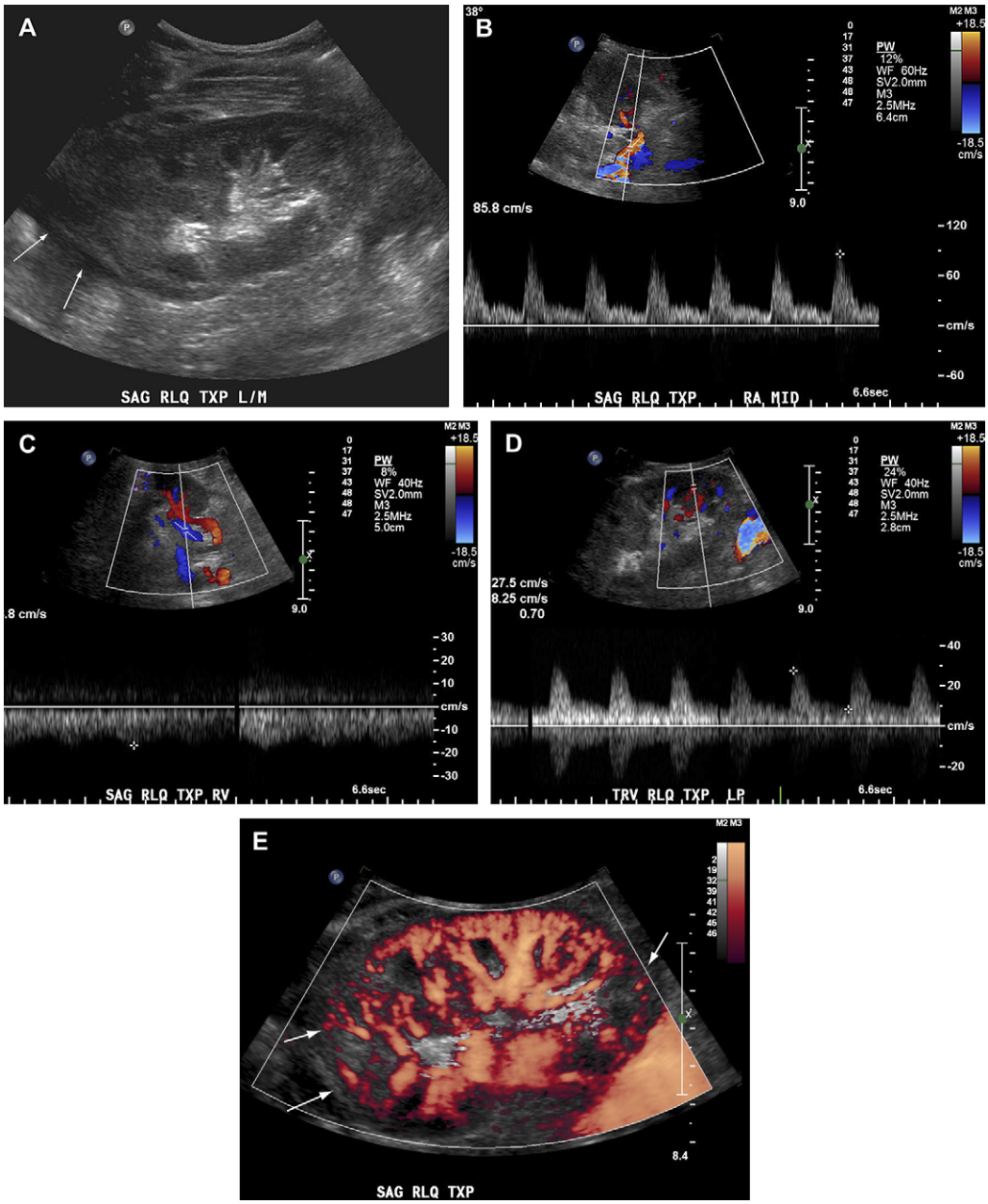

Fig. 2. Normal living related donor renal transplant 3 days after transplantation. (*A*) Sagittal gray-scale image demonstrating normal corticomedullary differentiation and a small postoperative fluid collection (*arrows*), likely a hematoma. (*B*) Spectral Doppler image of the main renal artery demonstrates normal low-resistance waveform with peak systolic velocity of 85.8 cm/s. Note appropriate technique with central placement of a narrow sampling gate. The orientation of the gate parallels the vessel and the Doppler angle is less than 60 degrees. (*C*) Spectral Doppler image of the main renal vein demonstrating normal continuous flow. (*D*) Spectral Doppler image demonstrating normal resistive index measurement (0.70) obtained from a lower pole interlobar artery. (*E*) Power Doppler image demonstrating normal cortical perfusion that extends to the edge of the renal cortex. Apparent paucity of flow at the renal poles (*arrows*) is attributable to loss of signal on the basis of a Doppler angle close to 90 degrees in these regions.

systolic velocity (PSV), acceleration time (AT), and resistive index (RI). Additional parameters that may also be assessed include pulsatility index and iliac artery to transplant artery PSV ratios. On spectral analysis, the Doppler angle should be kept between 30 and 60 degrees to minimize error in velocity calculation. The sample gate should be placed in the center part of the arterial lumen. The width of the gate should be adjusted to approximately one half of the diameter of larger vessels, such as the external iliac and main renal artery and veins, and at the smallest setting possible for the interlobar vessels [10]. Several spectral samples may be obtained in these vessels to detect the highest PSV. The upper limit of normal PSV in the renal artery is typically 200 to 250 cm/s (see Fig. 2A) [11]. The normal main renal vein demonstrates continuous low velocity flow, typically 40 to 60 cm/s (see Fig. 2B). The normal intrarenal arterial waveform is one of low resistance. The RI is considered to be normal if less than 0.7, indeterminate between 0.7 and 0.8, and elevated if greater than 0.8 (see Fig. 2C) [6]. A baseline Doppler examination is performed shortly after surgery and follow-up examinations are then performed as needed based on the patient's clinical status.

The overall vascularity of the transplant should be assessed by color Doppler examination, noting any focal areas of increased or decreased flow within the parenchyma. Power Doppler, a technique more sensitive to the low-velocity flow present in small vessels, may also be used to assess perfusion of the renal transplant, in particular cortical perfusion. When examined with a high-frequency (5 MHz or higher) linear transducer and appropriate power Doppler settings, a normal transplant should have detectable flow extending all the way to the renal cortex (see Fig. 2E) [12,13].

Parenchymal insults

Acute graft dysfunction is most commonly related to acute rejection, acute tubular necrosis (ATN), toxic levels of a calcineurin inhibitor (cyclosporin A or tacrolimus), or infection [1–3,5,6]. Unfortunately, although many sonographic features have been described with these parenchymal insults, sonography is not able to differentiate among the possible causes. Sonography is most useful to eliminate obstruction and vascular compromise as a possible cause of graft dysfunction.

Acute allograft rejection remains one of the most serious and common complications of renal transplantation. Virtually every patient experiences some degree of rejection, and differentiating rejection from other causes of graft dysfunction remains a challenging clinical problem. Acute rejection occurs in approximately 40% of patients in the early posttransplant period, peaking at 1 to 3 weeks following transplantation, and is characterized clinically by a rapid increase in serum creatinine, often a 25% or greater increase in 24 to 48 hours [3,4,14,15]. If acute rejection is diagnosed early it may be reversed by steroids or by antibody therapy. Acute rejection can be suspected based on a combination of clinical, laboratory, and sonographic findings, but an accurate diagnosis depends on transplant biopsy, a technique that carries a 4% mortality [15]. Although potentially completely reversible, the occurrence of acute rejection is viewed as an adverse long-term prognostic indicator for graft survival [3].

ATN occurs in the early postoperative period as result of ischemia before revascularization and is much more common with cadaveric transplantation than with living related donors [1,13,14]. Although this condition is self-limited, with most kidneys recovering in 2 to 3 weeks, 10% to 30% of patients require dialysis until the graft recovers [3]. Cyclosporin and tacrolimus are immunosuppressive agents that have proven to be a major advance in organ transplantation, but their nephrotoxicity remains an important problem. They produce reversible renal vasoconstriction acutely and interstitial fibrosis chronically, which may cause irreversible graft dysfunction. In general this diagnosis is made by renal biopsy or by response to alteration of drug levels [1,3].

Several sonographic findings have been reported in patients who have graft dysfunction (Fig. 3A), including poor corticomedullary differentiation, reduction in renal sinus echoes, both increased an decreased echogenicity of the pyramids, urothelial thickening, and enlargement of the kidney [3,6,16]. All these findings are nonspecific, however, and may be seen in patients who have acute rejection, ATN, infection, and cyclosporin toxicity, along with vascular complications. Additionally these sonographic findings often occur much later than the biochemical indicators of graft dysfunction, limiting their usefulness to allow early therapeutic intervention. There are some general trends, however. For example, the more severe and acute the rejection, the more marked the sonographic findings.

The spectral Doppler examination may show an elevated RI in all forms of graft dysfunction (Figs. 3B and 4B) [14,15]. The elevated RI results from any cause of interstitial edema, which is most reflected in the diastolic phase of the arterial waveform. A normal RI does not exclude graft dysfunction, however, and may be noted in up to 50% of patients who have biopsy-proven rejection [12,15]. Serial measurements of RI may be helpful

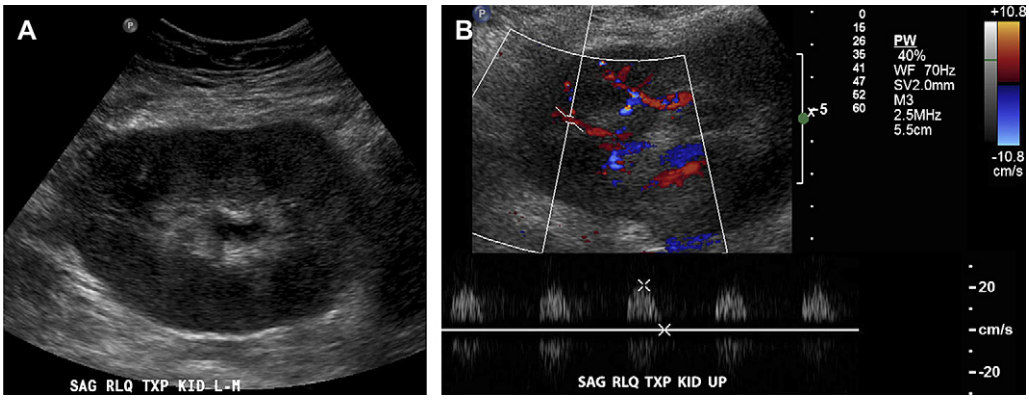

Fig. 3. Acute rejection. (*A*) Sagittal gray-scale image demonstrates loss of corticomedullary differentiation, enlarged size, and rounded configuration of the renal transplant in this patient who has elevated serum creatinine. (*B*) Spectral Doppler image demonstrates very high resistance waveform in an upper pole interlobar artery characterized by absence of diastolic flow. Renal biopsy revealed acute rejection.

to determine if the insult is worsening and to monitor therapeutic interventions [17]. Although RI cannot differentiate among the causes of early graft dysfunction, a normal RI in the immediate transplant period is a good predictor of immediate graft function [14].

Power Doppler examination is more sensitive than RI evaluation for the detection of the vascular changes of graft dysfunction. Alterations in the small vessels within the cortex of the transplant (Fig. 4A) may be the earliest sign of parenchymal insults, such as rejection and cyclosporin toxicity [12,13,15,17,18]. These patients may show patchy flow or complete lack of cortical flow on power Doppler examination of the parenchyma. Similar to the RI determinations, a normal examination does not exclude graft dysfunction [13,15].

Chronic rejection is defined as gradual deterioration in graft function beginning at least 3 months following transplantation in association with biopsy-proven interstitial fibrosis and tubular atrophy. The most common cause is previous episodes of acute rejection. With chronic rejection (Fig. 5) the kidney is small and demonstrates a thinned cortex, diffusely increased echogenicity, and reduced visibility of intrarenal vessels [3].

The sonographic findings of transplant infection are relatively nonspecific. The kidney may be enlarged and heterogeneous (Fig. 6), overlapping with the appearance of acute rejection and other causes of graft dysfunction. There may be regions of increased or decreased echogenicity or regions of altered parenchymal flow similar to rejection or segmental infarction. Focal pyelonephritis may

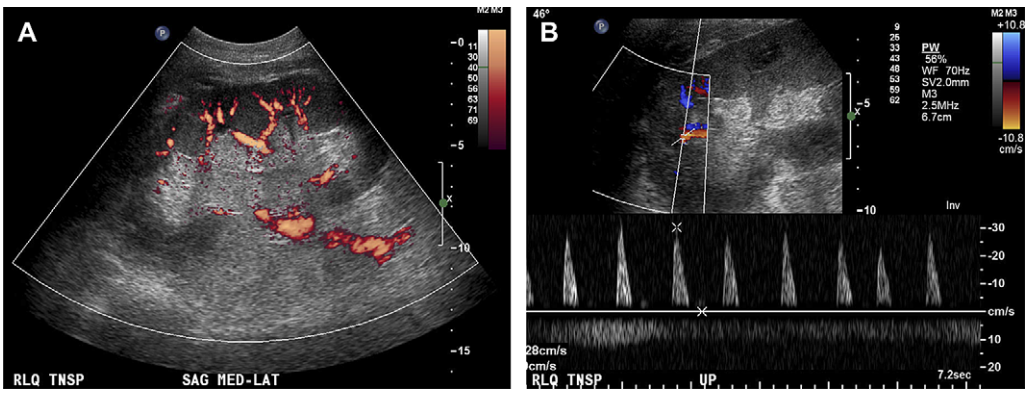

Fig. 4. Acute tubular necrosis. (*A*) Sagittal power Doppler image obtained 18 days after transplantation for continued graft dysfunction demonstrates paucity of vascularity and cortical pruning (compare with 2D). (*B*) Sampling of an upper pole interlobar artery revealed very a high resistance waveform with absence of diastolic flow, similar to 3B. Findings were suspected to represent acute rejection but biopsy revealed ATN, illustrating the nonspecific nature of the sonographic findings of acute allograft dysfunction and the role of renal biopsy in differentiating between possible causes.

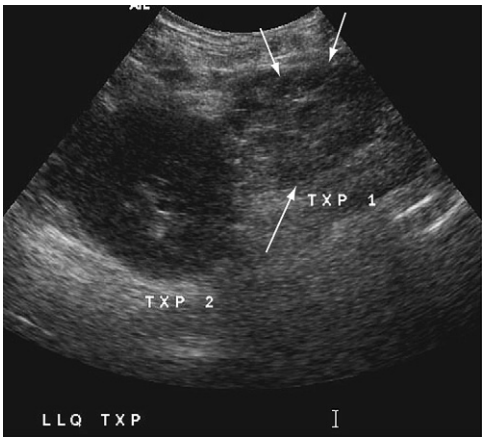

Fig. 5. Chronic rejection. Gray-scale image demonstrating a small, echogenic renal transplant (*arrows*), which was nonfunctioning secondary to chronic rejection, adjacent to a more recently placed renal transplant (labeled TXP 2), which has normal echogenicity and sonographic morphology.

appear mass-like, simulating a neoplastic process. Low-level echoes may be noted in the collecting system and there may be thickening of the urothelium [1,3,6].

Malignancy

Immunosuppressive therapy places the transplant recipient at 100 times the normal risk for developing cancer, in particular skin cancers and lymphomas [19]. The degree and duration of immunosuppression are important risk factors for the development of malignancy. Posttransplantation lymphoproliferative disorder (PTLD), a potentially malignant process, is a complication that occurs in 0.9% to 2.5% of all renal transplant recipients [20]. PTLD describes a heterogeneous group of lymphoid proliferations that histopathologically range from benign infectious mononucleosis-like lesions at one end of the spectrum to a monomorphic proliferation of B cells resembling a high-grade lymphoma at the other end [21]. The greatest risks for the development of PTLD are acute Epstein Barr virus infection following transplantation and the use of antilymphocyte antibodies, such OKT3 [22].

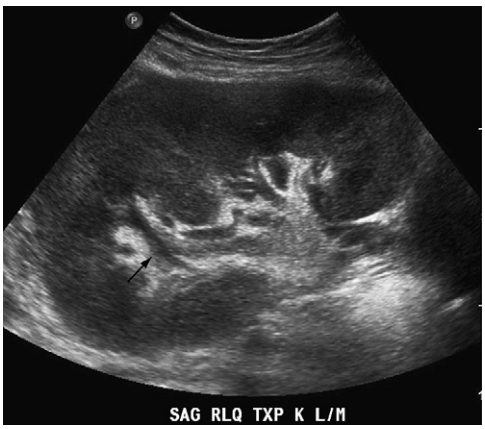

Fig. 6. Pyelonephritis. Sagittal gray-scale image in a patient who had fever and *Escherichia coli* bacteriuria demonstrates enlargement of the renal transplant, increased echogenicity of the renal sinus fat, subtle urothelial thickening (*arrow*), and mild prominence of the collecting system. Although the gray-scale findings were nonspecific, the presence of low resistive indices (0.61–0.62) and normal serum creatinine favored a diagnosis of infection over ATN or rejection. The findings resolved following antibiotic therapy.

Early PTLD typically affects younger patients, usually within a year of transplantation, and tends to be a less aggressive polyclonal proliferation of lymphocytes that can be treated with modulation of immunosuppression and antiviral therapy. Late-onset PTLD occurs on average 38 to 146 months following transplantation. This monoclonal proliferation follows a more aggressive course and is associated with poor outcome. PTLD presents with diffuse lymphadenopathy and single or multiple extranodal masses within the liver, spleen, lung, kidney, and the central nervous system and gastrointestinal tract [20]. Microscopic involvement of the renal hilum by PTLD is often noted on pathologic examination following graft removal [21]. Macroscopic involvement of the transplant presenting as a focal mass has now been noted by several authors [20,23]. Allograft-localized PTLD appears as a complex hypoechoic vascular mass within or adjacent to renal hilum, with mean size of 4.5 cm. The lesion may encase the main renal artery causing a focal stenosis and may involve the renal sinus and pelvis causing hydronephrosis in 50% of the cases reported [23].

A primary renal cell carcinoma should also be considered when a focal renal mass is noted by sonography. The prevalence of primary renal carcinoma may be increased in transplant recipients, with 90% occurring in the native kidneys and 10% in the transplant. Many cases are likely related to a high background incidence of acquired cystic disease of dialysis, with an estimated 9% of these patients developing tumors of the native kidneys [24]. Often patients are referred for imaging following an episode of gross hematuria. The diagnostic investigation of these patients must include imaging of the native and transplant kidneys and evaluation of the urothelium of all three ureters and the urinary bladder.

Graft thrombosis

Thrombosis of the renal vasculature following transplantation is a complication that requires rapid diagnosis to avoid graft loss. Renal artery thrombosis affects less than 1% of transplants and typically presents in the immediate postoperative period, but may occur at any time if the patient is at risk for hypercoagulation [6,25–28]. Acute and hyperacute rejection are the most common causes, but thrombosis may occur because of surgical technique in particular if associated with arthrosclerosis in donor or recipient, multiple renal vessels, or a pediatric donor kidney [2,3,25]. Thrombosis of the main renal artery often leads to complete infarction of the kidney. The patient may present with absence of urinary output, pain, swelling, and tenderness over the graft but may also be relatively asymptomatic [3]. The kidney becomes hypoechoic and enlarged; no arterial or venous flow is seen in the main vessels and the intrarenal vessels on color Doppler examination (Fig. 7) [2,3,5,29,30]. If the diagnosis is made early, some grafts have been salvaged by surgical or percutaneous thrombolysis [4]. Renal infarction due to hyperacute rejection (Fig. 8) may mimic the appearance of acute renal artery thrombosis; however, a patent main transplant renal artery is found at the time of surgical removal.

Segmental infarcts may occur as part of rejection or as a result of unassociated segmental thrombosis or vasculitis. The rate of polar infarcts from inadvertent ligature of a polar artery in the donor has dramatically decreased with the use of en bloc harvesting techniques [7]. Segmental infarcts may appear as a geographic region of hypoechogenicity or may

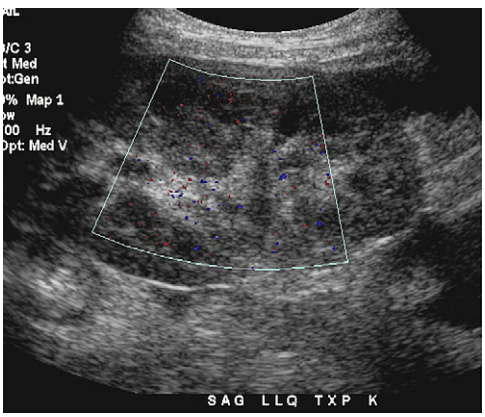

Fig. 7. Acute transplant main renal artery thrombosis. Color Doppler sagittal image 12 hours after transplantation reveals complete absence of flow in the renal transplant. On explant, the transplant renal artery was found to be completely thrombosed.

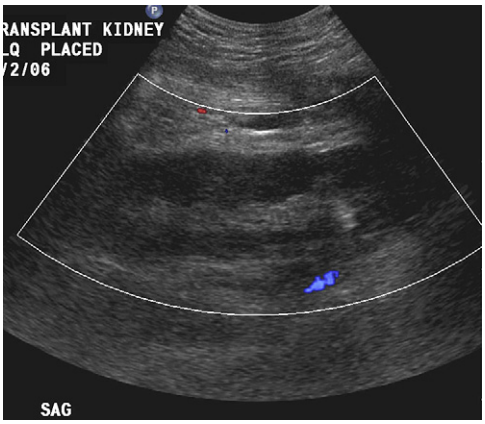

Fig. 8. Hyperacute rejection. Color Doppler sagittal image obtained 24 hours after transplantation demonstrates no flow to the kidney, concerning for acute renal artery thrombosis. At surgery, however, the main renal artery and vein were found to be patent. In this case, the allograft infarction and necrosis were caused by hyperacute rejection.

appear more masslike with a well-defined echogenic wall. On color Doppler they appear as wedge-shaped areas without flow (Fig. 9), a finding that may also be noted with severe pyelonephritis [2].

Renal vein thrombosis is more common than arterial thrombosis, occurring in about 5% of transplants, accounting for one third of all early graft failures [4,25–28]. It typically presents between

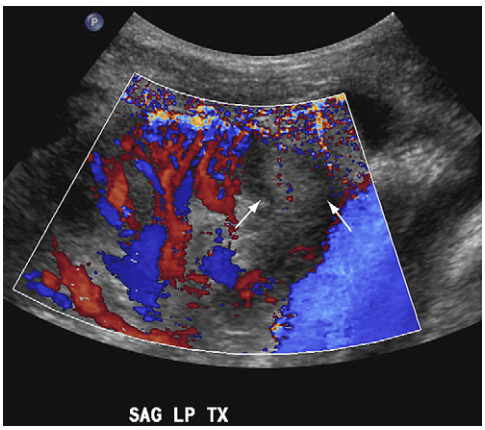

Fig. 9. Segmental renal infarct. Sagittal color Doppler shows a segmental area of increased parenchymal echogenicity and decreased vascularity (*arrows*) that corresponded to a photopenic defect on a renal scintigram obtained 1 day after transplantation (not shown). The findings were most likely related to a segmental infarct from surgical injury to the vascular supply of the lower pole. The differential diagnosis of focal decreased vascularity includes focal pyelonephritis in the appropriate clinical setting.

the third and eighth postoperative day [31,32]. Hypovolemia, compression from peritransplant collections, and slow flow secondary to rejection or caused by other allograft disease are common predisposing risk factors [2,31,32]. The patient may develop either abrupt or gradual cessation of renal function and may develop swelling and tenderness over the graft.

On gray scale, the kidney is enlarged and edematous. The main renal vein may be dilated and echogenic thrombus may be visible in the lumen. On color Doppler examination there is severely reduced or no detectable venous flow in the hilum of the transplant, often in combination with reversed diastolic arterial flow in the renal artery (Fig. 10) [29–32]. Reversal of diastolic arterial flow may occasionally be seen with severe acute rejection and ATN, but venous flow is present differentiating those conditions from renal vein thrombosis. In cases of partial renal vein thrombosis there may be diminished flow in the main renal vein with a visible nonocclusive thrombosis; other cases may only have a nonspecific increase in arterial resistance [5,32].

Renal artery stenosis

Renal artery stenosis accounts for 75% of all vascular complication, affecting 10% of transplants, usually in the first 3 years after surgery [4]. Renal artery stenosis should be suspected if the patient has persistent hypertension refractory to medical therapy, particularly if accompanied by audible bruit over the graft or unexplained graft malfunction in the absence of rejection [1,2,5,11]. More than half of the stenoses occur at the anastomosis secondary to focal intimal fibrosis and calcification caused by vessel perfusion injury, with end-to-end anastomoses at three times greater risk for stenosis than end-to-side anastomoses [27]. Stenoses that occur proximal to the anastomosis may be attributable to atherosclerotic disease in the donor vessel or clamp injury, whereas distal stenoses are caused by intimal hyperplasia in response to turbulent flow and are more commonly seen with end-to-side anastomosis. Other causes include transplant rejection, arterial twisting, kinking, or compression of the artery [5,6].

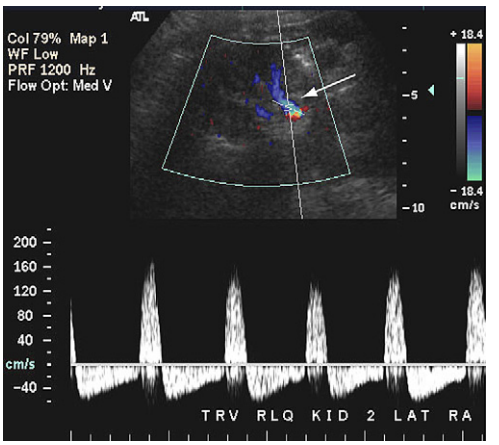

Fig. 10. Renal vein thrombosis. Spectral Doppler image obtained 1 day after transplantation in a patient who had abrupt decrease in urinary output demonstrates reversal of diastolic flow in the main renal artery. Note on color Doppler examination (*arrow*) that the direction of renal arterial flow is away from the kidney. This phenomenon was observed only during the diastolic phase of the cycle reflecting the high intrarenal pressure. Acute renal vein thrombosis was confirmed surgically. Reversal of diastolic flow may also be seen with severe ATN or rejection; however, in both of these conditions there would be a patent renal vein.

Gray-scale findings (Fig. 11A) of renal artery stenosis include focal luminal narrowing, mural thickening, and mural calcification. Color and spectral Doppler examination (Fig. 11B) shows focal color aliasing in the region of the narrowing, with downstream spectral broadening and an abnormal intrarenal tardus–parvus wave form [2,5]. In general, duplex sonography has a sensitivity of 87% to 94% and a specificity of 86% to 100% for the diagnosis of renal artery stenosis, with the range reflecting the varying parameters and threshold values used by different laboratories [4,10,11,33–36]. The PSV in the renal artery is considered by most authors to be the most reliable indicator of renal artery stenosis. A PSV of 200 to 250 cm/s should be viewed as suspicious for renal artery stenosis because it correlates with a stenosis of at least 50% in most patients [10,11,33]. Other authors have advocated using a higher threshold of 300 cm/s to improve specificity and reduce the number of patients referred for confirmatory arteriography, particularly when dealing with a low-risk or surveillance population [36]. Higher threshold PSV values, particularly greater than 400 cm/s, have the highest specificity for detecting severe RAS requiring intervention, but may miss moderate stenoses [10]. Other parameters suspicious for RAS include an AT of greater than 100 milliseconds in the renal or intrarenal arteries and a ratio of PSV in the transplant main renal artery to external iliac artery of 1.8 or greater [11,34,35].

Mimics of renal artery stenosis include tortuosity or transient kinking of the renal artery (Fig. 12), which may cause increased velocities and spectral broadening in normal vessels [6]. Improper velocity settings or incorrect Doppler angle correction may also yield spuriously high PSV readings. Elevated peak systolic arterial and venous velocities with

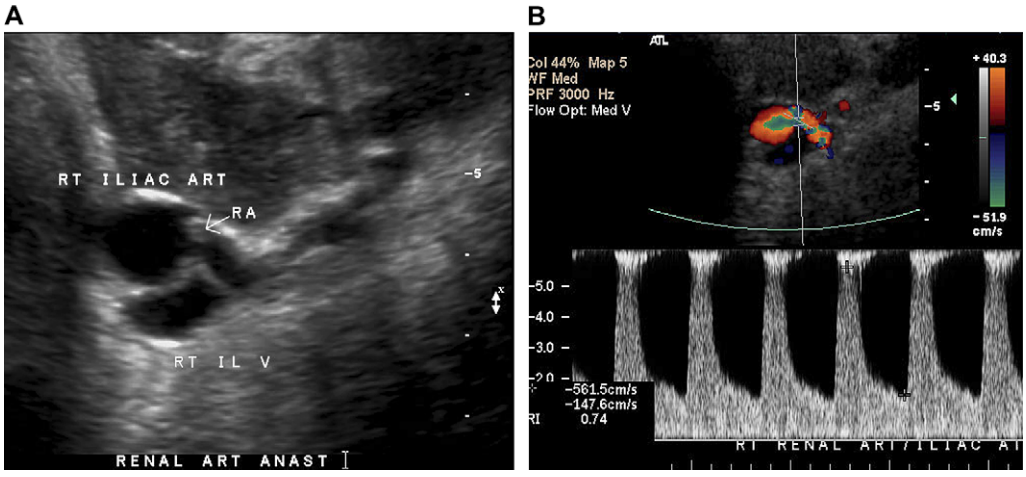

Fig. 11. Transplant main renal artery anastomotic stenosis 1 year after transplantation. (*A*) Transverse gray-scale image shows narrowing (*arrow*) of the transplant main renal artery at the anastomosis. (*B*) Spectral Doppler of the area of greatest luminal narrowing demonstrates spectral broadening, marked elevation of the PSV (561.5 cm/s), and elevation of the PSV ratio (transplant main renal artery compared with iliac artery) to 2.5. Findings indicate hemodynamically significant renal artery stenosis.

normal RI may be seen immediately after transplantation and decrease to normal at 1 to 3 months' follow-up. This finding suggests physiologic adaptation rather than true stenosis [37].

Biopsy complications

Intrarenal arteriovenous fistulas (AVFs) and pseudoaneurysms have been reported to complicate 1% to 18% of all renal transplants. The exact incidence is uncertain because most are small and resolve spontaneously [1,4]. They are almost exclusively attributable to needle biopsies. AVF results from vessel wall injury of an adjacent artery and vein, allowing a fistulous communication to be established. These are best detected on Color Doppler (Fig. 13) as a focal area of disorganized flow extending beyond the gray-scale borders of the vessels reflecting the vibration in the surrounding tissues caused by the high-velocity jet of arterial blood entering the adjacent vein. The feeding artery and

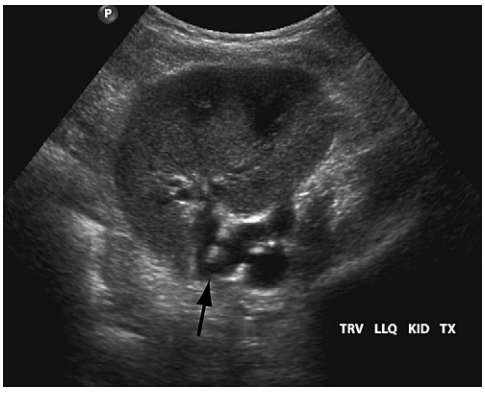

Fig. 12. Mimic of renal artery stenosis. Transverse gray-scale image demonstrates a tortuous transplant main renal artery with elevation of the peak systolic velocities (210–220 cm/s, not shown) in the region of maximal curvature (*arrow*), without gray-scale findings or a poststenotic jet to indicate hemodynamically significant renal artery stenosis.

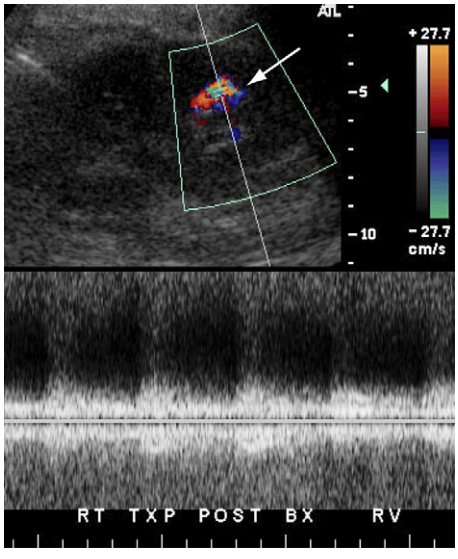

Fig. 13. Postbiopsy AVF. Color and spectral Doppler image 1 week after percutaneous biopsy in a patient who had hematuria demonstrates focal color aliasing in the transplant lower pole (*arrow*). Spectral Doppler of the area of aliasing reveals spectral broadening and low resistance flow characteristic of an AVF.

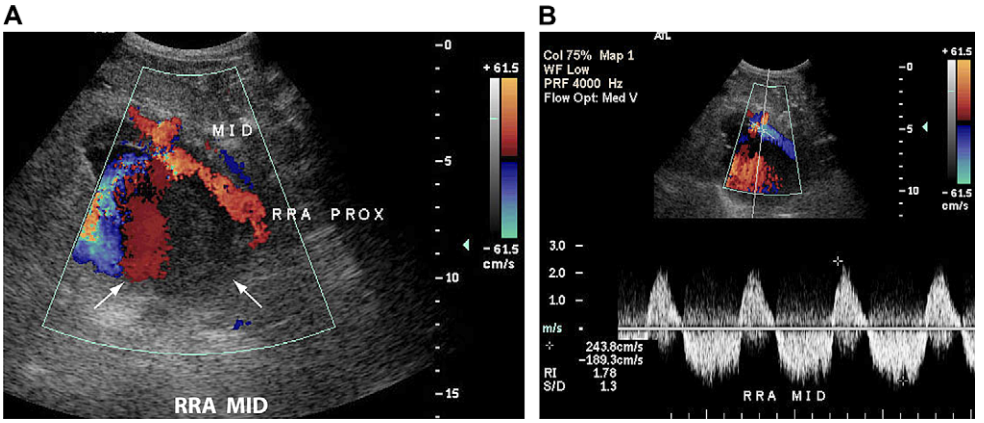

Fig. 14. Extrarenal pseudoaneurysm. (*A*) Color Doppler image demonstrating a partially thrombosed pseudoaneurysm arising from the main transplant renal artery, with characteristic yin-yang swirling internal flow dynamics in the lumen. Note the thrombus in the pseudoaneurysm (*arrows*). (*B*) Spectral Doppler image showing the characteristic to-and-fro flow in the aneurysm neck.

draining vein are often engorged and may be seen on gray-scale and color examination. The artery has a high-velocity, low-resistance waveform on spectral Doppler examination and the draining vein may have a pulsatile or "arterialized" waveform. The significance of an AVF depends on its size and the degree of shunting. Many small lesions can be managed conservatively and spontaneously resolve. Rarely some grow slowly over time causing graft dysfunction because of regional ischemia.

A pseudoaneurysm results from transmural injury to the artery creating a cavity that communicates with the main lumen by way of a neck. The arterial flow has a typical "to-and-fro" pattern in the neck on spectral Doppler and a "yin-yang" appearance in the aneurysm sac on color Doppler because of swirling of blood within this space (Fig. 14) [4]. Extrarenal pseudoaneurysms and arteriovenous fistulas are rare but may occur as a result of surgical technique or infection adjacent to the vessels. All PSAs require therapy because of the risk for spontaneous rupture [1].

Small perinephric hematomas are commonly noted following percutaneous renal biopsy procedures. Large or rapidly expanding hematomas may require angiography with embolization to control the hemorrhage (Fig. 15). Color Doppler may be able to identify active bleeding from the renal parenchyma or vessels in the surrounding soft tissue. Vascular injury during biopsy may be

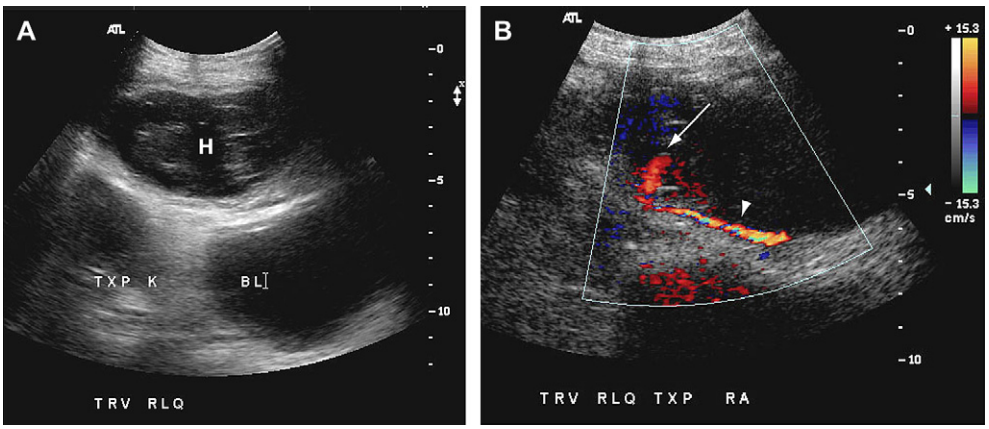

Fig. 15. Superficial postbiopsy hematoma. (*A*) Gray-scale image obtained 2 days after renal transplant biopsy in a hypotensive patient who had an expanding anterior abdominal wall mass demonstrates a complex superficial collection in keeping with a hematoma (H, hematoma), overlying the renal transplant. (*B*) Color Doppler image demonstrates active arterial extravasation indicated by the extraluminal jet of color flow (*arrow*) into the hematoma caused by inadvertent puncture of the inferior epigastric artery (*arrowhead*) during the biopsy procedure.

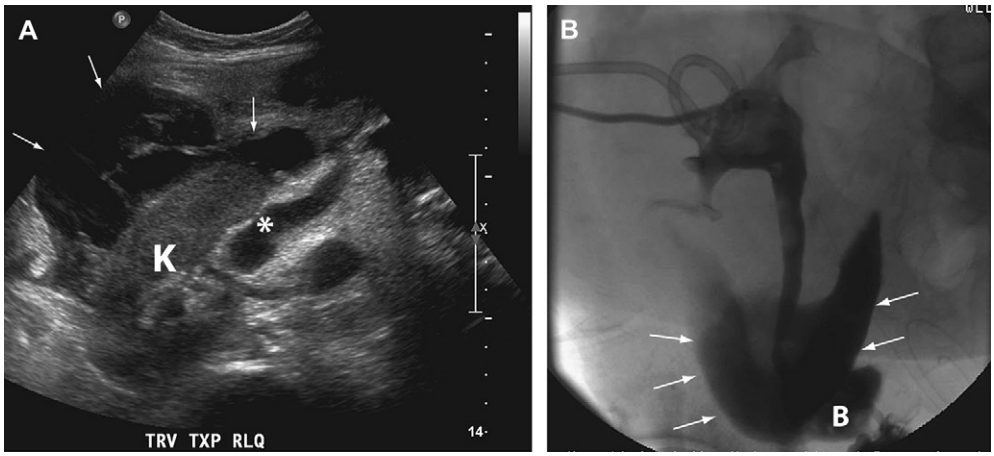

Fig. 16. Urinoma. (*A*) Sagittal gray-scale image obtained 20 days after transplantation in a patient who had new right leg swelling demonstrates a complex fluid collection (*arrows*) concerning for abscess. On drainage, the collection proved to be a sterile urinoma despite atypical appearance and location. Note also the hydronephrosis attributable to compression of the ureter by the urinoma. (*, ureter; K, kidney). (*B*) Nephrostogram showed extravasated contrast material (*arrows*) pooling between the distal ureter and bladder (B, bladder), in keeping with urinary leak arising from the region of the ureteroneocystostomy. Pathology revealed ischemic necrosis of the distal ureter.

minimized with use of US guidance to avoid a needle path into renal sinus.

Urinary complications

The prevalence of urinary tract complications has varied from 2.6% to 15% in large adult series, approaching 30% in pediatric recipients [38,39]. Urinary tract complications include urinary leak, obstruction, vesicoureteral reflux, and nephrolithiasis. The higher complication rates were more common in early studies when ureteroureterostomy or pyeloureterostomy were performed [2]. Recent improvements in graft harvesting and ureteral reimplantation techniques have reduced the rate to 2% to 5% with very low morbidity [38–42].

The most frequent urinary tract complication in the early postoperative period is urinary leakage (see Fig. 16). Most commonly this occurs at the level of the ureterovesical anastomoses, secondary to ureteral necrosis attributable to inadequate vascular supply of the distal ureter [38,40,41]. Rarely it may result from more proximal ureteral leakage or from calyceal rupture, which may be caused by high-grade obstruction or segmental ischemia, such as in patients who have accessory arteries

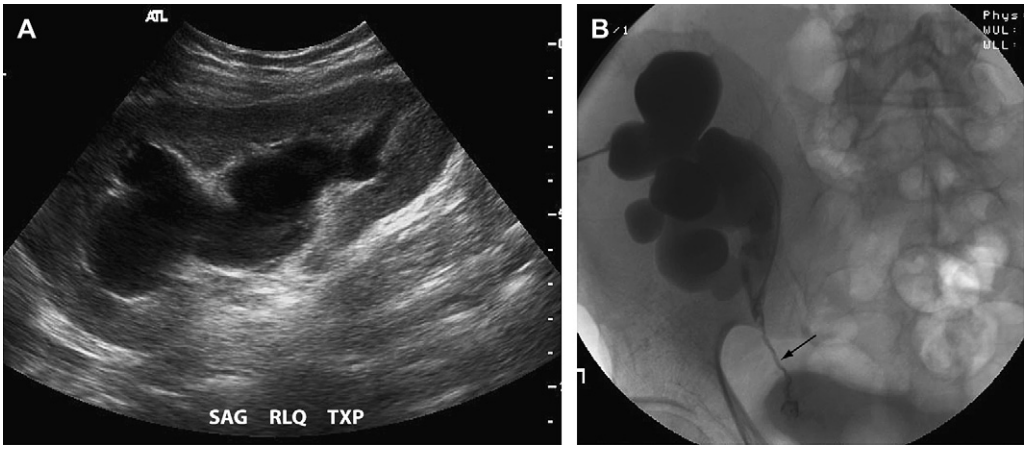

Fig. 17. Hydronephrosis caused by long ureteral stricture. (*A*) Sagittal gray-scale image in a patient who had rising creatinine 2 days after removal of a ureteral stent reveals marked hydronephrosis. (*B*) Nephrostogram demonstrating markedly narrowed distal ureter with irregular contour, likely reflecting an ischemic stricture.

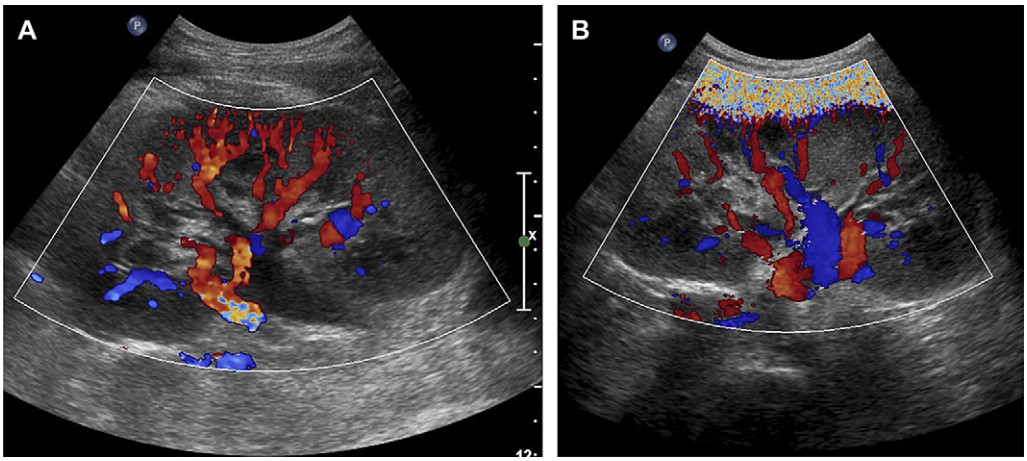

Fig. 18. Postoperative pyelocaliectasis caused by ureteral edema. (*A*) Sagittal color Doppler image 4 days after transplantation demonstrates mild pyelocaliectasis. (*B*) Sagittal color Doppler image 4 months later shows resolution of the pyelocaliectasis, which presumably was on the basis of postoperative edema at the ureteral anastomosis.

[2]. Improved ureteral vascularization is achieved by preservation of the hilar fat, periureteral tissue, and the lower pole renal artery branches that supply the distal ureter during harvesting [38,39]. Also the use of extravesical ureteroneocystostomy allowing the use of a shorter segment of ureter has proven to decrease the risk for ureteral ischemia and bladder injury [39,40,42]. Some surgeons have incorporated the use of ureteral stents at the time of transplantation, which has led to a lower risk for leakage and obstruction [39,43].

Ureteral necrosis may also be related to medical causes of vascular insufficiency; an increased incidence is noted with older donors and in those patients who have rejection or other causes of delayed graft dysfunction [40]. Infection may also play a role; there has been a parallel decrease in CMV infection and ureteral necrosis since the routine use of CMV prophylaxis in 1998 [40]. Urinary leaks are usually diagnosed 2 to 7 days after surgery. The patient may present with elevation of the serum creatinine, decreased urinary output, or mass effect symptoms from the enlarging urinoma [1,2]. If small, a urinary leak may be treated with nephrostomy and stent placement for 6 to 8 weeks to allow complete healing, with a success rate of 63% to 83% [4].

Urinary tract obstruction occurs in 1.3% to 10.2% of all transplants [38,39]. Early obstruction may be attributable to a blood clot within the ureter

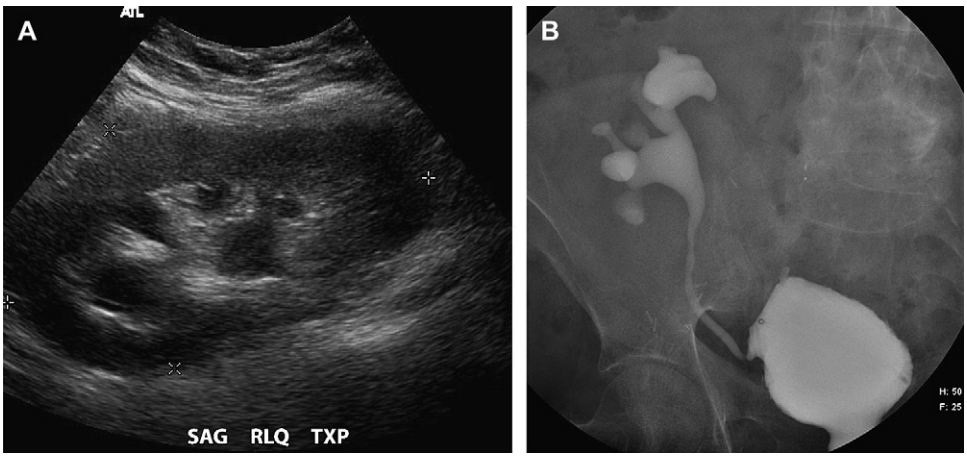

Fig. 19. Pyelocaliectasis caused by vesicoureteral reflux. (*A*) Sagittal gray-scale image demonstrates mild pyelocaliectasis. (*B*) Free vesicoureteral reflux is identified on this image from a voiding cystourethrogram, accounting for the pyelocaliectasis.

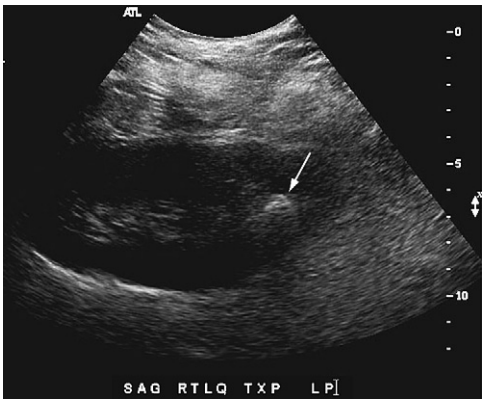

Fig. 20. Renal calculus. Sagittal gray-scale demonstrates an echogenic area with posterior acoustic shadowing in the lower pole of the transplant kidney (*arrow*), shown to be a non-obstructing renal calculus on a CT.

or bladder and can often be relieved by irrigation [3]. Beyond the immediate postsurgical period, obstruction is most likely to occur in the distal ureter secondary to a ureteral stricture occurring as a result of ischemia (Fig. 17) or prior acute rejection, or from suboptimal surgical technique in the creation of the ureteroneocystostomy or from kinking of the ureter [1,3,4]. Less common causes include periureteric fibrosis, calculi, sloughed papillae, and extrinsic compression by a pelvic fluid collection [2]. Obstruction should be considered in patients who have an increasing serum creatinine level and should be differentiated from medical causes of graft dysfunction. Percutaneous nephrostomy is often performed to relieve the urinary obstruction and allow percutaneous intervention, such as balloon dilation of ureteral strictures [3,4].

Hydronephrosis can be easily identified with sonography, but its significance should be made in conjunction with renal function [3,6]. Mild hydronephrosis immediately following surgery may reflect mild and reversible ureteral edema and can be reassessed by follow-up sonography (Fig. 18). Increasing dilatation of the transplant collecting system over time implies obstruction and allows distinction from mild dilatation secondary to diminished ureteral tone from denervation of the transplant and from acute rejection [2,5]. Conversely, obstruction may be present with little or no hydronephrosis early in the course of obstruction or in the case of a scarred, nondistensible collecting system [4]. Renal collecting system dilation in the absence of obstruction (Fig. 19) may also be noted in patients who have free vesicoureteral reflux, especially when the bladder is full [4]. Reflux has been noted in up to 86% of renal transplants, but its clinical significance is controversial [39]. Reflux may be important in patients who have recurrent urinary tract infections and may place the transplant at increased risk for pyelonephritis and graft dysfunction [44].

The incidence of transplant calculi (Figs. 20 and 21) is estimated to be 0.4% to 1%; however, it is anticipated that longer graft survival may lead to more frequent detection of calculi [45]. Transplant calculi have been noted more frequently in patients who have secondary hyperparathyroidism, hypercalcuria, urinary tract infection, and ureteral stents [2,45]. In some instances the kidney may be harvested with stones, a condition termed

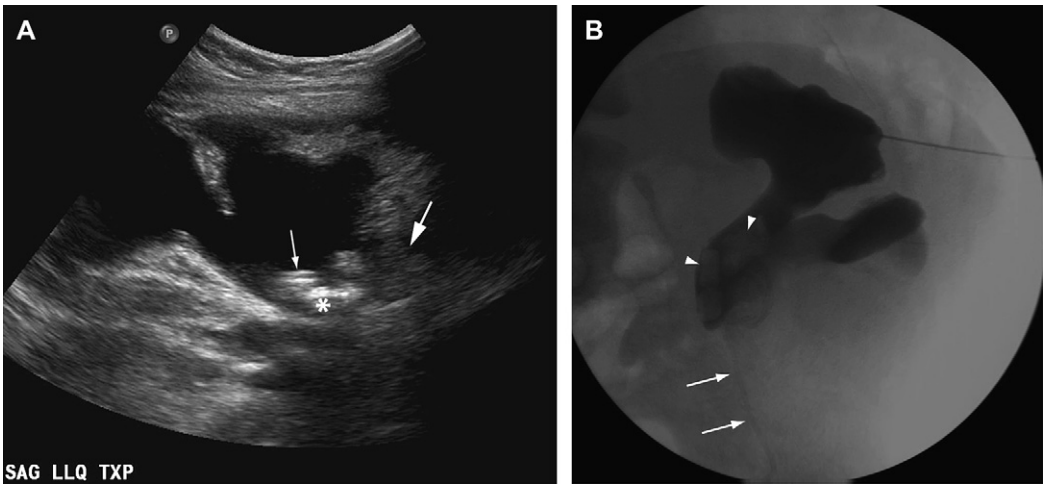

Fig. 21. Chronic hydronephrosis and multiple renal calculi. (*A*) Sagittal gray-scale image demonstrates an atrophic, hydronephrotic transplant kidney with indwelling proximal end of a double-J ureteral stent (*small arrow*) and debris (*large arrow*) and shadowing stones (*). (*B*) Nephrostogram showing obstruction of the encrusted ureteral stent (*arrows*) and multiple large nonradiopaque renal calculi (*arrowheads*).

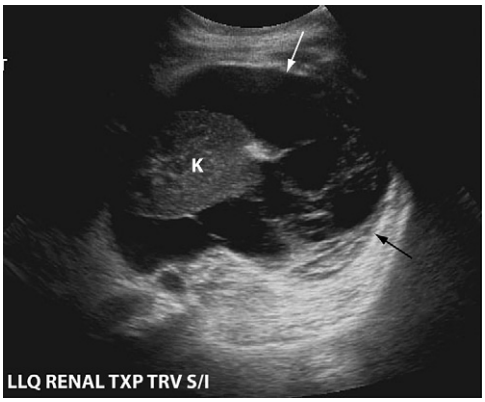

Fig. 22. Lymphocele. Transverse gray-scale image obtained 2 weeks after transplantation in a patient who had new right leg swelling demonstrates a thinly septated collection (*arrows*) around the transplant kidney (K, kidney) that proved to be a lymphocele on percutaneous drainage.

"donor-gifted allograft lithiasis." Small stones may pass spontaneously but larger ones may require treatment, including percutaneous nephrolithotomy or extracorporeal shock wave lithotripsy [4].

Peritransplant collections

Peritransplant collections have been reported in as many as 50% of renal transplant recipients [2]. Many are asymptomatic and are noted during routine sonographic evaluation of the kidney in the first 2 to 6 postoperative weeks [4,46,47]. Lymphoceles are the most common and characteristically have multiple thin septations (Fig. 22). They result from disruption of the donor kidney's lymphatics at the time of harvesting or from disruption of the recipient's lymphatics during dissection of the external iliac artery. They usually develop medial and inferior to the transplant or adjacent to the pelvic sidewall. Because the sonographic characteristics of all peritransplant collections are nonspecific, ultrasound-guided percutaneous aspiration maybe necessary to exclude urinary leak. Lymphoceles are rich in protein and cholesterol and have a creatinine level equal to serum. When small they may not necessarily require therapy, but 30% cause symptoms or ureteral compression (Fig. 23), requiring drainage and sclerosis [4,39].

Urinomas (see Fig. 16) vary in size and are most commonly noted between the transplant and the bladder, but may present in atypical locations, such as the thigh, scrotum, or labia [3]. On sonography, they are usually well-defined anechoic fluid collections without septations. Drainage is often performed under US guidance because of a high risk for secondary infection attributable to immunosuppression. Urinomas have a high creatinine level that distinguishes them from other pelvic fluid collections. Large urinomas may rupture, producing urinary ascites [4].

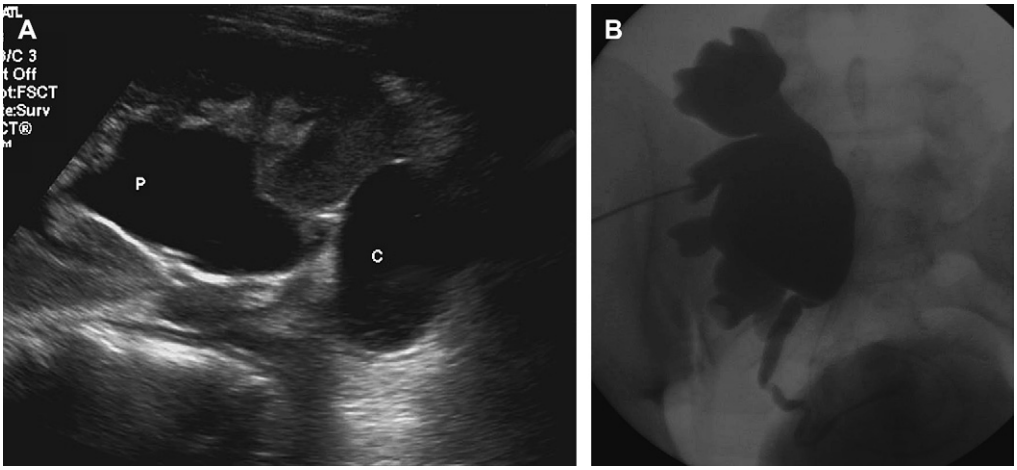

Fig. 23. Lymphocele contributing to hydronephrosis. (*A*) Gray-scale image obtained 10 weeks after transplantation in a patient who had rising creatinine demonstrates hydronephrosis secondary to compression of the proximal ureter by a lymphocele. (L, lymphocele; C, extrarenal collection which proved to be a lymphocele; P, dilated renal pelvis). The hydronephrosis did not completely resolve after drainage of the collection indicating that the obstruction was in part attributable to other factors. (*B*) Subsequent percutaneous nephrostomy revealed a poorly funneled ureteropelvic junction (UPJ) with sluggish drainage of contrast material from the pelvis into the ureter, characteristic of a congenital UPJ obstruction. The UPJ obstruction likely only became urodynamically significant as urine flow rates increased in the setting of improving renal function in the postoperative period.

Small crescent-shaped peritransplant collections surrounding the kidney transplant (see Fig. 2A), representing small hematomas or seromas, are almost considered an expected finding in the immediate postoperative period [2]. Acute hematomas tend to be more complex, echogenic, and solid appearing, whereas seromas and resolving hematomas are more cystic. Small collections do not require therapy; enlarging collections raise concern for an abscess or underlying vascular injury. Peritransplant abscesses are an uncommon complication and are most likely in the first few weeks after transplantation. They may occur secondary to development of transplant pyelonephritis or bacterial seeding of an adjacent lymphocele, hematoma, or urinoma. Patients are at risk secondary to immunosuppression, indwelling catheters, and frequent glycosuria. Abscesses tend to have a complex, cystic appearance on sonography and are indistinguishable from other complex peritransplant collections unless they contain gas.

Summary

Sonography is an important imaging technique in the evaluation of patients who have had renal transplantation. Sonographic examination can detect many of the potential urologic and vascular surgical complications that occur in the early postoperative period and threaten graft viability. Sonography is often able to guide diagnostic and therapeutic interventions when these complications are noted. Additionally, sonography provides an excellent noninvasive way to monitor the graft for late complications, such as renal artery stenosis.

Acknowledgments

The authors thank Andrea Kaldrovics for assistance preparing the figures.

References

[1] Brown ED, Chen MYM, Wolfman NT, et al. Complications of renal transplantation: evaluation with US and radionuclide imaging. Radiographics 2000;20:607–22.
[2] Akbar SA, Jafri SZ, Amendola MA, et al. Complications of renal transplantation. Radiographics 2005;25:1335–56.
[3] Baxter GM. Ultrasound of renal transplantation. Clin Radiol 2001;56:802–18.
[4] Sandhu C, Patel U. Renal transplantation dysfunction: the role of interventional radiology. Clin Radiol 2002;57:772–83.
[5] Pozniak MA, Dodd GD III, Kelcz F. Ultrasonographic evaluation of the renal transplant. Radiol Clin North Am 1992;30:1053–66.
[6] Friedewald SM, Molmenti EP, Friedewald JJ, et al. Vascular and nonvascular complications of renal transplants: sonographic evaluation and correlation with other imaging modalities, surgery and pathology. J Clin Ultrasound 2005;33:127–39.
[7] Basaran O, Moray G, Emiroglu R, et al. Graft and patient outcomes among recipients of renal grafts with multiple arteries. Transplant Proc 2004;36:102–4.
[8] Mancini M, Mainenti PP, Speranza A, et al. Accuracy of sonographic volume measurements of kidney transplant. J Clin Ultrasound 2006;34:184–9.
[9] Khosroshahi HT, Tarzamni M, Oskuii RA. Doppler ultrasonography before and 6 to 12 months after kidney transplantation. Transplant Proc 2005;37:2976–81.
[10] Li J, Ji Z, Cai S, et al. Evaluation of severe transplant renal artery stenosis with Doppler sonography. J Clin Ultrasound 2005;33:261–9.
[11] de Morais RH, Muglia VF, Mamere AE, et al. Duplex Doppler sonography of transplant renal artery stenosis. J Clin Ultrasound 2003;31:135–41.
[12] Hillburn MD, Bude RO, Murphy KJ, et al. Renal transplant evaluation with power Doppler ultrasound. Br J Radiol 1997;70:39–42.
[13] Sidhu MK, Gambir S, Jeffrey RB Jr, et al. Power Doppler imaging of acute renal transplant rejection. J Clin Ultrasound 1999;27:171–5.
[14] Chudek J, Kolonko A, Krol R, et al. The intrarenal resistance parameters measured by duplex Doppler ultrasound shortly after kidney transplantation in patients with immediate, slow and delayed graft function. Transplant Proc 2006;38:42–5.
[15] Datta R, Sandhu M, Saxena AK, et al. Role of duplex Doppler and power Doppler sonography in transplanted kidneys with acute renal parenchymal dysfunction. Australas Radiol 2005;49:15–20.
[16] Cochlin DLL, Wake A, Salaman JR, et al. Ultrasound changes in the transplant kidney. Clin Radiol 1988;39:373–6.
[17] Hollenbeck M, Hilbet N, Meusel F, et al. Increasing sensitivity and specificity of Doppler sonographic detection of renal transplant rejection with serial investigative technique. Clin Investig 1994;72:609–15.
[18] Trillaud H, Merville P, Tran L, et al. Colour Doppler sonography in early renal transplantation following follow-up: resistive index measurements versus power Doppler sonography. AJR Am J Roentgenol 1988;171:1611–5.
[19] Penn I, Bunson ME. Cancers after cyclosporine therapy. Transplant Proc 1998;20(Suppl 3):885–92.
[20] Kew CE, Lopez-Ben R, Smith JK, et al. Posttransplant lymphoproliferative disorder localized near the allograft in renal transplantation. Transplantation 2000;69:809–14.
[21] Jain M, Badwal S, Pandey R, et al. Post-transplant lymphoproliferative disorder after live donor

renal transplantation. Clin Transpl 2005;19: 668–73.
[22] Miller WT Jr, Siegel SG, Montone KT. Posttransplantation lymphoproliferative disorder: changing manifestations of disease in a renal transplant population. Crit Rev Diagn Imaging 1997;36:569–85.
[23] Lopez-Ben R, Smith JK, Kew CE, et al. Focal posttransplantation lymphoproliferative disorder at the allograft hilum. AJR Am J Roentgenol 2000; 175:14–7, 1422.
[24] Bretan PN Jr, Busch MP, Hricak H, et al. Chronic renal failure: a significant risk in the development of renal cysts and renal cell carcinoma. Cancer 1986;57:1871–9.
[25] Bakir N, Sluiter WJ, Ploeg RJ, et al. Primary renal graft thrombosis. Nephrol Dial Transplant 1996; 11:140–7.
[26] Orlic P, Vukas D, Drescik I, et al. Vascular complications after 725 kidney transplantations during 3 decades. Transplant Proc 2003;35:1381–4.
[27] Jordan ML, Cook GT, Cardella CJ. Ten years experience with vascular complications in renal transplantation. J Urol 1982;128:689–92.
[28] Penny MJ, Nankivell BJ, Disney AP, et al. Renal graft thrombosis. A survey of 134 consecutive cases. Transplantation 1994;58:565–9.
[29] Grenier N, Douws C, Morel D, et al. Detection of vascular complications in renal allografts with color Doppler flow imaging. Radiology 1991; 178:557–8.
[30] Dodd GD III, Tublin ME, Shah A, et al. Imaging of vascular complications associated with renal transplants. AJR Am J Roentgenol 1991;157: 449–59.
[31] Ojo AO, Hanson JA, Wolfe RA, et al. Dialysis modality and the risk of allograft thrombosis in adult renal transplant recipients. Kidney Int 1999;55:1952–60.
[32] Baxter GM, Morley R, Dall B. Acute renal vein thrombosis in renal allografts: new Doppler ultrasonic findings. Clin Radiol 1991;43:125–7.
[33] Baxter GM, Ireland H, Moss JG, et al. Colour Doppler ultrasound in renal transplant artery stenosis: which Doppler index? Clin Radiol 1995;50:618–22.
[34] Gottlieb RH, Lieberman JL, Pabico RC, et al. Diagnosis of renal artery stenosis in transplanted kidneys: value of Doppler waveform analysis of intrarenal arteries. AJR Am J Roentgenol 1995; 65:1441–6.
[35] Loubeyre P, Abidi H, Cahen R, et al. Transplanted renal artery: detection of stenosis with color Doppler US. Radiology 1997;203:661–5.
[36] Patel U, Khaw KK, Highes NC. Doppler ultrasound for the detection of renal transplant artery stenosis—threshold peak systolic velocity needs to be higher in low-risk or surveillance population. Clin Radiol 2003;58:772–7.
[37] Thalhammer C, Aschwnden M, Mayr M, et al. Duplex sonography after living donor kidney transplantation: new insights in the early postoperative phase. Ultraschall Med 2006;27: 141–5.
[38] Samhan M, Al-Mousawi M, Abdulhalim M, et al. Urologic complications after renal translation. Transplant Proc 2005;37:3075–6.
[39] Kocak T, Nane I, Ander H, et al. Urologic and surgical complications in 362 consecutive living related donor renal transplantations. Urol Int 2004;72:252–6.
[40] Karam G, Maillet F, Parant S, et al. Ureteral necrosis after kidney transplantation: risk factors and impact on graft and patient survival. Transplantation 2004;78:725–9.
[41] Makisalo H, Eklund B, Salmela K, et al. Urological complications after 2,084 consecutive kidney transplantations. Transplant Proc 1997;29: 152–3.
[42] Butterwroth PC, Horsburgh T, Veitch PS, et al. Urologic complications in renal transplantation:impact of a change of technique. Br J Urol 1997;79:499–502.
[43] Benoit G, Blanchet P, Eschwege P, et al. Insertion of double pigtail ureteral stent for the prevention of urological complications in renal transplantation: a prospective randomized study. J Urol 1996;156:881–4.
[44] Matthew TH, Kincaid-Smith P, Vikraman P. Risks of vesicoureteral reflux in the transplanted kidney. N Engl J Med 1997;297:414–8.
[45] Challacombe B, Dasgupta P, Tiptaft R, et al. Multimodal management of urolithiasis in renal transplantation. BJU Int 2005;96:385–9.
[46] Khauli RB, Stoff JS, Lovewell T, et al. Post-transplant lymphoceles: a critical look into risk factors, pathophysiology and management. J Urol 1993;150:22–6.
[47] Dubeaux VT, Oliveira RM, Moura VJ, et al. Assessment of lymphoceles incidence following 450 renal transplantations. Int Braz J Urol 2004;30:18-21.

ELSEVIER SAUNDERS

ULTRASOUND CLINICS

Ultrasound Clin 2 (2007) 89–104

Sonography of Pediatric Renal Tumors

Harriet J. Paltiel, MD

Ultrasonography (US) plays a crucial role in the imaging investigation of pediatric renal tumors because it is easily performed without the need for sedation or ionizing radiation. Gray-scale imaging can readily differentiate solid from cystic lesions. Color Doppler US with spectral analysis is used to evaluate the integrity of the renal vasculature. Once a solid lesion is demonstrated and a malignant neoplasm is suspected, cross-sectional imaging with CT or MR is performed to better delineate the extent of disease. Wilms' tumor is the most common pediatric solid renal mass. There are distinct clinical and imaging features that aid in differentiating Wilms' tumor from other renal masses of childhood.

Normal sonographic anatomy of the pediatric kidney

Renal size and parenchymal echogenicity vary with patient age. The most commonly used measurement of size is the upper to lower pole length [1]. Renal length measurements obtained with the patient in a supine or in a contralateral decubitus position tend to be slightly higher than those obtained with the patient prone [2].

Renal cortical echogenicity in neonates and infants tends to be greater than that of older children and adults. It is usually the same as or greater than the echogenicity of the adjacent liver or spleen (Fig. 1A), whereas the renal cortex in older individuals is hypoechoic relative to these organs (Fig. 1B). The increased cortical echogenicity in younger individuals is believed to be attributable to an increased cellularity and number of cortical glomeruli that leads to more acoustical interfaces. In healthy term infants renal cortical echogenicity is not usually greater than that of the liver or spleen. In contrast, renal cortical echogenicity in premature infants is often hyperechoic to these organs (Fig. 2). The more premature the infant, the greater the likelihood that the renal cortex will be hyperechoic [3]. During infancy the renal cortex decreases in echogenicity and by 1 year of age it is usually hypoechoic relative to the adjacent liver or spleen [4].

In infants less than 1 year of age the medullary pyramids appear more prominent and hypoechoic than in older children and adults (Fig. 3). This appearance is believed to be because of the larger medullary volume and smaller cortical volume in infants [4,5].

Department of Radiology, Children's Hospital Boston, 300 Longwood Avenue, Boston, MA 02115, USA
E-mail address: harriet.paltiel@childrens.harvard.edu

1556-858X/07/$ – see front matter
doi:10.1016/j.cult.2007.01.004
ultrasound.theclinics.com

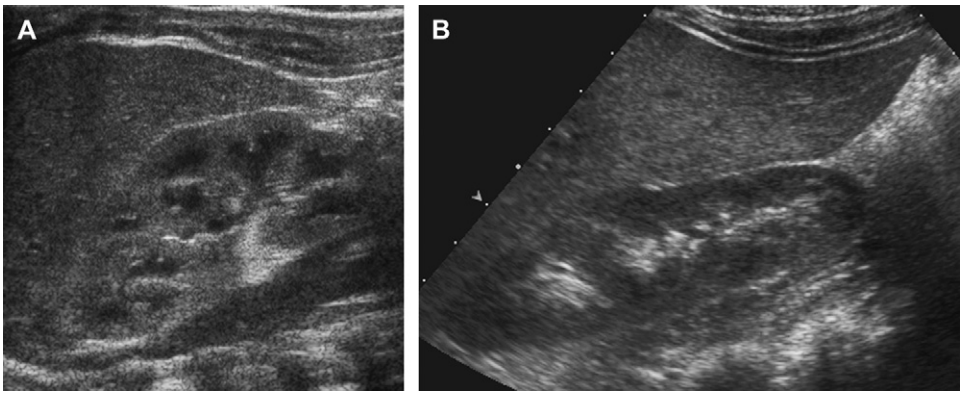

Fig. 1. Normal kidney. (*A*) Longitudinal sonogram of the normal right kidney in a 20-day-old full term neonate demonstrates renal cortex isoechoic to the adjacent hepatic parenchyma. (*B*) Longitudinal sonogram of a normal right kidney in a 5-year-old child demonstrates renal cortex hypoechoic to the adjacent hepatic parenchyma.

Finally, the renal sinus in neonates and infants is less echogenic than in older children and adults because of a relative paucity of fat in this location (see Figs. 1A, 2, 3). The echogenicity of the renal sinus increases with age and approaches that of the adult by adolescence [4,5].

Normally, the renal pelvis measures 10 mm or less in anteroposterior diameter and is not associated with calyceal dilation [6,7]. The walls of the normal collecting system are not visible. Mural thickening suggests the presence of urinary tract infection, vesicoureteral reflux, or chronic obstruction.

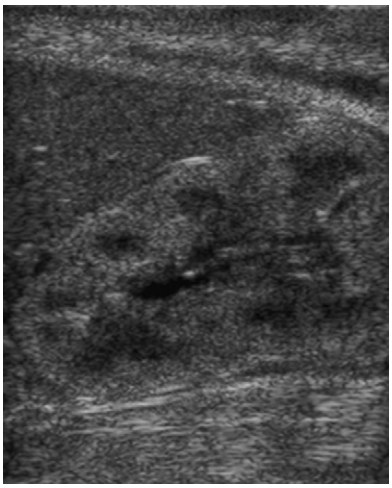

Fig. 2. Normal kidney in a 7-day-old premature infant born at a gestational age of 24 weeks. Longitudinal sonogram of the right kidney depicts renal cortex hyperechoic to the adjacent hepatic parenchyma.

Renal tumors

Wilms' tumor

Wilms' tumor represents approximately 6% of all childhood tumors and is the most common pediatric renal malignancy, with an incidence of approximately 500/y in the United States. Current 5-year survival is greater than 90% [8,9]. Most Wilms' tumors appear within the first 5 years of life, with a mean age at diagnosis for boys with unilateral disease of 41.5 months compared with 46.9 months for girls. For children presenting with bilateral disease the mean age at diagnosis is 29.5 months for boys and 32.6 months for girls [10,11]. Wilms' tumor is rare in neonates, with less than 0.16% of cases occurring in this age group [11]. Approximately 6% of Wilms' tumors are bilateral. Although most Wilms' tumors are sporadic, approximately 1% are familial [11]. The mode of inheritance is usually autosomal dominant with variable

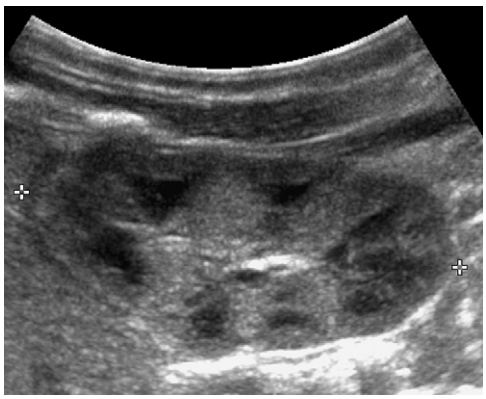

Fig. 3. Normal kidney (*between cursors*) in an 18-day-old infant. Note the prominent hypoechoic medullary pyramids.

penetrance and expressivity [12]. Extrarenal abnormalities occur in approximately 8% of patients who have Wilms' tumor, including congenital sporadic aniridia, and overgrowth disorders, such as hemihypertrophy [12,13]. Certain genetic syndromes are also associated with Wilms' tumor, including trisomy 18, Beckwith-Wiedemann syndrome, and WAGR (Wilms' tumor, aniridia, genitourinary abnormalities, mental retardation) and Drash (male pseudohermaphroditism and progressive glomerulonephritis) syndromes [10,13].

Two loci on chromosome 11 have been implicated in the development of a minority of Wilms' tumors, locus 11p13 (the WT1 gene), and locus 11p15 (the WT2 gene). An abnormal WT1 gene is present in patients who have the WAGR and Drash syndromes, whereas an abnormal WT2 gene has been identified in patients who have Beckwith-Wiedemann syndrome (macroglossia, macrosomia, visceromegaly, umbilical hernia or omphalocele, neonatal hypoglycemia) and hemihypertrophy. Additional genetic abnormalities have been found on chromosomes 1, 12, and 8 in other patients who have Wilms' tumor, all of which point to a multifactorial cause. Several potential genetic prognostic factors have also been identified, including loss of heterozygosity at chromosomes 1p and 16q. Children who have loss of heterozygosity at 16q seem to be at greater risk for relapse and mortality than children who do not have this genetic abnormality. According to the fifth National Wilms' Tumor Study (NWTS-5), tumor-specific loss of heterozygosity for both chromosomes 1p and 16q, identified in about 5% of patients who have favorable-histology Wilms' tumor, was shown to be associated with a significantly increased risk for relapse and death [14].

Wilms' tumor is presumed to develop as a result of abnormal histogenesis. Renal blastemal tissue is believed to be a precursor of Wilms' tumor. Development of the fetal kidney is complete by 36 weeks of gestation, and the kidneys of normal term infants contain no residual foci of renal blastema. Nodules of renal blastema are found in approximately 15% of kidneys harboring Wilms' tumor, however, and are particularly common when the tumor is bilateral [15,16]. Nephrogenic rests are of two distinct types, perilobar and intralobar, distinguished primarily by their position within the renal lobe. Perilobar rests are confined to the lobar periphery. Intralobar nephrogenic rests may be found anywhere within the renal lobe, in the walls of the pyelocalyceal system, and in the renal sinus. Nephrogenic blastemal cells arising earlier in gestation tend to be situated deeper in the lobe; there is an increased association between intralobar nephrogenic rests and subsequent development of Wilms' tumor [17]. Nephrogenic rests are classified into four subtypes based on gross and microscopic characteristics: incipient or dormant, regressing or sclerosing, hyperplastic, and neoplastic [18]. In the NWTS-4 report, 41% of the unilateral and 99% of the synchronous bilateral Wilms' tumors were associated with the presence of nephrogenic rests [17]. In children who have aniridia or the Denys-Drash syndrome the lesions are primarily intralobar, whereas in children who have hemihypertrophy or Beckwith-Wiedemann syndrome the lesions are mainly perilobar in distribution.

Histologically, Wilms' tumor contains epithelial, stromal, and blastemal elements. Tumor histology is the most important prognostic factor. Favorable histology occurs in approximately 90% of all tumors, consisting of fairly well-differentiated renal tissue with embryonic or abortive glomeruli and tubule formation surrounded by spindle cell stroma (Fig. 4). The tumor may have components of striated muscle, fibrous tissue, cartilage, bone, and adipose tissue. Unfavorable histology occurs in approximately 10% of tumors, with anaplastic features, including variability in size and shape of nuclei, enlarged hyperchromatic nuclei, and large numbers of mitotic figures (Fig. 5).

Wilms' tumor may arise from any portion of the kidney. It may be exophytic, but usually expands within the renal parenchyma to displace and distort the pyelocalyceal system. It is usually solid and has a pseudocapsule that separates it from normal renal parenchyma. The renal capsule is generally intact; rarely, the tumor breaks through the capsule and extends into the extrarenal space. Areas of central hemorrhage and necrosis may produce a cystic appearance. Local metastases to regional lymph nodes are frequent. Occasionally there may be urothelial spread. Wilms' tumor may invade the renal vein and inferior vena cava. It is important to document

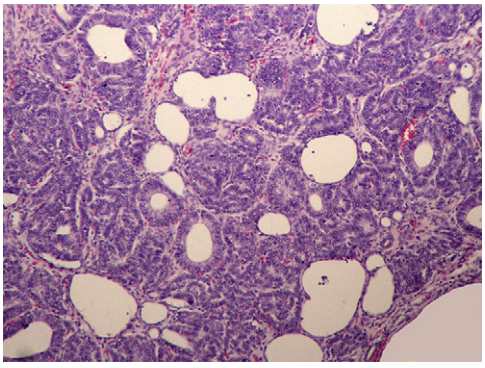

Fig. 4. Favorable histology Wilms' tumor showing predominantly epithelial components. Hematoxylin and eosin stain. (*Courtesy of* Antonio Perez-Atayde, MD, Boston, MA.)

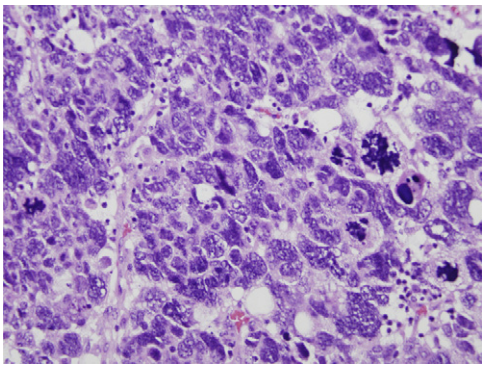

Fig. 5. Unfavorable histology Wilms' tumor showing marked anaplasia with atypical mitoses, nuclear pleomorphism, hyperchromatism, and unrest. Hematoxylin and eosin stain. (*Courtesy of* Antonio Perez-Atayde, MD, Boston, MA.)

venous extension preoperatively as its presence affects the surgical approach. Distant metastases most often occur to the lungs and liver. Renal vein extension explains the high frequency (12% to 20%) of hematogenous lung metastases at diagnosis. Although many lung metastases are detected by chest radiography, CT is important to verify the presence or absence of small metastases. Pneumothorax occasionally complicates metastases from the anaplastic form of Wilms' tumor.

Staging of Wilms' tumor occurs on the basis of information provided by imaging modalities, surgery, and pathologic examination. The staging system used by the National Wilms' Tumor Study Group (NWTSG) is outlined in Box 1 [9].

Imaging of Wilms' tumor should define the size and location of the primary tumor, local spread, and sites of distant metastases. Imaging is also used for surveillance of people at risk for primary or recurrent Wilms' tumor. Sporadic Wilms' tumor is usually diagnosed by observation of abdominal distention and palpation of an abdominal mass. Tumors associated with familial transmission and genetic syndromes are often detected by screening. Screening for Wilms' tumor in patients who have associated syndromes should begin at syndrome diagnosis with serial US every 3 to 4 months up to 5 to 7 years of age [19,20]. The duration of screening depends on the age range of Wilms' tumor presentation in the predisposing condition. After the age of 5 to 7 years, depending on the particular condition under surveillance, screening can be discontinued because the risk for developing Wilms' tumor decreases significantly [21,22].

US is usually the first imaging modality performed in a child who has a palpable abdominal mass. Wilms' tumor is typically large, sharply marginated, and hyperechoic relative to the normal renal parenchyma. Hypoechoic regions within the tumor may be attributable to hemorrhage, necrosis, or dilated calyces [23]. Because of the high frequency of extension of Wilms' tumor into the renal vein, inferior vena cava (IVC), and occasionally the right atrium, careful evaluation for tumor thrombus using color Doppler US with spectral analysis is mandatory. Venous extension is diagnosed when an intravascular echogenic focus is identified (Fig. 6). Because Wilms' tumors are usually large, however, precise sonographic evaluation of the IVC maybe difficult because of marked extrinsic displacement and compression by the tumor mass. This situation may prevent adequate US evaluation of venous structures, especially in uncooperative children. CT or MR imaging is usually helpful in defining vena caval patency (Fig. 7).

Current treatment of Wilms' tumor is surgical with adjuvant chemotherapy. The opposite kidney is explored to exclude synchronous bilateral tumor involvement. Radiation therapy may be used after surgery. Most oncologists consider that a 2-year

***Box 1:* National Wilms' Tumor Study Group staging system for renal tumors**

Stage I
Tumor confined to the kidney and completely resected. No penetration of the renal capsule or involvement of renal sinus vessels.

Stage II
Tumor extends beyond the kidney but is completely resected (negative margins and lymph nodes). At least one of the following has occurred: (a) penetration of the renal capsule, (b) invasion of the renal sinus vessels, (c) biopsy of tumor before removal.

Stage III
Gross or microscopic residual tumor remains postoperatively, including inoperable tumor, positive surgical margins, spillage of tumor preoperatively or intraoperatively, regional lymph node metastases, or transected tumor thrombus.

Stage IV
Hematogenous metastases or lymph node metastases outside the abdomen (eg, lung, liver, bone, brain).

Stage V
Bilateral renal Wilms' tumors.

From Dome JS, Perlman EJ, Ritchey ML, et al. Renal tumors. In: Pizzo PA, Poplack DG, editors. Principles and practice of pediatric oncology. 5th edition. Philadelphia: Lippincott Williams & Wilkins; 2006. p. 915; with permission.

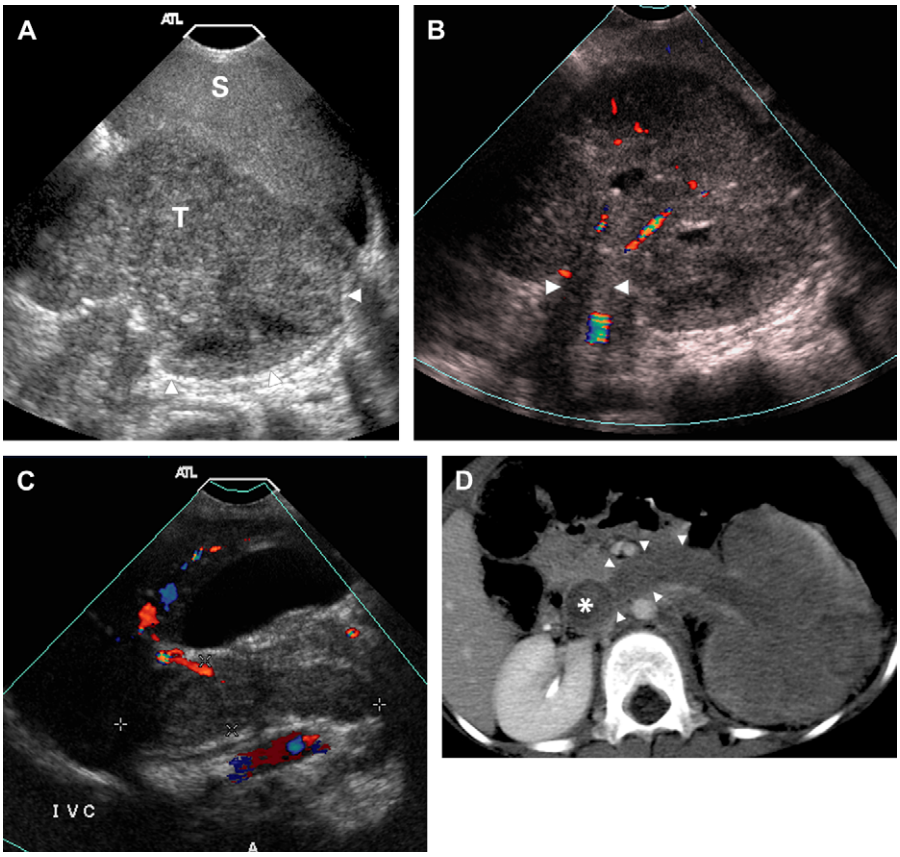

Fig. 6. Wilms' tumor. (*A*) Longitudinal sonogram shows a large, echogenic tumor (*T*) replacing most of the left kidney. Residual normal lower pole renal parenchyma is present along the inferior aspect of the tumor (*arrowheads*). S, spleen. (*B*) Transverse color Doppler sonogram of the left kidney demonstrates distention of the main renal vein by echogenic clot (*arrowheads*) with associated absence of venous flow. (*C*) Longitudinal color Doppler sonogram of the IVC depicts a large intraluminal clot (*between calipers*). (*D*) Contrast-enhanced axial CT image at the level of the tumor confirms invasion of the left renal vein (*arrowheads*) and IVC (*asterisk*).

disease-free survival after treatment indicates cure. Surgery with supplemental chemotherapy and irradiation has led to a 2-year survival rate of more than 90% in patients who have favorable histologic features. Mortality remains high in children who have unfavorable histologic features. Follow-up imaging after treatment includes serial chest CT and abdominal US, CT, or MR imaging.

Nephroblastomatosis

The term nephroblastomatosis refers to the presence of multiple or diffuse nephrogenic rests. The vast majority of nephrogenic rests regress spontaneously; their incidence in infants is approximately 100 times greater than that of Wilms' tumor (1/10,000 infants) [24]. Macroscopic nephrogenic rests are usually detected sonographically as hypoechoic masses. Diffuse hyperplastic perilobar nephroblastomatosis is a distinct disorder with unilateral or bilateral renal involvement. The affected kidney is massively enlarged but maintains a normal configuration because of a peripheral rind of abnormal parenchyma (Fig. 8). Sonographically the kidney may demonstrate diffusely decreased echogenicity with absent corticomedullary differentiation. MR imaging may be useful in following children who have nephroblastomatosis and in documenting a transition from nephrogenic rest to Wilms' tumor by alterations in imaging characteristics and growth [25]. Treatment of nephroblastomatosis is controversial. Although chemotherapy has been advocated by some to control the proliferative elements of the nephrogenic rests, there are no data to support its efficacy. Others recommend careful radiologic follow-up of enlarging masses. Nephrectomy is not performed [26,27].

Renal cell carcinoma

Renal cell carcinoma (RCC) is a malignancy that arises from the epithelial cells of the renal tubule.

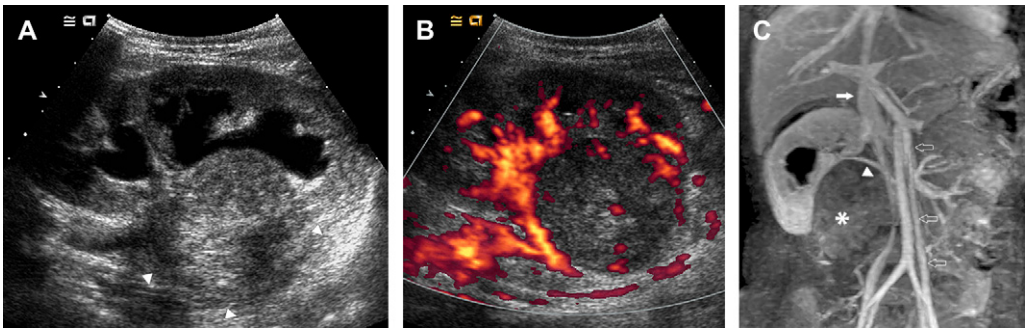

Fig. 7. Wilms' tumor. (*A*) Longitudinal sonogram depicts a right renal hilar mass (*arrowheads*) with associated hydronephrosis. (*B*) Power Doppler sonogram demonstrates marked displacement and distortion of the course of the hilar vessels. Patency of the main renal vein could not be determined with certainty. (*C*) Coronal image from an MR angiogram demonstrates superior displacement of the patent right renal vein (*arrowhead*) by the mass (*asterisk*). The IVC is patent (*arrow*). Incidental note is made of a duplicated left-sided IVC (*open arrows*).

Although it accounts for 90% to 95% of renal neoplasms in adults and is the sixth leading cause of adult cancer death in the United States [28,29], it is rare in the pediatric population, accounting for approximately 2.6% of solid renal malignancies in children [30]. Wilms' tumor is approximately 30 times more common than RCC in childhood [31], although their incidence is nearly equal in the second decade of life [32].

Recent studies have identified significant differences in clinical presentation and behavior of pediatric RCC compared with its adult counterpart [33–36], along with unique genetic abnormalities [34,37–39], an association with neuroblastoma [40], and distinct pathologic characteristics [32,33]. The mean age at diagnosis is about 10 years. Unlike RCC in adults, there is a female, not male, predominance [34,36,41]. Presenting signs

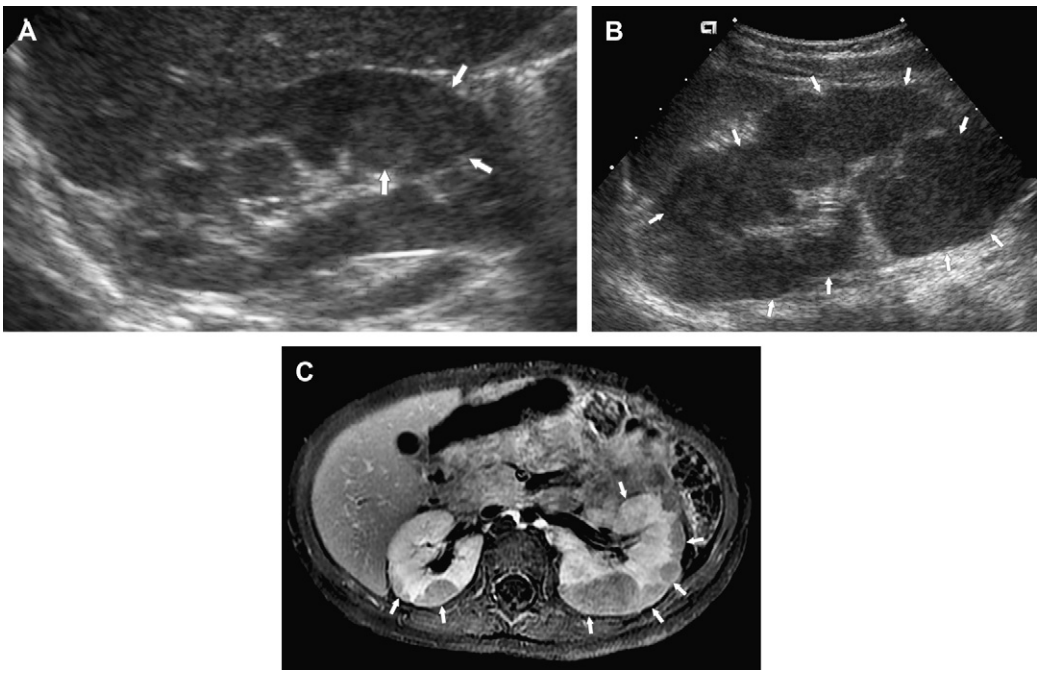

Fig. 8. Nephroblastomatosis. Longitudinal sonograms demonstrate thickening of the renal parenchyma, focally on the right (*A*; *arrows*) and more diffusely on the left (*B*; *arrows*). There is associated loss of normal corticomedullary differentiation. Contrast-enhanced, fat-suppressed axial T1-weighted MR image (*C*) depicts bilateral renal masses in a perilobar distribution (*arrows*). The masses are hypointense compared with the adjacent normal renal parenchyma.

and symptoms are generally related to the primary tumor instead of metastatic disease, and include abdominal or flank pain, a palpable abdominal mass, and hematuria. RCC is associated with von Hippel–Lindau syndrome in which the tumors tend to be multiple and present at a younger age [32]. There also seems to be an association with prior malignancy [41]. Several authors have reported a higher proportion of papillary histology in childhood RCC than in adults, in whom clear cell histology is predominant [41,42].

Pathologically, RCC may be well circumscribed by a pseudocapsule or infiltrating, with variable degrees of hemorrhage, necrosis, cystic degeneration, and calcification. The tumor invades locally with spread to adjacent retroperitoneal lymph nodes. Metastases to the lungs, bones, liver, or brain are found in approximately 20% of patients at diagnosis [43]. Although RCC tends to be smaller than Wilms' tumor, its gross morphology is similar, and the two can be indistinguishable preoperatively. Prognosis depends largely on tumor stage at presentation, with an overall 20-year survival of 55% in a recent series [36]. Both the Robson and TNM classifications are used for staging of RCC. Because these tumors are usually resistant to chemotherapy, treatment consists of radical nephrectomy and regional lymphadenectomy. A recent report noted equivalent survival in patients undergoing partial nephrectomy [42].

As with Wilms' tumor, imaging of RCC is used to define the size and location of the primary tumor, local spread, and sites of distant metastases. Sonographically the tumors have a variable appearance, depending on the presence or absence of necrosis, hemorrhage, and calcification. Invasion into the renal vein and IVC can be documented with gray scale and color Doppler US. CT and MR imaging are used to document local spread and metastatic disease (Fig. 9).

Clear cell sarcoma

Clear cell sarcoma of the kidney is a highly malignant neoplasm with a predilection for bone metastases. Approximately 20 new cases of clear cell sarcoma are diagnosed each year in the United States [44]. In a large series of 351 cases, including 182 patients entered on NWTSG trials 1 to 4, the male to female ratio was 2:1. The mean age at diagnosis for the NWTG patients was 36 months with a range of 2 months to 14 years [45]. Typical gross features included large size with a mean diameter of

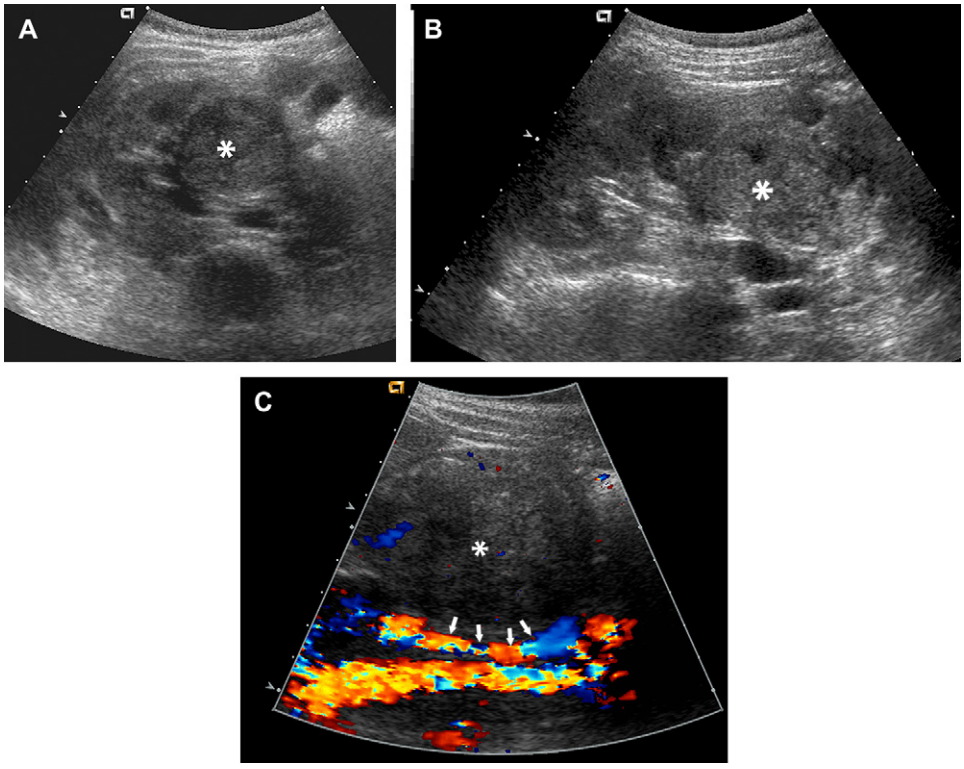

Fig. 9. Renal cell carcinoma. Transverse (*A*) and sagittal (*B*) sonograms demonstrate a mildly heterogeneous solid mass arising from the lower pole of the right kidney (*asterisk*). Color Doppler sonogram (*C*) depicts indentation of the IVC (*arrows*) by the mass (*asterisk*) without invasion.

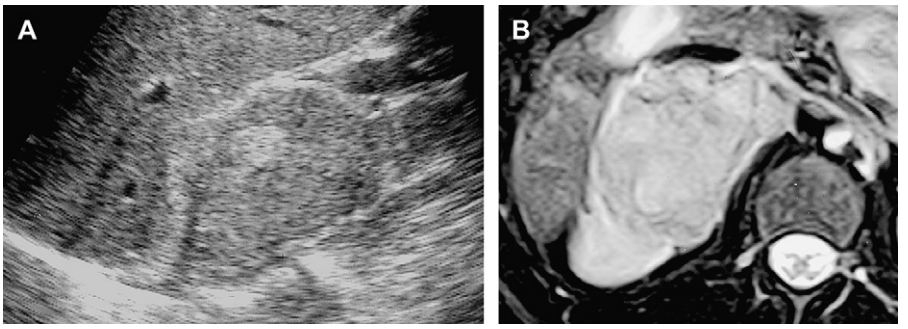

Fig. 10. Clear cell sarcoma. Sagittal sonogram (*A*) and T2-weighted axial MR image (*B*) depict a heterogeneous, solid mass arising from the upper pole of the right kidney.

11.3 cm, mucoid texture, cyst formation, and foci of necrosis. Nine major histologic patterns were identified with all tumors containing multiple patterns. Overall survival was 69% with a 98% survival for stage 1 patients. Independent prognostic factors for survival include age at diagnosis, stage, tumor necrosis, and treatment with doxorubicin.

Ipsilateral renal lymph nodes are common sites of metastatic spread at presentation. Bone metastases are the most common mode of relapse followed by lung, abdominal/retroperitoneal, brain, and liver metastases. Late relapses are not uncommon, especially among patients treated with doxorubicin [44]. Imaging features are indistinguishable from Wilms' tumor (Fig. 10).

Malignant rhabdoid tumor

Malignant rhabdoid tumor of the kidney is a rare, aggressive tumor of infancy and early childhood that has a high association with primary brain tumors and a propensity to metastasize to the brain [46,47]. Metastatic spread to the lungs and liver is also common. There is a high relapse rate and a mortality of more than 80%. Imaging findings of malignant rhabdoid tumor tend to be indistinguishable from Wilms' tumor. Although the characteristic appearance of a peripheral fluid collection attributable to subcapsular hematoma (Fig. 11) and a thickened, irregular renal capsule with tumor implants has been described, these findings are not pathognomonic and may occur in patients who have other forms of renal malignancy as well [48,49]. Because of the association with primary central nervous system tumors, imaging of the brain should be performed routinely.

Medullary carcinoma

Renal medullary carcinoma is a recently recognized tumor with distinctive clinical and pathologic features that is believed to arise in collecting duct epithelium. Almost all patients who have renal medullary carcinoma have sickle cell trait. It has

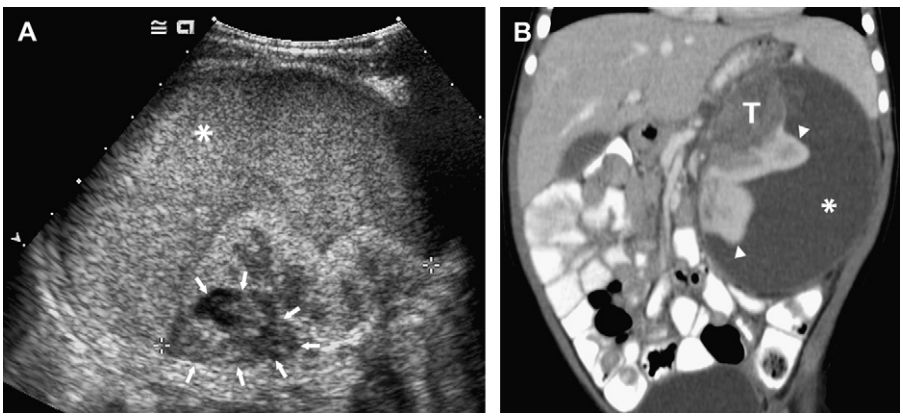

Fig. 11. Malignant rhabdoid tumor. Sagittal sonogram (*A*) of the left flank demonstrates the presence of a large fluid collection (*asterisk*) surrounding the left kidney (*between cursors*). There is a heterogeneous, hypoechoic upper pole renal mass (*arrows*). (*B*) The subcapsular hematoma (*asterisk*) and left upper pole renal tumor (T) are well depicted on a contrast-enhanced coronal CT image. Note compression of the renal parenchyma (*arrowheads*) by the hematoma.

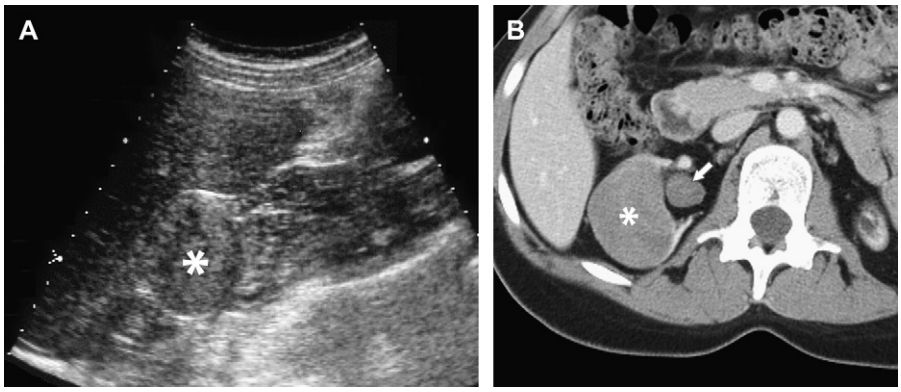

Fig. 12. Renal medullary carcinoma arising in a native kidney after renal transplantation. Sagittal sonogram (*A*) depicts a well-circumscribed mass (*asterisk*) in the upper renal pole of an atrophic right kidney. Axial contrast-enhanced CT image (*B*) demonstrates the mass within the right kidney (*asterisk*) with extension into the renal pelvis (*arrow*).

been postulated that the epithelium of the renal papilla undergoes chronic ischemic damage related to sickling erythrocytes, and that renal medullary carcinoma originates in a setting of chronic regeneration of this damaged epithelium. Renal medullary carcinoma is an aggressive tumor that typically occurs in young patients between the ages of 10 and 40 years with a mean age of 22 years. There is a male predominance before the age of 24 years, after which the tumors occur equally among men and women. Abdominal and flank pain, weight loss, and gross hematuria are common presenting complaints, and some patients present with symptoms of metastatic cancer. A palpable abdominal mass is often noted. The tumors typically occupy the renal medulla and are poorly circumscribed, lobulated, and demonstrate varying degrees of hemorrhage and necrosis. Satellite nodules are commonly present as is extension into the perinephric and sinus fat. Microscopically, there are various morphologic patterns. The most common is a reticular or microcystic growth pattern that resembles yolk sac tumor of the testis [50,51]. Characteristic imaging findings include an infiltrative renal mass with associated caliectasis and retroperitoneal adenopathy (Fig. 12) [52,53].

Renal lymphoma

Primary lymphoma of the kidney is extremely rare. Renal involvement is often present in the terminal phases of the disease, however, particularly in the setting of non-Hodgkin lymphoma. There may be many small renal nodules, large confluent masses, or diffuse parenchymal infiltration resulting in bilateral renal enlargement. Diffuse renal involvement usually produces a decrease in parenchymal echogenicity by US. Lymphomatous nodules may appear hypoechoic or anechoic. There may be distortion of the renal contours and disruption of normal renal architecture (Fig. 13). There is almost always coexistent retroperitoneal or mesenteric adenopathy [54,55].

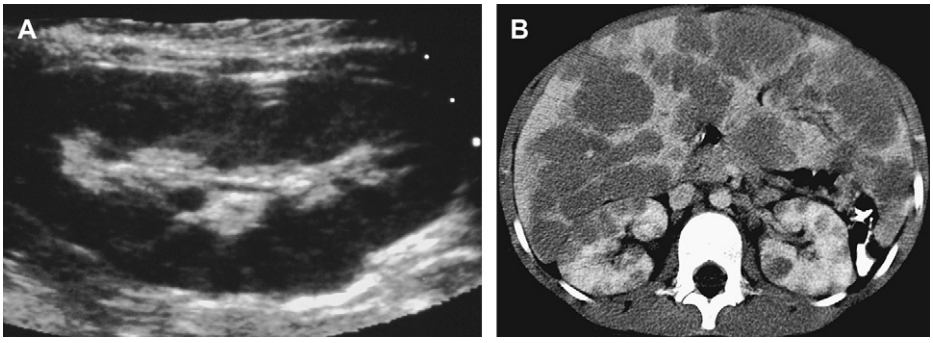

Fig. 13. Renal involvement in patient with Burkitt's lymphoma. (*A*) Sagittal sonogram of the left kidney shows loss of normal renal corticomedullary differentiation. There are multiple hypoechoic tumor nodules replacing much of the renal parenchyma. (*B*) Contrast-enhanced axial CT depicts extensive involvement of kidneys, liver, and retroperitoneal nodes by lymphoma.

Multilocular cystic tumors

Multilocular cystic renal tumors include two histologically distinct but otherwise identical lesions: multilocular cystic nephroma (multilocular renal cyst, cystadenoma) and cystic partially differentiated nephroblastoma (CPDN) [56,57]. Multilocular cystic nephroma is a cystic mass containing multiple septa composed entirely of differentiated tissues, without blastemal, embryonal, or other malignant elements. CPDN is also a multilocular lesion without solid or nodular components. Its septa contain blastemal or other embryonal cells, however. Grossly, multilocular cystic renal tumors consist of a solitary, well-circumscribed, multiseptated mass of noncommunicating, fluid-filled cysts surrounded by a thick, fibrous capsule. Cyst herniation into the renal pelvis has been described [58].

Multilocular cystic tumors mainly affect boys in early childhood, in whom a substantial portion of lesions contain embryonal elements (CPDN), and women, whose lesions commonly contain only mature cells (multilocular cystic nephroma). Children who have multilocular cystic renal tumors present with a painless abdominal mass. Symptoms (pain, hematuria, urinary tract infection) are more common in adults.

Multilocular cystic nephroma and CPDN cannot be distinguished by imaging. On US, the tumor usually consists of multiseptated, cystic mass. Lesions with small cysts and numerous acoustic interfaces may resemble a solid mass, however [59]. On CT and MR imaging the septa demonstrate enhancement after contrast administration. The attenuation of the cyst contents is similar to water by CT, whereas MR imaging demonstrates variable signal intensity, presumably because of differing concentrations of protein and blood products (Fig. 14) [56,60,61].

The histogenesis of multilocular cystic renal tumors is unknown. Most authorities consider the neoplasms to be benign equivalents of nephroblastoma or hamartoma [62]. It is highly unlikely that they represent congenital cystic dysplasia. It is impossible to distinguish accurately, by imaging alone, a benign multilocular cystic nephroma from CPDN or from multilocular cystic nephroma containing foci of renal blastema, Wilms' tumor, or renal cell carcinoma. The presence of thick or irregular septa on examination with US, CT, or MR imaging is suggestive of CPDN [63]. This type of multilocular nephroma frequently contains blastemal elements within the cyst wall and is considered a cystic variant of Wilms' tumor. Demonstration of fine, linear septa by imaging suggests benignity. The treatment of multilocular cystic nephroma, with or without Wilms' tumor or blastemal elements, is nephrectomy. Regular postoperative surveillance is advised in patients who have the CPDN variant [57].

Congenital mesoblastic nephroma

Congenital mesoblastic nephroma (mesenchymal hamartoma) is the most common neonatal renal neoplasm [64,65]. It is almost always discovered during the first few months of life, although rarely it is detected in older children or even adults. Occasionally it is detected as a solid renal mass in utero, and may be associated with polyhydramnios, hydrops fetalis, or dystocia [66]. The neonate usually presents with a large, nontender abdominal mass with no other abnormalities. Hematuria is occasionally present. The mean age at diagnosis is 3.4 months and there is a 2:1 male predominance [67]. In the past it was believed that Wilms' tumor occurring in neonates had a better prognosis than in older children. In fact, most solid renal tumors presenting in the first weeks of life are benign

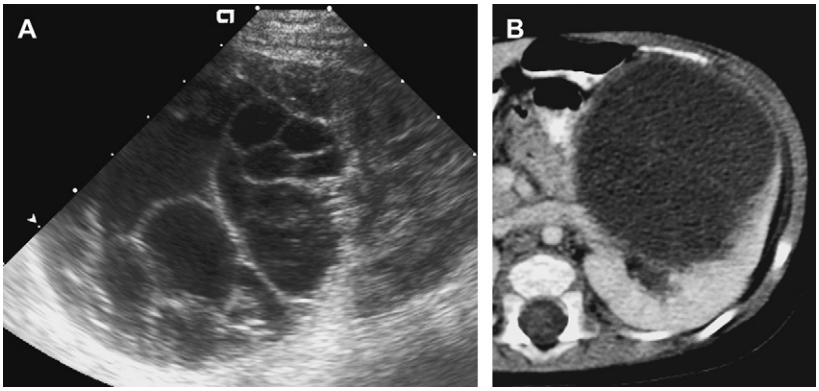

Fig. 14. Multilocular cystic nephroma in a 6-month-old boy. Sagittal sonogram of the left kidney (*A*) depicts a cystic upper pole mass containing numerous delicate septa. Axial CT (*B*) demonstrates a low-attenuation cystic mass with very faintly enhancing septa.

mesoblastic nephromas [65]. Mesoblastic nephroma is distinguished from Wilms' tumor by its earlier presentation, distinct histologic features, and more favorable outcome.

Pathologically the typical lesion is an unencapsulated mass with a whorled appearance on cut section that resembles a uterine fibroid. The tumor margins blend imperceptibly with normal renal parenchyma and may penetrate the renal capsule with extension into the perinephric space or retroperitoneum. Mesoblastic nephroma is histologically benign and does not invade the renal pedicle, extend into the renal pelvis, or metastasize to remote sites. Local recurrence may result from capsular penetration or incomplete resection. Hemorrhage and necrosis are uncommon, although the neoplasm may show grossly cystic changes, especially at the junction of the tumor and uninvolved kidney. Microscopically mesoblastic nephroma consists of benign-appearing spindle cells. The histologic appearance is so distinctive that it is considered a unique hamartomatous lesion unrelated to Wilms' tumor [68]. At the interface with normal kidney, sheets of spindle cells grow between intact nephrons. Foci of calcification may be present. A subgroup of patients has a form of mesoblastic nephroma that is highly cellular with an extremely large number of mitotic cells and occasional aggressive behavior, including local recurrence and distant metastases [69].

US usually demonstrates a large, echogenic mass that is either homogeneous in echotexture or heterogeneous as a result of hemorrhage or necrosis (Fig. 15). A distinctive sonographic "ring sign" has been described in some tumors [70]. Differentiation between mesoblastic nephroma and a rare neonatal Wilms' tumor is not generally possible based solely on imaging features, however. Imaging also cannot differentiate between a typical mesoblastic nephroma and the potentially more aggressive cellular form of the tumor.

The prognosis after compete surgical removal is excellent in most patients. In children who have the cellular form of mesoblastic nephroma, the age at diagnosis determines prognosis. Patients undergoing resection when they are younger than 3 months of age are less likely to develop local recurrence or metastatic disease than older children [69]. Chemotherapy and radiation are therefore generally reserved for children older than 3 months of age who have extensive local tumor metastases or recurrent disease [67,69].

Angiomyolipoma

Angiomyolipoma is a benign tumor that consists histologically of a disordered arrangement of fatty, vascular, and smooth muscle elements. Two types of angiomyolipoma have been described: isolated angiomyolipoma and angiomyolipoma associated with tuberous sclerosis. Isolated angiomyolipoma, which occurs sporadically, is often solitary and accounts for 80% of the tumors. Mean patient age at presentation is 43 years, and is approximately four times more common in women than in men. Angiomyolipoma associated with tuberous sclerosis accounts for 20% of the tumors; these lesions are typically larger than isolated angiomyolipoma and are often multiple and bilateral. Angiomyolipomas occur in 80% of patients who have tuberous sclerosis. The sex distribution of angiomyolipoma in patients who have tuberous sclerosis is closer to being equal, although females still outnumber males in prevalence [71].

In childhood, angiomyolipoma is rare in the absence of tuberous sclerosis. In contrast, 80% of children who have tuberous sclerosis develop angiomyolipomas by the age of 10 years [72]. In patients who have tuberous sclerosis, angiomyolipomas tend to be bilateral and multiple. Although classified as benign tumors, they may be locally aggressive, replacing renal parenchyma and extending into prevertebral tissues and local lymph nodes.

Symptoms are related to the development of intratumoral aneurysmal hemorrhage. Tumors less than 4 cm in diameter are generally asymptomatic.

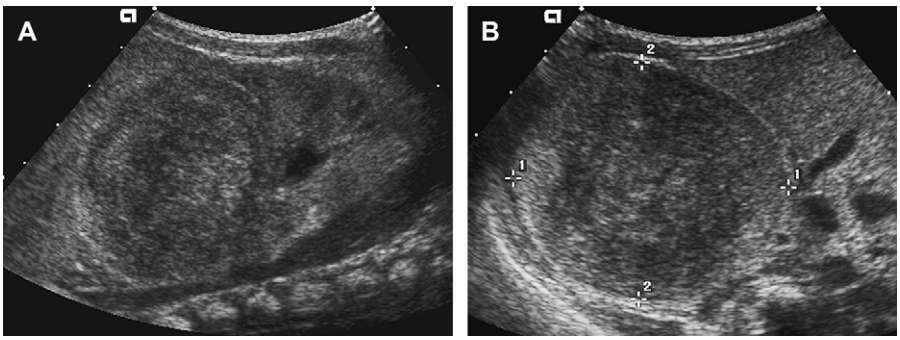

Fig. 15. Mesoblastic nephroma. Sagittal (*A*) and transverse (*B*) sonograms demonstrate a mildly heterogeneous solid mass (*between cursors*) arising from the upper pole of the right kidney.

Tumors larger than 4 cm in diameter are more likely to undergo spontaneous hemorrhage resulting in hematuria and flank or abdominal pain [73]. Occasionally life-threatening hemorrhage may occur [74].

The imaging appearance of angiomyolipoma depends on the type and relative amount of histologic elements present within a particular tumor. By US, angiomyolipomas usually appear as multiple small hyperechoic renal cortical foci without associated distal shadowing. Less commonly they may replace the entire renal cortex, resulting in a diffusely echogenic appearance of the parenchyma with loss of corticomedullary differentiation, or appear as a solitary intrarenal mass. CT and MR imaging are diagnostic when fat is identified within the lesion (**Fig. 16**) [75,76]. Angiomyolipomas may be cystic rather than solid [77] and may occasionally be numerous enough to cause renal failure.

Currently, US evaluation of patients who have tuberous sclerosis is recommended every 2 to 3 years before puberty and yearly thereafter to identify enlarging lesions [72]. Embolization, partial nephrectomy, or other treatments, such as cryotherapy and radiofrequency ablation, can be performed in symptomatic patients [78].

Ossifying renal tumor of infancy

Ossifying renal tumor of infancy is an extremely rare benign neoplasm with distinct imaging and morphologic features [64,79,80]. These tumors are attached to the renal medulla and develop predominantly within the pyelocalyceal system. Histologically, three major components are identified: an osteoid core, osteoblasts within and at the periphery of the core, and spindle cells. The proportions of these components vary, although the relative amount of osteoid tends to increase with increasing age of the patient. Investigators have suggested that this tumor is related to intralobar nephrogenic rests.

Most reported cases have presented with gross hematuria. Intravenous urography reveals dilation and distortion of the collecting system with filling defects or minimal obstruction. Ossifying renal tumor of infancy may be confused with a staghorn calculus. US shows an echogenic mass containing calcifications or stones. CT demonstrates a well-defined mass with minimal contrast enhancement (**Fig. 17**). Treatment consists of surgical excision. Chemotherapy and radiotherapy are unnecessary.

Metanephric neoplasms

Metanephric neoplasms represent a spectrum of differentiated lesions that seem to be related to Wilms' tumor. These tumors include a pure epithelial lesion (metanephric adenoma), a pure stromal lesion (metanephric stromal tumor), and a mixed epithelial-stromal lesion (metanephric adenofibroma). The continuity of these lesions with Wilms' tumor has been demonstrated best in the epithelial lesions. The relationship of Wilms' tumor, metanephric adenofibroma with mitoses or combined metanephric fibroma/Wilms' tumor lesions, and usual metanephric fibroma or usual metanephric adenoma has been viewed as analogous to that of neuroblastoma, differentiating neuroblastoma, and ganglioneuroma, in which progressively more mature or differentiated counterparts of malignant embryonal lesions are associated with a greater probability of benign clinical behavior [81–84]. Metanephric adenoma also has morphologic similarities to papillary renal cell neoplasms but is distinguished from them by genetic markers. Although the overwhelming majority of

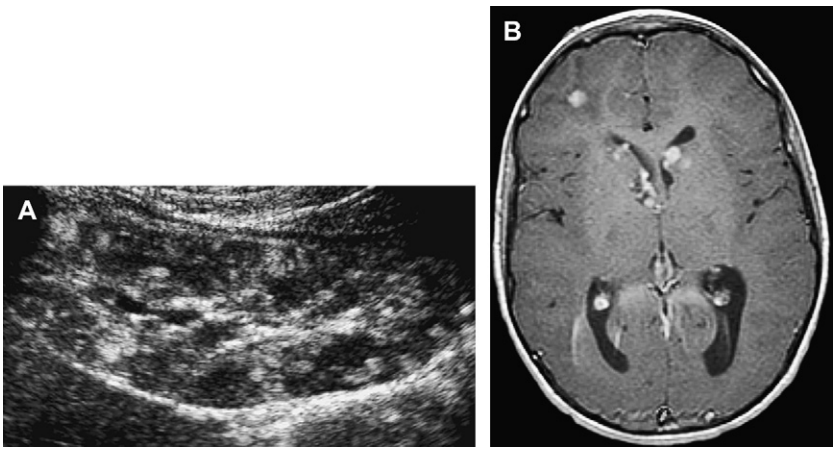

Fig. 16. Thirteen-year-old boy with tuberous sclerosis and seizures. (*A*) Sagittal sonogram of the right kidney reveals the presence of innumerable small cortical echogenic foci corresponding to angiomyolipomas. (*B*) Axial T1-weighted MR image of the brain shows enhancing bilateral subependymal nodules and right frontal tuber.

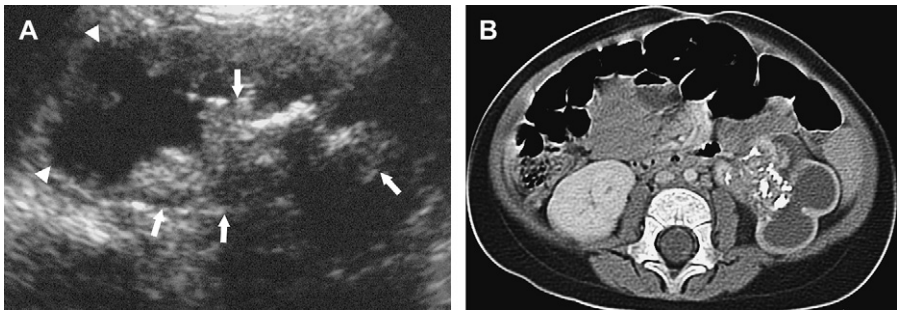

Fig. 17. Ossifying renal tumor of infancy. (*A*) Coronal sonogram reveals an echogenic, shadowing mass in the mid- and lower left kidney (*arrows*) with associated upper pole hydronephrosis (*arrowheads*). (*B*) Contrast-enhanced axial CT image depicts the calcified tumor within the left renal pelvis.

metanephric neoplasms are benign, malignant transformation has been described. Genetic predictors of malignant transformation are as yet unknown.

Patients who have metanephric neoplasms may present with polycythemia, hypertension, or hematuria. Tumor size is variable, ranging from 0.3 to 15 cm. On gross pathologic examination, tumors are usually solitary and unencapsulated. Metanephric adenoma usually occurs in the renal cortex, whereas metanephric stromal tumor and metanephric adenofibroma are usually centered in

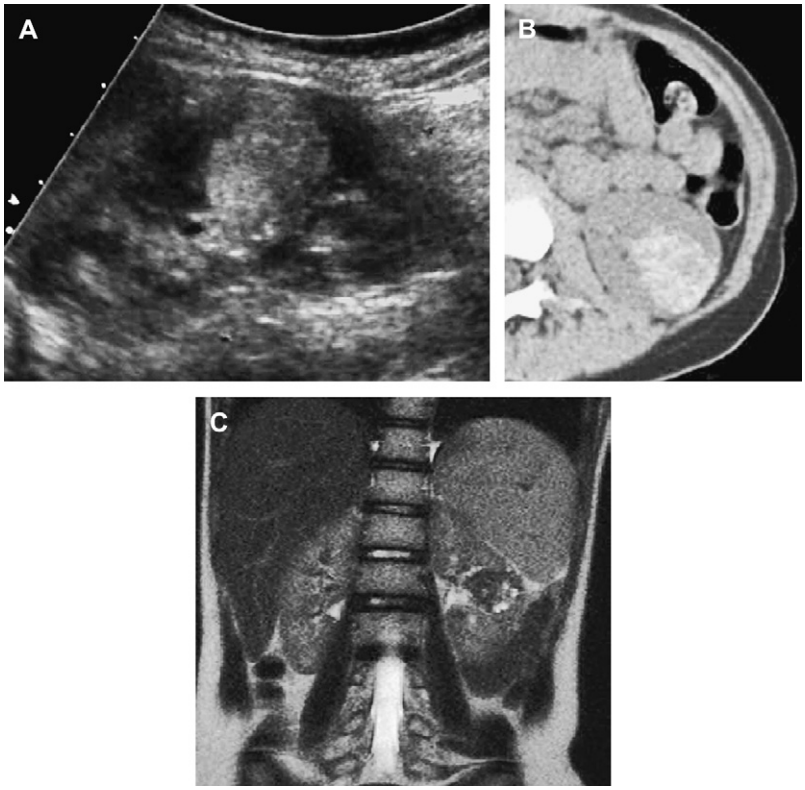

Fig. 18. Metanephric adenoma. (*A*) Longitudinal sonogram demonstrates an echogenic mass of the mid-left kidney. (*B*) Unenhanced axial CT image through mid-left kidney reveals a hyperdense mass. (*C*) The tumor is hypointense to the adjacent normal renal parenchyma on T2-weighted MR imaging. Small hyperintense foci correspond to cystic areas within the tumor. (*Adapted from* Amodio JB, Shapiro E, Pinkney L, et al. Metanephric adenoma in an 8-year-old child: case report and review of the literature. J Pediatr Surg 2005;40:E25–8; with permission.)

the medulla. Because of the occasional association with Wilms' tumor or low-grade renal cell carcinoma, complete resection is indicated.

The imaging features of metanephric tumors have been described in a few cases [85–90]. By US these tumors appear as sharply defined solid masses that are either hypoechoic or hyperechoic to normal parenchyma. A single report noted decreased perfusion by power Doppler imaging relative to normal parenchyma [86]. On unenhanced CT tumors may be iso- or hyperdense relative to normal renal parenchyma, and are hypointense on T1 and T2-weighted MR imaging (Fig. 18). They may demonstrate enhancement after contrast administration, but generally to a lesser degree than normal renal parenchyma.

Summary

US plays a vital role in the investigation and characterization of renal masses in children because of its ease of performance and the absence of ionizing radiation or need for iodinated contrast material, sedation, or prolonged immobilization. Cystic and solid lesions are easily differentiated and the integrity of the renal vasculature is readily assessed.

References

[1] Rosenbaum DM, Korngold E, Teele RL. Sonographic assessment of renal length in normal children. AJR Am J Roentgenol 1984;142:467–9.
[2] Carrico CW, Zerin JM. Sonographic measurement of renal length in children: does the position of the patient matter? Pediatr Radiol 1996; 26:553–5.
[3] Cramer BC, Jequier S, de Chadarevian JP. Factors associated with renal parenchymal echogenicity in the newborn. J Ultrasound Med 1986;5: 633–8.
[4] Vade A, Lau P, Smick J, et al. Sonographic renal parameters as related to age. Pediatr Radiol 1987;17:212–5.
[5] Han BK, Babcock DS. Sonographic measurements and appearance of normal kidneys in children. AJR Am J Roentgenol 1985;145:611–6.
[6] Davey MS, Zerin JM, Reilly C, et al. Mild renal pelvic dilatation is not predictive of vesicoureteral reflux in children. Pediatr Radiol 1997;27: 908–11.
[7] Walsh G, Dubbins PA. Antenatal renal pelvis dilatation: a predictor of vesicoureteral reflux? AJR Am J Roentgenol 1996;167:887–90.
[8] Erlich PF. Wilms tumor: progress to date and future considerations. Expert Rev Anticancer Ther 2001;1:555–64.
[9] Beckwith JB. National Wilms' tumor study: an update for pathologists. Pediatr Dev Pathol 1998;1:79–84.
[10] Dome JS, Perlman EJ, Ritchey ML, et al. Renal tumors. In: Pizzo PA, Poplack DG, editors. Principles and practice of pediatric oncology. 5th edition. Philadelphia: Lippincott Williams & Wilkins; 2006. p. 905–32.
[11] Charles AK, Vujanic GM, Berry PJ. Renal tumours of childhood. Histopathology 1998;32:293–309.
[12] Matsunanga E. Genetics of Wilms tumor. Hum Genet 1981;57:231–46.
[13] White KS, Grossman H. Wilms' and associated renal tumors of childhood. Pediatr Radiol 1991;21:81–8.
[14] Grundy PE, Telzerow PE, Breslow N, et al. Loss of heterozygosity for chromosomes 16q and 1p in Wilms' tumors predicts an adverse outcome. Cancer Res 1994;54:2331–3.
[15] Crist WM, Kun LE. Common solid tumors of childhood. N Engl J Med 1991;324:461–71.
[16] Malcolm AW, Jaffe N, Folkman MJ, et al. Bilateral Wilms tumor. Int J Radiat Oncol Biol Phys 1980; 6:167–74.
[17] Beckwith JB, Kiviat NB, Bonadio JF. Nephrogenic rests, nephroblastomatosis, and the pathogenesis of Wilms tumor. Pediatr Pathol 1990;10: 1–36.
[18] Beckwith JB. Precursor lesions of Wilms tumor: clinical and biological implications. Med Pediatr Oncol 1993;21:158–68.
[19] Scott RH, Walker L, Olsen ØE, et al. Surveillance for Wilms tumour in at-risk individuals—pragmatic recommendations for best practice. Arch Dis Child 2006;91:995–9.
[20] McNeil DE, Brown M, Ching A, et al. Screening for Wilms tumor and hepatoblastoma in children with Beckwith-Wiedemann syndromes: a cost-effective model. Med Pediatr Oncol 2001;37:349–56.
[21] Lonergan GJ, Martinez-Leon MI, Agrons GA, et al. Nephrogenic rests, nephroblastomatosis, and associated lesions of the kidney. Radiographics 1998;18:947–68.
[22] Beckwith JB. Children at increased risk for Wilms tumor: monitoring issues. J Pediatr 1998;132: 377–9.
[23] Lowe LH, Isuani BH, Heller RM, et al. Pediatric renal masses: Wilms tumor and beyond. Radiographics 2000;20:1585–603.
[24] Bennington JL, Beckwith JB. Tumors of the kidney, renal pelvis, and ureter. In: Atlas of tumor pathology, 2nd series, fascicle 12. Washington, DC: Armed Forces Institute of Pathology; 1975. p. 31–91.
[25] Gylys-Morin V, Hoffer FA, Kozakewich H, et al. Wilms' tumor and nephroblastomatosis: imaging characteristics by gadolinium-enhanced MR imaging. Radiology 1993;188:517–21.
[26] Laberge JM. Nephroblastomatosis update. Med Pediatr Oncol 2003;41:96–7.
[27] Prasil P, Laberge JM, Bond M, et al. Management decisions in children with nephroblastomatosis. Med Pediatr Oncol 2000;35:429–32.
[28] Curti BD. Renal cell carcinoma. JAMA 2004;292: 97–100.

[29] Chow WH, Devesa SS, Warren JL, et al. Rising incidence of renal cell cancer in the United States. JAMA 1999;281:1628–31.
[30] Bernstein L, Linet M, Malcolm A, et al. Cancer incidence and survival among children and adolescents 1975–1995. SEER pediatric monograph. Available at: http://seer.cancer.gov/publications/childhood/renal.pdf. Accessed March 5, 2007.
[31] Lack EE, Cassady JR, Sallan SE. Renal cell carcinoma in childhood and adolescence: a clinical and pathological study of 17 cases. J Urol 1985;133:822–8.
[32] Hartman DS, Davis CJ Jr, Madewell JE, et al. Primary malignant renal tumors in the second decade of life: Wilms tumor versus renal cell carcinoma. J Urol 1982;127:888–91.
[33] Geller JI, Dome JS. Local lymph node involvement does not predict poor outcome in pediatric renal cell carcinoma. Cancer 2004;101:1575–83.
[34] Carcao MD, Taylor GP, Greenberg ML, et al. Renal-cell carcinoma in children: a different disorder from its adult counterpart? Med Pediatr Oncol 1998;31:153–8.
[35] Asanuma H, Nakai H, Takeda M, et al. Renal cell carcinoma in children: experience at a single institution in Japan. J Urol 1999;162:1402–5.
[36] Indolfi P, Terenziani M, Casale F, et al. Renal cell carcinoma in children: a clinicopathologic study. J Clin Oncol 2003;21:530–5.
[37] Bruder E, Passera O, Harms D, et al. Morphologic and molecular characterization of renal cell carcinoma in children and young adults. Am J Surg Pathol 2004;28:1117–32.
[38] Zambrano E, Reyes-Mugica M. Renal cell carcinoma with t(X;17): singular pediatric neoplasm with specific phenotype/genotype features. Pediatr Dev Pathol 2003;6:84–7.
[39] Renshaw AA. Pediatric renal cell carcinomas: where do they fit in the new histologic classification of renal cell carcinoma? Adv Anat Pathol 2000;7:135–40.
[40] Fleitz JM, Wootton-Gorges SL, Wyatt-Ashmead J, et al. Renal cell carcinoma in long-term survivors of advanced stage neuroblastoma in early childhood. Pediatr Radiol 2003;33:540–55.
[41] Estrada CR, Suthar AM, Eaton SH, et al. Renal cell carcinoma: Children's Hospital Boston experience. Urology 2005;66:1296–300.
[42] Cook A, Lorenzo AJ, Salle JL. Pediatric renal cell carcinoma: single institution 25-year case series and initial experience with partial nephrectomy. J Urol 2006;175:1456–60.
[43] Geller E, Smergel EM, Lowry PA. Renal neoplasms of childhood. Radiol Clin North Am 1997;35:1391–413.
[44] Beckwith JB. Renal tumors. In: Stocker JT, Askin FB, editors. Pathology of solid tumors in children. New York: Chapman & Hall Medical; 1998. p. 1–23.
[45] Argani P, Perlman EJ, Breslow NE, et al. Clear cell sarcoma of the kidney (CCSK): a review of 351 cases from the National Wilms' Tumor Study Group Pathology Center. Am J Surg Pathol 2000;24:4–18.
[46] Weeks D, Beckwith J, Mierau G, et al. Rhabdoid tumor of the kidney: a report of 111 cases from the National Wilms' Tumor Study Pathology Center. Am J Surg Pathol 1989;13:439–58.
[47] Rorke LB, Packer R, Biegel J. Central nervous system atypical teratoid/rhabdoid tumors of infancy and childhood. J Neurooncol 1995;24: 21–8.
[48] Sisler CL, Siegel MJ. Malignant rhabdoid tumor of the kidney: radiologic features. Radiology 1989;172:211–2.
[49] Agrons GA, Kingsman KD, Wagner BJ, et al. Rhabdoid tumor of the kidney in children: a comparative study of 21 cases. AJR Am J Roentgenol 1997;168:447–51.
[50] Steele EL, MacLennan GT. Renal medullary carcinoma. J Urol 2005;174:1449.
[51] Davis CJ, Mostofi FK, Sesterhenn IA. Renal medullary carcinoma. Am J Surg Pathol 1995;19: 1–11.
[52] Davidson AJ, Choyke PL, Hartman DS, et al. Renal medullary carcinoma associated with sickle cell trait: radiologic findings. Radiology 1995; 195:83–5.
[53] Blitman NM, Berkenblit RG, Rozenblit AM, et al. Renal medullary carcinoma: CT and MRI features. AJR Am J Roentgenol 2005;185:262–72.
[54] Weinberger E, Rosenbaum DM, Pendergrass TW. Renal involvement in children with lymphoma: comparison of CT with sonography. AJR Am J Roentgenol 1990;155:347–9.
[55] Fernbach SK, Glass RB. Uroradiographic manifestations of Burkitt's lymphoma in children. J Urol 1986;135:986–8.
[56] Agrons GA, Wagner BJ, Davidson AJ, et al. Multilocular cystic renal tumor in children: radiologic-pathologic correlation. Radiographics 1995;15: 653–69.
[57] Joshi VV, Beckwith JB. Multilocular cyst of the kidney (cystic nephroma) and cystic partially differentiated nephroblastoma. Cancer 1989;64: 366–79.
[58] Madewell JE, Goldman SM, Davis CJ, et al. Multilocular cystic nephroma: a radiographic-pathologic correlation of 58 patients. Radiology 1983; 146:309–21.
[59] Banner MP, Pollack HM, Chatten J, et al. Multilocular renal cysts: radiologic-pathologic correlation. AJR Am J Roentgenol 1981;136:239–47.
[60] Abara OE, Liu P, Churchill BM, et al. Magnetic resonance imaging of cystic, partially differentiated nephroblastoma. Urology 1990;36:424–7.
[61] Dikengil A, Benson M, Sanders L, et al. MRI of multilocular cystic nephroma. Urol Radiol 1988;10:95–9.
[62] McAlister WH, Siegel MJ, Askin FB, et al. Multilocular renal cysts. Urol Radiol 1979;1:89–92.
[63] Kirks DR, Kaufman RA, Babcock DS. Renal neoplasms in infants and children. Semin Roentgenol 1987;22:292–302.

[64] Glick RD, Hicks MJ, Nuchtern JG, et al. Renal tumors in infants less than 6 months of age. J Pediatr Surg 2004;39:522–5.
[65] Moore SW, Satge D, Sasco AJ, et al. The epidemiology of neonatal tumours. Report of an international working group. Pediatr Surg Int 2003;19: 509–19.
[66] Hartman DS, Lesar MS, Madewell JE, et al. Mesoblastic nephroma: radiologic-pathologic correlation of 20 cases. AJR Am J Roentgenol 1981;136: 69–74.
[67] Howell CG, Othersen HB, Kiviat NE, et al. Therapy and outcome in 51 children with mesoblastic nephroma: a report of the National Wilms Tumor study. J Pediatr Surg 1982;17:826–31.
[68] Bolande RP, Brough AJ, Izant RJ Jr. Congenital mesoblastic nephroma of infancy. A report of eight cases and the relationship to Wilms' tumor. Pediatrics 1967;40:272–8.
[69] Beckwith JB. Wilms tumor and other renal tumors of childhood: an update. J Urol 1986;136:320–4.
[70] Chan HS, Cheng MY, Mancer K, et al. Congenital mesoblastic nephroma: a clinicoradiologic study of 17 cases representing the pathologic spectrum of the disease. J Pediatr 1987;111:64–70.
[71] Eble JN. Angiomyolipoma of kidney. Semin Diagn Pathol 1998;15:21–40.
[72] Ewalt DH, Sheffield E, Sparagana SP, et al. Renal lesion growth in children with tuberous sclerosis complex. J Urol 1998;160:141–5.
[73] Steiner MS, Goldman SM, Fishman EK, et al. The natural history of renal angiomyolipoma. J Urol 1993;150:1782–6.
[74] Henske EP. Tuberous sclerosis and the kidney: from mesenchyme to epithelium, and beyond. Pediatr Nephrol 2005;20:854–7.
[75] Lemaitre L, Claudon M, Dubrulle F. Imaging of angiomyolipomas. Semin Ultrasound CT MR 1997;18:100–14.
[76] Casper KA, Donnelly LF, Chen B, et al. Tuberous sclerosis complex: renal imaging findings. Radiology 2002;225:451–6.
[77] Mitnick JS, Bosniak MA, Hilton S, et al. Cystic renal disease in tuberous sclerosis. Radiology 1983;147:85–7.
[78] Hadley DA, Bryant LJ, Ruckle HC. Conservative treatment of renal angiomyolipomas in patients with tuberous sclerosis. Clin Nephrol 2006;65: 22–7.
[79] Sotel-Avila C, Beckwith JB, Johnson JE. Ossifying renal tumor of infancy: a clinicopathologic study of nine cases. Pediatr Pathol Lab Med 1995;15: 745–62.
[80] Vazquez JL, Barnewolt CE, Shamberger RC, et al. Ossifying renal tumor of infancy presenting as a palpable abdominal mass. Pediatr Radiol 1998;28:454–7.
[81] Argani P, Beckwith JB. Metanephric stromal tumor: report of 31 cases of a distinctive pediatric renal neoplasm. Am J Surg Pathol 2000;24: 917–26.
[82] Davis CJ Jr, Barton JH, Sesterhenn IA, et al. Metanephric adenoma: clinicopathological study of fifty patients. Am J Surg Pathol 1995;19:1101–14.
[83] Arroyo MR, Green DM, Perlman EJ, et al. The spectrum of metanephric adenofibroma and related lesions: clinicopathologic study of 25 cases from the National Wilms Tumor Study Group Pathology Center. Am J Surg Pathol 2001;25: 433–44.
[84] Argani P. Metanephric neoplasms: the hyperdifferentiated, benign end of the Wilms tumor spectrum? Clin Lab Med 2005;25:379–92.
[85] Comerci SC, Levin TL, Ruzal-Shapiro C, et al. Benign adenomatous kidney neoplasms in children with polycythemia: imaging findings. Radiology 1996;198:265–8.
[86] Navarro O, Connolly B, Taylor G, et al. Metanephric adenoma of the kidney: a case report. Pediatr Radiol 1999;29:100–3.
[87] Amodio JB, Shapiro E, Pinkney L, et al. Metanephric adenoma in an 8-year-old child: case report and review of the literature. J Pediatr Surg 2005;40:E25–8.
[88] Fielding JR, Visweswaran A, Silverman SG, et al. CT and ultrasound features of metanephric adenoma in adults with pathologic correlation. J Comput Assist Tomogr 1999;23:441–4.
[89] Araki T, Hata H, Asakawa E. MRI of metanephric adenoma. J Comput Assist Tomogr 1998;22: 87–90.
[90] Hwang SS, Choi YJ. Metanephric adenoma of the kidney: case report. Abdom Imaging 2004;29: 309–11.

ELSEVIER SAUNDERS

ULTRASOUND CLINICS

Ultrasound Clin 2 (2007) 105–114

New Advances in Genitourinary Ultrasound

Jared D. Christensen, MD, Vikram S. Dogra, MD*

Ultrasound is one of the most widely used and versatile imaging modalities in medicine. It allows providers directed real-time imaging without exposing the patient to ionizing radiation or nephrotoxic contrast agents. The technology is relatively inexpensive and portable, especially when compared with alternative modalities, such as magnetic resonance (MR) and computed tomography (CT). Ultrasonography has become an integral component of daily medical practice not only for its inherent diagnostic value, but also as a key modality for procedural guidance (eg, ultrasound-guided biopsies) and ultrasound-based therapies (eg, high-intensity focused ultrasound ablations). Since its clinical introduction in the 1940s, advances in ultrasound technology and modality-specific clinical research have broadened the role of ultrasonography in the diagnosis, management, and follow-up of patients who have urologic disorders [1]. This article reviews the basic concepts of ultrasound imaging and describes new advances in technology and its clinical applications for genitourinary evaluation.

Basic ultrasound physics

Ultrasound as an imaging modality is based upon the propagation of mechanical waves through tissue and the detection of reflected echoes occurring at tissue interfaces. The fundamental concepts governing ultrasound are the piezoelectric effect, the pulse-echo principle, and acoustic impedance.

The piezoelectric effect

To create an image, mechanical waves are generated from electronic impulses and transmitted through tissue; the returning echoes must be detected and

University of Rochester Medical Center, 601 Elmwood Avenue, Box 648, Rochester, NY 14642, USA
* Corresponding author.
E-mail address: vikram_dogra@urmc.rochester.edu (V.S. Dogra).

1556-858X/07/$ – see front matter
doi:10.1016/j.cult.2007.01.008
ultrasound.theclinics.com

changed back into an electrical signal to undergo processing to form a conventional ultrasound image. These steps are performed by the ultrasound transducer. In general, a transducer is a device that converts energy from one form to another. The piezoelectric effect explains how mechanical energy and electrical energy are interconverted [2].

Electrical signals applied to a piezoelectric material induce mechanical vibrations; conversely, when a mechanical pressure is applied to a piezoelectric material, an electrical charge is created that is proportional to the inciting force. Most modern ultrasound transducers use piezoelectric elements composed of man-made lead zirconate or lead titanate crystals. Changing the polarity of the applied voltage causes the crystal to expand and contract, thereby generating and transmitting a mechanical vibration or sound wave.

Reflected echoes are in turn detected by the ultrasound transducer and cause the piezoelectric element to vibrate. These vibrations are converted by the piezoelectric crystal back into electrical signals that may undergo further processing, such as amplification, compensation, demodulation, or compression, before being displayed as an image [3].

The pulse-echo principle

Electricity is applied to the piezoelectric crystals at a specific pulse rate. This allows for transmission of sound waves and receipt of the returning echoes. Generally, the transducer sends pulses of 1 microsecond duration with a repetition period of 999 microseconds. Thus, far more time is devoted to receiving echoes than to generating sound waves. The pulse-echo principle states that the electrical impulse generated by reflected sound waves is proportional to the strength of the returning echo [2]. Differences in echo strength are therefore indicative of the tissue properties that form the basis of imaging contrast.

Acoustic impedance

The generation of echoes results from the interaction of sound waves with structures within the transmitting medium. Acoustic impedance (Z) is a tissue-specific characteristic that determines the extent of sound wave reflection and is defined as $Z = \rho\ c$, where ρ represents tissue density and c the velocity of sound within tissue (average of 1540 m/sec for biologic tissues) [2]. The degree to which ultrasound waves are reflected toward the transducer is proportional to the density differences encountered between varying tissues, which are referred to as acoustic interfaces. The differential acoustic impedance between air and tissue is so large that nearly all sound waves are reflected back toward the transducer; therefore, a coupling medium, such as ultrasound gel, is used to decrease the differential impedance between the transducer and skin to facilitate the transmission of ultrasound waves.

When an area is scanned by the ultrasound transducer, the majority of the energy imparted by the mechanical waves is attenuated by absorption, refraction, and scattering, with only a small portion of the incident sound wave being reflected to form an image [2]. Absorption is the most common of these interactions, with the energy loss being transferred as heat to the surrounding tissue. The degree of attenuation, or weakening of the sound wave's amplitude or intensity as it travels through tissue, is proportional to the frequency of the sound wave and to the distance it has traversed. Higher frequencies provide greater axial and lateral resolution than low frequencies but have shorter wavelengths and are more readily absorbed by tissue, resulting in less penetration. Therefore, whenever feasible, transducers of the highest permissible frequency should be used for scanning with regard to the required depth of penetration. For genitourinary evaluation, the following frequencies have been recommended: kidneys and bladder, 3.5 to 5 MHz; uterus and adnexa, 7 to 10 MHz; prostate, 6 to 10 MHz; testes and penis, 10 to 14 MHz.

Types of ultrasound

Conventional grayscale (B-mode)

The fundamental physics described in the previous section are the basis for two-dimensional (2D) grayscale ultrasound, where the signal intensity of reflected echoes is proportional to the image display brightness or echogenicity. Pulse-echo brightness mode (B-mode) is the most commonly used format in ultrasound imaging; the routine examination of genitourinary structures is no exception (**Fig. 1**).

Doppler ultrasound

The Doppler effect represents the change in frequency or wavelength of transmitted sound waves that occurs when there is relative motion between the transducer (sound source) and reflecting surfaces (red blood cells) [4]. The frequency, or Doppler, shift between the transmitted and received frequencies is measured in Hertz and is related to the contraction or expansion of wavelengths ahead of or behind the moving object. The shift provides information of flow directionality and can be represented visually with color or by an audible signal.

Color flow Doppler technique calculates the mean frequency shift over a series of locations along the beam axis. This color information is displayed over a conventional 2D grayscale image in

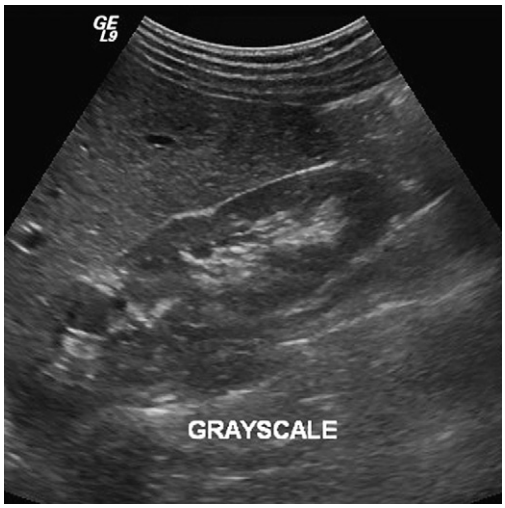

Fig. 1. Longitudinal B-mode sonogram of normal kidney demonstrates characteristic parenchymal echogenicity.

real-time and is broadly used to document vascularity or the lack thereof (eg, distinguishing hydronephrosis from a vessel at the renal hilum). Absence of color flow in the ovaries or testis with high clinical index of suspicion is virtually diagnostic of torsion (Fig. 2) [5,6]. Additionally, color flow Doppler is useful in the evaluation of erectile dysfunction.

Power Doppler ultrasound presents 2D Doppler information by color-encoding the strength of the Doppler shifts. Power Doppler enhances the sensitivity of detecting blood flow by at least five times that of color flow Doppler ultrasound but does not provide a flow vector (directionality) or velocity [7]. Power Doppler scanning is valuable in scrotal ultrasonography because of its increased sensitivity to low-flow states and its independence from Doppler angle correction (see Fig. 2) [5,6].

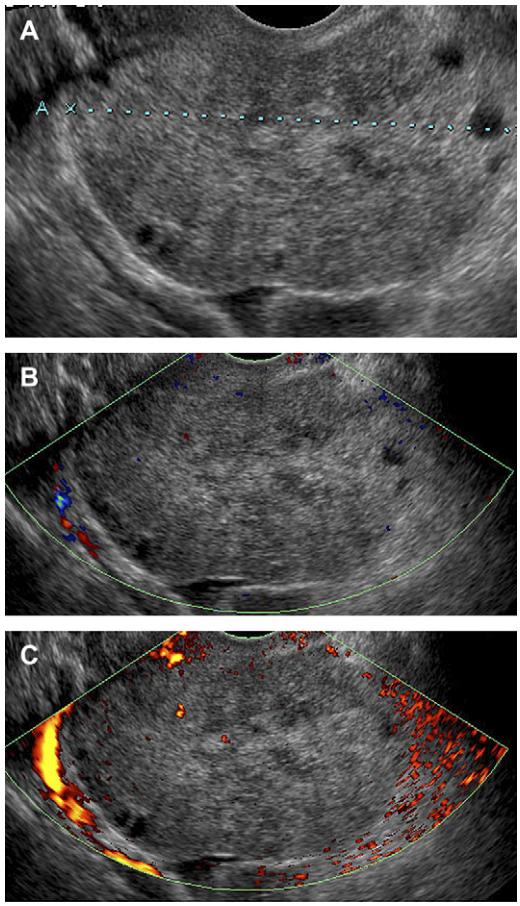

Fig. 2. Ovarian torsion. (*A*) Grayscale ultrasound demonstrating an enlarged, heterogenous right ovary. (*B*) Colorflow Doppler reveals a lack of parenchymal vascularity consistent with torsion. (*C*) Power Doppler confirms the lack of flow.

Acquisition and processing enhancements

Harmonic imaging

As sound waves are applied to the body, the tissue compresses and then relaxes until the next wave is applied. This mechanical alteration produces peaks and troughs in the pulse wave pattern because the speed of sound is slightly higher in compressed than in noncompressed tissue. These repetitive changes are more pronounced with each serial pulse, resulting in low-amplitude harmonic echoes that intensify as the beam propagates deeper. Multiple harmonics are produced; however, the initial echo of the fundamental transmitted pulse—the second harmonic—is typically the only one sufficiently strong for use in clinical applications [8]. Harmonics reinforce the data supplied by the initial fundamental echo but are much less susceptible to artifacts, resulting in an improved signal-to-noise ratio (SNR), which is the ratio of the amplitude of the desired signal (echoes forming the image) to the amplitude of unwanted signals (electronic noise not contributing to image formation). Other advantages include improved resolution of objects closer to the transducer (near-field resolution) and improved contrast resolution (Fig. 3).

Pulse inversion harmonic imaging consists of the transmission of identical ultrasonic pulses with opposite polarities. Because the polarities are reversed, the linear aspects of the returning echoes cancel each other out, leaving only the nonlinear components (harmonic and subharmonic ultrasound waves) to generate the image [9]. This technique enhances the nonlinear echoes formed by pulse inversion and is commonly used with ultrasound contrast agents and in the evaluation of low-flow states [6].

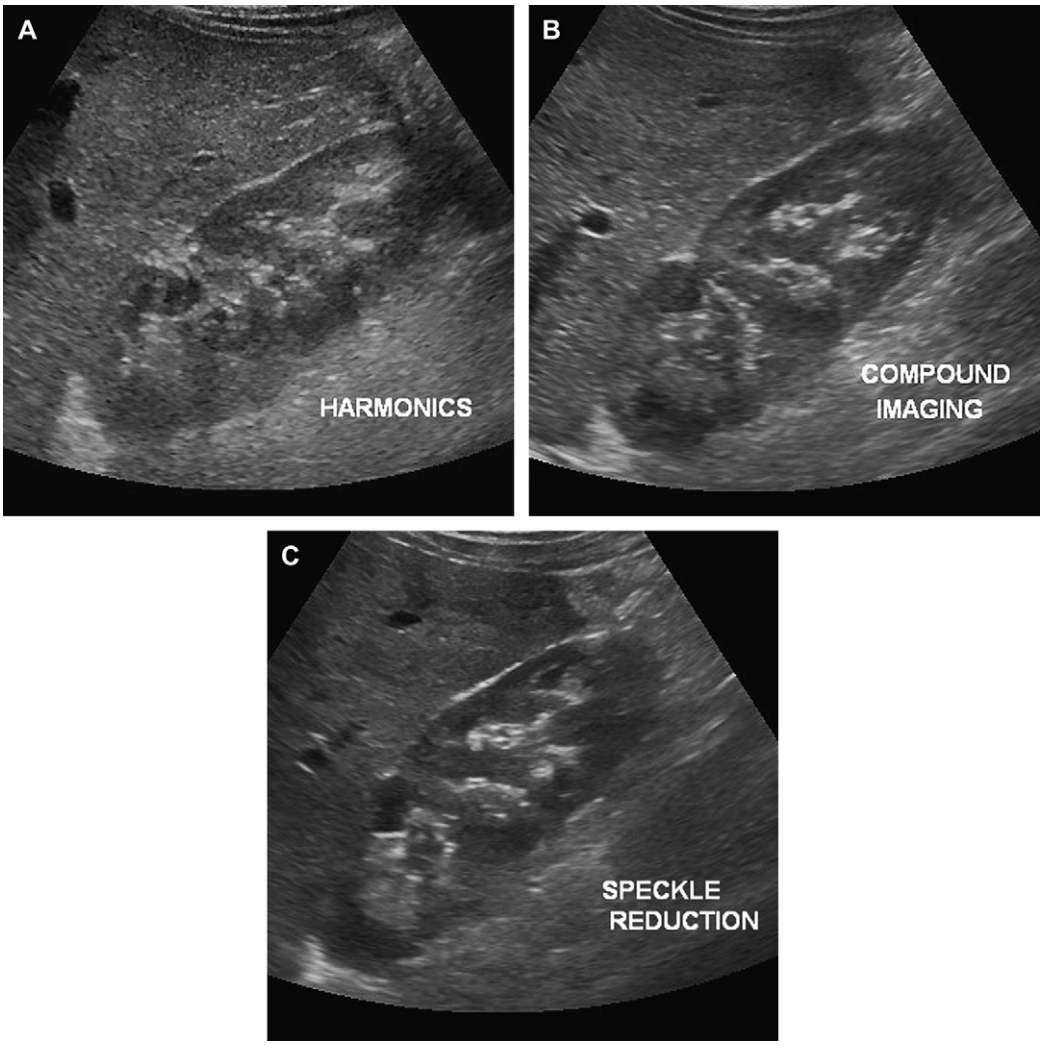

Fig. 3. Comparison of techniques to improve ultrasound imaging resolution. (*A*) Harmonic imaging of a normal kidney reveals improved tissue contrast with better corticomedullary differentiation in comparison to conventional B-mode ultrasound (see Fig. 1). (*B*) Spatial compound imaging. (*C*) Speckle reduction.

Spatial compound imaging

In conventional real-time ultrasound, each target is insonated at a single, constant angle. Compound sonography uses an array transducer with electronic beam steering to image the target tissue from multiple angles via the generation of parallel sound waves in offset directions [2]. The multiple returning echoes obtained from differing spatial orientations are averaged together to form a single compound image with an overall reduction in noise, speckle, shadowing, and artifacts. Because multiple echoes are used to produce the composite image, there is an increased computational time and therefore a slower frame rate; however, the resulting image has improved contrast and margin definition in comparison to conventional B-mode ultrasound (see Fig. 3) [10].

Speckle reduction imaging

Ultrasound images contain an inherent artifact called speckle, which is caused by complex interference between sound waves that reduce spatial and contrast resolution. Speckle reduction imaging reduces speckle artifact and increases the SNR and thereby improves contrast resolution (see Fig. 3) [11].

Extended field of view

One of the inherent drawbacks of conventional ultrasound is the limited field of view because many structures cannot be assessed with a single static image. The use of 2D array transducers with mechanical or electronic beam steering can overcome this limitation by extended filed of view processing. As the transducer is translated laterally across the

desired area, multiple images are obtained from varying angles. The images are reconstructed into a single, panoramic display by registering sequential areas of overlap through comparison of signal and position information (Fig. 4) [2].

Three-dimensional ultrasound

Advances in array transducers and imaging processing have allowed the development of three-dimensional ultrasound (3D US). In general, 3D images may be acquired in one of two ways. A conventional transducer producing 2D images may be coupled to a tracking mechanism storing precise location and spatial orientation information, allowing for 3D image construction. Alternatively, 2D arrays may be used to generate 3D images directly; the transducer is held stationary over the target while electronic beam-steering sweeps 360° through a tissue volume. The returning echoes are detected by the 2D array and processed in real-time to display a volume-rendered, or 3D, image [12].

Three-dimensional volume acquisition allows for multiplanar image reconstruction (Fig. 5), increased measuring accuracy, and better appreciation of anatomic relationships between the area of interest and surrounding structures (Fig. 6) [12,13]. Furthermore, the problems associated with user-dependent variability are eliminated, allowing for improved exam-to-exam comparison and long-term follow-up. In the adult population, 3D US has been shown to provide more accurate calculations of prostate specific antigen density and improved treatment mapping for brachytherapy [12]. Additionally, 3D US may be used for routine evaluation of the testis. The primary advantages of this technique are a short image acquisition time and the ability to manipulate the image in any plane, thereby improving diagnostic confidence. 3D US applications are also useful in the evaluation of patients who have erectile dysfunction (Fig. 7).

Despite its benefits, 3D US technique does have limitations. Most relevant is the potential for imaging artifacts introduced during the initial scan or during image processing, which may result in possible misdiagnosis. Centers interested in the technology must also consider the large initial investment in ultrasound equipment and the necessary supportive infrastructure, including hardware, software, storage, and specialized technologists who are trained to obtain and manipulate the large data sets generated for volume reconstructions.

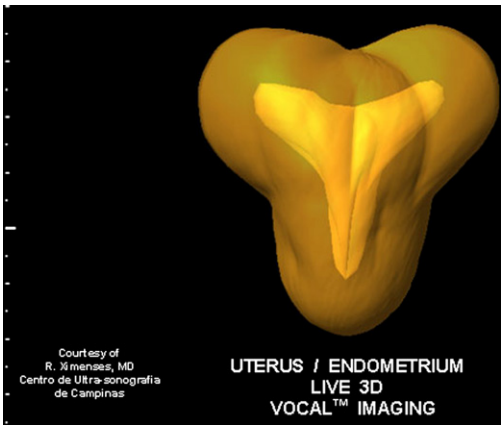

Fig. 5. Three-dimensional volume acquisition of the uterus in the coronal plane with surface rendering illustrates normal myometrium and endometrium. (*Courtesy of* Philips Medical Systems; with permission.)

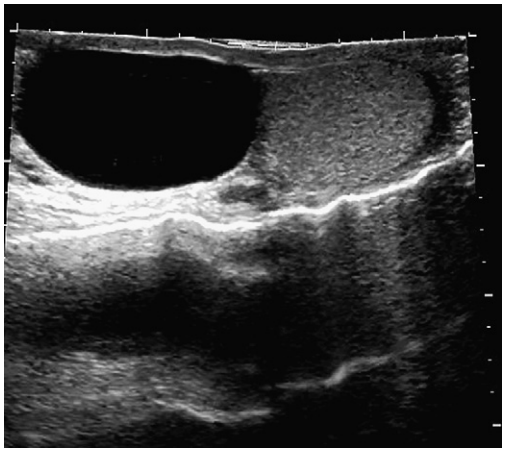

Fig. 4. Gray-scale sonogram of left testis with extended field of view demonstrating the full extent of a spermatocele and its relation to the adjacent testis.

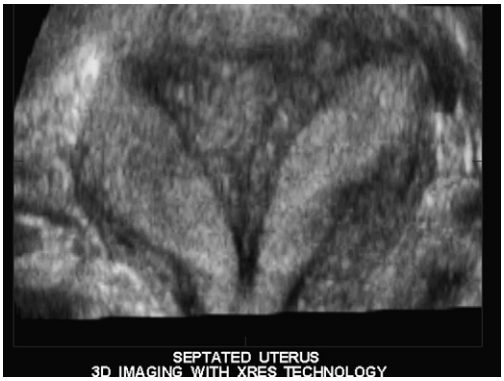

Fig. 6. Three-dimensional volume acquisition of septate uterus. Three-dimensional imaging assists in defining the anatomic relationships of the uterine cornua, fundus, and muscular septum. (*Courtesy of* Philips Medical Systems; with permission.)

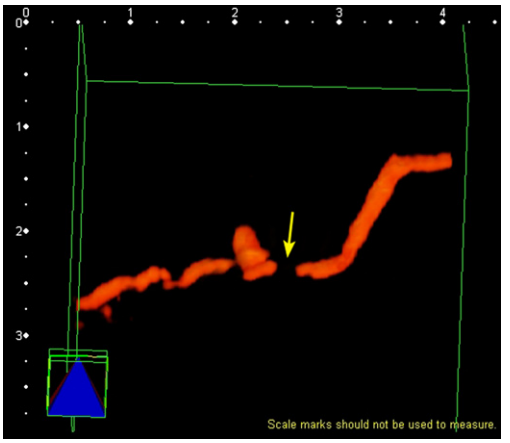

Fig. 7. Three-dimensional power Doppler sonogram with maximum intensity projection algorithm shows tortuous cavernosal artery caused by atherosclerosis with severe segmental stenosis (*arrow*) in a patient who has erectile dysfunction.

Four-dimensional ultrasound

Four-dimensional ultrasound (4D US) incorporates a temporal component to 3DUS: Successive 3D volumes are acquired and rendered in real time as the 2D array transducer is moved over the patient [2]. This approach is useful for performing volume assessments as a function of time in dynamic systems, such as the cardiac cycle [14,15]. The utility of 4D US applications for interventional procedures, such as solid organ biopsy, is also being explored [16]. Won and colleagues [16] reported that 4D US is a more intuitive modality for performing biopsies because familiar 2D images can be displayed for the operator while volumetric processing is performed. Additionally, the presentation of 4D reconstructions is continuous, thereby preventing time delays experienced with 3D imaging. The limitations of this technology are similar to those found with 3D US.

Innovations in ultrasound

Contrast agents

Ultrasound contrast agents consist of intravenously injected microbubbles that significantly improve the contrast between vascular structures and the surrounding tissues. As the microbubbles circulate and pass through the target ultrasound pressure field, they begin to resonate. The differential acoustic impedance between the blood and the gas within the microbubble core is high, resulting in reflection of nearly all of the incident sound waves with little to no transmission. Optimal scattering is produced at the resonant frequency of the contrast agent, which is approximately equal to 3/R, where R represents the microbubble radius in micrometers [6]. For example, the resonant frequency for a typical 1-μm bubble is 3 MHz, which is within the diagnostic ultrasound frequency range.

Despite near total reflection of the acoustic wave, the fundamental returning echoes are typically not ideal for generating adequate image contrast due to the small size of the microbubbles, their relative low concentration within the circulation, and a high background of returning echoes from adjacent structures [17]. These limitations can be overcome through the use of harmonic imaging, which exploits the nonlinear behavior of microbubbles. The spectrum of the scattered ultrasound signal contains higher harmonics of the fundamental frequency. Ultrasound contrast agents produce harmonics much more readily than the surrounding tissue; therefore, the detected harmonic frequency is almost entirely produced by the microbubbles [18]. The second harmonic is routinely selected; therefore, a unit producing ultrasounds at a given frequency (eg, 3.5 MHz) receives an ultrasound signal twice as powerful (ie, 7 MHz), representing only the contrast agent. Harmonic technique therefore eliminates artifacts from surrounding anatomic structures, resulting in a markedly improved SNR.

Contrast sonography was first used in cardiac and hepatic imaging but is finding broader application, particularly in the evaluation of genitourinary disease (Fig. 8). Robbin and colleagues [17] indicated that the technology has the potential to evaluate renal masses by first performing a noncontrast ultrasound examination followed by contrast sonography to assess for enhancement of hypervascular lesions. They also proposed a contrast ultrasound classification pattern for complex renal

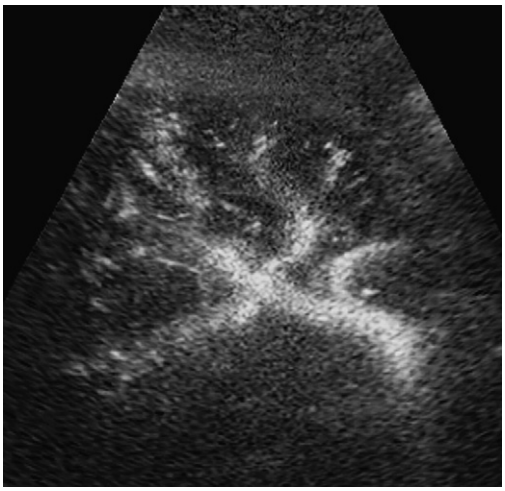

Fig. 8. Ultrasound contrast on grayscale imaging outlining the renal arterial blood supply.

cysts—a modification of the Bosniak criteria used in CT [17]. Further evaluation of the utility of ultrasound contrast agents is ongoing, with work assessing applications in renal perfusion, pyelonephritis, and intraoperative localization of tumors [17].

The indications for using ultrasound contrast agents often overlap with those for contrast CT; however, contrast sonography may offer several advantages in that patients are not exposed to ionizing radiation, there are no nephrotoxic or allergic effects, and the examination may be performed at bedside for patients unable to be transported [19]. In addition to enhanced tissue definition, ultrasound contrast agents may be used to assess organ perfusion and quantitative blood volume [20]. The use of ultrasound contrast agents for biologic targeting is also under investigation. Microbubbles are tagged with a protein ligand specific for a particular biologic marker, injected intravenously, and imaged by delayed ultrasound. Bound microbubbles retained in target tissue may be indicative of pathology. For example, most cancers express specific receptor sets promoting angiogenesis, such as vascular endothelial growth factor. Microbubbles tagged to vascular endothelial growth factor ligands may be used to visualize potential tumors [21]. If proven feasible, targeted ultrasound contrast agents may ultimately be used for the delivery of gene or pharmaceutical therapies [22].

High-intensity focused ultrasound

Conventional ultrasound is performed with sound waves of very low signal intensity without any major risk of tissue damage. Conversely, high-intensity focused ultrasound (HIFU) uses much stronger mechanical waves, resulting in intense deposition of heat at a focal point through tissue absorption [23]. Although conventional ultrasound is diagnostic, HIFU can be used in therapeutic and surgical applications, such as the minimally invasive treatment of prostate cancer. This procedure uses a transrectal ultrasound transducer producing sound waves of greater than 100 W/pulse. The energy is focused into a small area, creating intense heat of 80 to 100°C, which results in localized coagulation necrosis. Given that ultrasound is nonionizing, tissue in the entry and exit path of the HIFU beam is not injured [23].

HIFU for the treatment of prostate cancer offers several advantages over standard therapies. HIFU may be performed at the time of diagnostic transrectal ultrasound without the necessary delays of surgical or radiation planning; the treatment zone is much more precise than with radiation or surgical intervention, thereby preserving adjacent normal tissue; and the projected cost is less than that of standard therapies [24]. Aside from primary therapy, HIFU may be used for salvage therapy after failed radiation, cryosurgery, or radical prostatectomy [23]. Palliative treatment by tumor debulking is also possible. The published clinical experience with HIFU for the treatment of prostate cancer is limited but promising [24–26]. Although the FDA has not approved the procedure for use in the United States, HIFU is approved with increasing use and acceptance in Europe, Japan, China, and other countries [26].

Compact ultrasound systems

Advances in technology in ultrasound components and computers have allowed for the development of progressively smaller ultrasound systems. Stationary units that once filled a small room are now handheld devices weighing less than 6 lb. The miniaturization of ultrasound units has, in most cases, not come at the expense of image quality or production costs. With better image resolution, new features, and affordable prices, these compact systems are more accessible to medical specialists in all fields and have helped to expand the role of ultrasound in routine medical practice [2,27]. The American Institute of Ultrasound in Medicine formed a multidisciplinary panel of experts to address the opportunities and challenges inherent in the dissemination of ultrasound technology, including concerns over imaging quality control, credentialing, accurate interpretation, self-referral, and over use [27]. The forum concluded that all practitioners independently performing ultrasound be appropriately trained in its use and committed to ongoing education, professional development, and outcomes-based research to ensure optimal patient care.

Emerging technologies

Sonoelastography

Contrast in conventional gray-scale ultrasound relies upon varying acoustic properties between adjacent structures; if these properties are similar, the tissues cannot be visually differentiated, which explains why some lesions are undetected. Sonoelastography is a developing technology that relies upon differences in a tissue's elastic, rather than acoustic, characteristics. Several techniques are under investigation. A common methodology uses a modified Doppler technique to detect shear waves produced by mechanical tissue vibration [28]. The images provide a real-time depiction of viscoelasticity ("stiffness")—a property typically assessed by manual palpation (Fig. 9) [29]. Sonoelastography may therefore be used to increase the sensitivity and objectivity of physical examination and to perform "virtual" palpation in organs not routinely

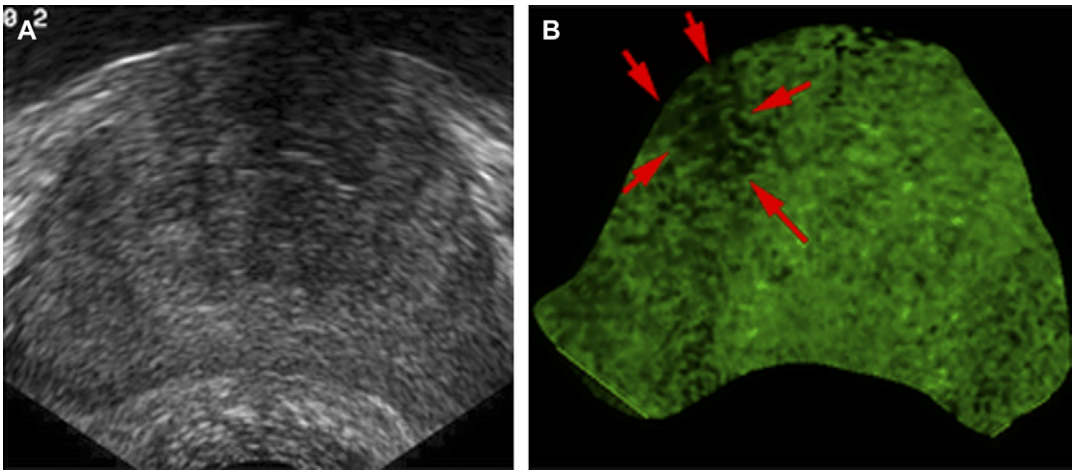

Fig. 9. Apparent normal two-dimensional grayscale image of the prostate (*A*). The corresponding sonoelastogram (*B*) reveals a discrete peripheral mass (*arrows*) seen as a dark area within normal parenchyma (*green*). Note that the color overlay corresponds to tissue elasticity, with black being most hard or stiff. This lesion was subsequently biopsied and proven to represent prostatic carcinoma. (*Courtesy of* Kenneth Hoyt, Rochester, NY.)

accessible on physical examination. Recent studies have demonstrated the accuracy of sonoelastography in the detection of prostate cancer. 3D applications are under investigation for brachytherapy treatment planning and disease surveillance [28].

Near-infrared ultrasound

Ultrasound is helpful in differentiating cystic from solid lesions. However, its specificity in genitourinary tumor diagnosis is often not sufficiently high due to overlapping characteristics of benign and malignant lesions. CT or MR examinations are therefore routinely recommended for further evaluation of suspect lesions. Optical imaging based on diffusive near-infrared (NIR) light has the potential to differentiate tumors from normal parenchyma through the assessment of tissue parameters, such as blood volume, blood O_2 saturation, tissue light scattering, and the concentration and retention of exogenous contrast agents [30]. Low spatial resolution and artifacts due to the intense scattering of light in tissue plague NIR imaging. These drawbacks can be mitigated by a hybrid imaging modality using NIR diffusive light in conjunction with high-resolution ultrasound, incorporating the ultrasound transducer and NIR source-detector into a single probe.

The feasibility of NIR hybrid or stand-alone systems has been documented for breast lesions, and promising applications in the evaluation of genitourinary conditions have been reported [30]. NIR permits the visualization of nerves, tissue perfusion, and lymph nodes during urologic surgery. Clinical trials in patients who have renal malignancy are being performed to evaluate the clinical utility of infrared imaging and the accuracy of tumor margin identification as correlated by histopathology. In addition, intraoperative infrared ultrasound may be beneficial in the evaluation of renal perfusion after partial nephrectomy. Recent developments in hybrid NIR technologies have also been applied to the identification of cavernous nerves in an animal model; the accurate identification ofneurovascular bundles allows cavernous nerves to be spared during radical prostatectomy, thereby reducing the rate of postoperative erectile dysfunction [31]. The assessment of testicular torsion by NIR with quantification of reperfusion after torsion reduction has also proven feasible in an animal model [32].

Animal imaging in genitourinary ultrasound

Documenting efficacy in an animal model remains an integral step in the clinical development of new imaging technologies. High-resolution ultrasound machines are available for animal research and are being investigated for genitourinary applications. These systems use extremely high-frequency transducers of 40 MHz and incorporate 2D and 3D capabilities.

Capacitative micromachined ultrasonic transducers

Most widely available ultrasound transducers are based upon single ceramic or piezoelectric crystals, which have a limited frequency range, thereby requiring multiple transducers of specific frequencies to perform different examinations. Furthermore, it

Table 1: **Ultrasound innovations and the potential imaging benefits**

Innovation	Benefit
Improved ergonomics	Decreased work-related injuries
Improved image resolution	Enhanced definition of tissue interfaces; potential increased diagnostic accuracy
Compact size	Portable, bedside imaging
Three- and four-dimensional US	Volumetric images with multiplanar viewing
Harmonic imaging	Improved tissue definition; US contrast agent imaging
Compound imaging	Edge enhancement; decreased artifacts
Extended field of view	View larger area of interest
Contrast agents	Assess tissue vascularity; enhancement without nephrotoxicity; potential targeted gene or drug therapy
High-intensity focused US	Minimally invasive treatment therapies
Sonoelastography	Earlier tumor detection
Near-infrared US	Assess perfusion status; earlier tumor detection; improved surgical outcomes
Capacitative micromachined transducers	Multifrequency single transducer

Abbreviation: US, ultrasound.

is often necessary to exchange transducers during a single examination to optimize imaging of some structures. Capacitative micromachined ultrasound transducers are constructed of nonresonant silicon membranes. An applied voltage causes the membrane to deflect by electrostatic forces, which in turn produces acoustic waves. The voltage can be altered, resulting in sound waves of varying wavelengths and frequencies being produced by a single transducer [33].

Summary

Ultrasound technology and its application in the evaluation of genitourinary disease continue to improve (Table 1). Advances in signal acquisition and processing have resulted in better spatial resolution and image quality, particularly for conventional 2D applications. Multidimensional imaging provides detailed spatial relationships that can be reconstructed from any viewing angle and readily compared over time. New transducer materials and components allow for volumetric imaging and real-time variable frequency selection. A role for ultrasound as a therapeutic modality is being established through broadening applications of HIFU. Ultrasound contrast agents and emerging hybrid technologies incorporating NIR diffusive imaging permit the assessment of vascularity and flow states previously achievable only with CT and MR imaging. The rapid rate of new advances in ultrasound applications requires close consultation and collaboration with nonimaging specialists to ensure that patients receive the highest standard of care.

References

[1] Resnick MI. Ultrasonography of the prostate and testes. J Ultrasound Med 2003;22:869–77.

[2] Hangiandreou NJ. AAPM/RNSA physics tutorial for residents: topics in US. B-mode US: basic concepts and new technology. Radiographics 2003; 23:1019–33.

[3] McAchran SE, Dogra V, Resknick MI. Office urologic ultrasound. Urol clin North Am 2005;32: 337–52.

[4] Boote EJ. AAPM/RSNA physics tutorial for residents: topics in US. Doppler US techniques: concepts of blood flow detection and flow dynamics. Radiographics 2003;23:1315–27.

[5] Dogra V, Bhatt S. Acute painful scrotum. Radiol Clin North Am 2004;42:349–63.

[6] Dogra V, Rubens D, editors. Ultrasound secrets. Philadelphia: Hanley & Belfus; 2004.

[7] Hamper UM, DeJong MR, Caskey CI, et al. Power Doppler imaging: clinical experience and correlation with color Dopper US and other imaging modalities. Radiographics 1997;17:499–513.

[8] Rosenthal SJ, Jones PH, Wetzel LH. Phase inversion tissue harmonic sonographic imaging: a clinical utility study. AJR Am J Roentgenol 2001; 176:1393–8.

[9] Kim TK, Choi BI, Han JK, et al. Hepatic tumors: contrast agent-enhancement patterns with pulse-inversion harmonic US. Radiology 2000;216: 411–7.

[10] Jespersen SK, Wilhjelm JE, Sillesen H. Multiangle compound imaging. Ultrason Imaging 1998;20: 81–102.

[11] Wagner RF, Insana MF, Smith SW. Fundamental correlation lengths of coherent speckle in medical ultrasound images. IEEE Trans Ultrason Ferroelectr Freq Control 1998;35(1):34–43.

[12] Downey DB, Fenster A, Williams JC. Clinical utility of three-dimensional US. Radiographics 2000;20:559–71.

[13] Riccabona M, Fritz GA, Schollnast H, et al. Hydronephrotic kidney: pediatric three-dimensional US for relative renal size assessment—initial experience. Radiology 2005;236(1):275–83.
[14] Bhat AH, Corbett VN, Liu R, et al. Validation of volume and mass assessments for human fetal heart imaging by four-dimensional spatiotemporal image correlation echocardiography. J Ultrasound Med 2004;23:1151–9.
[15] Nguyen LD, Leger C, Debrun D, et al. Validation of a volumic reconstruction in 4d echocardiography and gated SPECT using a dynamic cardiac phantom. Ultrasound Med Biol 2003;29(8): 1151–60.
[16] Won HG, Han JK, Do KH, et al. Values of four-dimensional ultrasonography in ultrasonographically guided biopsies of hepatic masses. J Ultrasound Med 2003;29(8):1151–60.
[17] Robbin ML, Lockhart ME, Barr RG. Renal imaging with ultrasound contrast: current status. Radiol Clin North Am 2003;41:963–78.
[18] Burns PN. Harmonic imaging with ultrasound contrast agents. Clin Radiol 1996;51(Suppl 1): 50–5.
[19] Goldberg BB, Liu JB, Forsberg F. Ultrasound contrast agents: a review. Ultrasound Med Biol 1994; 20:319–33.
[20] Delorme S, Krix M. Contrast-enhanced ultrasound for examining tumor biology. Cancer Imaging 2006;6:148–52.
[21] Wink MH, Lagerveld BW, Laguna MP, et al. Cryotherapy for renal-cell cancer: diagnosis, treatment, and contrast-enhanced ultrasonography for follow-up. J Endourol 2006;20(7):456–8.
[22] Rahim A, Taylor SL, Bush NL, et al. Physical parameters affecting ultrasound/microbubble-mediated gene delivery efficiency in vitro. Ultrasound Med Biol 2006;32(8):1269–79.
[23] Gardner TA, Koch MA. Prostate cancer therapy with high-intensity focused ultrasound: comprehensive review. Clin Genitourin Cancer 2005; 4(3):187–92.
[24] Thuroff S, Chaussy C, Vallanaen G, et al. High-intensity focused ultrasound and localized prostate cancer: efficacy results from the European multicentric study. J Endourol 2003;17(8): 673–77.
[25] Illing RO, Leslie TA, Kennedy JE, et al. Visually directed high-intensity focused ultrasound for organ-confined prostate cancer: a proposed standard for the conduct of therapy. BJU Int 2006; 98(6):1187–92.
[26] Blana A, Walter B, Rogenhofer S, et al. High-intensity focused ultrasound for the treatment of localized prostate cancer: 5-year experience. Urology 2004;63(2):297–300.
[27] Greenbaum LD, Benson CB, Nelson LH, et al. Proceedings of the compact ultrasound conference sponsored by the American Instititute of Ultrasound in Medicine. J Ultrasound Med 2004;23:1249–54.
[28] Taylor LS, Rubens DJ, Porter BC, et al. Prostate cancer: three-dimensional sonoelastography for in vitro detection. Radiology 2005;237(3):981–5.
[29] Hall TJ. AAPM/RSNA physics tutorial for residents: topics in US. Beyond the basics: elasticity imaging with US. Radiographics 2003;23: 1657–71.
[30] Chen NG, Guo P, Yan S, et al. Simultaneous near-infrared diffusive light and ultrasound imaging. Appl Opt 2001;40(34):6367–80.
[31] Golijanin DJ, Wood RW, Madeb R, et al. Intraoperative visualization of cavernous nerves using near infrared fluorescence of indocyanine green in the rat. J Endourol 2006;20(Suppl 1):A1–75 [Virtual Poster Session].
[32] Capraro GA, Mader TJ, Coughlin BF, et al. Feasibility of using near-infrared spectroscopy to diagnose testicular torsion: an experimental study in sheep. Ann Emerg Med, in press.
[33] Erguan AS, Huang Y, Zhuang X, et al. Capacitative micromachined ultrasonic transducers: fabrication technology. IEEE Trans Ultrason Ferroelectr Freq Control 2005;52:2242–58.

ELSEVIER SAUNDERS

ULTRASOUND CLINICS

Ultrasound Clin 2 (2007) 115–120

Ultrasound-Guided Genitourinary Interventions

Preet S. Kang, MD*, Raj Mohan Paspulati, MD

Interventional uroradiology is a specialized field dedicated to image-guided minimally invasive management of a wide variety of urinary tract diseases [1–5]. Although this field was founded on the basis of fluoroscopy for providing imaging guidance, the application of real-time ultrasound has had a significant impact. Fluoroscopy and ultrasound are complementary to each other for providing guidance making procedures safer and widely applicable [3,6,7]. This article predominantly discusses the use of ultrasound in the performance of urinary interventions.

Percutaneous access into the pelvicaliceal system is the first and foremost step, which opens the door to a host of diagnostic and therapeutic urinary procedures. Ultrasound and fluoroscopy are used to gain safe and reliable access into the pelvicaliceal system. After antegrade access is obtained diagnostic procedures, such as urine sampling, antegrade nephrostogram, and Whitaker test can be performed. Commonly the antegrade nephrostogram is coupled with a therapeutic procedure, such as percutaneous nephrostomy (PCN) catheter placement for urinary decompression or diversion. This procedure may be done alone or combined with nephroureteric catheter placement or double-J ureteral stent placement. Based on the underlying disease percutaneous nephrostomy can provide access for nephrolithotomy/lithotripsy or foreign body removal, stricture dilatation, biopsy, or instillation of medications [1–3]. The indications and steps in detail are discussed in the section about PCN.

Diagnostic procedures

Antegrade nephrostogram

The main purpose of antegrade nephrostogram is to determine the presence, degree, and level of obstruction in the urinary collecting system. Once needle access is gained into the urinary collecting system, contrast injection is performed for its opacification [2,3]. As a diagnostic test antegrade nephrostogram has limited application with the availability of several noninvasive imaging modalities, such as ultrasound, CT, or MR imaging. In almost all instances percutaneous antegrade access to the renal collecting system is performed with the intent of proceeding with a therapeutic procedure.

Whitaker test

The Whitaker test is used to determine the presence and severity of obstruction in the urinary system when the results of noninvasive imaging, such as

Department of Radiology, Case School of Medicine, University Hospitals of Cleveland, 11100 Euclid Avenue, Cleveland, OH 44106, USA
* Corresponding author.
E-mail address: kang@uhrad.com (P.S. Kang).

1556-858X/07/$ – see front matter
doi:10.1016/j.cult.2007.01.011
ultrasound.theclinics.com

ultrasound, CT scan, and diuretic renogram, are equivocal. This test is used in pediatric patients in the presence of dilated but nonrefluxing ureter or in adults to determine if pelvicaliceal dilatation attributable to ureteropelvic dysfunction is a result of obstruction. The test involves simultaneous antegrade access into the pelvicaliceal system and the urinary bladder with manometry. Fluid is infused into the pelvicaliceal system and pressures obtained. At different rates of fluid infusion the gradients are recorded and the degree of obstruction classified. Based on the results a PCN or a ureteral stent can be placed [4].

Therapeutic procedures

Percutaneous nephrostomy

First described in 1955, PCN has now become a routinely performed procedure [5]. The first step of the technique after selection and preparation of the patient is the percutaneous antegrade access to the pelvicaliceal system. Although it can be performed with fluoroscopic guidance alone as initially described, ultrasound is useful for obtaining initial access into the urinary collecting system [3,6–8]. There are some reports of using ultrasound exclusively for the whole procedure [9–12], including the use of diuretics to distend a nondilated urinary tract to facilitate ultrasound-guided needle access [12]. The applications of this procedure include emergency indications, such as pyonephrosis or worsening kidney function in the setting of obstruction. In other instances PCN provides an antegrade access into the urinary system for subsequent interventions. This procedure is applicable to both the native and the transplant kidney.

Indications

The indications for PCN are outlined in Box 1.

In some cases the percutaneous nephrostomy is performed because of an unsuccessful attempt at cystoscopic retrograde stent placement, usually by the urologist. Most patients of PCN require close cooperation between the interventional radiologist and the urologist for a successful outcome [2,3].

Preprocedure preparation

Laboratory tests As a prerequisite to PCN, a coagulation profile, including PTT and INR, and complete blood counts, including platelets, are essential [1–3,6,8]. This profile is particularly significant for patients who are on anticoagulation medication, who have renal or liver failure, who have a history of abnormal bleeding, or if a reliable history is not available. The INR should be less than 1.5 and the platelet count greater than 50 thousand. The INR can be reversed with fresh frozen plasma based on the emergent need for PCN. Platelet count less than 50 thousand requires platelet transfusion to avoid bleeding complications.

Box 1: Indications for percutaneous nephrostomy

Urinary obstruction
Stone
Malignancy: genitourinary or extrinsic
Pyonephrosis
Ureteral stricture
Nonfunctioning ureteral stent

Percutaneous access for further interventions
Nephrolithotomy/lithotripsy
Dilatation of ureteral stricture
Endopyelotomy
Ureteral double-J stent placement
Foreign body removal (eg, stent)
Whitaker test
Biopsy
Instillation of medications (eg, antifungal agents)

Urinary diversion
Vesical fistula
Ureteral transaction
Hemorrhagic cystitis: prevention and therapy

Preprocedure antibiotics Most outpatient low-risk PCN patients can be given a single intravenous dose of 1 g cefazolin. Patients who have a history of allergy may be given vancomycin 500 mg intravenously. For high-risk patients (positive urine culture or history of infection) broad-spectrum intravenous antibiotics are given, usually a combination of ampicillin with gentamicin, and continued after the procedure.

Sedation and analgesia

Most PCNs are performed under conscious sedation using intravenous midazolam and fentanyl with local anesthesia using 1% to 2% lidocaine. For the purpose of sedation the patient should be fasting for at least 6 hours after a meal or at least 2 hours if taking liquids only.

Procedure

The procedure is usually performed in the interventional radiology suite with the patient prone on the table. C-arm fluoroscopy and ultrasound are used for guidance. For access to a transplant kidney the patient is positioned supine. Ultrasound is performed before skin preparation to localize the kidney, including depth, and to plan for suitable pelvicaliceal access. The appropriate area is then prepped and draped using aseptic precautions. Ultrasound guidance is used in real time using either

a needle guide mounted on the probe or the free-hand technique. Sterile ultrasound probe covers are used. The ideal location for needle puncture is below the 12th rib and lateral to the erector spinae muscle (Fig. 1A, B). The kidney is approached from the posterolateral aspect keeping in mind the relatively avascular Brödel's plane [13]. Attempt is made to puncture the mid or lower pole posterior calyx (Fig. 2A). A 22-gauge needle is used. Following return of urine, a sample is obtained for culture in cases of infection. Limited contrast is then injected under fluoroscopy to opacify the collecting system (Fig. 2B). Care is taken to avoid overdistension of a potentially infected kidney.

Antegrade nephrogram is obtained and further management undertaken. If the calyceal access is considered to be satisfactory then a 0.018-in Cope mandril wire is placed by way of the needle into the collecting system, followed by placement of the coaxial dilators of the introduction set under fluoroscopic guidance. A 0.035- or 0.038-in guidewire is placed alongside the Cope mandril wire (safety wire) after removing the inner dilator. The guidewire is looped in the collecting system or advanced down the ureter. Based on the access and patient profile, predilatation of the tract with appropriate dilators or the use of a peel-away sheath may be required. A locking loop multiside-hole nephrostomy drainage catheter, usually 8 or 10 French, is then placed over the guidewire. The catheter is secured to the skin and sterile dressing applied [1–3,6–8].

Special circumstances

Transplant kidney The patient is placed supine because the transplant kidney is anterior in position and usually in the right or left lower abdominal quadrant. Access is obtained into an anterior calyx. Care is taken to access the kidney from the lateral aspect to avoid penetration of the peritoneum [1,2].

Access for percutaneous nephrolithotomy In such cases the access may be guided by the location of the calculi, necessitating access into the upper pole calyx or even dual access. Ultrasound may be of limited value if the calculi are radiopaque and seen easily by fluoroscopy. Once suitable access has been obtained the tract is dilated and nephrolithotomy performed [1,2].

Renal cysts Presence of numerous cysts in the kidney can be problematic during the placement of PCN. The nature of fluid returned from a cyst can be confused with urine and may result in malplacement of the nephrostomy. Use of ultrasound can be helpful to avoid cyst puncture and guide the needle into the urinary collecting system [9,10].

Nondilated collecting system These are particularly challenging cases in which the pelvicaliceal system is not distended either because of leakage or injury. Urinary diversion in a nondilated kidney is at times indicated in the management of severe hemorrhagic cystitis. There is a report of using ultrasound guidance for PCN in nondilated kidney, facilitated by diuretic-induced transient dilatation of the calyces. In two of five cases fluoroscopic guidance was used in addition to complete the procedure [12].

Pregnant and pediatric patients Ultrasound guidance is extremely valuable in pregnant or pediatric patients to eliminate or significantly decrease the need for fluoroscopy for placement of PCN [9–11].

Complications

The most common major complication following percutaneous nephrostomy is hemorrhage

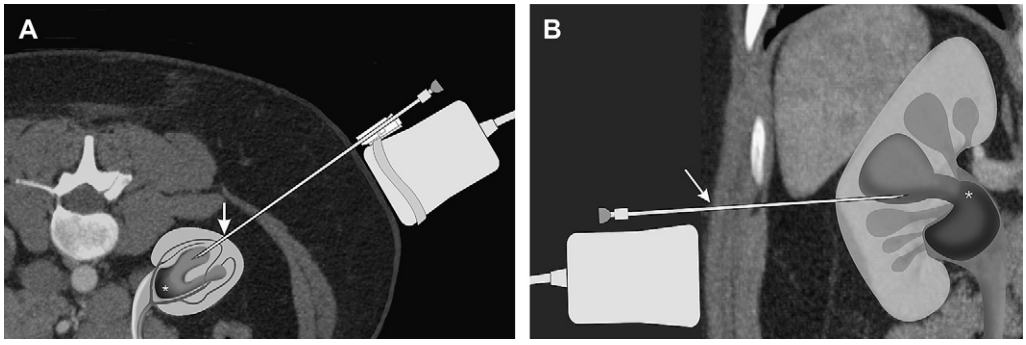

Fig. 1. (*A*) Axial illustration of needle access (*arrow*) into a dilated renal collecting system (*) by way of the posterior calyx through a relatively avascular Brödel's plane, using ultrasound guidance with needle attachment. (*B*) Coronal illustration of needle access (*arrow*) into a dilated renal collecting system (*) using ultrasound guidance with free hand technique (without needle guide).

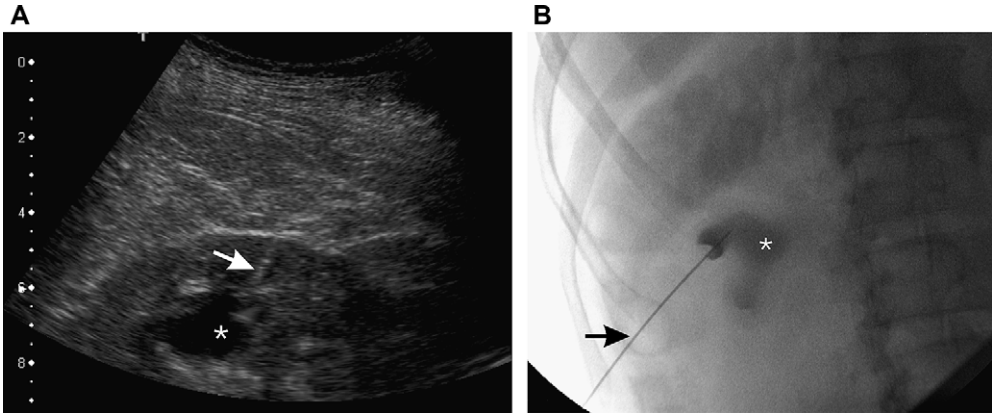

Fig. 2. (*A*) Ultrasound of kidney in longitudinal plane showing an echogenic needle (*arrow*) accessing a dilated collecting system. The tip of the needle is within the renal pelvis (*). (*B*) Corresponding fluoroscopic image with contrast injection demonstrating the needle (*arrow*) entering the collecting system (*) by way of a posterior calyx.

requiring transfusion in about 3% of patients followed by septicemia in approximately 1% of patients [3]. Minor tube-related complications are seen in about 2.5% of all cases [3].

Percutaneous cyst drainage and sclerotherapy

Renal cysts are usually asymptomatic and are incidental findings on imaging. Only those renal cysts that are symptomatic or complicated need treatment. Large renal cysts may present with pain or a palpable mass. Infection of the cyst, hypertension, and hydronephrosis because of the mass effect over the renal vasculature and renal pelvis are other complications of a renal cyst in which treatment is indicated [14–16]. Surgical management of renal cysts is by laparoscopic excision or unroofing [17–19]. Ultrasound is useful in the diagnosis of renal cysts and guidance for percutaneous cyst interventions. A cystic renal neoplasm has to be excluded by imaging before percutaneous management of a renal cyst. Association between patient symptoms and presence of a renal cyst must be established before any invasive procedure. The patient is then screened for any contraindications, such as bleeding diathesis. The patient preparation and procedure techniques are similar to those for percutaneous nephrostomy. It is recommended to perform cyst drainage at the first instance and observe the patient for relief of symptoms. If the patient benefits from cyst drainage and the symptoms recur with reaccumulation of fluid in the cyst, then sclerotherapy is indicated. Cyst ablation can be performed with instillation of sclerosing agents, such as absolute alcohol, tetracycline, or ethanolamine [1].

Bean [20] first reported imaging-guided renal cyst sclerotherapy with 95% ethanol in 1981. Subsequently, there have been several reports of varied techniques of percutaneous renal cyst sclerotherapy. Simple cyst aspiration has a high failure rate because of rapid reaccumulation of fluid from the lining secretory epithelium. The renal cyst is punctured under ultrasound guidance and a 6- to 8-French pigtail catheter is introduced into the cyst over a guidewire [15,21]. Another option for drainage catheter placement is the single step trocar technique if suitable access to the cyst is available. The cyst contents are completely aspirated and the aspirated volume is recorded. Water-soluble iodide contrast medium is injected into the cyst under fluoroscopy to document smooth lining of the cyst wall, internal filling defects or loculations, and communication of the cyst with the collecting system, such as calyceal diverticulum. Communication of the cyst with the collecting system is an absolute contraindication for sclerotherapy [21]. Some 25% of the aspirated cyst fluid volume is replaced with a sclerosing agent. Various sclerosing agents have been used for effective sclerotherapy. These include 95% alcohol, tetracycline, minocycline hydrochloride, iophendylate, and ethanolamine oleate [22]. Ethanol is the most widely used sclerosant and various concentrations of ethanol have been used. The most widely accepted concentration is 95% ethanol. There are several reports of 99% ethanol to be a more effective sclerosant with low recurrence rates [23]. The retention period of the sclerosant within the cyst varies from 30 minutes to 4 hours. Chung and colleagues [24] reported multiple sessions of sclerotherapy to be superior to a single injection of sclerosant. Lin and colleagues [21] reported that a single session with prolonged

retention of the sclerosant is safe and efficacious. They also concluded that there is no difference in the therapeutic efficacy between 2-hour and 4-hour retention of the sclerosant. The procedure is associated with minor complications; major complications are uncommon. Pain and tenderness after the procedure are the most common complications, which are transient and well controlled with medications. There are also reports of transient drunkenness following ethanol sclerotherapy [21]. Low-grade fever and microscopic hematuria are other minor complications described after the procedure [22]. Frank hematuria and perinephric hemorrhage are uncommon complications. Frank hematuria has been reported with cysts communicating with collecting system [21]. Patients are followed with ultrasound at 1- to 3-month intervals for 1 to 2 years [15,21]. Symptomatic patients who have recurrence of cysts are treated with further sessions of sclerotherapy.

Summary

Ultrasound has made a significant impact in the field of urinary interventions, with the principle role being imaging guidance. Ultrasound guidance has made procedures safer and shorter, limiting the number of needle punctures required and decreasing or sometimes eliminating radiation. In most of its applications it is complementary to fluoroscopy for providing image guidance for different urinary procedures [1–3,21–23]. Ultrasound before performing PCN helps to plan the procedure and access site. The particular renal calyx and the skin puncture site can be selected before prepping the patient. The depth of the target and angulation of needle access can be planned, keeping in mind the avascular Brödel's line [13]. Usually the posterior calyx is selected and ultrasound can provide radiation-free real-time imaging guidance for the needle puncture. It decreases the procedure time and the number of needle punctures, thereby decreasing the chance of potential complications [3,12]. Ultrasound eliminates the need for intravenous contrast administration, which is at times used during fluoroscopic-guided urinary access. In a poorly functioning kidney intravenous contrast may not even be feasible because of limited excretion, in which case ultrasound is valuable for single needle puncture access [10,12]. Ultrasound also helps avoid cysts during access for PCN because they may cause confusion attributable to the aspirated fluid. Once antegrade access is obtained into the urinary system, fluoroscopy is generally better for guidewire manipulation and drainage catheter placement. Antegrade nephrostogram can be obtained if indicated and further intervention planned. Ultrasound has a complementary role to fluoroscopy in the performance of PCN, making it a shorter and safer procedure [1–3,6–8].

Similarly for renal cyst aspiration and sclerotherapy ultrasound provides diagnostic and therapeutic functions. It is limited, however, for visualizing connection of a renal cyst with the collecting system, for which contrast injection under fluoroscopic imaging is better suited. Ultrasound provides accurate imaging for follow-up of renal cysts and their management with the inherent safety of being radiation-free [15,23].

Several other procedures, such as perinephric abscess drainage [25] or percutaneous cystostomy [26], can be assisted with ultrasound guidance. In the placement of double-J stents by the urologist by way of the cystoscopic route, ultrasound can help localize the proximal end of the stent in the upper collecting system. This is useful in pregnant patients in whom fluoroscopy is unsafe because of radiation exposure [27,28]. Ultrasound continues to expand and define its role in urinary interventions.

Acknowledgments

The authors thank Elena Dupont for her assistance in the preparation of the figures for this article.

References

[1] Banner MP. Radiologic interventions: uroradiology. Baltimore (MD): Williams & Wilkins; 1998. p. 3–27, 73–7.
[2] Dyer RB, Assimos DG, Regan JD. Update on interventional uroradiology. Urol Clin North Am 1997;24:623–52.
[3] Farrell TA, Hicks ME. A review of radiologically guided percutaneous nephrostomies in 303 patients. J Vasc Interv Radiol 1997;8:769–74.
[4] Whitaker RH. An evaluation of 170 diagnostic pressure flow studies of the upper urinary tract. J Urol 1979;121(5):602–4.
[5] Goodwin WE, Casey WC, Woolf W. Percutaneous trocar (needle) nephrostomy in hydronephrosis. JAMA 1955;157:891–4.
[6] Maher MM, Fotheringham T, Lee MJ. Percutaneous nephrostomy. Semin Intervent Radiol 2000; 17:329–39.
[7] Zegel HG, Pollack HM, Banner MC, et al. Percutaneous nephrostomy: comparison of sonographic and fluoroscopic guidance. AJR Am J Roentgenol 1981;137(5):925–7.
[8] Stables DP. Percutaneous nephrostomy: techniques, indications, and results. Urol Clin North Am 1982;9:15–29.
[9] Pedersen JF. Percutaneous nephrostomy guided by ultrasound. J Urol 1974;112(2):157–9.
[10] Baron RL, Lee JK, McClennan BL, et al. Percutaneous nephrostomy using real-time sonographic

guidance. AJR Am J Roentgenol 1981;136(5): 1018–9.
[11] von der Recke P, Nielsen MB, Pedersen JF. Complications of ultrasound-guided nephrostomy. A 5-year experience. Acta Radiol 1994;35(5): 452–4.
[12] Gupta S, Gulati M, Suri S. Ultrasound-guided percutaneous nephrostomy in non-dilated pelvicaliceal system. J Clin Ultrasound 1998;26(3): 177–9.
[13] Papanicolaou N. Renal anatomy relevant to percutaneous interventions. Semin Intervent Radiol 1995;12:163–72.
[14] Mohsen T, Gomha MA. Treatment of symptomatic simple renal cysts by percutaneous aspiration and ethanol sclerotherapy. BJU Int 2005; 96(9):1369–72.
[15] Akinci D, Akhan O, Ozmen M, et al. Long-term results of single-session percutaneous drainage and ethanol sclerotherapy in simple renal cysts. Eur J Radiol 2005;54(2):298–302.
[16] Hoard TD, O'Brien DP 3rd. Simple renal cyst and high renin hypertension cured by cyst decompression. J Urol 1976;115(3):326–7.
[17] Rubenstein SC, Hulbert JC, Pharand D, et al. Laparoscopic ablation of symptomatic renal cysts. J Urol 1993;150(4):1103–6.
[18] Hemal AK. Laparoscopic management of renal cystic disease. Urol Clin North Am 2001;28(1): 115–26.
[19] Dunn MD, Clayman RV. Laparoscopic management of renal cystic disease. World J Urol 2000; 18(4):272–7.
[20] Bean WJ. Renal cysts: treatment with alcohol. Radiology 1981;138(2):329–31.
[21] Lin YH, Pan HB, Liang HL, et al. Single-session alcohol-retention sclerotherapy for simple renal cysts: comparison of 2- and 4-hr retention techniques. AJR Am J Roentgenol 2005;185(4):860–6.
[22] Yamamoto K, Sakaguchi H, Anai H, et al. Sclerotherapy for simple cysts with use of ethanolamine oleate: preliminary experience. Cardiovasc Intervent Radiol 2005;28(6):751–5.
[23] Paananen I, Hellstrom P, Leinonen S, et al. Treatment of renal cysts with single-session percutaneous drainage and ethanol sclerotherapy: long-term outcome. Urology 2001;57(1):30–3.
[24] Chung BH, Kim JH, Hong CH, et al. Comparison of single and multiple sessions of percutaneous sclerotherapy for simple renal cyst. BJU Int 2000;85(6):626–7.
[25] Elyaderani MK, Moncman J. Value of ultrasonography, fine needle aspiration, and percutaneous drainage of perinephric abscesses. South Med J 1985;78(6):685–9.
[26] Aguilera PA, Choi T, Durham BA. Ultrasound-guided suprapubic cystostomy catheter placement in the emergency department. J Emerg Med 2004;26(3):319–21.
[27] Fainaru O, Almog B, Gamzu R, et al. The management of symptomatic hydronephrosis in pregnancy. BJOG 2002;109(12):1385–7.
[28] Jarrard DJ, Gerber GS, Lyon ES. Management of acute ureteral obstruction in pregnancy utilizing ultrasound-guided placement of ureteral stents. Urology 1993;42(3):263–7.

ELSEVIER SAUNDERS

ULTRASOUND CLINICS

Ultrasound Clin 2 (2007) 121–132

Saline Infusion Sonohysterography

Chiou Li Ong, MD, MBBS, FRCR

Saline infusion sonohysterography (SIS) is a useful adjunct to transvaginal ultrasonography (US) for the evaluation of the endometrial cavity. The procedure is also known as hysterosonography, saline contrast sonohysterography, and sonohysterography. It involves the instillation of sterile saline into the endometrial cavity by means of a fine catheter. The resultant distension of the endometrial cavity helps to outline irregularities, deformities, or growth that may be present in the endometrium. Patients who may benefit from this technique include pre- and postmenopausal women who have abnormal endometrial thickening, women who have submucosal fibroids, and women undergoing screening before in vitro fertilization. Submucosal fibroids may be assessed for suitability for transcervical hysteroscopic resection. The technique has been combined with three-dimensional (3D) US for better depiction of the endometrial cavity. More recently, there have been a number of reports describing the use of sonohysterography to guide the resection of polyps.

Background

Abnormal vaginal bleeding is one of the most common indications for performing a pelvic ultrasound. Of importance is the evaluation of postmenopausal bleeding. Although an endometrial thickness of 4 mm or less practically rules out endometrial pathology, patients who have thickened endometrium require further evaluation. In premenopausal women, endometrial thickness varies throughout the menstrual cycle, ranging from 1 to 4 mm during menstruation and from 4 to 8 mm during the early proliferative phase to 14 mm in the late proliferative/early secretory phase. Such cyclical change needs to be taken into consideration when assessing the endometrium.

Although endometrial biopsy or dilatation and curettage is effective at providing histologic material for the diagnosis of endometrial carcinoma, they may miss focal lesions that could be responsible for the abnormal bleeding. In this regard, SIS is

Department of Diagnostic Imaging, KK Women's and Children's Hospital, 100 Bukit Timah Road, Singapore 229899
E-mail address: ong.chiou.li@kkh.com.sg

1556-858X/07/$ – see front matter
doi:10.1016/j.cult.2007.01.009
ultrasound.theclinics.com

useful because it provides a means to visualize the endometrium and is a more accurate technique for guiding the decision to proceed to endometrial biopsy, dilatation, and curettage for generalized endometrial thickening or hysteroscopy and biopsy for focal lesions. Many studies have shown its accuracy in evaluating the endometrial cavity. Besides providing additional useful information on anomalies that are detected on transvaginal US, it can also reveal anomalies not demonstrated on conventional transvaginal US [1]. Studies show a high level of sensitivity of 98% to 100% for SIS, compared with 75% to 92% for transvaginal US [2–4]. Specificity ranges from 72% to 94%. Positive and negative predictive values range from 85% to 95% and 97% to 98%, respectively [2–5]. The influence of SIS findings on patient management can be significant. In a study by Bree and colleagues [5], treatment decisions in 80% of the patients were based on findings from SIS.

Indications for performing saline sonohysterography

The indications for performing SIS include investigation of abnormal endometrial thickening in pre- and postmenopausal women, assessment of submucosal fibroids, and screening before in vitro fertilization. For women who have abnormal endometrial thickening, the procedure allows differentiation between focal abnormalities (eg, polyps) and diffuse thickening. It facilitates triaging of patients to hysteroscopy for focal lesions or "blind" dilatation and curettage for patients who have diffuse thickening.

Technique

Patient preparation

For premenopausal patients, the procedure should be scheduled during the early part of the proliferative phase of the menstrual cycle, soon after menstruation has ceased. In most cases, it should not be performed beyond the tenth day of the cycle. During this time of the cycle, the endometrium is at its thinnest and is less likely to produce redundant mucosa, which may be mistaken for polyps or abnormal thickening. Blood clots and fibrin strands may be present if the procedure is performed before menstruation has ceased. Most workers recommend performing the procedure from day 6 to day 10 of the cycle. Patients who may be pregnant or who have signs or symptoms of pelvic inflammation are excluded from the examination. Some centers prescribe oral analgesics before the procedure. Prophylactic antibiotics are not prescribed unless there is a history of chronic pelvic inflammation or cardiac valvular disorders. Patients should be asked if they have latex allergy before latex sheaths are used to cover the vaginal probe. Verbal or signed consent for the procedure is taken depending on institutional practice.

Catheters

Various catheters have been used. They include catheters with and without retaining balloons. The types of catheters used include insemination catheters, 6-8F Foley catheters, hysterosalpingography catheters, and 6-8F infant feeding tubes. Dessole and colleagues [6] compared six different catheters commonly used in sonohysterography and found no statistically significant difference among the catheters. Balloon catheters provide a seal on the cervical canal and help to keep the endometrial cavity distended. When such catheters are used, slow infusion of saline is recommended to minimize the cramping sensation that the patient may feel with uterine distension. With nonballoon catheters, the operator may encounter difficulty in keeping the endometrial cavity distended in some patients, and faster rates of infusion may be required.

Procedure

During the procedure, the patient is placed in the lithotomy position. A preliminary transvaginal US is performed to evaluate the uterus, ovaries, and adnexal regions. In patients who have dilated fallopian tubes, the study should be deferred, and the patient should be treated with antibiotics. Laparoscopy may be performed instead for these patients.

Cleansing of the external genitalia is performed, followed by the insertion of a vaginal speculum to expose the vagina, cervix, and external os for cleansing, Cleansing solutions such as povidone iodine or chlorhexidine may be used after excluding allergies to the lotions. The external cervical os is identified, and a fine catheter that has been filled with saline to expel the air is inserted.

An endovaginal transducer that has been covered with a sterile sheath (the author uses a sterile glove for the probe and a sterile plastic sheath for the probe cable) is then inserted into the vagina. A nonlatex sheath should be used in patients who are allergic to latex. Under real-time US, sterile normal saline is infused by an assistant to slowly distend the endometrium.

Imaging

While the endometrial cavity is distended with saline, the entire endometrial cavity is surveyed for abnormal thickening, polypoidal lesions, synechia, or submucosal masses. Images of the uterus are obtained in sagittal and coronal sections. Real-time information may also be recorded on video for review. For 3D imaging, a volume dataset may be

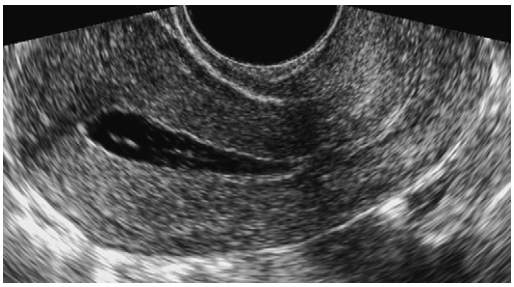

Fig. 1. Normal sonohysterogram in a premenopausal woman before undergoing in vitro fertilization. Smooth and regular endometrium revealed with saline infusion during the early proliferative phase of menstrual cycle.

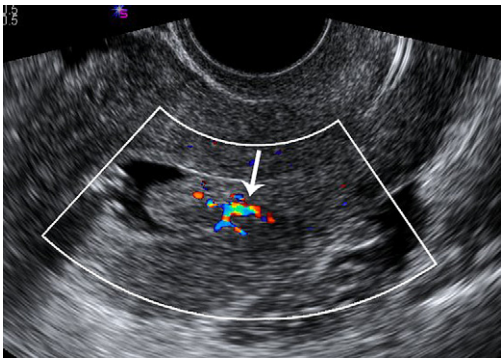

Fig. 3. Color Doppler sonohysterogram showing a vascular pedicle (*arrow*) extending into a benign endometrial polyp, a common feature of polyps.

acquired using an automated transducer or freehand scanning, depending on the equipment available. The endometrial cavity may be displayed in the coronal plane to show its triangular configuration. Such a display is useful for demonstrating congenital anomalies of the uterus.

Guidelines for the procedure have been jointly developed by the American College of Radiologists, the American College of Obstetricians and Gynecologists, and the American Institute of Ultrasound in Medicine and have been published in their respective websites and official journals [7,8]. In these guidelines, the key requisites for the physician performing the procedure are training, experience, skill in transcervical placement of catheters, and competence in gynecologic US.

Complications

Complications from the procedure are rare and self-limiting. The patient may experience mild lower abdominal cramps during the procedure and, in some cases, soon after the procedure. Discomfort may be minimized with slow infusion of saline when the balloon catheter is used. Slight per vaginal spotting may occur for 1 or 2 days after the procedure. Infection is uncommon at around 1% to 2% and usually presents as endometritis [8,9]. The success rate of the procedure varies in different reports [10,11], depending on the patient's age group. A higher rate of failure is encountered in a study with a higher composition of older postmenopausal patients due to cervical stenosis and failure in cannulating the uterus [11].

The risk of inadvertent dissemination of malignant cells is a worrisome aspect when performing this procedure on women who have postmenopausal bleeding. A study by Nagele and colleagues [12] found a rate of 23.3% dissemination of endometrial cells during hysteroscopy when saline was used as the distending medium for the uterine cavity. The pressure of the saline infusion for that study ranged from 100 to 150 mm Hg. Endometrial cells were present before hysteroscopy in 6.7% of their cases. In another study by Dessole and colleagues

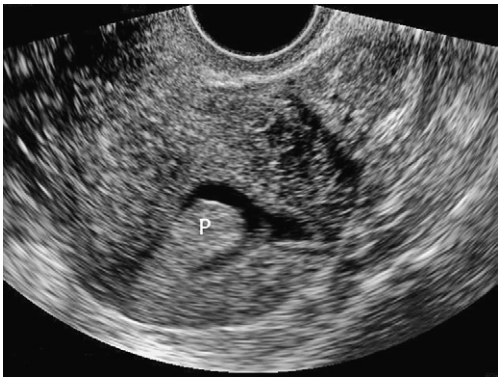

Fig. 2. Axial sonohysterogram of a 30-year-old woman investigated for infertility, showing an endometrial polyp (P) situated in the right cornual region in another woman investigated for infertility.

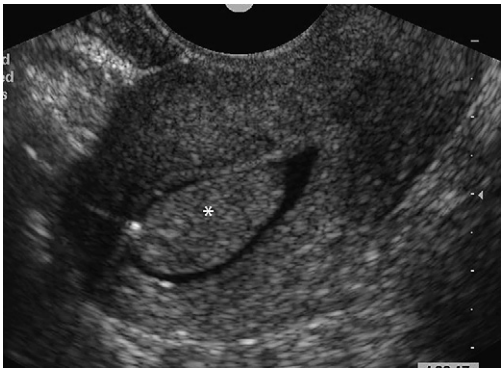

Fig. 4. Longitudinal sonohysterogram showing a large benign endometrial polyp (*asterisk*).

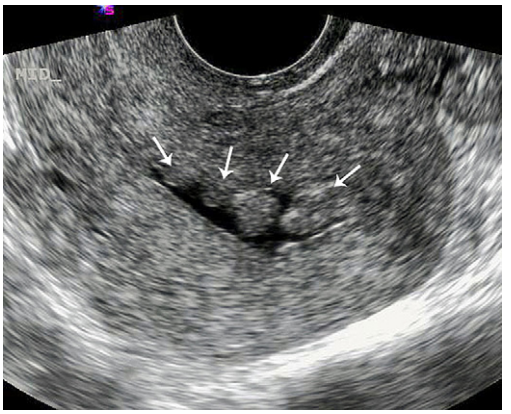

Fig. 5. Premenopausal woman investigated for infertility. Multiple polyps (*arrows*) along the posterior wall of the retroflexed uterus are demonstrated in a longitudinal sonohysterogram.

[13] on 32 women who had endometrial carcinoma, malignant cells were found in fluid spilled from the fallopian tubes during saline infusion in two patients (6.25%), and suspicious cells were found in another six women (18.75%). Alcazar and colleagues [14] found in an earlier study involving 14 patients who had stage I endometrial carcinoma that one patient (7.1%) showed malignant cells in the spilled fluid from the fallopian tube. The prognostic significance of such an occurrence is unclear because no randomized study has been done to evaluate this. A possible clue to this may lie in a study on x-ray hysterosalpingography (HSG) that showed no difference in the survival rates of patients who had endometrial carcinoma between those who had spillage of contrast into the peritoneal cavity and those who did not [15]. Because the process of instilling fluid into the endometrial cavity is similar in SIS and HSG, it is likely that patients who undergo SIS would have a similar outcome as those who had HSG.

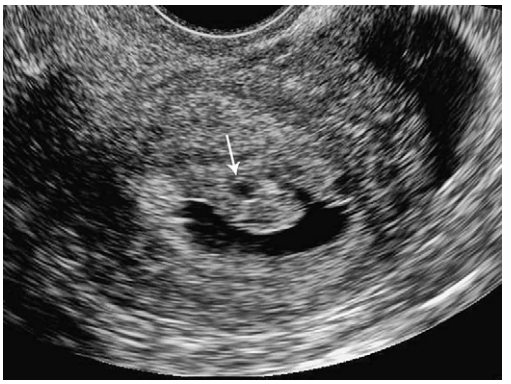

Fig. 6. Cyst (*arrow*) within an endometrial polyp on an axial sonohysterogram.

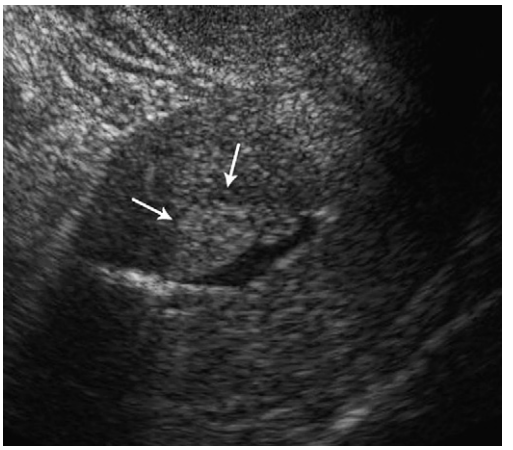

Fig. 7. A 59-year-old woman presenting with nonhemorrhagic vaginal discharge. Longitudinal sonohysterogram reveals focal thickening (*arrows*) of the endometrium in the anterior wall of the uterus due to sessile benign polyps. Differential diagnosis includes endometrial carcinoma.

Sonohysterographic findings

Normal

The normal endometrium should have a smooth outline with no focal thickening or irregularity (Fig. 1). The endometrial cavity should be clear of structures or stranding. In postmenopausal patients, the thickness of the two layers of the endometrium should not measure more than 4 mm.

Anomalies

The anomalies that may be revealed on SIS include polyps, submucosal fibroids, synechia, and diffuse thickening that may be due to hyperplasia or neoplasia.

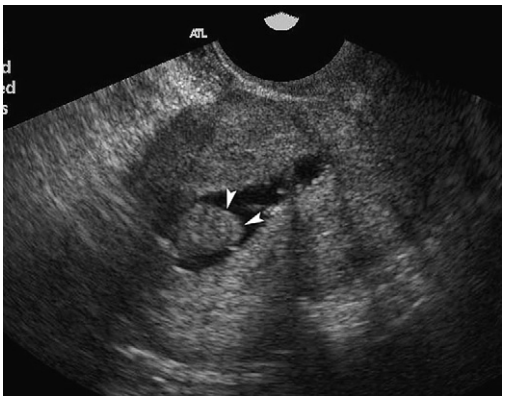

Fig. 8. A 55-year-old woman presenting with prolonged irregular per vaginal bleeding. Polypoidal mass (*arrowheads*) isoechoic to myometrium revealed within endometrial cavity. Histopathology revealed fibroid.

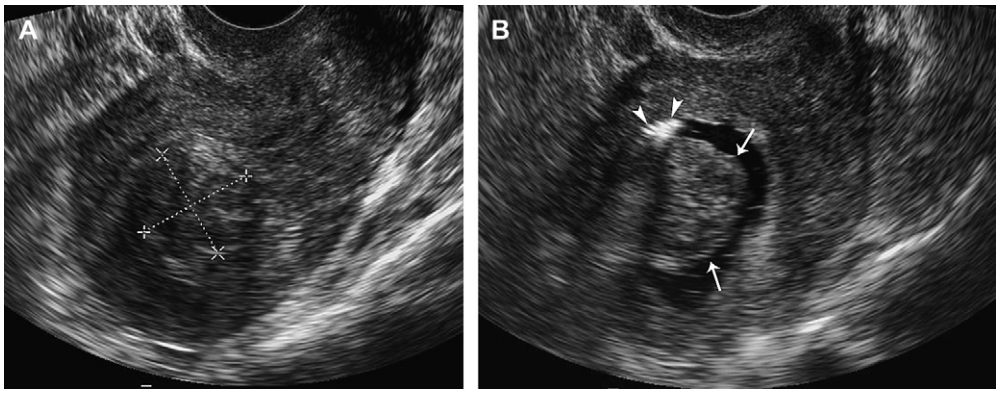

Fig. 9. (*A*) Longitudinal transvaginal US showing a central fibroid (*within cursors*) with distortion of the endometrium. (*B*) Longitudinal sonohysterogram reveals fibroid (*arrows*) with less than 50% extension into the myometrium. TI lesion. Air bubbles (*arrowheads*).

Polyps

Polyps are the most common anomalies that are revealed on SIS. They may or may not be associated with abnormal uterine bleeding. These lesions are due to focal hyperplasia of endometrial glands and stroma. They account for approximately 30% of postmenopausal bleeding [16]. In premenopausal women, they may cause infertility and intermenstrual bleeding. The majority of polyps are benign, but about 1.5% to 3% may be malignant [17–19]. In one study [19], the malignant polyps were found only in postmenopausal women.

The usual appearance of a polyp on SIS is a well defined echogenic pedunculated lesion that arises from the endometrium (Fig. 2). There is no disruption of the endometrial–myometrial junction. One or two vessels arising from the subendometrial myometrium may be seen extending into the polyp (Fig. 3). The rest of the endometrium is usually unaffected and should show normal thickness and contour.

Polyps may be large (Fig. 4), may be multiple (Fig. 5), may contain cysts (Fig. 6), may be sessile or broad based (Fig. 7), and may have heterogeneous or hypoechoic echotexture.

Submucosal leiomyomas

Compared with leiomyomas (fibroids) in other locations, submucosal leiomyomas tend to cause more symptoms. They distort the endometrial cavity and are more likely to cause abnormal uterine bleeding, severe bleeding, failure of embryo implantation, and infertility. Advances in operative hysteroscopy have enabled the removal of these lesions with significant reduction in morbidity, postoperative recovery time, and costs compared with open abdominal myomectomy. It is important to preoperatively identify fibroids that are suitable for hysteroscopic resection. An important determinant of such fibroids is the proportion of the fibroid that lies within the uterine cavity and its intramural extension. A classification system adapted by the European Society of Hysteroscopy grades fibroids into three categories (T0, TI, and TII) according to their intramural myometrial extension. T0 are pedunculated fibroids (Fig. 8), TI are fibroids with less than 50% extension into the myometrium (Fig. 9A, B), and TII (Fig. 10) are lesions where more than 50% of the fibroid is within the myometrium. A study by Wamsteker and colleagues [20] found that with more extensive intramural involvement, success in achieving complete resection was reduced, and the number of procedures required increased. Although transvaginal US can demonstrate submucosal lesions, SIS is more accurate in determining the extent of myometrial extension and resectability [21,22].

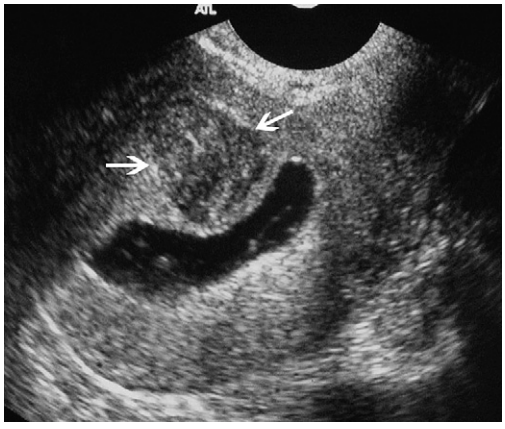

Fig. 10. Fibroid (*arrows*) with more than 50% extension into the myometrium. TII lesion.

On SIS, submucosal fibroids are hypoechoic lesions partially covered by the echogenic endometrium as it protrudes into the endometrial cavity. Occasionally, pedunculated fibroids may extend to the endocervical canal, making it impossible to carry out the procedure.

Endometrial hyperplasia and malignancy

Endometrial hyperplasia is a proliferative disorder of the endometrium usually caused by unopposed estrogen exposure. It is further classified as simple or complex and by the presence or absence of cellular atypia. Endometrial proliferative disorders range from simple hyperplasia to endometrial carcinoma. The classification is useful in predicting the risk of developing endometrial carcinoma in a given patient. Cellular atypia and complex endometrial hyperplasia increase the risk of cancer development. Another related condition, endometrial metaplasia, refers to change in the endometrial cell to resemble cells in the other parts of the genital tract (eg, squamous cells, ciliated cells). It may also cause abnormal uterine bleeding.

On SIS, endometrial hyperplasia, metaplasia, and carcinoma can present as diffuse thickening of the endometrium. The thickening may not be distinguishable from secretory endometrium. Lobular thickening may be seen in hyperplasia, resembling polyps or endometrial carcinoma [23].

Irregularity, heterogeneity of the endometrium, and focal abnormality are features of endometrial malignancy but may also be seen in hyperplasia. Poor distension of the endometrial cavity was demonstrated in another study [24] in all of its malignant cases (3 out of 63 cases). The presence of fluid in the endometrial cavity in these conditions would obviate the need to perform SIS (Figs. 11 and 12). In cases where the transvaginal US is highly suspicious of malignancy (Fig. 13), it may be prudent not to proceed with SIS [13].

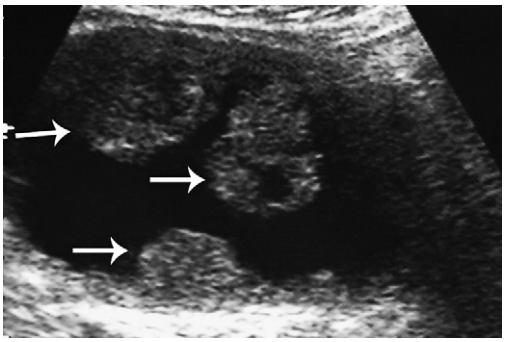

Fig. 12. A 71-year-old woman who had previous radiation therapy for cervical cancer presented with a pelvi-abdominal mass due to uterine distension. Transabdominal ultrasonography shows a fluid-filled endometrial cavity revealing multiple polypoidal masses (*arrows*) due to malignant mixed mullerian tumor.

Synechiae

Uterine synechiae or adhesions may be responsible for unexplained infertility, recurrent pregnancy loss, and reduced menstrual flow. There is usually a history of previous dilatation and curettage. Synechiae

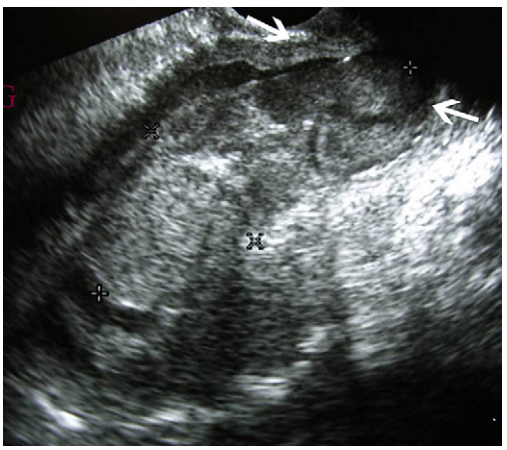

Fig. 11. A 76-year-old woman with per vaginal bleeding. Malignant mixed mullerian tumor presenting as large polypoidal intracavitary mass (*within cursors*) extending from the uterine body to the cervix (*arrows*) on transvaginal US.

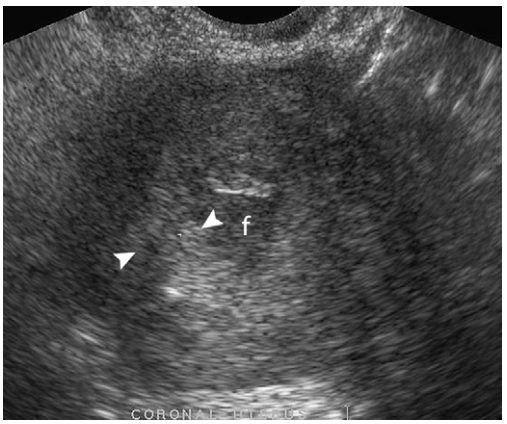

Fig. 13. A 56-year-old woman with postmenopausal bleeding. Axial transvaginal US shows diffuse irregular thickening of the endometrium (*arrowheads*) outlined by fluid (f) with low-level echoes. Histopathology of hysteroscopic dilatation and curettage specimen showed moderately differentiated endometrioid adenocarcinoma with myometrial invasion.

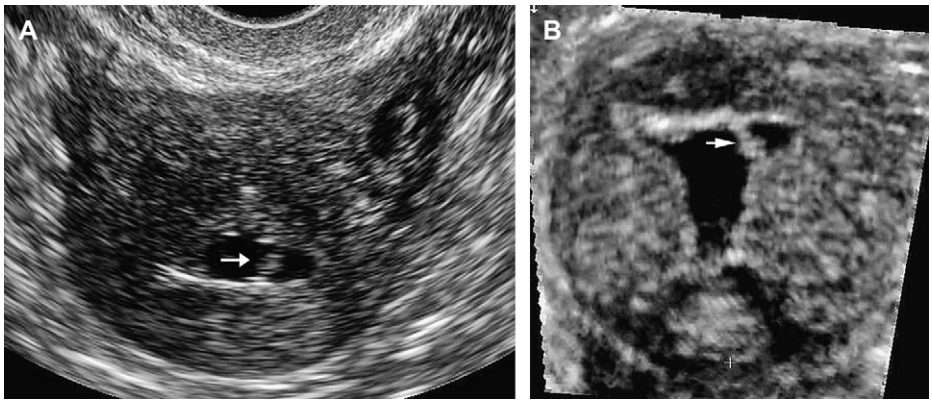

Fig. 14. (*A*) Patient who has had recurrent miscarriage. Sonohysterogram shows echogenic band (*arrow*) across the left side of the endometrial cavity due to synechia. (*B*) Coronal plane of the endometrial cavity constructed from 3D US showing location of the synechia (*arrow*) extending across the left cornu of the uterus.

may present as echogenic bridging bands (Fig. 14A, B) in the endometrial cavity, thin membranous undulating structures, or as a focus of adherent endometrial lining that cannot be separated (Fig. 15). When extensive, endometrial distension is often difficult and is one of the causes of a failed study. Patients who have extensive adhesions often complain of reduced menstruation.

Role of saline infusion sonohysterography in the assessment of infertility

HSG is the primary imaging method for the investigation of infertility. Although it is a good method for depicting the fallopian tubes, studies [4,25] describe shortcomings in the evaluation of the endometrial cavity, with false-positive rates as high as 35% [25]. In comparison, SIS offers a higher sensitivity and specificity for evaluating the uterine cavity. Using air and saline as contrast media, tubal patency may be assessed, making the technique a possible alternative to HSG [26].

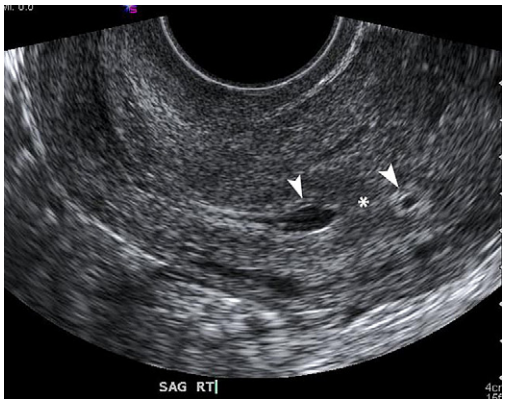

Fig. 15. Longitudinal sonohysterogram revealing adhesion (*asterisk*) between endometrial lining of the anterior and posterior uterine walls in a patient who has a past history of miscarriage with dilatation and curettage. Endometrial cavity with fluid (*arrowheads*).

Endometrial changes due to tamoxifen

Tamoxifen is widely used as adjuvant therapy in breast cancer patients for its antiestrogenic effects on breast tissue. Tamoxifen has a mild estrogenic effect on the endometrium. According to a study of 700 patients on tamoxifen [27], slightly over a third of cases had an abnormal endometrium, whereas the rest had atrophic or functional endometrium. Endometrial changes related to the tamoxifen treatment, including endometrial malignancy, are well documented [27–30]. The various endometrial pathologies include hyperplasia, polyps, atrophy, carcinoma, and sarcoma, with the most common being polyps [30]. Despite its low specificity, transvaginal US is often used to screen women on tamoxifen for endometrial anomalies. Thickening of the endometrium has been observed in postmenopausal women treated with tamoxifen [31]. There is little consensus on the cut-off value for normal endometrial thickness in asymptomatic women on tamoxifen. In a study of 117 asymptomatic postmenopausal women on tamoxifen, Fong and colleagues [32] found 6 mm to be the optimal cut-off value for normal endometrial thickness on transvaginal US. In their study, endometrium exceeding 6 mm in thickness or showing focal finding of a mass or thickening had a sensitivity of 85.1%, a specificity of 55.7%, a positive predictive value of 56.3%, a negative predictive value of 84.8%, and a positive likelihood ratio of 1.92 for the detection

of endometrial pathology. They also found that sonohysterography (called hysterosonography in their study) improves specificity (79.2% in their study). Sonohysterography is also more sensitive than endometrial biopsy in the detection of endometrial lesions [33].

The most common abnormal manifestation of tamoxifen treatment on a transvaginal US is a thickened endometrium with multiple cystic spaces (Fig. 16). This feature is nonspecific. It may be caused by hyperplasia (Fig. 17) or pseudo thickening due to subendometrial cysts (Fig. 18) lined by atrophic endometrium. The latter does not require further intervention. Such a distinction in the endometrial findings can be accurately assessed only by sonohysterography.

Role of sonohysterography in postmenopausal bleeding

Transvaginal US is generally accepted as the first imaging investigation for the evaluation of the endometrium in postmenopausal bleeding. In patients who are not on hormone therapy, an endometrial thickness of 4 mm is generally accepted as the cut-off limit of normal on transvaginal US. The use of SIS or direct hysteroscopy as the next investigation in cases of increased endometrial thickness remains a controversial issue. An algorithmic approach in the diagnostic work-up of postmenopausal patients who have abnormal uterine bleeding has been suggested elsewhere [34]. SIS may be offered to patients who have endometrial thickening (Fig. 19A, B) to determine if the thickening is due to a focal lesion or diffuse abnormality and to help in directing these patients to hysteroscopy or routine endometrial biopsy, respectively.

In patients on hormone therapy, there is no clear consensus on the cut-off limit for normal endometrial thickness. Differences in endometrial thickness

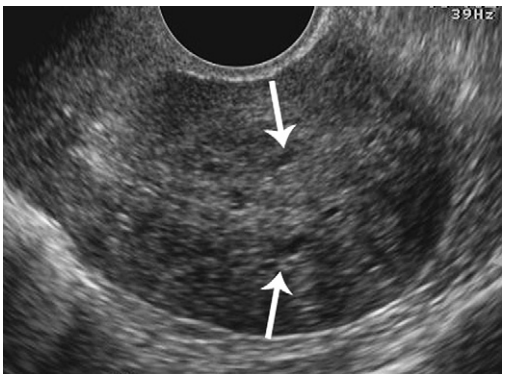

Fig. 16. Transvaginal US of a postmenopausal woman on tamoxifen showing thickened endometrium with cystic spaces (*arrows*).

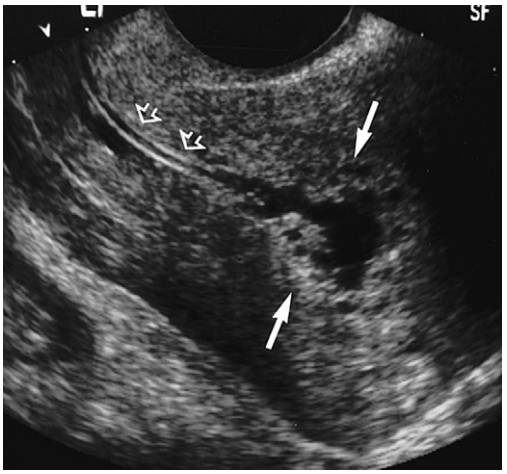

Fig. 17. A 55-year-old woman undergoing tamoxifen treatment for 5 years. Sonohysterogram shows circumferential thickening of the endometrium (*closed arrows*) measuring 12 mm and containing cystic spaces. The catheter (*open arrows*) is in the cervix. Histopathology from hysteroscopy with dilatation and curettage showed endometrial hyperplasia with atypia. (*From* LE Hann, Gretz EM, Bach AM, Francis SM. Sonohysterography for evaluation of the endometrium in women treated with tamoxifen. AJR Am J Roentgenol 2001;177:339; with permission.)

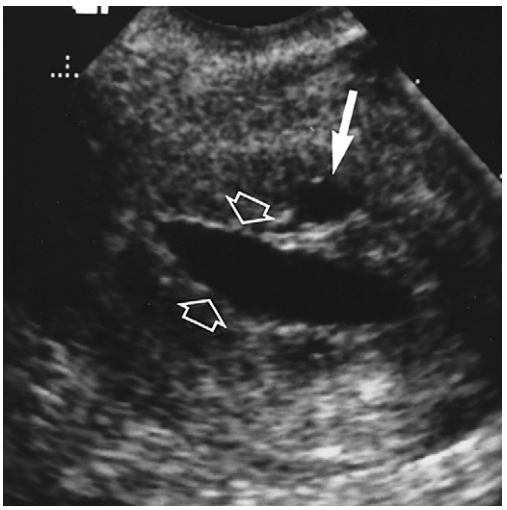

Fig. 18. A 63-year-old woman with tamoxifen who required no further examination after sonohysterography revealed that apparent endometrial thickening on transvaginal US was due to subendometrial cysts. On longitudinal sonohysterogram, the endometrium (*open arrows*) appears normal, and a subendometrial cyst (*closed arrow*) is seen. (*From* LE Hann, Gretz EM, Bach AM, Francis SM. Sonohysterography for evaluation of the endometrium in women treated with tamoxifen. AJR Am J Roentgenol 2001;177:341; with permission.)

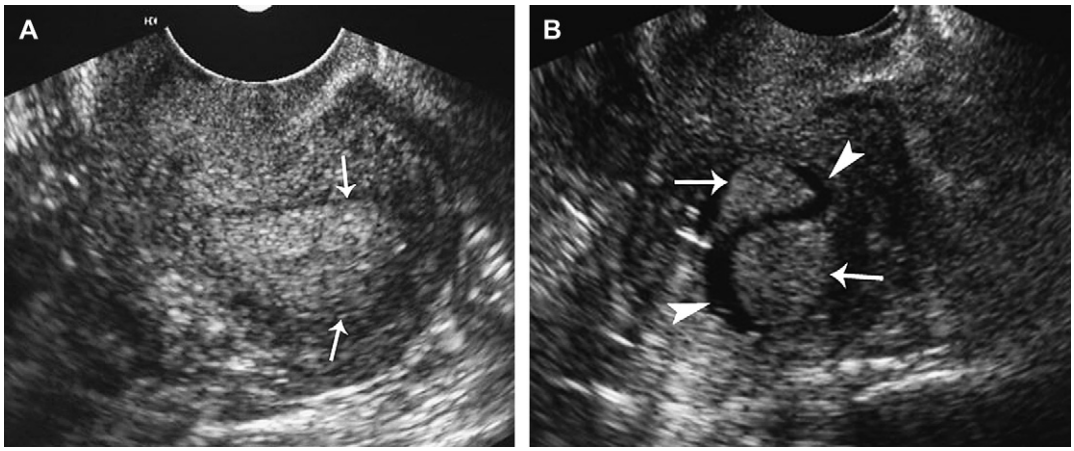

Fig. 19. (*A*) A 60-year-old woman presented with postmenopausal bleeding with thickened endometrium (*arrows*) on transvaginal US. (*B*) Sonohysterogram reveals two polyps (*arrows*). The rest of the endometrium is atrophic (*arrowheads*). Transcervical hysteroscopy confirmed the findings. Histopathology revealed benign endometrial polyps.

were observed in different therapy regimens, with greater thickening observed with unopposed estrogen compared with continuous combined and sequential estrogen-progestogen therapy [35,36]. Patients taking sequential therapy undergo cyclical bleeding, similar to premenopausal women, normally occurring after the last intake of progestogen. In studies where the scans of patients on sequential therapy were timed (usually between day 5 to 10 after the last progestogen intake and after withdrawal bleeding has taken place), a thinner endometrium was observed [37,38] compared with earlier studies [36,39] where the scans were not timed. The mean thickness observed in the studies with timing ranged from 3.5 mm (±1.2 mm) [37] to 4.3 mm (±1.2 mm) [38]. Women on continuous combined estrogen-progestogen therapy do not have endometrial thickness that is significantly different from those on sequential therapy [37].

In patients who present with unscheduled bleeding, a lower cut-off of 4 mm is suggested as a safe limit [36] for the diagnosis of endometrial atrophy as the cause of the bleeding. It is generally accepted that no further intervention is required for these patients apart from regular follow-up. In asymptomatic women, where there is less inclination toward intervention, an upper limit of 6 mm may be appropriate [34,36]. Some studies

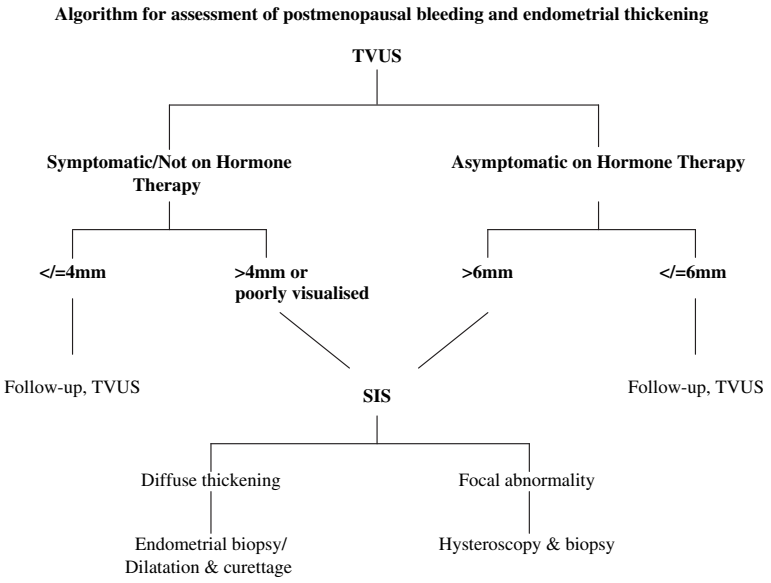

Fig. 20. Algorithm for assessment of symptomatic and asymptomatic postmenopausal women.

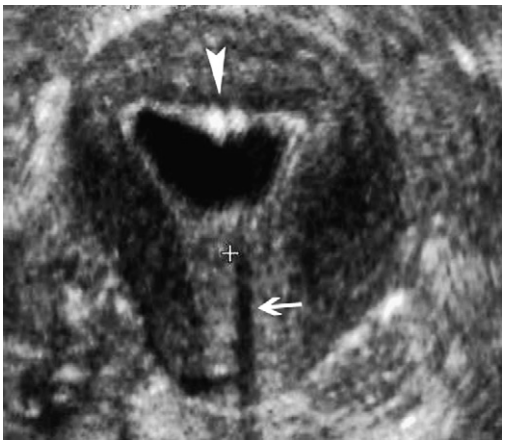

Fig. 21. Coronal image of the uterus reconstructed from 3D US revealing normal triangular endometrial cavity. The shadowing is due to the catheter (*arrow*) and air bubbles (*arrowhead*).

recommend endometrial sampling for patients who have endometrial thickness of over 4 mm [40,41]. An illustration of the diagnostic algorithm for the management of abnormal endometrial thickening and postmenopausal bleeding is presented in Fig. 20. Besides further diagnostic or surgical intervention, some clinicians have opted to change hormonal regimen and re-evaluate on transvaginal US. Other nonhormonal medications (tibolone and raloxifene) have little or no stimulatory effect on the endometrium.

Three-dimensional saline infusion sonohysterography

3D US, when performed with saline infusion, can yield additional useful information about the uterus, the endometrial cavity, and lesions that may occur within [42,43]. It provides detailed information of the internal and external contours of the uterus (Fig. 21), obviating the need to perform surgery for diagnosis alone. There is better depiction of endometrial lesion location (Fig. 22). More recently, a 3D sonographic inversion rendering was introduced that converts anechoic voxels to echogenic ones. Fluid-filled structures are made echogenic and displayed in three dimensions. With this technique, a digital "cast" of the endometrial cavity may be made and further studied [44].

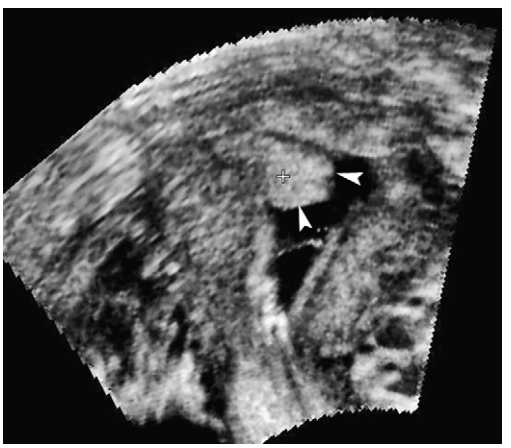

Fig. 22. Coronal image of the uterus reconstructed from 3D US of the patient shown in Fig. 2 showing right cornual endometrial polyp (*arrowheads*) and triangular endometrial cavity.

Saline infusion sonohysterography–guided interventional procedures on endometrial lesions

Initial feasibility studies using various catheters and techniques have indicated that it is possible to obtain adequate tissue samples of the endometrium [45,46] and to perform polypectomy [47] with SIS guidance.

Summary

SIS adds useful diagnostic information to transvaginal US in the evaluation of abnormal endometrial thickening, submucosal leiomyomas, endometrial changes due to tamoxifen, and other endometrial anomalies, such as synechia. Its applications continue to grow with the addition of 3D US techniques and its use in guiding biopsies or polypectomies within the endometrial cavity. It is simple to perform and well tolerated by patients.It should be included as part of the training curriculum for physicians performing gynecologic US.

References

[1] Laifer-Narin S, Ragavendra N, Parmenter EK, et al. False-normal appearance of the endometrium on conventional transvaginal sonography. AJR Am J Roentgenol 2002;178:129–33.
[2] Ragni G, Diaferia D, Vegetti W, et al. Effectiveness of sonohysterography in infertile patient work-up: a comparison with transvaginal ultrasonography and hysteroscopy. Gynecol Obstet Invest 2005;59(4):184–8.
[3] Dueholm M, Forman A, Jensen ML, et al. Transvaginal sonography combined with saline contrast sonohysterography in evaluating the uterine cavity in premenopausal patients with abnormal uterine bleeding. Ultrasound Obstet Gynecol 2001;18(1):54–61.
[4] Soares SR, Barbosa dos Reis MM, Camargos AF. Diagnostic accuracy of sonohysterography, transvaginal sonogaphy, and hysterosalpingography

in patients with uterine cavity diseases. Fertil Steril 2000;73(2):406–11.
[5] Bree RL, Bowerman RA, Bohm-Velez M, et al. US evaluation of the uterus in patients with postmenopausal bleeding: a positive effect on the diagnostic decision making. Radiology 2000;216: 260–4.
[6] Dessole S, Farina M, Capobianco G, et al. Determining the best catheter for sonohysterography. Fertil Steril 2001;76(3):605–9.
[7] Hamper UM, Piccoli CW (Principal drafters), Collaborative subcommittee from American Institute of Ultrasound in Medicine (AIUM), American College of Obstetricians and Gynecologists, AIUM clinical standards committee, and American College of Radiology. AIUM standard for the performance of saline infusion sonohysterography. J Ultrasound Med 2003;22:121–6.
[8] Breitkopf D, Goldstein SR, Seeds JW, ACOG committee on Gynecologic Practice. Saline infusion sonohysterography: ACOG technology assessment in obstetrics and gynecology. Obstet Gynecol 2003;102:659–62.
[9] Bonnamy L, Marret H, Perrotin F, et al. Sonohysterography: a prospective survey of results and complications in 81 patients. Eur J Obstet Gynecol Reprod Biol 2002;102:42–7.
[10] Dubinsky TJ, Parvey HR, Gormaz G, et al. Transvaginal hysterosonography: comparison with biopsy in the evaluation of postmenopausal bleeding. J Ultrasound Med 1995;14:887–93.
[11] Meng K, Branam JD, Nghiem HV, et al. The short-term clinical outcomes after saline infusion sonohysterography in women with post-menopausal bleeding. Acad Radiol 2005;12:136–41.
[12] Nagele F, Wieser F, Deery A, et al. Endometrial cell dissemination at diagnostic hysteroscopy: a prospective randomized cross-over comparison of normal saline and carbon dioxide uterine distension. Hum Reprod 1999;14(11):2739–42.
[13] Dessole S, Rubattu G, Farina M, et al. Risks and usefulness of sonohysterography in patients with endometrial carcinoma. Am J Obstet Gynecol 2006;194(2):362–8.
[14] Alcazar JL, Errasti T, Zornoza A. Saline infusion sonohysterography in endometrial cancer: assessment of malignant cells dissemination risk. Acta Obstet Gynecol Scand 2000;79(4):321–2.
[15] Devore GR, Schwartz PE, Morris JM. Hysterography: a 5-year follow-up in patients with endometrial carcinoma. Obstet Gynecol 1982;60: 369–72.
[16] O'Connell LP, Fries MH, Zeringue E, et al. Triage of abnormal postmenopausal bleeding: a comparison of endometrial biopsy and transvaginal sonohysterography versus fractional curettage with hysteroscopy. Am J Obstet Gynecol 1998; 178:956–61.
[17] Bakour SH, Khan KS, Gupta JK. The risk of premalignant and malignant pathology in endometrial polyps. Acta Obstet Gynecol Scand 2000; 79(4):317–20.
[18] Anastasiadis PG, Koutlaki NG, Skaphida PG, et al. Endometrial polyps: prevalence, detection, and malignant potential in women with abnormal uterine bleeding. Eur J Gynaecol Oncol 2000;21(2):180–3.
[19] Shushan A, Revel A, Rojansky N. How often are endometrial polyps malignant? Gynecol Obstet Invest 2004;58(4):212–5.
[20] Wamsteker K, Emanuel MH, de Kruif JH. Transcervical hysteroscopic resection of submucous fibroids for abnormal uterine bleeding: results regarding the degree of intramural extension. Obstet Gynecol 1993;82(5):736–40.
[21] Becker E Jr, Lev-Toaff AS, Kaufman EP, et al. The added value of transvaginal sonohysterography over transvaginal sonography alone in women with known or suspected leiomyomas. J Ultrasound Med 2002;21:237–47.
[22] Leone FP, Lanzani C, Ferrazzi E. Use of strict sonohysterographic methods for preoperative assessment of submucous myomas. Fertil Steril 2003;79(4):998–1002.
[23] Jorizzo JR, Chen MY, Martin D, et al. Spectrum of endometrial hyperplasia and its mimics on saline hysterosonography. AJR Am J Roentgenol 2002;179:385–9.
[24] Laifer-Narin SL, Ragavendra N, Lu DS, et al. Transvaginal saline hysterosonography: characteristics distinguishing malignant and various benign conditions. AJR Am J Roentgenol 1999; 172:1513–20.
[25] Mencaglia L, Colafranceschi M, Gordon AG, et al. Is hysteroscopy of value in the investigation of female infertility? Acta Eur Fertil 1988;19:239–41.
[26] Exacoustos C, Zupi E, Carusotti C, et al. Hysterosalpingo-contrast sonography compared with hysterosalpingography and laparoscopic dye perturbation to evaluate tubal patency. J Am Assoc Gynecol Laparosc 2003;10:367–72.
[27] Deligdisch L, Kalir T, Cohen CJ, et al. Endometrial histopathology in 700 patients treated with tamoxifen for breast cancer. Gynecol Oncol 2000; 78(2):181–6.
[28] Van Leeuwen FE, Benraadt J, Coebergh JW, et al. Risk of endometrial cancer after tamoxifen treatment of breast cancer. Lancet 1994;343(8895): 448–52.
[29] Hulka CA, Hall DA. Endometrial abnormalities associated with tamoxifen therapy for breast cancer: sonographic and pathologic correlation. AJR Am J Roentgenol 1993;160(4):809–12.
[30] Cohen I. Endometrial pathologies associated with postmenopausal tamoxifen treatment. Gynecol Oncol 2004;94:256–66.
[31] Gerber B, Krause A, Muller H, et al. Effects of adjuvant tamoxifen on the endometrium in postmenopausal women with breast cancer: a prospective long-term study using transvaginal ultrasound. J Clin Oncol 2000;18:3464–70.
[32] Fong K, Kung R, Lytwyn A, et al. Endometrial evaluation with transvaginal US and hysterosonography in asymptomatic postmenopausal

women with breast cancer receiving tamoxifen. Radiology 2001;220:765–73.
[33] Hann LE, Kim CM, Gonen M, et al. Sonohysterography compared with endometrial biopsy for evaluation of the endometrium in tamoxifen-treated women. J Ultrasound Med 2003;22:1173–9.
[34] Davis PC, O'Neill MJ, Yoder IC, et al. Sonohysterographic findings of endometrial and subendometrial conditions. Radiographics 2002;22: 803–16.
[35] Lin MC, Gosink BB, Wolf SI, et al. Endometrial thickness after menopause: effect of hormone replacement. Radiology 1991;180:427–32.
[36] Holbert TR. Transvaginal ultrasonographic measurement of endometrial thickness in postmenopausal women receiving estrogen replacement therapy. Am J Obstet Gynecol 1997;176:1334–9.
[37] Omodei U, Ferrazzi E, Ramazzotto F, et al. Endometrial evaluation with transvaginal ultrasound during hormone therapy: a prospective multicenter study. Fertil Steril 2004;81:1632–7.
[38] Affinito P, Palomba S, Sammartino A, et al. Ultrasonographic endometrial monitoring during continuous–sequential hormonal replacement therapy regimen in postmenopausal women. Maturitas 2001;39:239–44.
[39] Levine D, Gosink BB, Johnson LA. Change in endometrial thickness in postmenopausal women undergoing hormone replacement therapy. Radiology 1995;197:603–8.
[40] Vuento MH, Pirhonen JP, Makinen JI, et al. Screening for endometrial cancer in asymptomatic postmenopausal women with conventional and colour Doppler sonography. Br J Obstet Gynaecol 1999;106:14–20.
[41] Omodei U, Ferrazi E, Ruggeri C, et al. Endometrial thickness and histological abnormalities in women on hormonal replacement therapy: a transvaginal ultrasound/hysteroscopic study. Ultrasound Obstet Gynecol 2000;15:317–20.
[42] Lev-Toaff AS, Pinheiro LW, Bega G, et al. Three-dimensional multiplanar sonohysterography: comparison with conventional two-dimensional sonohysterography and X-ray hysterosalpingography. J Ultrasound Med 2001;20:295–306.
[43] Bega G, Lev-Toaff AS, O'Kane P, et al. Three-dimensional ultrasonography in gynecology: technical aspects and clinical applications. J Ultrasound Med 2003;22:1249–69.
[44] Timor-Tritsch IE, Monteagudo A, Tsymbal T, et al. Three-dimensional inversion rendering: a new sonographic technique and its use in gynecology. J Ultrasound Med 2005;24:681–8.
[45] Dubinsky TJ, Reed S, Mao C, et al. Hysterosonographically guided endometrial biopsy: technical feasibility. AJR Am J Roentgenol 2000;174: 1589–91.
[46] Wei AY, Schink JC, Pritts EA, et al. Saline contrast sonohysterography and directed extraction, resection and biopsy of intrauterine pathology using a Uterine Explora Curette. Ultrasound Obstet Gynecol 2006;27:202–5.
[47] Lee C, Ben-Nagi J, Ofili-Yebovi D, et al. A new method of transvaginal ultrasound-guided polypectomy: a feasibility study. Ultrasound Obstet Gynecol 2006;27:198–201.

ELSEVIER SAUNDERS

ULTRASOUND CLINICS

Ultrasound Clin 2 (2007) 133–153

Sonography of Adnexal Masses

Mukund Joshi, MD, FAMS*, Karthik Ganesan, DNB, Harsha Navani Munshi, DNB, Subramania Ganesan, MD, Ashwin Lawande, DNB

Transabdominal and transvaginal sonography are the community standard for the performance of pelvic sonography. Since their introduction, transvaginal probes have become the principal tools for evaluating the female pelvis [1]. Transabdominal imaging provides a global anatomic survey, whereas transvaginal imaging provides improved texture determination and characterization of the internal architecture of the ovary, vascular anatomy, and adnexal area. The location, size, consistency, and origin of adnexal masses may be defined with a combination of transvaginal and transabdominal scanning [2,3]. Transrectal ultrasound is performed whenever there is a contraindication to transvaginal scan, such as in the evaluation of the pediatric pelvis or in women who have never been sexually active. Transperineal scans also have a role to play in determining the origin and extent of some tumors. This article presents grayscale, color, and power Doppler features of common and uncommon benign and malignant adnexal masses.

Sonographic evaluation of the adnexal mass

The benefit of ultrasound lies in its ability to characterize the mass and give significant insight as to its probable nature. Correlation of sonographic images with pathologic findings has led to a substantial understanding of adnexal abnormalities. The development of scoring systems to characterize and define ovarian lesions, first based on morphologic characteristics and later including color Doppler flow data, brought us closer to a relatively reliable distinction between benign and malignant lesions, or at least to a negative predictive value in the range of 97% to 99%. The use of grayscale ultrasound morphology to characterize a pelvic mass is based on "pattern recognition." Subjective evaluation of ovarian masses based on pattern recognition can achieve sensitivity of 88% to 100% and specificity of 62% to 96%. Such subjective evaluation is found to be superior to scoring systems. Pattern recognition is superior to all other ultrasound methods (eg, simple classification systems, scoring

Dr. Joshi's Imaging Clinic, 809 Harjivandas Estate, Dr. Ambedkar Road, Next to Babubhai Jagjivandas, Dadar T.T, Mumbai 400014, Maharashtra, India
* Corresponding author.
E-mail address: drmukundjoshi@gmail.com (M. Joshi).

1556-858X/07/$ – see front matter
doi:10.1016/j.cult.2007.03.001
ultrasound.theclinics.com

systems, and mathematical models for calculating the risk of malignancy) for discrimination between benign and malignant extrauterine pelvic masses [4,5].

Benign adnexal lesions

The majority of ovarian masses are simple cysts (Fig. 1), most of which are benign. In this context, it is important to remember that the diagnosis of a "simple cyst" is based purely on ultrasound findings.

Functional ovarian cysts

Functional ovarian cysts result when a mature follicle does not rupture and the follicle continues to grow. Functional cysts include follicular cysts, serous inclusion cysts, corpus luteum, corpus albicans cysts, hemorrhagic cysts, and theca lutein cysts [2,3,6]. Most of these are simple cysts. Sonographically they appear unilocular, round, and anechoic with an imperceptible wall and posterior through transmission [4]. Functional cysts can become quite large but are usually less than 10 cm in size. These may produce discomfort or delayed menses but can be observed to regress within two menstrual cycles, although some persist for several months.

Corpus luteum cysts occur in the secretory phase of the menstrual cycle. Corpus luteal cyst in pregnancy reaches its maximum size by 7 weeks, and resolution occurs by 16 weeks. The corpus luteum can have a wide range of appearances on ultrasound (US) in the first trimester of pregnancy. The most common appearance is that of a round, thin-walled hypoechoic structure that demonstrates diffuse, homogeneous, low-level echoes. Other reported grayscale appearances (in order of decreasing frequency) include a cyst with a thick wall and anechoic center, a cyst that contains scattered internal echoes (Fig. 2A), and a thin-walled simple cyst that is similar in appearance to a follicular cyst [7]. On color flow Doppler sonography, it shows a typical "ring of fire" (Fig. 2B), and spectral Doppler examination reveals prominent diastolic flow [8]. The "ring of fire" appearance is secondary to increased vascularity in the periphery and is a nonspecific sign, because this may be seen in a mature Graafian follicle as well. Corpus luteal cyst of pregnancy is very vascular because of its hormonal status and may present with hemorrhage (known as a hemorrhagic corpus luteum), but the physiologic features are the same regardless of size [2,3,9].

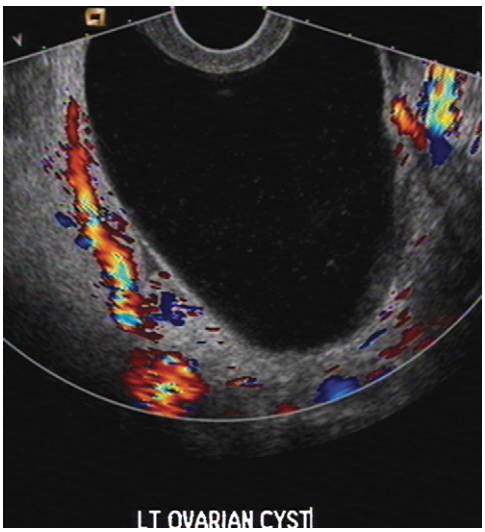

Fig. 1. Simple ovarian cyst. Transvaginal color flow Doppler image demonstrates a large simple ovarian cyst.

Any functional cyst may hemorrhage within and present as a hemorrhagic cyst (HC). The internal echo pattern varies with the stage of hemorrhage and the amount of fluid within the cyst. Evidence of posterior through transmission is typically present because of the cystic composition [10,11].

The average diameter of an HC is 3.0 to 3.5 cm (range: 2.5–8.5 cm). The cyst wall is thin (2–3 mm), well defined, and regular [12]. US appearance of HC may have diffuse echogenic material within, diffuse echoes with visible fibrin strands, retracting thrombus, or a fluid–fluid level. Jain [13] described the occurrence of fibrin strands within an HC as a "fishnet" appearance (Fig. 3A). The presence of a retracting thrombus adhering to the wall of a cyst is an additional sonographic feature. This finding may be occasionally confused with a focal mural nodule. A retracting clot typically has a concave margin, whereas mural nodules have convex margins. Retracting clots also appear to have a variable central echogenic pattern, whereas most mural nodules appear isoechoic in relation to the wall of the cyst. Okai and colleagues [14] serially followed 28 cases of hemorrhagic ovarian cysts that regressed spontaneously within 8 weeks. Color Doppler flow studies do not reveal any blood flow within a retracting clot or the fibrin strands (Fig. 3B) [2,3,9].

Theca lutein cysts (also called lutein cysts, *hyperreactio luteinalis*) are luteinized follicle cysts that form as a result of overstimulation from high hCG levels or hypersensitivity to human chorionic gonadotrophin (hCG) in normal pregnancy. Bilateral multiseptated cystic adnexal masses in a woman who has gestational trophoblastic disease (Fig. 4), multiple gestation, ovarian hyperstimulation, or a pregnancy complicated by fetal hydrops are likely to represent theca lutein cysts, rather than malignancy. Theca lutein cysts are reported with

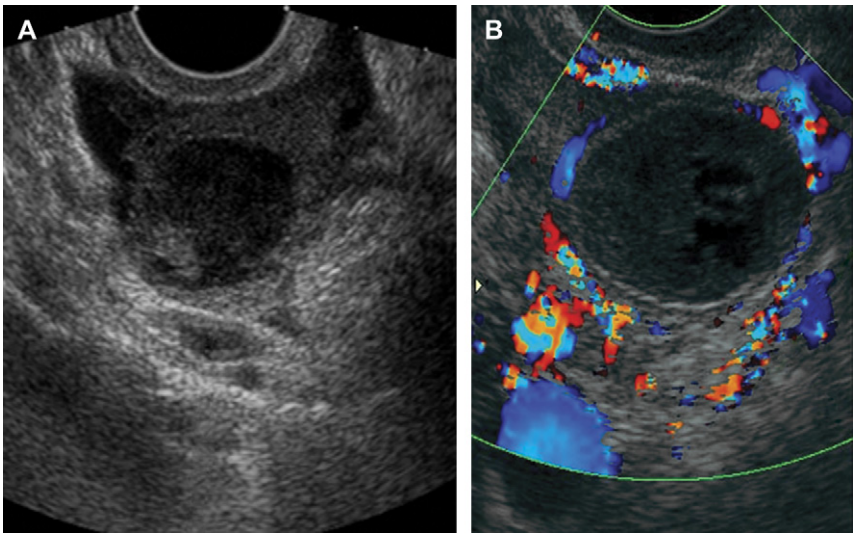

Fig. 2. Corpus luteum cyst. (*A*) Transvaginal grayscale image of the left ovary demonstrates a cyst with debris within, suggestive of hemorrhage in a corpus luteum cyst. (*Courtesy of* A. Khurana, MD, India). (*B*) Corresponding color flow Doppler image demonstrates peripheral vascularity—called the "ring of fire."

complete hydatidiform moles 14% to 30% of the time [15]. In normal pregnancy, the cysts gradually resolve weeks to months after the source of hCG is eliminated. Complications include torsion, infarction, and hemorrhage.

Endometriosis

Endometriosis is defined as the presence of functional endometrial tissue outside the uterine cavity and the myometrium. The most common site of involvement in endometriosis is the ovary, followed by the uterine ligaments (posterior broad ligament, uterosacral ligament), pelvic cul-de-sac, pelvic peritoneum, fallopian tubes, rectosigmoid, and bladder. Endometriotic cysts (endometriomas) usually occur within the ovaries and result from repeated cyclic hemorrhage. More than 90% of endometriomas are pseudocysts formed by invagination of the ovarian cortex, which is sealed off by adhesions. Endometriomas may completely replace normal ovarian tissue. Cyst walls are usually thick and fibrotic, frequently with dense fibrous adhesions and areas of discoloration. Cyst content generally is composed of thick, dark, degenerate blood products, and this appearance has been called "chocolate cyst" [12].

The sonographic features of endometriomas are varied, ranging from anechoic cysts to cysts with diffuse low-level echoes to solid-appearing masses. Fluid–fluid or debris–fluid levels may also be

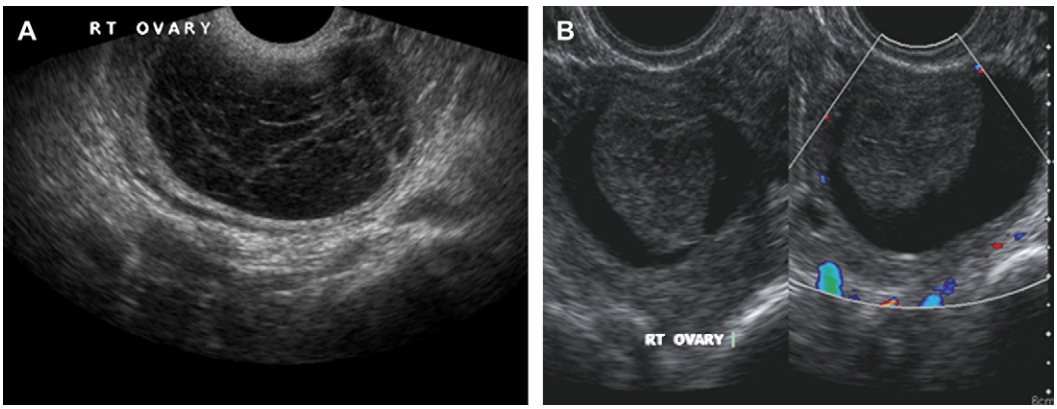

Fig. 3. Hemorrhagic ovarian cyst. (*A*) Transvaginal grayscale image of the right ovary demonstrates a typical "fish-net" appearance. (*B*) Grayscale and color flow Doppler image of the right ovarian cyst with a retracting blood clot adherent to the cyst wall and absent vascularity.

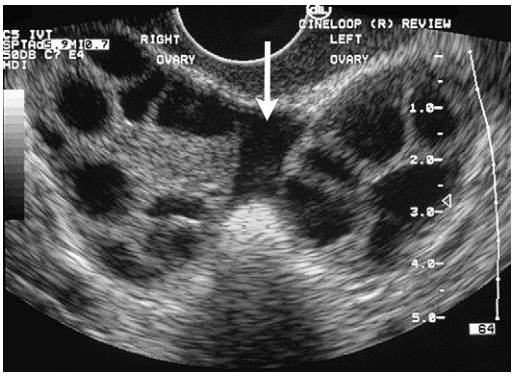

Fig. 4. Theca lutein cysts. Transvaginal grayscale image of the pelvis demonstrates multiple simple bilateral ovarian cysts in this patient with a hydatidiform mole. A pocket of free fluid is present between the two ovaries (*arrow*). (*From* Webb EM, Green GE, Scoutt LM. Adnexal mass with pelvic pain. Radiol Clin North Am 2004;42:335; with permission.)

seen. They may be unilocular or multilocular with thin or thick septations [7].

One of the more common appearances of endometrioma is that of an adnexal mass with diffuse low-level echoes (Fig. 5A). This appearance is seen in 95% of endometriomas [16]. Typical endometriomas do not show any vascularity [17]. The presence of hyperechoic wall foci (punctate peripheral echogenic foci) on sonographic examination is very specific for endometriomas. Echogenic wall foci differ from wall nodularity and are an important discriminating feature. A mass with low-level internal echoes, hyperechoic wall foci, and no neoplastic features is 32 times more likely to be an endometrioma than another adnexal mass. This echogenic wall focus was found to be the highest single predictor of endometrioma and is believed to represent cholesterol deposits [12,16].

In a recent study, the appearance of "kissing ovaries" is suggested as an indirect sign of endometriosis, especially in diagnosing adhesions and the most severe form of the disease, which is significant pelvic extension of the endometriosis with dense adhesions. The diagnosis of kissing ovaries is made when both ovaries are joined behind the uterus in the cul-de-sac and cannot be separated by pushing the transvaginal probe or by manipulating the uterus transabdominally (Fig. 5B). The detection of kissing ovaries by US is strongly associated with the presence of endometriosis and is a marker of the most severe form of this disease [18].

Certain reports have suggested that solid areas or polypoid projections are suggestive of malignancy in an endometrioma. Malignant transformation has been documented in 0.3% to 0.8% of patients who have ovarian endometriosis. For a high level of sonographic confidence in detection of endometriomas, attention must be focused on assessment of wall nodularity to exclude a malignancy [2,3,9,19].

Hydrosalpinx

Hydrosalpinx is characterized by obliteration of the fimbriated end and dilatation of the fallopian tube, usually the ampullary and infundibular portions. If the ovary is first involved by tubo-ovarian adhesions, the dilated tube may compress the ovary. The tube usually contains clear, serous fluid. Most cases of hydrosalpinx have a typical appearance and may be easily distinguished from ovarian abnormalities. Hydrosalpinges are tubular, elongated, extraovarian structures, and some show longitudinal folds (Fig. 6).

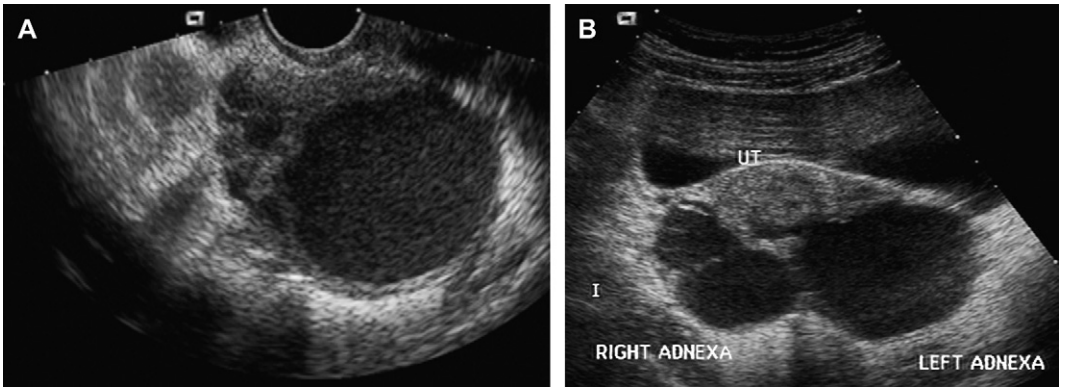

Fig. 5. Endometrioma. (*A*) Transvaginal grayscale image demonstrates a left ovarian cyst with low-level echoes. (*B*) Transabdominal grayscale image of the pelvis with bilateral endometriomas demonstrates the "kissing ovaries" sign. (UT, uterus.)

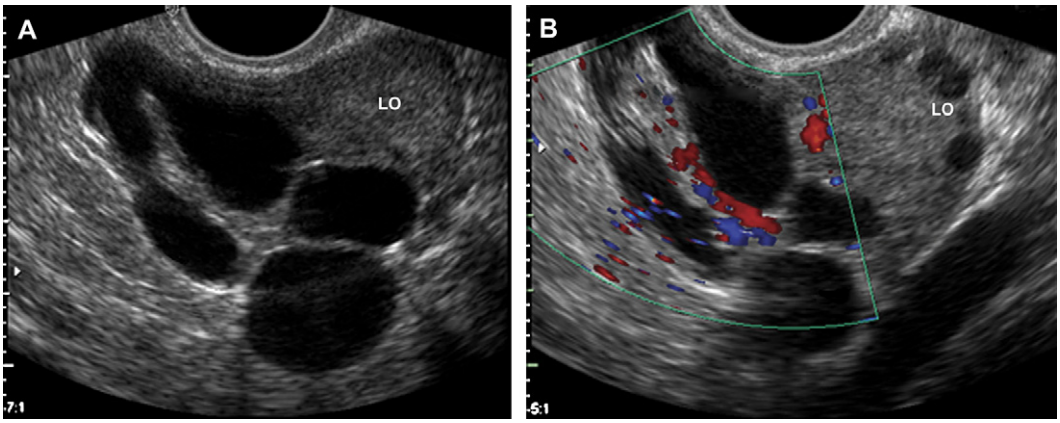

Fig. 6. Hydrosalpinx. Transvaginal grayscale (*A*) and color flow Doppler (*B*) images of the left adnexa demonstrate serpiginous, tubular, anechoic, and avascular structures in the left adnexa. (LO, left ovary.)

Tessler and colleagues [20] described a tubular structure with folded configuration and incomplete septations as the most consistent sonographic feature in 12 cases of hydrosalpinx. Timor-Tritsch and colleagues [21] also analyzed the shape of the mass, wall structure, wall thickness, and ovarian involvement. They suggested that many hydrosalpinges appear as ovoid or pear-shaped fluid collections with incomplete septae, multiple hyperechoic mural nodules (beads-on-a-string sign), and short linear projections (cogwheel sign). A waist sign has been described in cases of hydrosalpinges, representing the diametrically opposed indentations along the wall of the mass lesion.

Patel [22] reported that the combination of the waist sign and tubular shape of the mass had no false positives for diagnosis of hydrosalpinx, leading to a calculated likelihood ratio exceeding 18:9. In their study, incomplete septations and short linear projections were findings predictive of hydrosalpinx; however, independently each sign was less predictive than the tubular shape of the mass or the waist sign. They suggested that incomplete septations were less useful as a diagnostic sign, because these can also be detected in some cystic tumors. The sonographic detection of a normal-appearing ovary ipsilateral to a cystic adnexal mass aids in accurate diagnosis of the mass as representing a hydrosalpinx rather than an ovarian mass. However, in some cases the ovary may also be involved in the disease process, extending to form a chronic tubo-ovarian mass.

Pelvic inflammatory disease

Pelvic inflammatory disease (PID) is one of the most common causes of acute pelvic pain in women, and imaging findings vary with the stage of disease. The sonographic findings may be normal early in the course of the disease. Sonographic markers for tubal inflammatory disease have been described as 1) thickening of the tube wall of 5 mm or more; 2) the cogwheel sign, defined as a sonolucent, cogwheel-shaped structure visible in a cross-section of a tube with thick walls, correlating with inflammatory changes in acute salpingitis; 3) incomplete septa, correlating with folds or kinks in the dilated tube, which may be sonolucent or contain low-level echoes (Fig. 7A); 4) the beads-on-a-string sign, defined as hyperechoic mural nodules (about 2–3 mm) seen on the cross-section of a fluid-filled, distended structure; 5) Tubo-ovarian complex, in which the ovaries and tubes are recognized, but the ovary cannot be separated from the tube; 6) tubo-ovarian abscess with marked probe tenderness, formation of a conglomerate mass, or fluid collection; and 7) cul-de-sac fluid.

A tubo-ovarian abscess may present as an asymptomatic probable adnexal mass that did not completely resolve previously. The US appearance varies according to its appearance at the time of stabilization of the inflammatory process. The mass may be purely cystic, have multiple loculations, have thick septations, and contain complex debris (Fig. 7B). Much less common than a tubo-ovarian abscess is an abscess confined to the ovary. An ovarian abscess is typically a result of direct or lymphatic spread of organisms from a nongynecologic pelvic inflammatory process (eg, diverticulitis, appendicitis, infection following pelvic surgery) [2,4,9]. Presence of any free fluid is worrisome, and the possibility of pus must be considered. Although the combination of sonographic and clinical findings is often quite specific for PID, there are several other common diagnoses in the

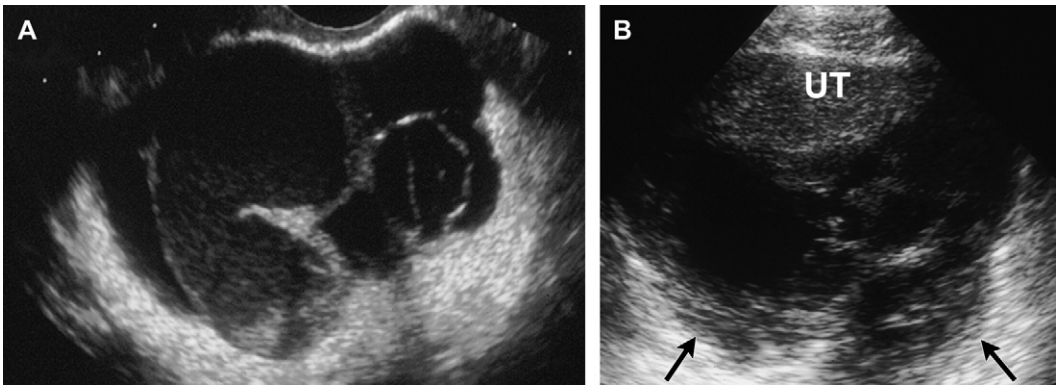

Fig. 7. Pelvic inflammatory disease. (*A*) Transvaginal grayscale image demonstrates debris within the dilated fallopian tube. (*B*) Transabdominal grayscale image in patient with fever and confirmed PID reveals pelvic abscess (*arrows*). (UT, uterus.)

differential diagnosis. The most common alternative diagnoses, with findings that simulate PID by the presence of an indistinct uterus and complex pelvic fluid, are ruptured endometrioma or HC and perforated appendicitis [23]. Perihepatitis associated with PID is known as Fitz-Hugh-Curtis Syndrome [23].

Mature cystic teratoma

Mature cystic teratoma constitutes 20% to 25% of pelvic masses. Mean age of presentation is 30 years, and 12% are bilateral. Mature cystic teratomas grow slowly at an average rate of 1.8 mm each year, prompting some investigators to advocate nonsurgical management of smaller (<6 cm) tumors. The presence of fat opacity or fat signal intensity in an ovarian lesion is highly specific for a teratoma. Mature cystic teratomas are predominantly cystic with dense calcifications, whereas immature teratomas are predominantly solid with small foci of lipid material and scattered calcifications. Although dermoids have a wide spectrum of sonographic appearances, depending on the elements present (ectoderm, mesoderm, or endoderm), certain distinct features occur with a degree of consistency. Among these are dermoid mesh with hyperechoic calcifications, indicating the presence of bone, teeth, or other ectodermal derivatives in a predominantly cystic medium, hyperechoic solid mural components, and hair–fluid levels [2–4,24].

Sonographic appearance, in order of decreasing frequency, is cystic lesion with a densely echogenic tubercle (Rokitansky nodule); diffusely or partially echogenic mass, with the echogenic area usually demonstrating sound attenuation; and multiple thin echogenic bands caused by hair in the cyst. These sonographic criteria have 58% sensitivity and 99% specificity [25]. Sometimes the presence of echogenic focus (secondary to calcification) results in a curvilinear interface with acoustic shadowing and may obscure the visualization of mature cystic teratoma; hence this is called the "tip of the iceberg" sign (Fig. 8).

Unusual findings in mature cystic teratoma may result in occasional diagnostic difficulties. Multiple spherical structures (fat balls) floating free in a large cystic mass is one of the rarer patterns that can be mistaken for malignancy. The sonographic feature of intracystic floating echogenic balls is probably pathognomonic for mature teratoma and is easily detected in most cases [26]. In cases with sonographic features simulating malignancy, color Doppler mapping may be helpful. Color Doppler sonography is helpful in differentiating these benign nodules (small balls) from malignant tumor

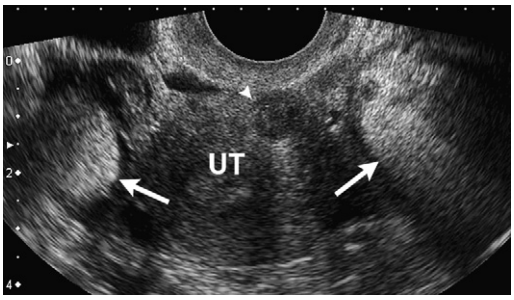

Fig. 8. Bilateral mature cystic teratoma. Transverse grayscale image demonstrates bilateral mature cystic teratomas (*arrows*). This image also shows the "tip of the iceberg" sign. Incidentally seen is a fibroid (*arrowhead*) in the anterior wall of the uterus (UT). *(Courtesy of* V. Dogra, MD, Rochester, NY.)

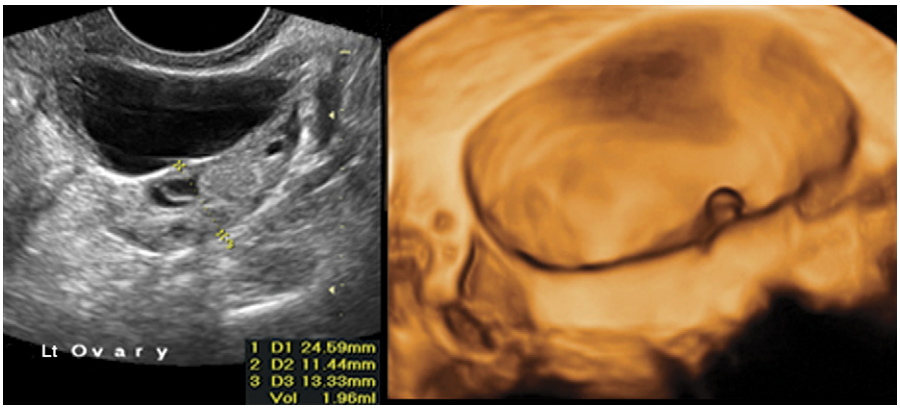

Fig. 9. Parovarian cyst. Transvaginal grayscale image demonstrates a left parovarian cyst with a corresponding four-dimensional US reformatted image that demonstrates better delineation and extent of the cyst. (*Courtesy of* A. Khurana, MD, India.)

[26]. The most common tumor associated with ovarian torsion is mature cystic teratoma [27].

Parovarian/paratubal cysts

Parovarian/paratubal cysts may arise from mesonephric (Wolffian) structures, paramesonephric (Mullerian) structures, or mesothelial inclusions. The hydatid of Morgagni is by far the most common paramesonephric cyst and is found arising from the fimbrial end of the fallopian tube. Sonographically, these have thin, deformable walls that are not surrounded by ovarian stroma and appear as simple cysts adjacent to the ovary (Fig. 9). They may be easily missed or mistaken for ovarian cysts but are confirmed by separating the cyst from the ovary on transvaginal examination. These cysts can arise anywhere in the adnexal structures; if they are large, their point of origin may not be clear. Their size does not change with the hormone cycle [2,3].

Peritoneal inclusion cysts

Although fairly common, peritoneal inclusion cysts are less well-recognized entities on imaging of the female pelvis. Peritoneal inclusion cysts, also known as peritoneal pseudocysts and inflammatory cysts of the pelvic peritoneum, present with a variety of imaging appearances, which can be confused with various adnexal masses of the female pelvis.

Peritoneal inclusion cysts occur predominantly in premenopausal women who have a history of previous abdominal surgery, trauma, PID, or endometriosis [28]. Peritoneal adhesions extend to the surface of the ovary and may distort the ovarian contour but not penetrate the ovarian parenchyma. When the adhesions surround the ovary, and fluid accumulates, complex cystic masses form. The entrapped ovary appears like a spider in a web and may be mistaken for a solid nodular portion of the tumor with surrounding septations. Sometimes the ovary is eccentrically located to the adhesions. This is called spider-web pattern (entrapped ovary) (Fig. 10) [29]. These cysts may simulate hydrosalpinx, pyosalpinx, or even an ovarian mass. Sonographic diagnosis depends on the presence of normal ipsilateral ovary with surrounding loculated fluid conforming to the peritoneal space [29]. The fluid is usually anechoic but may contain echoes in some compartments, owing to hemorrhage or proteinaceous fluid. Peritoneal inclusion cyst must be differentiated from parovarian cysts and hydrosalpinx [2,3].

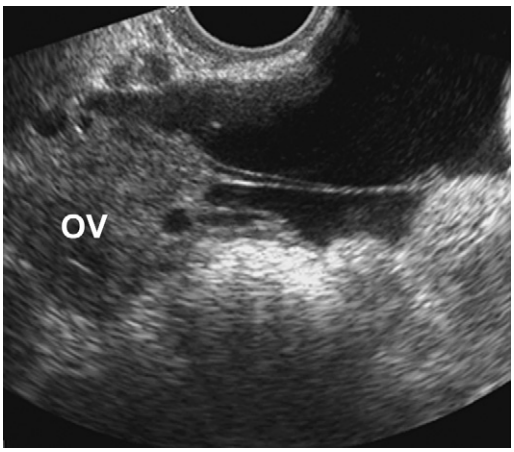

Fig. 10. Peritoneal inclusion cyst. Transvaginal grayscale image of the right adnexa demonstrates a spider-web pattern with presence of loculated fluid and an eccentric right ovary (OV).

Polycystic ovaries

Polycystic ovaries occur in approximately 17% of women of reproductive age. The classic signs and symptoms result from excessive androgen production, inappropriate gonadotropin secretion, and chronic anovulation and are manifested by acne, hirsutism, and menstrual irregularity [30]. Polycystic ovarian disease (PCOD), or Stein-Leventhal syndrome, is a common cause of infertility that is accompanied by secondary amenorrhea, hirsutism, and/or obesity [31]. The morphologic hallmark of the disease is mild enlargement of both ovaries, which contain multiple small cysts. Discrete cysts, however, are not sonographically visible in the majority of patients [32], and as many as 30% of patients who have PCOD have ovaries that are within normal size limits [33]. The number of follicles necessary to establish the diagnosis of polycystic ovaries has been reported to vary from more than five to 10 or at least 15 [34–36]. In a study by Pache and colleagues [37], a maximum of 11 follicles could be detected in normal ovaries, and a considerable number of ovaries in patients who had PCOD contained fewer than 11 follicles. Increased ovarian echogenicity is an additional criterion for diagnosing PCOD but is very subjective. A combination of follicular size and ovarian volume is the most sensitive objective parameter. It has a sensitivity of 92% and a specificity of 97% (Fig. 11).

Postmenopausal cysts

Small simple cysts are common in postmenopausal patients [38]. Fifteen percent of postmenopausal women may show simple cystic adnexal structures as large as 5 cm (Fig. 12). A cystic structure that is less than 30 mm in size, unilateral, and unilocular, has no internal echoes, solid areas, or nodules, and is avascular on color flow mapping may be re-evaluated 6 and 12 weeks later and then annually if it does not increase in size or change in morphology. A simple unilocular cyst without solid components is highly unlikely to be malignant. Any mass with abnormal vascularity and all masses greater than 50 mm in size warrant surgical evaluation. All masses associated with a rising CA-125 level warrant surgical exploration [39].

Ectopic pregnancy

Ectopic pregnancy is one of the most common gynecologic emergencies that presents as vaginal bleeding or abdominal pain. Ectopic pregnancy most commonly (95%) occurs in the ampullary or isthmic portions of the fallopian tube. An ectopic pregnancy can be diagnosed with confidence when an adnexal mass that contains a yolk sac or viable embryo is identified (Fig. 13A). In the absence of a visualized yolk sac or fetal pole, the so-called "echogenic adnexal" (or tubal) ring sign is the second most specific US finding for ectopic pregnancy [40]. It may be difficult to differentiate the tubal ring of an ectopic pregnancy from an exophytic corpus luteal cyst. An anechoic structure with an echogenic, vascular rim truly located within the ovary is statistically much more likely to be a corpus luteal cyst, because true intraovarian ectopic pregnancies are rare [7].

Differentiation between an ectopic pregnancy and an exophytic corpus luteal cyst can be aided by gently tapping on the ovary with the transducer. Independent movement of the ovary indicates an extraovarian location of the adnexal ring, which confirms ectopic pregnancy [7]. The demonstration of the embryonic cardiac activity confirms intrauterine pregnancy. (However, gestations earlier than 5 to 6 weeks may not show evidence of cardiac activity.)

As many as 20% of patients who have ectopic pregnancy demonstrate an intrauterine pseudogestational sac, which should be differentiated from the double decidual sac of an intrauterine pregnancy. The pseudogestational sac does not contain a living embryo or yolk sac and is located in the center of the endometrial cavity (unlike the burrowed gestational sac, which is placed eccentrically). Color Doppler imaging plays an important role in differentiating an ectopic pregnancy from a corpus luteum (CL). Both demonstrate abundant vascularity at the periphery—"ring of fire" on color flow imaging (Fig. 13B)—which is by itself a nonspecific sign and may also be seen around a mature ovarian follicle or HC.

It has been found that low (<0.39) and high (>0.7) resistive indices (RIs) are specific for ectopic pregnancy (100% specificity and positive predictive value). A higher RI suggests the presence of less active trophoblasts and therefore a spontaneous resolution of the ectopic pregnancy. Color Doppler evaluation of the endometrium may help discriminate between ectopic pregnancy and CL. Ectopic pregnancies may show endometrial blood flow, but the RI is usually greater than 0.55, and peak systolic velocity (PSV) is less than 15 cm/s. Demonstration of the presence of trophoblastic tissue in the endometrium, even in the absence of a visible double decidual sac, is suggestive of an intrauterine pregnancy and excludes ectopic pregnancy. Trophoblastic tissue is identified by the detection of low resistance flow in the endometrium with RI less than 0.55 and PSV greater than or equal to 15 cm/s. Screening of the upper abdomen as a routine part of the pelvic examination is mandatory to search for free fluid in Morison's pouch or along the flanks. Echogenic free fluid does not always mean

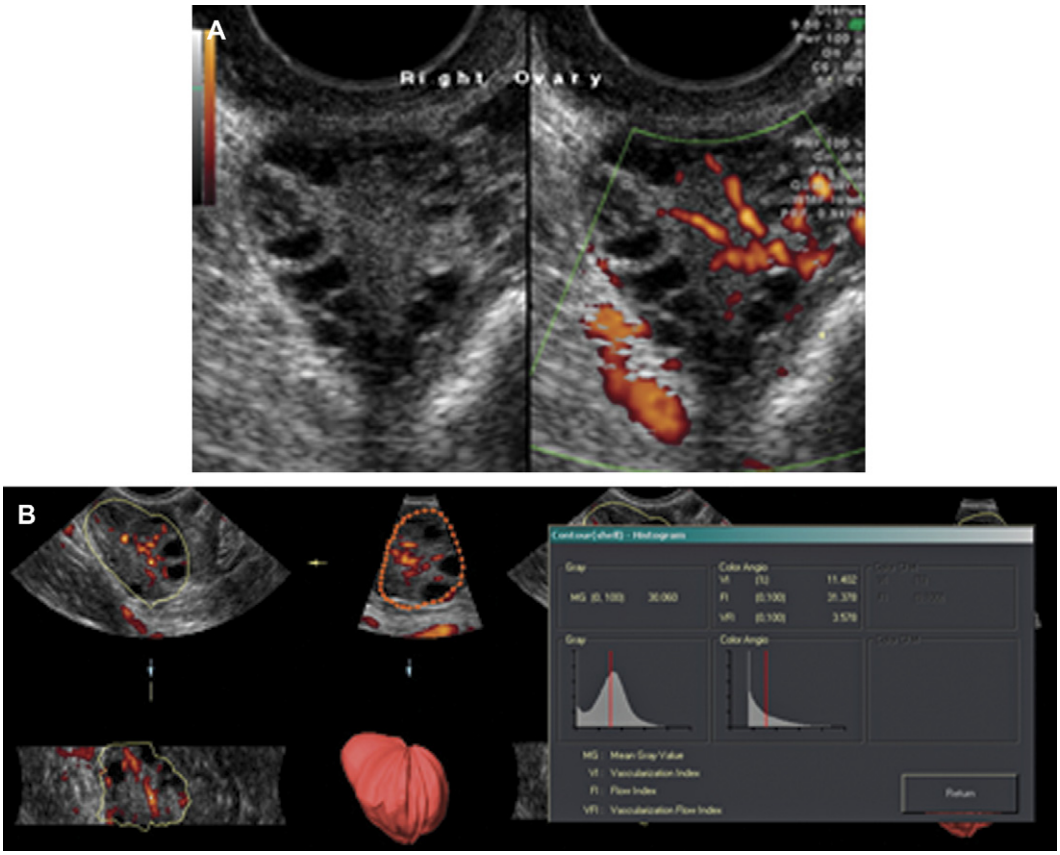

Fig. 11. Polycystic ovarian disease. (*A*) Power Doppler image of bilateral ovaries demonstrates multiple follicles. (*B*) Corresponding four-dimensional images demonstrate ovarian volume calculation in polycystic ovaries. (*Courtesy of* A. Khurana, MD, India.)

a ruptured ectopic pregnancy, although the greater the quantity of fluid, the greater the chance of finding a ruptured ectopic pregnancy [3,9,41,42].

The sonographer should remember that in as many as 26% of ectopic pregnancies, no intrauterine pregnancy or adnexal abnormality may be detectable by endovaginal sonography. Clinical correlation and close follow-up are of paramount importance [43].

Ovarian remnant syndrome

Ovarian remnant syndrome, a complication of oophorectomy, usually occurs in patients who have distorted anatomy resulting from adhesions and

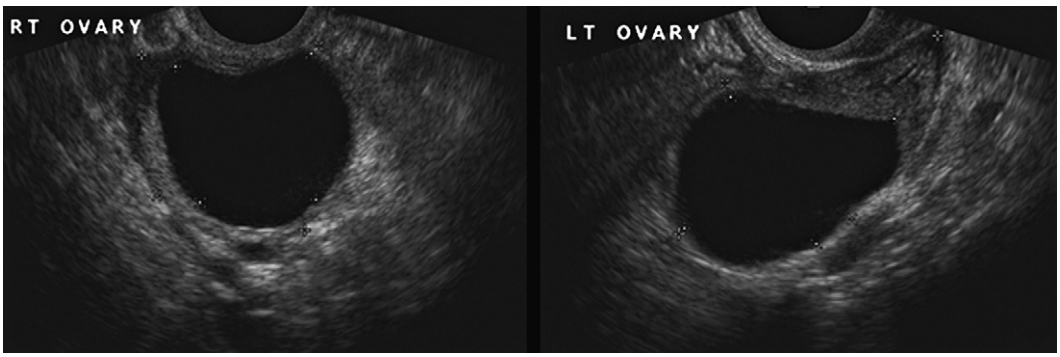

Fig. 12. Postmenopausal cysts. Transvaginal grayscale images of both ovaries demonstrate simple cysts bilaterally in a postmenopausal woman.

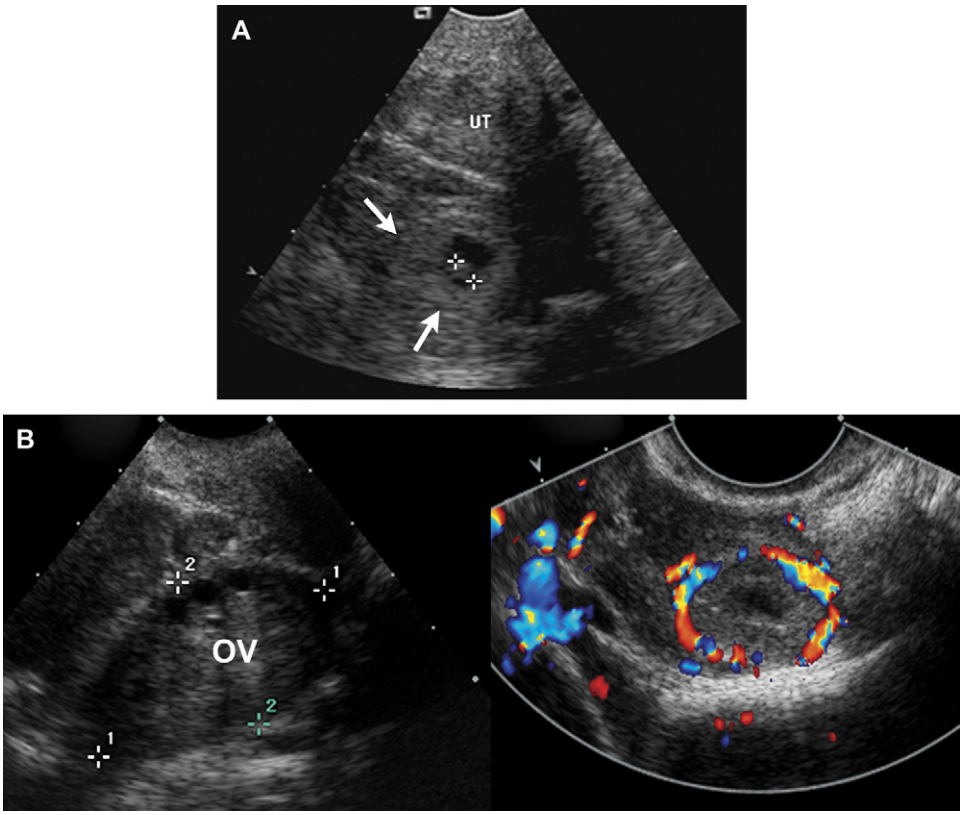

Fig. 13. Ectopic pregnancy. (*A*) Transvaginal grayscale image demonstrates an extraovarian mass with an embryonic pole (*within calipers*) and a tubal ring sign (*arrows*). (*B*) Grayscale and color flow Doppler image demonstrates a nonovarian adnexal mass with tubal ring sign and peripheral vascularity (ring of fire). (OV, ovary.)

endometriosis, making surgical dissection difficult. Residual ovarian tissue under hormone stimulation can become functional and produce pelvic pain, extrinsic compression of the distal ureter, or both. These cysts can be significantly symptomatic despite their small size because of the surrounding adhesions. Seen as complex cystic masses on ultrasonography, the cysts vary from small to relatively large completely cystic or complex masses. A thin rim of ovarian tissue is usually present in the wall of the cyst (Fig. 14) [2,3]. Laparoscopic ultrasonography has been reported to be a useful tool adjunct in laparoscopic surgery for ovarian remnant syndrome.

Serous cystadenoma

Serous cystadenoma is a very common tumor and may mimic a physiologic cyst or, occasionally, an atypical mature cystic teratoma that lacks the characteristic eccentric mural nodule. Serous cystadenomas arise from the surface epithelium of the ovary and are lined by cuboidal epithelium. They constitute 20% of all benign ovarian neoplasms and are usually encountered during the reproductive years. In 7% to 12% of patients, these tumors are bilateral. They are thin walled and uni- or multilocular and range in size from 5 cm to more than 20 cm (Fig. 15). They may have fine septa. The inner lining may be smooth or have areas with grossly visible papillary projections. Color Doppler flow studies obtained from the mural nodule may detect low resistance flow pattern [2–4,44].

Mucinous cystadenoma

Mucinous cystadenoma is a less common, almost always simple or septate, thin-walled multilocular cyst; it may be large (Fig. 16). In many of these tumors, the imaging appearance of the individual loculues may vary as a result of differences in degree of hemorrhage or protein content, often with internal echoes, with compartments differing in echogenicity. Apart from the septa that divide the cavities of the masses into smaller independent compartments, no solid areas are seen [2–4]. The sonographic detection of variable echogenicity in the contents of an adnexal multilocular cyst strongly suggests a mucinous tumor [45]. The difference in the chemical composition of fluids, rather than the difference in viscosity, is responsible for the different sonographic echogenicities. This sign may not appear in all mucinous tumors, because some

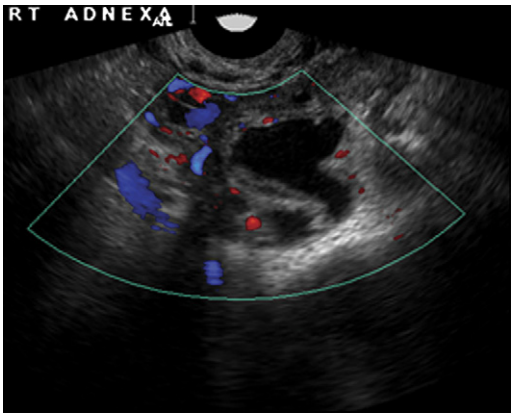

Fig. 14. Ovarian remnant syndrome. Transvaginal color flow Doppler image of right adnexa in a patient with history of oophorectomy demonstrates an ovarian cystic structure with surrounding ovarian tissue secondary to hormone stimulation.

may have small differences in the chemical composition of the contents of the different cavities that are undetectable on sonography [45].

Furthermore, some of the tumors are unilocular and have one type of mucin. Preoperative knowledge of the mucinous nature of the tumor is of crucial importance, because many of these tumors are resected laparoscopically, and spillage may occur. Spillage should be prevented, to avert both the potential spread of cells (in the event tumor turns out to be malignant) and pseudomyxoma peritoneii [4].

Fibromas

Fibromas are the most common benign, solid neoplasms of the ovary. Their malignant potential is low, less than 1%. These tumors compose approximately 5% of benign ovarian neoplasms and approximately 20% of all solid tumors of the ovary. Fibromas occur at all ages but are most frequently seen in middle-aged women.

These tumors are commonly misdiagnosed as exophytic fibroids or primary ovarian malignancy. Meigs' syndrome is the association of an ovarian fibroma, ascites, and hydrothorax. Both the ascites and the hydrothorax resolve after removal of the ovarian tumor [2]. The diameter of a fibroma is important clinically, because the incidence of associated ascites is directly proportional to the size of the tumor. Ascites is present in 10% to 15% of cases of ovarian fibromas greater than 10 cm in diameter. On sonography, fibromas appear as solid, typically hypoechoic masses, but hyperechoic appearance has been reported with attenuation of the acoustic beam. Dense calcifications are known to occur in fibromas, which produce extensive posterior acoustic shadowing. Less than 10% of fibromas have calcifications or small areas of hyaline or cystic degeneration. Bilateral ovarian fibromas are commonly found in women who have rare, genetically transmitted basal cell nevus syndrome.

Malignant adnexal masses

Considerable overlap in morphologic characteristics and corresponding imaging features may prevent definitive preoperative characterization of ovarian masses as benign or malignant. Nonetheless, features suggestive of malignant epithelial tumors include a thick, irregular wall; thick septa; papillary projections; and a large soft tissue component with necrosis (Fig. 17A, B) [4,44]. Calcifications may be present. Solid elements or bilateral tumors [46] suggest malignancy. Ascites form secondary to peritoneal surface implantation

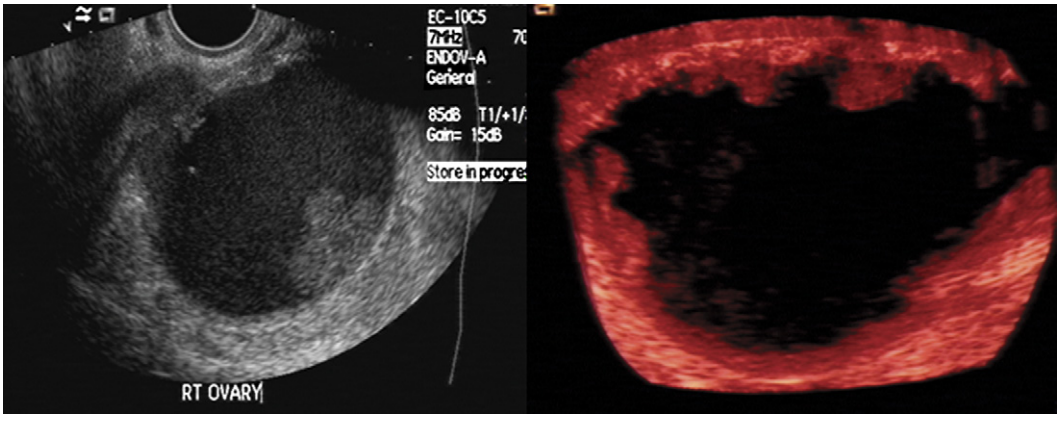

Fig. 15. Surgically confirmed serous cystadenoma. Transvaginal grayscale and corresponding three-dimensional US image of the right ovary demonstrate a complex cystic mass with a mural nodule that shows vascularity on the three-dimensional image.

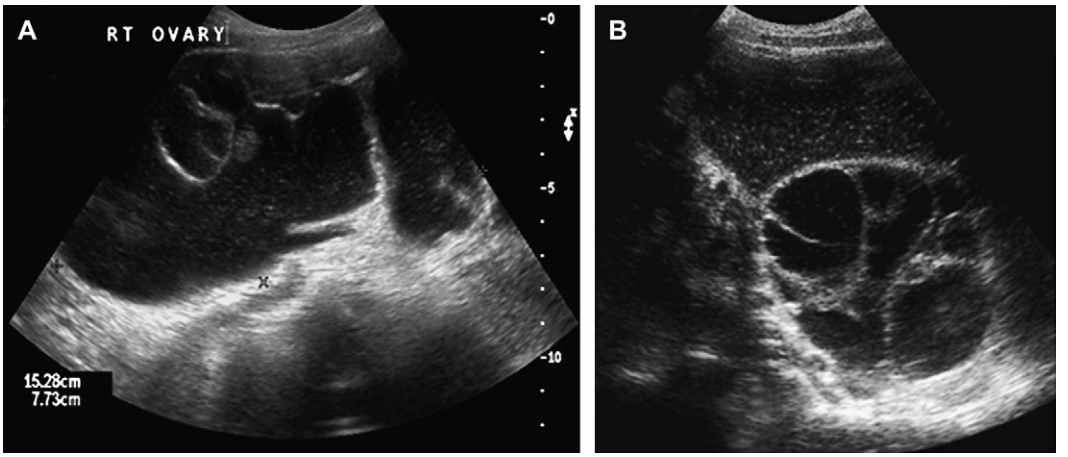

Fig. 16. Surgically confirmed mucinous cystadenoma. *(A, B)* Grayscale images in two different patients demonstrate multiloculated cystic lesion with septations.

(Fig. 17C). The tumor may spread to the lymph nodes (ie, the periaortic, mediastinal, supraclavicular, or peritoneum) (Fig. 17D) [4,47,48].

Other features supporting malignancy include papillary protrusions greater than 2 to 3 mm in thickness. The mass may show solid cystic components with bizarre, irregular vessels, with changing calibers and occasional vascular "lakes" [49]. The presence of a mural nodule is an additional feature supporting the diagnosis of malignancy and may demonstrate internal blood flow on color flow Doppler.

Descriptive morphologic scoring may overcome the subjectivity of interpretation of morphologic characteristics in small masses and, at the same time, may incorporate criteria that prevent simplistic description of a complex mass (Table 1).

With a score of 8 or higher, the likely ratio of malignancy was 3.61, sensitivity was 92%, specificity was 76.9%, and positive predictive value was 25.6%. Thus, sonographic morphologic characteristics could represent a cornerstone of the differential diagnosis of small adnexal masses from their first observation [50]. Approximately 90% of primary ovarian cancers are epithelial tumors, arising from the surface epithelium, and the rest arise from stromal and germ cells [51].

Rulin and Preston [52] analyzed 150 adnexal tumors in women older than 50 and noted 103 benign and 47 malignant tumors. Only one tumor of 32 that was smaller than 5 cm proved to be malignant, whereas 6 of 55 tumors 5 to 10 cm in size and 40 of 63 tumors larger than 10 cm were malignant. The majority of the malignant tumors in this age group were epithelial, and most were greater than 10 cm. The size criteria for malignancy and benignity are based on this study; in a reproductive age group, a tumor smaller than 5 cm is usually benign, and a tumor larger than 5 cm needs further investigation, irrespective of age.

Cystadenocarcinomas

Serous cystadenocarcinoma is the most common malignant tumor seen in all age groups but is rare before age 40. Serous cystadenocarcinomas are bilateral in more than 50% of cases, with peak age of presentation being 70 to 75 years. The typical imaging finding is a large-volume ascites out of proportion to the size of bilateral complex adnexal masses, of irregular shape with polypoid excrescences on the surface. Widespread peritoneal carcinomatosis with omental infiltration by the tumor (so-called "omental caking") is invariably present in cases of serous papillary carcinoma [51].

Mucinous cystadenocarcinoma neoplasms are seen in older patients with a peak age of 75 to 80 years. These tumors manifest as large, unilateral, multiseptated masses with a variable ratio of solid to cystic components. The presence of an enhancing solid component within a multicystic mass is a strong indicator of malignant cause. These tumors may be associated with pseudomyxoma peritoneii (Fig. 18). Pseudomyxoma peritoneii appear as loculated ascites with mass effect; on sonography they appear as hypoechoic fluid with bright punctate echoes [4].

Less common varieties of epithelial tumors are endometrioid, clear cell, Brenner, and undifferentiated carcinoma. These cannot be distinguished sonographically. Endometrioid cancers are usually bilateral mixed solid and cystic masses, which may be associated with endometrial hyperplasia and even concomitant endometrial carcinoma. Clear cell tumor manifests at the younger age of

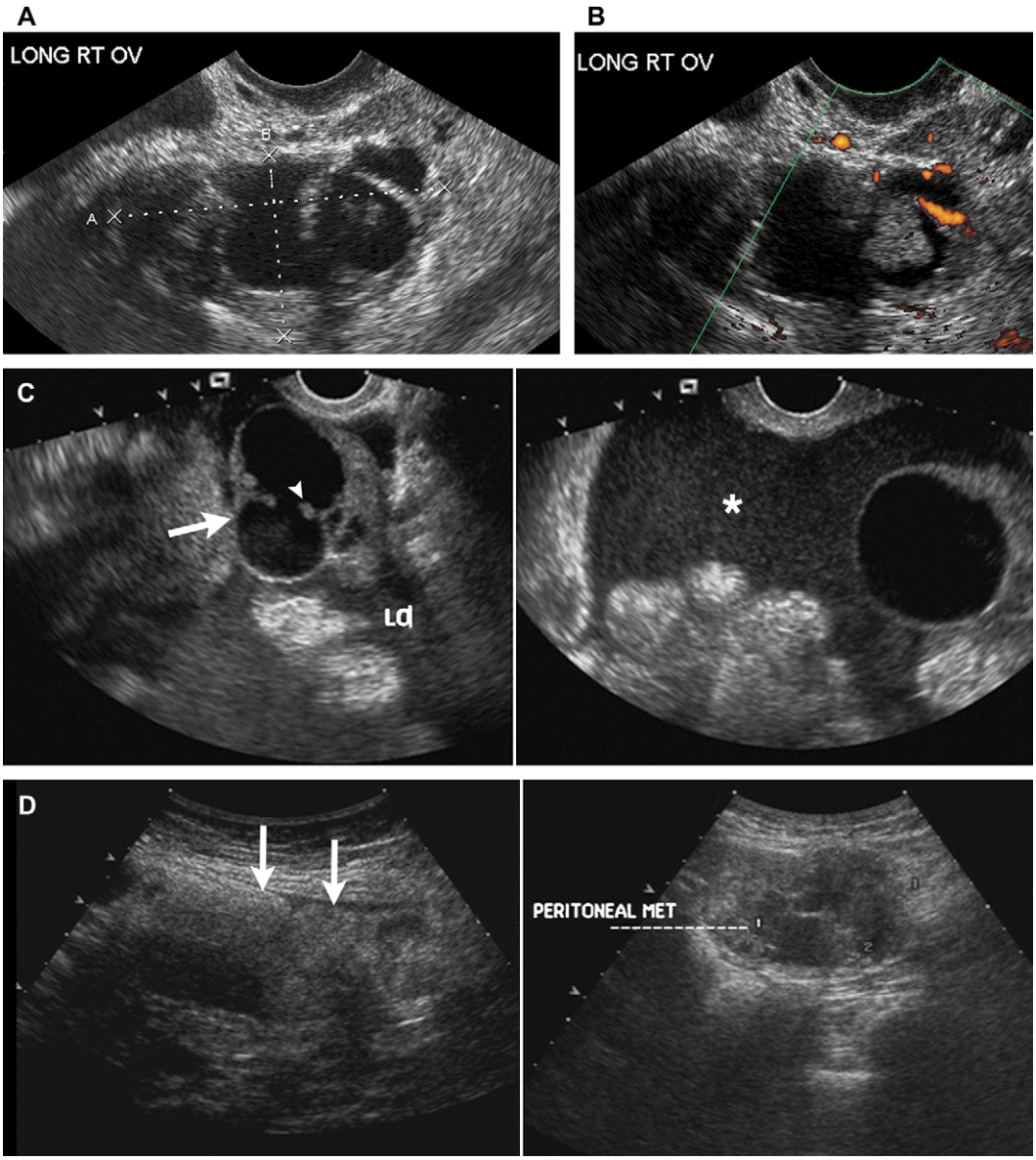

Fig. 17. Malignant adnexal masses. *(A)* Transvaginal grayscale image demonstrates a large right adnexal complex mass with solid and cystic components. *(B)* Corresponding power Doppler image shows increased vascularity within the septae. Spectral Doppler (not shown) confirmed resistive index of less than 0.4, suggesting an ovarian carcinoma. *(C)* Mucinous cystadenocarcinoma. Transvaginal grayscale images of left adnexa demonstrate a cystic left ovarian mass (*arrow*) with mural nodulations (*arrowhead*) and low-level echoes with complex free fluid (*asterisk*), consistent with malignant ascites. *(D)* Omental and peritoneal metastases. Grayscale US of the abdomen demonstrates omental caking (*arrows*) and peritoneal metastasis in a known case of ovarian carcinoma.

55 to 59 years and has the typical appearance of a solitary complex cystic mass with a vascular solid mural nodule. It is associated with endometriosis and occasionally may arise within endometriomas [53,54].

Malignant germ cell tumors include dysgerminoma and endodermal sinus tumors. Dysgerminomas are the most common malignant ovarian germ cell tumor, and they are the female equivalent of testicular seminomas [55]. If diagnosed when less than 10 cm in size, they have a good prognosis for a cure with surgical resection. Dysgerminomas are bilateral in 10% to 20% of cases [56]. These are large, predominantly solid masses that are more common in younger women (second and third decades of life) (Fig. 19). These tumors manifest as

Table 1: **Sonographic morphologic score for adnexal masses**

Score	Capsule	Septa	Papillary excrescences	Echogenicity
1	<3 mm	Absent	Absent	Anechoic
2	>3 mm	Thin (≤3 mm)	…	Low echogenicity/ ground glass
3	…	Thick (>3 mm)	…	…
4	Irregular, solid	…	<3 mm	With solid areas
5	Irregular, not applicable	…	<3 mm	Inhomogeneous, solid

Data from Ferrazzi E, Lissoni AA, Dordoni D, et al. Differentiation of small adnexal masses based on morphologic characteristics of transvaginal sonographic imaging: a multicenter study. J Ultrasound Med 2005;24:1469.

a large, solid, round, oval or lobulated, slightly glistening fibrous capsule and can be as large as 50 cm. Calcification may be present in a speckled pattern. Characteristic imaging findings include multilobulated solid masses with prominent fibrovascular septa [2,3]. Patients treated conservatively should be closely followed with periodic pelvic US or CT imaging evaluations, or both. Occasionally the serum lactic dehydrogenase is elevated as a nonspecific tumor marker [57].

Ovarian metastasis

Approximately 5% to 30% of malignant ovarian tumors are metastatic in origin. The ovary is a common site of tumor metastasis from the bowel (Krukenberg tumor) (Fig. 20), breast, and endometrium, as well as from melanoma and lymphoma. The most common gastrointestinal tract origin for these tumors is the stomach, and the next most frequent is the large intestine. At least 80% of Krukenberg tumors are bilateral.

Metastatic disease to the ovaries is often associated with ascites. Metastatic lesions are usually solid or have a "moth-eaten" cystic pattern. The presence of a purely solid tumor indicates a higher probability of metastatic carcinoma than of primary ovarian cancer. However, with the use of grayscale and color Doppler sonography, it is difficult to differentiate primary ovarian carcinomas from metastatic tumors to the ovary [58]. Metastases are frequently bilateral and, at imaging, they range from solid enhancing lesions with different degrees of necrosis to complex cystic masses of various sizes. Although multilocularity at US or MR imaging favors the diagnosis of primary rather than secondary neoplasm, accurate distinction between primary and secondary ovarian tumor is difficult [59].

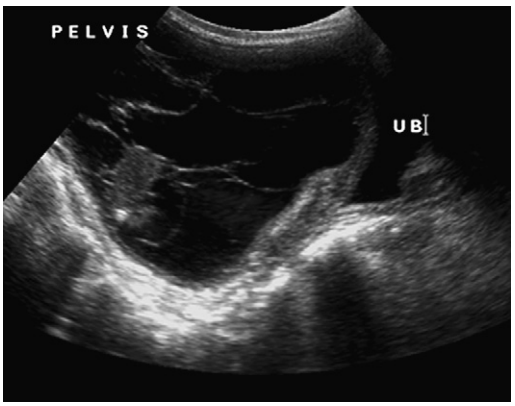

Fig. 18. Pseudomyxoma peritoneii. Transabdominal grayscale image of the pelvis in a known case of mucinous cystadenocarcinoma demonstrates presence of loculated ascites. (UB, urinary bladder.)

Other (nongynecologic) pelvic masses

Not all pelvic masses are gynecologic in origin: others include postoperative masses such as abscesses, hematomas, lymphoceles, urinomas, seromas, and postpartum complications (Fig. 21). Bladder flap hematoma is a common complication following cesarean section. It may be diagnosed sonographically as a complex or anechoic mass located adjacent to the scar and between the lower uterine segment and posterior bladder wall; echogenicity varies depending on the degree of organization within the hematoma. Presence of air inside is highly suggestive of an infected hematoma. Subfascial hematomas are extraperitoneal in location, contained within the prevesical space and caused by disruption of the inferior epigastric vessels or their branches during cesarean section or traumatic vaginal delivery. Sonographically, a complex or cystic mass is seen anterior to the bladder, although CT is the initial imaging modality of choice for

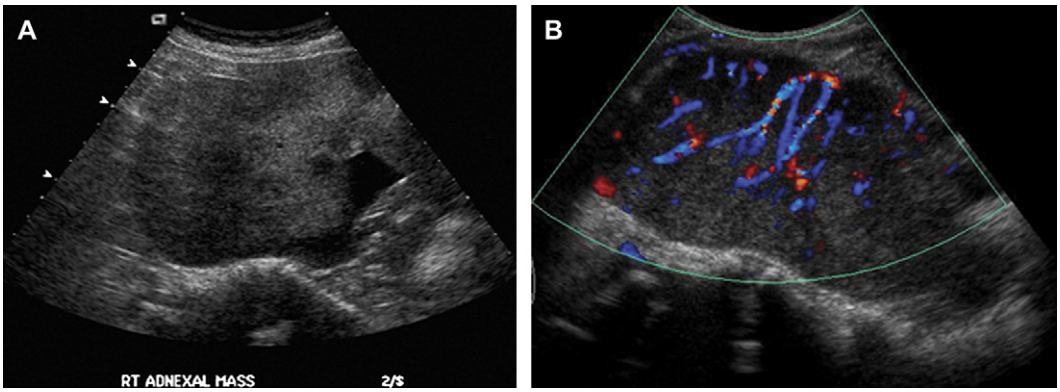

Fig. 19. Dysgerminoma. Grayscale *(A)* and color flow Doppler *(B)* images of the right ovary demonstrate a solid mass with increased vascularity.

postoperative complications such as pelvic abscess and hematoma. Uterine perforation may result from dilatation and curettage or occur after delivery and may appear as an enhancing parametrial fluid collection and discontinuity of the uterus [3].

Adnexal masses in pregnancy

Occasionally an adnexal mass, such as an ovarian or parovarian cyst or a dermoid, may be coexistent in a gravid woman. US features of an ovarian cyst or a dermoid may occasionally be seen with the pregnancy.

Mimics of an adnexal mass

Subserosal leiomyomas are the exophytic fibroids that protrude from the outer surface of the uterus. Leiomyomas create a uterine contour abnormality and may mimic an adnexal mass (Fig. 22) [41]. Leiomyomas usually demonstrate a peripheral rim of vascularity in the pseudocapsule (covering almost three fourths of the circumference); this feature aids in the identification of isoechoic intramural myomas and the diagnosis of subserosal myomas.

The presence of multiple vessels between the uterus and the presumed adnexal mass is called the vascular bridging sign (VBS). Demonstration of a VBS or a vascular pedicle between the uterus and the periuterine mass helps one to differentiate a subserosal leiomyoma from a true adnexal mass [41]. The VBS is secondary to recruitment of multiple vessels feeding the exophytic uterine fibroid and confirms the origin of the vascular blood supply in uterine fibroids from the uterine arteries, implying that the tissue is uterine, not ovarian. Color flow Doppler may also demonstrate a solitary vessel originating from the uterine artery that supplies the subserosal leiomyoma, called the vascular pedicle sign. Demonstration of a common source of blood for the mass and the uterus implies the mass originates in the uterus [41].

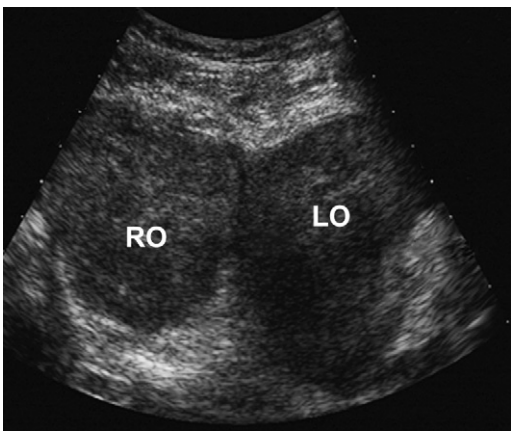

Fig. 20. Krukenberg tumors. Grayscale US image of the pelvis demonstrates bilateral solid ovarian tumors in a known case of stomach cancer. (LO, left ovary; RO, right ovary.)

Role of three-dimensional ultrasound

Three-dimensional ultrasound (3D US) and real-time 3D US are increasingly used to understand spatial relations and vascular morphology. The qualitative and quantitative assessment of sonographic volume data is now possible with the use of several analysis tools, such as multiplanar imaging, surface and volume rendering, and semiautomated volume calculation using a technique known as virtual organ computer-aided analysis [60]. Virtual organ aided analysis overcomes some limitations of conventional two-dimensional sonography, allowing a more detailed assessment of morphologic features of the object studied, with no restriction on the number and orientation of the scanning planes [61].

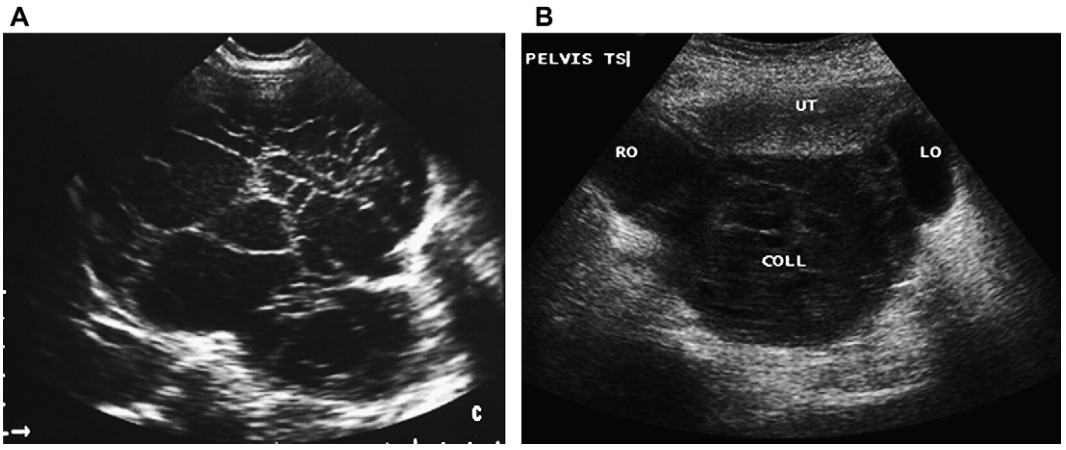

Fig. 21. Nongynecologic pelvic masses. *(A)* Lymphocele. Grayscale image of the pelvis demonstrates a complex septated fluid collection. *(B)* Postpartum collection. Grayscale image of the pelvis demonstrates a complex collection (coll) in the cul-de-sac, consistent with hemorrhage. (LO, left ovary; RO, right ovary; UT, uterus.)

3D US is particularly superior for (1) evaluating for papillary projections, (2) showing characteristics of cystic walls, (3) identifying the extent of capsular infiltration of tumors, and (4) calculating ovarian volume (Fig. 23A). 3D US may also be used to assess the location of masses in relation to normal ovarian tissue [62]. It assists in identification of tumor vascularity and tumor angiogenesis, thereby distinguishing between normal and tumor vessels in benign and malignant tumors. Precise evaluation of tumor morphology and vascular patterns is obtained without a significant increase in scan times. The 3D approach allows visualization of multiple overlapping tumor vessels, the vascular network, and the relationship of the mass to the vessels (Fig. 23B) [63,64].

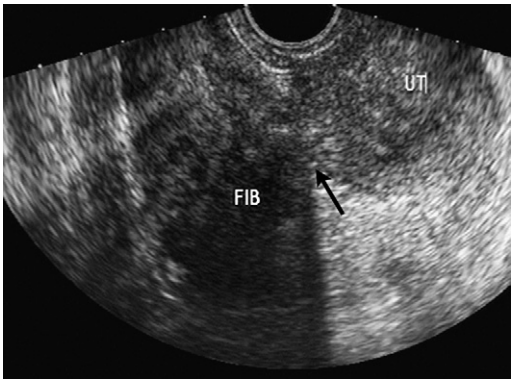

Fig. 22. Subserosal fibroid. Transvaginal grayscale US image of the pelvis demonstrates a large solid adnexal lesion (Fib) arising from the uterus (*arrow*). (UT, uterus.)

Role of color flow Doppler

Doppler examination should be performed when any abnormality of the ovary is detected. In cysts, color Doppler is helpful in differentiating an echo-free potential cyst from adjacent vascular structures. Using "color as morphology" and understanding its meaning can support a diagnosis or rule out the structure as benign (eg, the lack of color signals in benign cystic teratomas, simple cysts, or endometriomas) or as physiologic (eg, the characteristic "ring of fire" of a CL) (see Fig. 2B).

Color may also be used to localize flow for pulsed Doppler, which should be obtained on all ovarian masses. Pulsed Doppler of the adnexal branch of the uterine artery, the ovarian artery, or intratumoral flow is performed to determine the RI or pulsatility index (PI). Patients who have normal menstrual cycles are best scanned in the first 10 days of the cycle to avoid confusion with normal changes in intraovarian blood flow, because high diastolic flow occurs in luteal phase around the CL.

A debate exists in the literature regarding the value of the RI in distinguishing between benign and malignant adnexal masses. The largest study in the literature uses a cut-off point of greater than 0.4 as a normal RI in a nonfunctioning ovary; others describe a PI of greater than 1 as normal. Intratumoral vessels, low-resistance flow, and absence of a normal diastolic notch in the Doppler waveform are all worrisome signs for malignancy; however, abnormal waveforms can be seen in inflammatory masses, in metabolically active masses (including ectopic pregnancy), and in corpus luteum. The most significant problem with the use of RI is that it is not a sensitive indicator

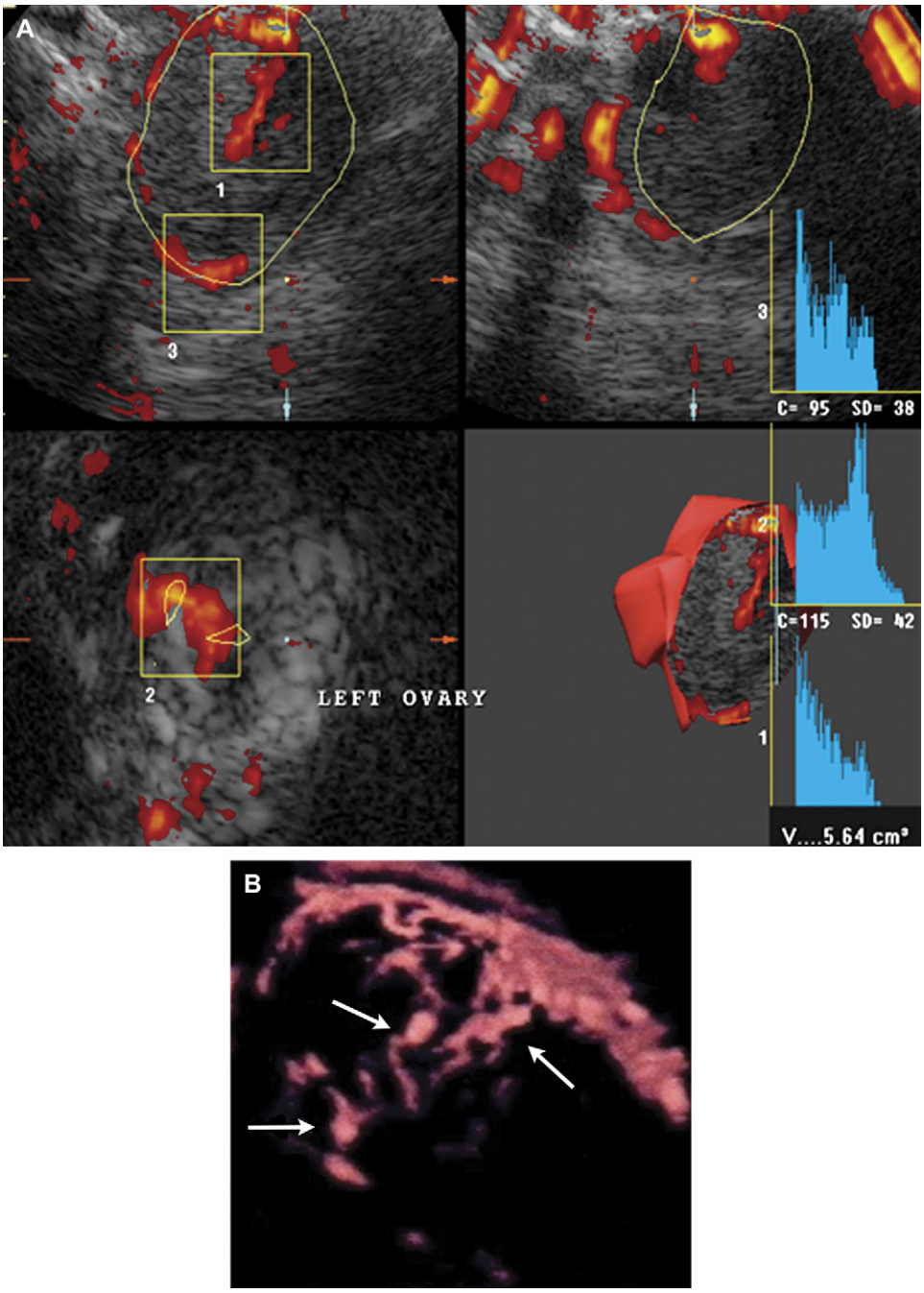

Fig. 23. 3D US. *(A)* Multiple 3D US images of the left ovary being used to calculate the ovarian volume. *(B)* 3D US also helps better to demonstrate the tumor vascularity (*arrows*).

of malignancy: a low RI is seen in only 25% of malignant lesions.

When a large number of erratic vessels with changing calibers, unusual anastomoses, and vascular lakes are seen entering an adnexal structure with centrally located flow within the mass, regardless of the RI, these findings may be considered highly suggestive of malignancy. The same may be said of the detection of blood vessels in papillae. If the papillary protrusions show blood flow, are 3 mm or larger, and are observed to be numerous, these findings should also raise the possibility of malignancy. On color Doppler, tumors tend to have vessels with low impedance, because of the lack of

muscular media in the vessel wall and arteriovenous shunts, and the vessels tend to be clustered [41,65–68].

Power Doppler imaging

Though spectral Doppler sonography and color Doppler US have been used successfully in the evaluation of adnexal tumor vascularity, they have inherent limitations, such as lack of sensitivity to slow flow, angle dependency, and aliasing. Further contributors to the confusion are a nonuniversal selection of Doppler parameters (RI or PI), the choice of highest, lowest, or mean impedance values, and the selection of vessels for investigations, together with operator variance and system sensitivity.

Power Doppler improves visualization of intratumoral vascularity, which may aid in detection of malignant adnexal tumors. Tumor vasculature consists of vessels recruited from the pre-existing network of host vasculature and vessels grown from the host vessels under the influence of the angiogenic factors. The organization of this tumor vasculature is completely different from that of the host vasculature, depending on the tumor's type, growth rate, and location. The architecture differs among various tumor types and also between the primary tumor and its transplants. It is possible with three-dimensional power Doppler to visualize vessel continuity more completely (in three orthogonal projections) and to demonstrate vessel branching more clearly (three-dimensional vascular reconstruction) (Fig. 24).

Physiologic angiogenesis is seen in folliculogenesis, embryogenesis, and implantation and in some benign neoplasms. The mesovarium vessels entering the hilum can be depicted as extending gradually to the stroma with increasing numbers and branches of fine vessels during the preovulatory phase. After ovulation, luteal cyst formation may be seen. The luteal vessels are usually fewer and seldom have complicated branching patterns or encircle the cyst, in contrast to the findings in malignant neoplasms. In endometriotic cysts, the vessels are usually straight and regularly branching; they generally emerge from a hilar vessel and run along the surface of a tumor.

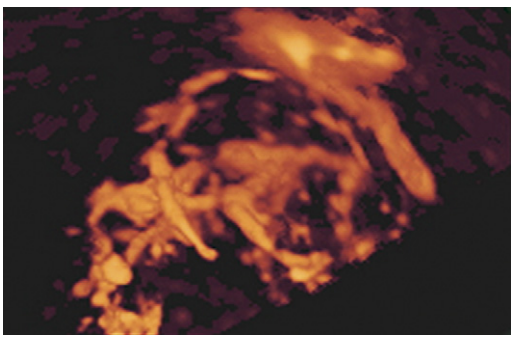

Fig. 24. Three-dimensional power Doppler. Three-dimensional reconstruction of power Doppler image of the ovarian mass demonstrates better vascular continuity and branching.

Tumor vasculature consists of vessels recruited from a pre-existing network of vasculature and vessels produced by neoangiogenesis under the influence of angiogenic factors produced by tumor cells. Within a tumor, variable territories exhibiting one or the other type of vascular pattern may be visualized on color Doppler studies. Tumor vascularity can be differentiated from a normal vascular network by certain characteristics. These include a single elongated and coiled branch, variable in caliber, a nonhierarchical vascular network, absence of normal precapillary architecture with dichotomous branching, absence of decrease in diameter of the higher-order branches, and an incomplete vascular wall with multiple breaks in the endothelial lining and basement membrane. Tumor vessels may also appear tortuous or saccular and may contain tumor cells within these walls. Tumor blood flow is commonly associated with anomalous veno–veno communications and arteriovenous shunts [49,69].

Quantitated color Doppler sonography

Progressive improvement and development of the technology has led to three-dimensional quantification of blood flow using three-dimensional color histograms that measure the color percentage and flow amplitudes in the region of interest [70]. Quantitative sonographic criteria for tumor vascularity analyzed include the vascularity index (VI) (which quantifies the difference between the total number of pixels and the number of pixels containing no color divided by the total $\times$ 100) and the power-weighted pixel density (PWPD), which weights the strength of the signal divided by the total. With a VI of greater than 2.3, a sensitivity of 75% and specificity of 90% were obtained for malignancies. When this was combined with a PWPD of greater than 4555, sensitivity improved to 88% and specificity improved to 93%—as compared with morphologic analysis, which had a sensitivity of 72% and specificity of 76% for malignancies [71]. Additional indices such as flow index (FI) and vascularization flow index are being studied to provide the insight needed to differentiate benign from malignant adnexal masses. VI and FI are suspected to be reliable predictors for tumoral neoangiogenesis. This method has been found helpful in distinguishing benign from malignant ovarian masses [70].

Box 1: Key points of adnexal masses

- The majority of adnexal masses in women in the reproductive years are follicle cysts of the ovary.
- The most common benign neoplastic tumors of the ovary are serous cystadenoma and benign cysts.
- The most common benign cystic neoplasms of the ovary in the 20- to 44-year-old group are benign cystic teratoma, serous cystadenoma, and mucinous cystadenoma.
- Most benign cystic teratomas are 10 cm or less in diameter, but about one sixth are larger.
- Serous cystadenocarcinoma is the most common malignant tumor in all age groups, from 20 to 75 years old.
- Dysgerminoma and teratoma are the most common solid adnexal tumors in young women.
- Of women in the reproductive years, 30% develop myoma of the uterus. By age 50, 40% will have developed myomas.
- A total of 95% of all endometriosis occurs in women in the reproductive years.
- Of 150 adnexal tumors in women older than 50, 103 were benign. Of the malignant tumors in this age group, most were epithelial tumors. Tumors less than 5 cm were usually benign, but 40 of 63 tumors larger than 10 cm were malignant.

Data from Stenchever MA, Droegemueller W, Herbst AL, et al. Comprehensive gynecology. 4th edition. Saint Louis: Mosby; 2001.

Contrast-enhanced, three-dimensional power Doppler

Use of US contrast agents may aid in distinguishing benign from malignant ovarian masses. Intravascular sonographic contrast agents enhance depiction of tumor vessels by providing a stronger Doppler signal [72]. Contrast agents may improve the diagnostic ability of sonography to identify early microvascular changes that are known to be associated with early-stage ovarian cancer, but only a few small published studies have used contrast agents for gynecologic purposes. Use of a contrast agent makes it possible to gain a more accurate map of the vascular anatomy by enhancing the signal strength from power Doppler sonography, increasing the number of large vessels and allowing recruitment of small vessels [73–75]. Tumors have a longer wash-out time, perhaps a reflection of the presence of tumor angiogenesis.

The vascular distribution in adnexal masses may be classified into three patterns using three-dimensional power Doppler US: pattern 0, no signal pattern (no detectable vessels); pattern 1, peripheral pattern (blood vessels are peripheral and surround the lesion); pattern 2, penetrating pattern (blood vessels arise outside the lesion and course toward its center); and pattern 3, mixed penetrating and peripheral pattern. The pattern of irregularly branching penetrating vessels in an adnexal mass, with or without contrast enhancement, is an important factor in predicting the likelihood of malignancy. The use of a US contrast agent with three-dimensional power Doppler sonography increases the diagnostic efficiency of nonenhanced three-dimensional power Doppler sonography from 86.7% to 95.6% [69].

Summary

Transabdominal sonography combined with high-frequency endovaginal US is considered the community standard for the performance of pelvic US for evaluation of an adnexal mass [36,46,76]. Subjective evaluation of ovarian masses based on pattern recognition can achieve a sensitivity of 88% to 100% and specificity of 62% to 96%. Addition of color and power Doppler to grayscale imagingfor pelvic mass evaluation increases the specificity in the range of 82% to 97% and increases the positive predictive value to 63% to 91% [4], aiding in subsequent evaluation and management [5]. Pelvic sonography can confidently diagnose most of the benign adnexal masses and helps with triage of patients for surgical management in collaboration with tumor markers. The key points of adnexal masses are presented in Box 1 [77].

Acknowledgments

The authors are extremely thankful to Vikram Dogra, MD, and Shweta Bhatt, MD, for their editorial advice and assistance in preparation of this manuscript. They would also like to express their sincere thanks to Dr. Ashok Khurana, MD, for his contribution.

References

[1] Timor-Tritsch IE, Goldstein SR. The complexity of a "complex mass" and the simplicity of a "simple cyst." J Ultrasound Med 2005;24:255–8.
[2] Dill-Macky MJ, Atri M. Ovarian sonography. 4th edition. Philadelphia: W.B.Saunders; 2000.
[3] Salem S, Wilson SR. Gynecologic ultrasound. 3rd edition. St. Louis (MO): Mosby; 2005.
[4] Arger PH. Asymptomatic palpable adnexal masses. New York: Thieme; 2000.
[5] Valentin L. Use of morphology to characterize and manage common adnexal masses. Best Pract Res Clin Obstet Gynaecol 2004;18:71–89.

[6] de Kroon CD, van der Sandt HA, van Houwelingen JC, et al. Sonographic assessment of non-malignant ovarian cysts: does sonohistology exist? Hum Reprod 2004;19:2138–43.
[7] Webb EM, Green GE, Scoutt LM. Adnexal mass with pelvic pain. Radiol Clin North Am 2004; 42:329–48.
[8] Durfee SM, Frates MC. Sonographic spectrum of the corpus luteum in early pregnancy: gray-scale, color, and pulsed Doppler appearance. J Clin Ultrasound 1999;27:55–9.
[9] Pellerito JS. Acute pelvic pain. New York: Thieme; 2000.
[10] Nemoto Y, Ishihara K, Sekiya T, et al. Ultrasonographic and clinical appearance of hemorrhagic ovarian cyst diagnosed by transvaginal scan. J Nippon Med Sch 2003;70:243–9.
[11] Swire MN, Castro-Aragon I, Levine D. Various sonographic appearances of the hemorrhagic corpus luteum cyst. Ultrasound Q 2004;20: 45–58.
[12] Bhatt S, Kocakoc E, Dogra VS. Endometriosis: sonographic spectrum. Ultrasound Q 2006;22: 273–80.
[13] Jain KA. Sonographic spectrum of hemorrhagic ovarian cysts. J Ultrasound Med 2002;21:879–86.
[14] Okai T, Kobayashi K, Ryo E, et al. Transvaginal sonographic appearance of hemorrhagic functional ovarian cysts and their spontaneous regression. Int J Gynaecol Obstet 1994;44:47–52.
[15] Montz FJ, Schlaerth JB, Morrow CP. The natural history of theca lutein cysts. Obstet Gynecol 1988;72:247–51.
[16] Patel MD, Feldstein VA, Chen DC, et al. Endometriomas: diagnostic performance of US. Radiology 1999;210:739–45.
[17] Alcazar JL, Laparte C, Jurado M, et al. The role of transvaginal ultrasonography combined with color velocity imaging and pulsed Doppler in the diagnosis of endometrioma. Fertil Steril 1997;67:487–91.
[18] Ghezzi F, Raio L, Cromi A, et al. "Kissing ovaries": a sonographic sign of moderate to severe endometriosis. Fertil Steril 2005;83:143–7.
[19] Woodward PJ, Sohaey R, Mezzetti TP Jr. Endometriosis: radiologic–pathologic correlation. Radiographics 2001;21:193–216 [questionnaire: 288–94].
[20] Tessler FN, Perrella RR, Fleischer AC, et al. Endovaginal sonographic diagnosis of dilated fallopian tubes. AJR Am J Roentgenol 1989;153:523–5.
[21] Timor-Tritsch IE, Lerner JP, Monteagudo A, et al. Transvaginal sonographic markers of tubal inflammatory disease. Ultrasound Obstet Gynecol 1998;12:56–66.
[22] Patel MD. Practical approach to the adnexal mass. Ultrasound Clinics 2006;1:335–56.
[23] Horrow MM. Ultrasound of pelvic inflammatory disease. Ultrasound Q 2004;20:171–9.
[24] Outwater EK, Siegelman ES, Hunt JL. Ovarian teratomas: tumor types and imaging characteristics. Radiographics 2001;21:475–90.
[25] Mais V, Guerriero S, Ajossa S, et al. Transvaginal ultrasonography in the diagnosis of cystic teratoma. Obstet Gynecol 1995;85:48–52.
[26] Tongsong T, Wanapirak C, Khunamornpong S, et al. Numerous intracystic floating balls as a sonographic feature of benign cystic teratoma: report of 5 cases. J Ultrasound Med 2006;25: 1587–91.
[27] Rha SE, Byun JY, Jung SE, et al. CT and MR imaging features of adnexal torsion. Radiographics 2002;22:283–94.
[28] Sohaey R, Gardner TL, Woodward PJ, et al. Sonographic diagnosis of peritoneal inclusion cysts. J Ultrasound Med 1995;14:913–7.
[29] Jain KA. Imaging of peritoneal inclusion cysts. AJR Am J Roentgenol 2000;174:1559–63.
[30] Dolz M, Osborne NG, Blanes J, et al. Polycystic ovarian syndrome: assessment with color Doppler angiography and three-dimensional ultrasonography. J Ultrasound Med 1999;18:303–13.
[31] Ginsburg J, Havard CW. Polycystic ovary syndrome. Br Med J 1976;2:737–40.
[32] Hann LE, Hall DA, McArdle CR, et al. Polycystic ovarian disease: sonographic spectrum. Radiology 1984;150:531–4.
[33] Parisi L, Tramonti M, Derchi LE, et al. Polycystic ovarian disease: ultrasonic evaluation and correlations with clinical and hormonal data. J Clin Ultrasound 1984;12:21–6.
[34] Yeh HC, Futterweit W, Thornton JC. Polycystic ovarian disease: US features in 104 patients. Radiology 1987;163:111–6.
[35] Adams J, Franks S, Polson DW, et al. Multifollicular ovaries: clinical and endocrine features and response to pulsatile gonadotropin releasing hormone. Lancet 1985;2:1375–9.
[36] Fox R, Corrigan E, Thomas PA, et al. The diagnosis of polycystic ovaries in women with oligoamenorrhoea: predictive power of endocrine tests. Clin Endocrinol (Oxf) 1991;34:127–31.
[37] Pache TD, Wladimiroff JW, Hop WC, et al. How to discriminate between normal and polycystic ovaries: transvaginal US study. Radiology 1992; 183:421–3.
[38] Wolf SI, Gosink BB, Feldesman MR, et al. Prevalence of simple adnexal cysts in postmenopausal women. Radiology 1991;180:65–71.
[39] Khurana A, Jha U. Ultrasound for pelvic assessment in menopausal women. New Delhi (India): Jaypee brothers; 2004.
[40] Brown DL, Doubilet PM. Transvaginal sonography for diagnosing ectopic pregnancy: positivity criteria and performance characteristics. J Ultrasound Med 1994;13:259–66.
[41] Bhatt S, Dogra V. Doppler imaging of the uterus and adnexae. Ultrasound Clinics 2006;1:201–21.
[42] Levine D. Ectopic pregnancy. 4th edition. Philadelphia: W.B.Saunders; 2000.
[43] Russell SA, Filly RA, Damato N. Sonographic diagnosis of ectopic pregnancy with endovaginal probes: what really has changed? J Ultrasound Med 1993;12:145–51.

[44] Fried AM. Family history of ovarian carcinoma. New York: Thieme; 2000.
[45] Caspi B, Hagay Z, Appelman Z. Variable echogenicity as a sonographic sign in the preoperative diagnosis of ovarian mucinous tumors. J Ultrasound Med 2006;25:1583–5.
[46] Lee SI. Radiological reasoning: imaging characterization of bilateral adnexal masses. AJR Am J Roentgenol 2006;187:S460–6.
[47] Jeong YY, Outwater EK, Kang HK. Imaging evaluation of ovarian masses. Radiographics 2000; 20:1445–70.
[48] Woodward PJ, Hosseinzadeh K, Saenger JS. From the archives of the AFIP: radiologic staging of ovarian carcinoma with pathologic correlation. Radiographics 2004;24:225–46.
[49] Kurjak A, Kupesic S, Breyer B. The assessment of ovarian tumor angiogenesis by three dimensional power Doppler. New York: Parthenon publishing; 2000.
[50] Ferrazzi E, Lissoni AA, Dordoni D, et al. Differentiation of small adnexal masses based on morphologic characteristics of transvaginal sonographic imaging: a multicenter study. J Ultrasound Med 2005;24:1467–73 [quiz: 1475–6].
[51] Mironov S, Akin O, Pandit-Taskar N, et al. Ovarian cancer. Radiol Clin North Am 2007;45:149–66.
[52] Rulin MC, Preston AL. Adnexal masses in postmenopausal women. Obstet Gynecol 1987;70: 578–81.
[53] Green GE, Mortele KJ, Glickman JN, et al. Brenner tumors of the ovary: sonographic and computed tomographic imaging features. J Ultrasound Med 2006;25:1245–51 [quiz: 1252–4].
[54] Wu TT, Coakley FV, Qayyum A, et al. Magnetic resonance imaging of ovarian cancer arising in endometriomas. J Comput Assist Tomogr 2004; 28:836–8.
[55] Stepanian M, Cohn DE. Gynecologic malignancies in adolescents. Adolesc Med Clin 2004;15: 549–68.
[56] Chen VW, Ruiz B, Killeen JL, et al. Pathology and classification of ovarian tumors. Cancer 2003;97: 2631–42.
[57] Schwartz PE, Morris JM. Serum lactic dehydrogenase: a tumor marker for dysgerminoma. Obstet Gynecol 1988;72:511–5.
[58] Alcazar JL, Galan MJ, Ceamanos C, et al. Transvaginal gray scale and color Doppler sonography in primary ovarian cancer and metastatic tumors to the ovary. J Ultrasound Med 2003;22:243–7.
[59] Brown DL, Zou KH, Tempany CM, et al. Primary versus secondary ovarian malignancy: imaging findings of adnexal masses in the Radiology Diagnostic Oncology Group Study. Radiology 2001;219:213–8.
[60] Benacerraf BR, Benson CB, Abuhamad AZ, et al. Three- and 4-dimensional ultrasound in obstetrics and gynecology: Proceedings of the American Institute of Ultrasound in Medicine Consensus Conference. J Ultrasound Med 2005; 24:1587–97.
[61] Alcazar JL, Galan MJ, Garcia-Manero M, et al. Three-dimensional sonographic morphologic assessment in complex adnexal masses: preliminary experience. J Ultrasound Med 2003;22:249–54.
[62] Pretorius DH, Nelson TR, Lev-Toaff AS. Three dimensional ultrasound in obstetrics and gynecology. 4th edition. Philadelphia: W.B.Saunders; 2000.
[63] Downey DB, Fenster A. Vascular imaging with a three-dimensional power Doppler system. AJR Am J Roentgenol 1995;165:665–8.
[64] Kurjak A, Kupesic S, Sparac V, et al. Three-dimensional ultrasonographic and power Doppler characterization of ovarian lesions. Ultrasound Obstet Gynecol 2000;16:365–71.
[65] Alcazar JL, Ruiz-Perez ML, Errasti T. Transvaginal color Doppler sonography in adnexal masses: which parameter performs best? Ultrasound Obstet Gynecol 1996;8:114–9.
[66] Timor-Tritsch LE, Lerner JP, Monteagudo A, et al. Transvaginal ultrasonographic characterization of ovarian masses by means of color flow–directed Doppler measurements and a morphologic scoring system. Am J Obstet Gynecol 1993;168:909–13.
[67] Valentin L, Sladkevicius P, Marsal K. Limited contribution of Doppler velocimetry to the differential diagnosis of extrauterine pelvic tumors. Obstet Gynecol 1994;83:425–33.
[68] Zanetta G, Vergani P, Lissoni A. Color Doppler ultrasound in the preoperative assessment of adnexal masses. Acta Obstet Gynecol Scand 1994; 73:637–41.
[69] Kupesic S, Kurjak A. Contrast-enhanced, three-dimensional power Doppler sonography for differentiation of adnexal masses. Obstet Gynecol 2000;96:452–8.
[70] Pairleitner H. Three dimensional color histogram using three dimensional power Doppler. New York: Parthenon publishing; 2000.
[71] Wilson WD, Valet AS, Andreotti RF, et al. Sonographic quantification of ovarian tumor vascularity. J Ultrasound Med 2006;25:1577–81.
[72] Deng CX. Contrast agents for ultrasound imaging. In: Dogra V, Rubens DJ, editors. Ultrasound secrets. Philadelphia: Hanley & Belfus; 2004. p. 23–9.
[73] Abramowicz JS. Ultrasonographic contrast media: has the time come in obstetrics and gynecology? J Ultrasound Med 2005;24:517–31.
[74] Orden MR, Jurvelin JS, Kirkinen PP. Kinetics of a US contrast agent in benign and malignant adnexal tumors. Radiology 2003;226:405–10.
[75] Marret H, Tranquart F, Sauget S, et al. Sonographic diagnosis of ovarian tumors: pre-operative Doppler evaluation. J Radiol 2003;84:1725–31.
[76] Fogata ML, Jain KA. Degenerating cystic uterine fibroid mimics an ovarian cyst in a pregnant patient. J Ultrasound Med 2006;25:671–4.
[77] Pelvic and lower abdominal masses. In: Stenchever MS, Droegemueller W, Herbst A, et al, editors. Comprehensive gynecology. 4th edition. Saint Loius: Mosby, Inc; 2001. p. 70–2.

ELSEVIER SAUNDERS

ULTRASOUND CLINICS

Ultrasound Clin 2 (2007) 155–166

The Sonographic Diagnosis of Ovarian Torsion: Pearls and Pitfalls

Rochelle F. Andreotti, MD*, Libby L. Shadinger, MD, Arthur C. Fleischer, MD

Adnexal torsion is the fifth most common gynecologic emergency, with a reported incidence of 3% in some series, primarily affecting women of reproductive age or younger [1,2]. This process involves twisting of the ovary, the fallopian tube, or both structures, causing vascular compromise with resulting ovarian edema and eventual necrosis. Torsion may be partial or complete, and acute or chronic. Not infrequently, torsion is intermittent with periods of spontaneous remission of symptoms. Although the most consistent presenting symptom is abdominal and pelvic pain, the diagnosis of torsion is complicated by its vague clinical presentation. Early diagnosis and intervention before infarction may not only permit ovarian preservation but also prevent the life-threatening complications of peritonitis.

Sonography has been the modality of choice for imaging evaluation of lower abdominal and pelvic pain, because it is noninvasive, radiation free, cost-effective, and widely available, as well as having the ability accurately to delineate uterine and ovarian architecture and assess vascular flow. However, there may be patients in whom the sonographic findings are subtle or not straightforward. This article endeavors to provide an imaging approach to the diagnosis of ovarian torsion that will avoid the pitfalls often encountered and improve the identification of this often elusive condition.

Background

To understand the variable sonographic findings in ovarian torsion, one should be aware of the blood supply to the ovary and tube (Fig. 1). The ovary is chiefly supplied by the ovarian artery, a branch of the hypogastric (internal iliac) artery, but it usually receives additional arterial flow from the ovarian branches of the uterine artery. The veins tend to parallel the arteries. From the ovarian pampiniform plexus, the right ovarian vein drains directly into the inferior vena cava, whereas the left ovarian vein empties into the left renal vein.

The ovaries are suspended in the pelvis by several ligaments, which also contain vascular, lymphatic, and nervous supplies to the organs. These include

Department of Radiology and Radiological Sciences, Vanderbilt University Medical Center, CCC-1121 Medical Center North, 1161 21st Avenue South, Nashville, TN 37232-2675, USA
* Corresponding author.
E-mail address: rochelle.f.andreotti@vanderbilt.edu (R.F. Andreotti).

1556-858X/07/$ – see front matter
doi:10.1016/j.cult.2007.02.001
ultrasound.theclinics.com

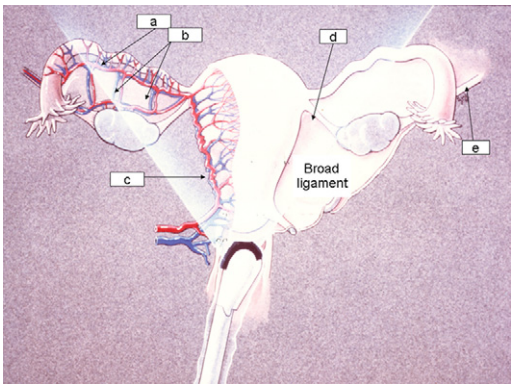

Fig. 1. Artist's rendering of the ovarian vasculature and ligaments. Ovarian artery and vein (*a*), branching arterioles supplying the ovary (*b*), uterine artery and vein (*c*), utero-ovarian ligament (*d*), and infundibulo-pelvic ligament (*e*).

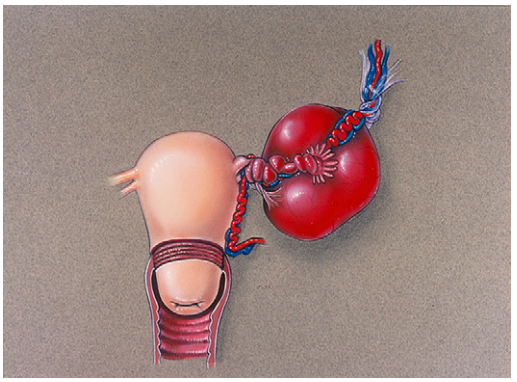

Fig. 2. Artist's rendering of a twisted ovarian pedicle containing broad ligament and fallopian tube with associated engorgement of the ovary.

the broad ligament, the ovarian ligament, and the infundibulo-pelvic ligament. The right and left broad ligaments are folds of peritoneum that extend from the lateral aspects of the uterus to the lateral pelvic side walls. The free border of the broad ligament contains the fallopian tube within its superior margin, which is referred to as the mesosalpinx [3]. The ovary is attached to the posterior layer of broad ligament by reflections of peritoneum called the mesovarium. The ovarian ligaments include the suspensory ligament (infundibulo-pelvic ligament), through which course the ovarian vessels and nerves, and the utero-ovarian ligament. Encompassing the superior and lateral margins of the broad ligament is the suspensory ligament. Arising from the uterine cornu posterior to the tubes and attaching to the inferior aspect of the ovary is the utero-ovarian ligament [4]. Coursing superior and adjacent to the utero-ovarian ligament is the ovarian branch of the uterine artery. Derived from the main ovarian artery and the ovarian branch of the uterine artery are numerous arterioles that extend to the capsule of the ovary and small penetrating arteries within the ovary itself. The ovarian blood supply may vary from five to six branches that penetrate the capsule to two large branches with multiple twigs. Torsion is caused by the rotation of the ovary or adnexa on its axis, with resulting arterial, venous, or lymphatic obstruction (Fig. 2).

Most cases of ovarian torsion (50% to 80%) are associated with adnexal pathologic conditions such as ovarian tumors or cysts. An ipsilateral ovarian mass may act as a fulcrum to potentiate torsion due to increased ovarian volume or weight within adnexal structures. Although torsion is associated with a neoplasm in as many as 50% of cases, previous studies have indicated that the lesions are usually benign, because the inflammatory and invasive changes caused by malignant lesions may be protective against ovarian mobility [1,5–7]. Torsion is also a common complication of non-neoplastic ovarian cysts. It is associated with 1 in 1800 pregnancies, most commonly in the first trimester or immediately post partum [8]. Women undergoing ovulation induction appear to be at high risk secondary to the development of large theca lutein cysts, which can cause twisting of the ovary on its pedicle [9].

In contrast to that of adults, the affected ovary in the pediatric population is normal in as many as 25% of cases [10]. Possible mechanisms that have been proposed to explain torsion of a normal ovary include tortuosity and elongation of the fallopian tube or mesosalpingeal vessels, congenitally long supportive ligaments, and tubal spasm. An active lifestyle or sudden changes in movement such as those involved in vomiting or coughing, more common in the younger population, have also been suggested as possible causes [1].

Pathophysiology

Initially the venous and lymphatic systems are compromised, producing edema and adnexal enlargement. However, until venous and arterial thrombosis has occurred, reperfusion may permit complete recovery. Because the ovary has a dual arterial blood supply, torsion in one arterial system may be compensated by increased vascular flow in the other. Thrombus within the ovarian vein may contribute to venous engorgement of the ovary. Thrombi may also be demonstrated within the smaller intraovarian veins. Chronic torsion may be associated with the establishment of collateral arterial and venous flow, and repeated episodes may even be associated with a reactive hyperemia. Complete and unalleviated torsion can progress

rapidly from interference with venous and lymphatic drainage to occlusion of the arterial circulation. The organ may quickly become black in color because of hemorrhage, necrosis, and gangrenous changes (Fig. 3). When necrosis occurs in the adnexa of the very young patient, the twisted adnexal components may be resorbed, resulting in unilateral adnexal absence, or they may become calcified [11,12].

Clinical presentation

Although it is a relatively infrequent gynecologic emergency, ovarian torsion may pose a diagnostic dilemma. Predisposing factors that should increase the suspicion of torsion include unilateral ovarian tumors (usually benign), ovarian hormone induction leading to ovarian hyperstimulation syndrome, pregnancy, and hypermobile adnexa. Although the pelvic examination usually demonstrates tenderness at least on the affected side, the enlarged ovary is frequently difficult to palpate, so physical examination findings may not suggest the diagnosis. The only consistent symptom cited in most studies is abdominal pain, usually localized to a lower quadrant [5,9,13]. The pain may be colicky or constant and is usually intense and progressive, frequently out of proportion to other findings.

Unfortunately, the differential considerations for abdominal pain in female patients include multiple gynecologic causative agents, such as pelvic inflammatory disease, ruptured ovarian cysts, and ectopic pregnancy, as well as nongynecologic causes such as appendicitis, mesenteric adenitis, cholecystitis, and urinary calculi. Other nonspecific signs and symptoms that are more variably present include fever, nausea, vomiting, and leukocytosis. The literature reports leukocytosis in 59% to 82% of patients [5,14], fever in 19% to 29% [5,14,15], and nausea and vomiting in 50% to 73% [5,14,16]. An observed right-sided predominance has been attributed to the presence of the sigmoid colon on the left or the hypermobility of the cecum on the right [5,9,17].

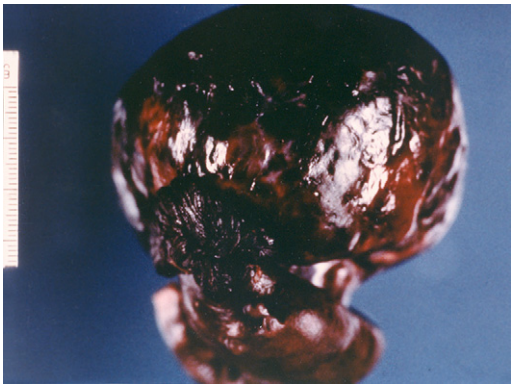

Fig. 3. Surgical pathology specimen of a hemorrhagic, necrotic ovary resulting from ovarian torsion.

The complications of untreated ovarian torsion include peritonitis, pulmonary embolism, and death [13,18,19]. Early intervention has been shown not only to decrease the incidence of these complications but also to improve ovarian salvage rates and consequently some aspect of reproductive capacity. Anders and Powell [6] report that pediatric patients taken to surgery within 8 hours of the onset of symptoms had an ovarian salvage rate of 40%, whereas patients who went to surgery more than 24 hours later had a salvage rate of 0%.

The use of pelvic sonography has enhanced our ability accurately to evaluate patients at risk for ovarian torsion. Nevertheless, gynecologists often delay surgery because of misleading ultrasound findings, only to discover nonviable tissue on exploration. Consequently, an appropriately high index of suspicion should be maintained when evaluating patients who present with unilateral pelvic pain, even if the sonographic findings appear to be negative. The remainder of this article explores both the assistance the modality can provide and its pitfalls.

Sonographic findings

The initial role of sonography in the evaluation of patients at risk for ovarian torsion is to help exclude other causes of acute abdominal pain, such as appendicitis, pelvic inflammatory disease, ruptured ovarian cyst, and ectopic pregnancy [20,21]. Characteristic findings may be routinely seen by transvaginal and transabdominal sonography, although appearances may be nonspecific. For example, the most common sonographic grayscale finding of ovarian torsion is an enlarged ovary or ovarian/tubal complex (Fig. 4). The presence of an adnexal mass or enlarged ovary has been documented in all subjects in several studies. Ovarian volumes within these studies have ranged from 26 to 4308 cm^3 [22–25]. However, if the twisted ovary is located in the right lower quadrant of the abdomen, it may be mistaken for an appendiceal abscess [22].

Several distinguishing grayscale appearances of ovarian torsion have been described using transabdominal sonography in children and adolescents. A large cystic mass with internal debris has been shown to be fairly specific for torsion in neonates (Fig. 5) [26–29]. In older children and adolescents, a unilaterally enlarged ovary containing dilated peripheral follicular cysts has been described as characteristic of torsion in as many as 74% of cases (Fig. 6) [22,25,30]. Weed and Collins [31], in an

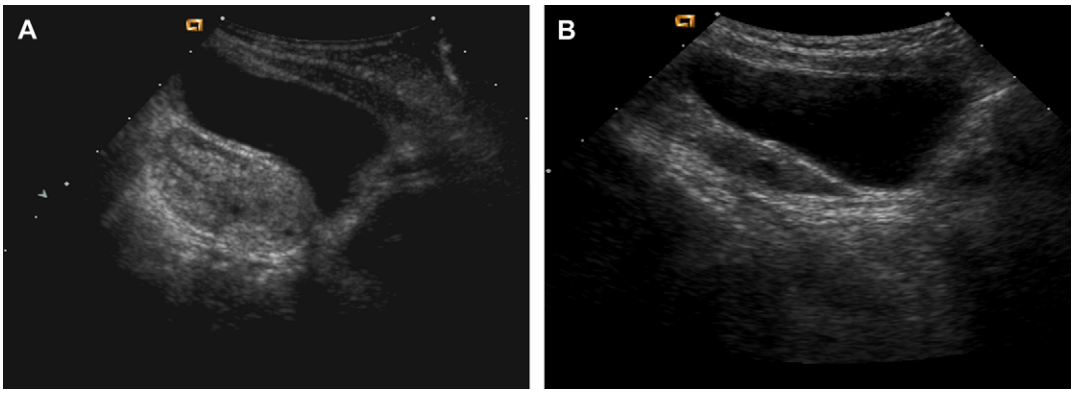

Fig. 4. Enlargement of a normal ovary following ovarian torsion. Three-year-old girl with abdominal pain. (*A*) Transabdominal sonogram of the right adnexa demonstrating extensive hemorrhage and engorgement due to torsion, without evidence of an adnexal mass. (*B*) Normal left ovary, which is significantly smaller than the torsed right ovary.

experimental study using an animal model, produced passive congestion and cystic dilatation of follicles by ligating the ovarian vessels. Follicular enlargement was ascribed at least partially to transudation of fluid into the follicles due to vascular impairment. Reports of cases of massive ovarian edema, a condition attributed to partial torsion of the ovary, describe similar follicular structures in the cortex of an enlarged ovary [32]. It is possible to conclude that this combination of findings is specific for ovarian torsion in the prepubertal age group where follicular enlargement is not expected.

In the postmenarchal population, ovarian appearances are more difficult to interpret. An irregular internal texture of the ovary appears to correlate with intraovarian hemorrhage (Fig. 7). Peripherally placed follicles and homogeneous echoes seen centrally, consistent with areas of edema within enlarged ovaries, have also been reported [25,30], although these descriptors are nonspecific. Entities such as endometriomas, hemorrhagic cysts, tubo-ovarian complexes, and hyperstimulated ovaries undergoing ovulation induction are often described. Free fluid within the cul-de-sac is another nonspecific finding frequently described in association with cases of ovarian torsion [30]. The fluid may be a transudate from the ovarian capsule secondary to obstruction of veins and lymphatic vessels [33]. However, a small amount of fluid is often physiologic in women of reproductive age.

The advent of color and spectral Doppler analysis of ovarian arterial and venous waveforms occasioned the assumption that this would prove to be an accurate tool for the evaluation of ovarian torsion. In actuality, studies of Doppler flow patterns in torsion are variable, with the Doppler findings varying with the degree of torsion and its chronicity.

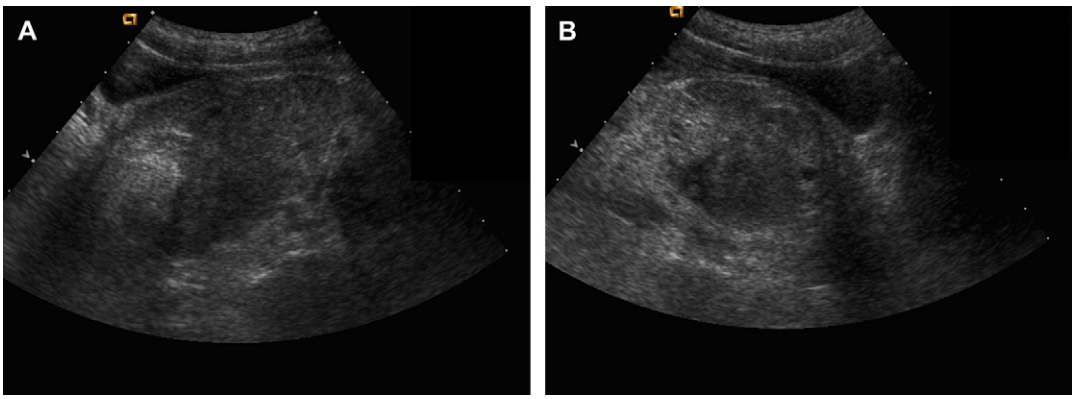

Fig. 5. An ovarian mass acting as a fulcrum to potentiate torsion in a pediatric patient. Five-year-old girl with left lower quadrant pain. Transabdominal sonography in transverse (*A*) and sagittal (*B*) planes demonstrates an enlarged ovary containing a pathology-proven mature teratoma, as well as hemorrhage and infarction.

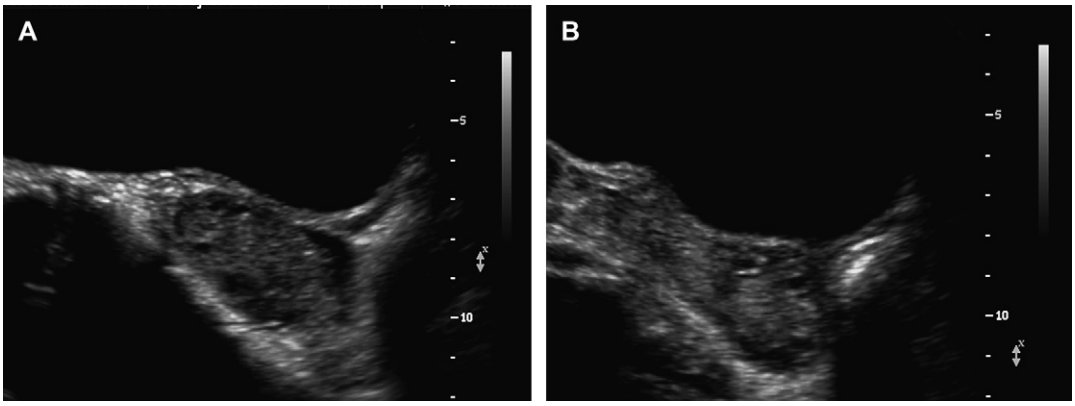

Fig. 6. Enlarged ovary containing peripheral follicular cysts in a prepubertal patient. Nine-year-old girl presenting with right lower quadrant pain. Transabdominal sonography demonstrates sagittal (*A*) and transverse (*B*) images of an edematous ovary with peripheral follicular cysts, which is a characteristic appearance of torsion in the prepubertal age group.

In some cases of torsion, there may be focal areas of blood flow, whereas no intraovarian venous or arterial flow is present in those cases that are more complete (Fig. 8). Lack of arterial and venous Doppler flow should enable confident diagnosis. (However, false-positive diagnoses may be obtained when the depth of penetration exceeds the capabilities of the ultrasound beam, when Doppler or grayscale priority settings are improper, or when filter pulse repetition frequency settings are too high [34–36].) Conversely, ovarian color Doppler signal has been reported frequently in cases of surgically proven torsion [22,23].

Multiple studies have supported the use of Doppler interrogation of the ovary in the evaluation of torsion. Ben-Ami and colleagues [34] reported a positive predictive value of 94% for torsion in the absence of venous flow and showed that torsion is highly unlikely when Doppler interrogation reveals venous flow. Fleischer and colleagues [35] and Lee and colleagues [36] assert that the presence of arterial and venous flow in adnexa that are found to be torsed on subsequent surgical exploration is predictive of the ultimate viability of the organs. The study by Lee and colleagues [36] found that grayscale and color Doppler sonography preoperatively identified twisting of the vascular pedicle in 28 of 32 patients who had surgically confirmed torsion (Fig. 9). The same study described 57% of cases as having both arterial and venous flow within the vascular pedicle. But the authors later concluded, using pathologic findings or clinical follow-up after a procedure to uncoil the twisted vascular pedicle, that 15 of these 16 ovaries with Doppler flow were viable organs. Investigations by Fleischer and colleagues [35] showed no venous Doppler flow centrally in all 10 cases of surgically proven nonviable ovaries. Additionally, venous Doppler signal was seen centrally in all three surgically proven viable ovaries.

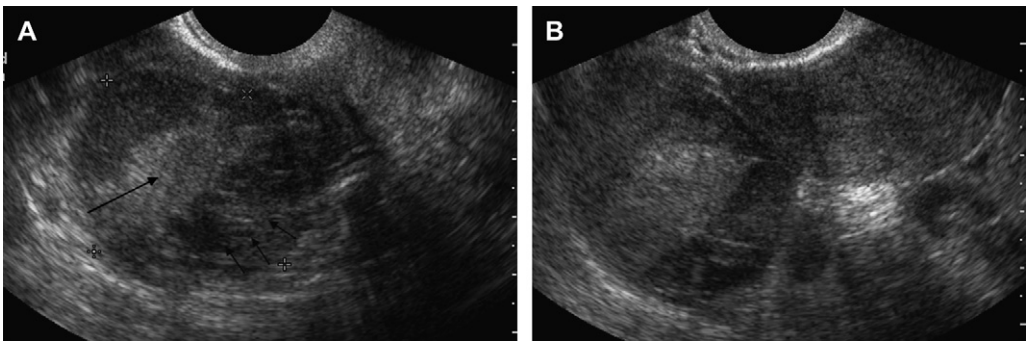

Fig. 7. Intraovarian hemorrhage manifested by an irregular internal texture of the ovary. Twenty-two-year-old woman with recurring right lower quadrant pain. A hemorrhagic, edematous ovary with an associated hemorrhagic cyst, the presumed fulcrum for torsion, was seen laparoscopically. Detorsion was performed by cyst drainage. Transvaginal sonography in sagittal (*A*) and transverse (*B*) planes demonstrates an irregular, heterogeneous consistency peripherally, due to parenchymal hemorrhage and edema (*long arrow*). A more circumscribed homogeneous echogenic area seen centrally corresponds to hemorrhage within a cyst (*short arrows*).

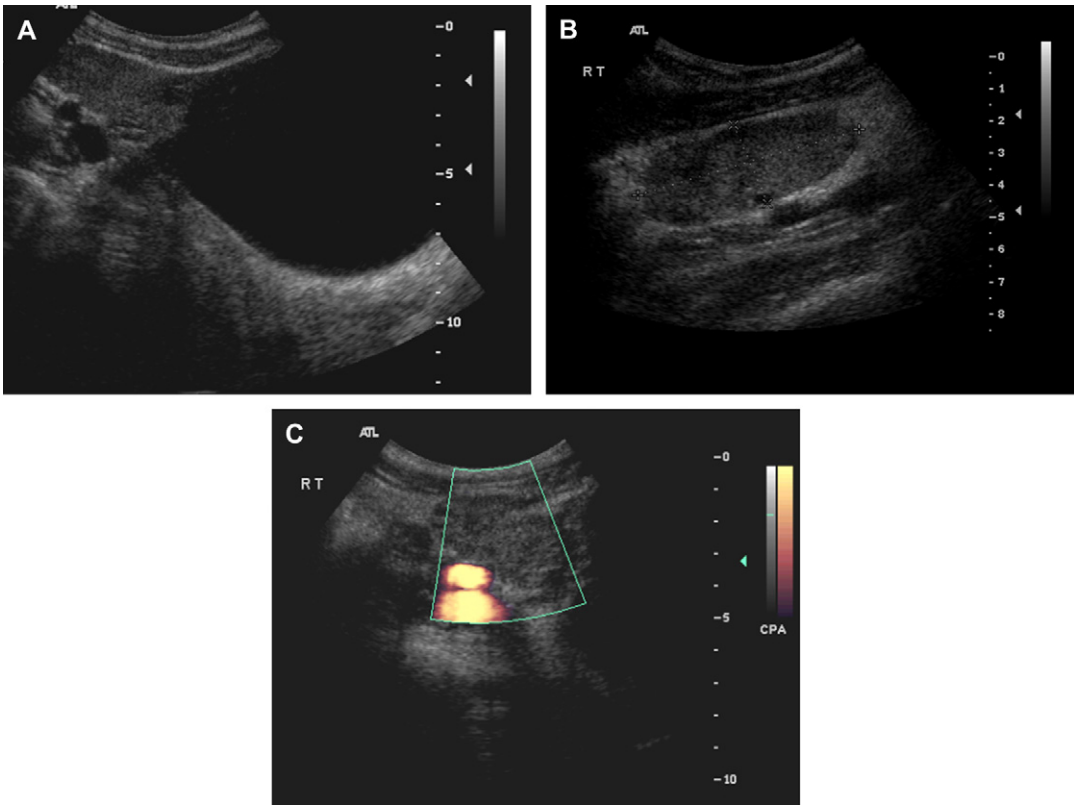

Fig. 8. Absence of color Doppler signal secondary to ovarian torsion. Nineteen-year-old woman with surgically and pathologically proven torsion. (*A*) A large paratubal cyst is seen adjacent to the ovary, most likely the fulcrum for torsion. (*B*) Enlarged ovary containing homogeneous echoes centrally. This pattern has been described in association with edema. (*C*) Power Doppler evaluation fails to demonstrate color signal within the ovary.

However, these findings were not confirmed in another series by Tepper and colleagues [37].

Other investigators have found Doppler findings to be less reliable. Several case reports and retrospective studies of adnexal torsion diagnosed at the time of surgical intervention have described an abnormal appearance of the ovary with normal arterial and venous Doppler signal (Fig. 10) [22,23,38,39]. In a retrospective series by Albayram and Hamper [23] that evaluated 15 pathologically proven torsed ovaries, 53% demonstrated some degree of arterial signal, and 27% showed evidence of venous signal within the ovary. Interestingly, in 14 of the 15 cases, abnormal Doppler flow was described when compared with Doppler flow within the normal contralateral ovary.

Similar results were found in an unpublished retrospective series of 39 patients who had pathologically proven ovarian torsion, performed at Vanderbilt University Medical Center [40]. Twenty-one patients (54%) had documented arterial Doppler signal within the torsed ovary, and 13 (33%) had documented venous flow. At the time of surgical exploration, none of these ovaries appeared grossly viable, so the patients underwent salpingo-oophoectomy or oophorectomy. However, only 23 of these 39 specimens (59%) were given pathologic descriptors such as "infarcted," "gangrenous," or "necrotic," implying irreversible damage. The studies by Fleischer [35] and Lee [36] have also described normal arterial and venous Doppler signal in association with ovaries that appeared visibly infarcted and torsed on surgical exploration.

Based on these assumptions, ovaries that appear irreversibly damaged on gross assessment during surgical exploration but have demonstrated arterial and venous signal, centrally or within the vascular pedicle, should be considered potentially viable ovaries. Conversely, these studies support the presence of a nonviable ovary when there is no evidence of arterial or venous Doppler signal. Several studies do recommend an attempt at conservative treatment regardless of the appearance of the ovary [14,15,41]. However, the authors have found no research into methods of determining which of these necrotic-appearing ovaries are irreversibly ischemic and which may eventually become viable following detorsion or partial oophorectomy.

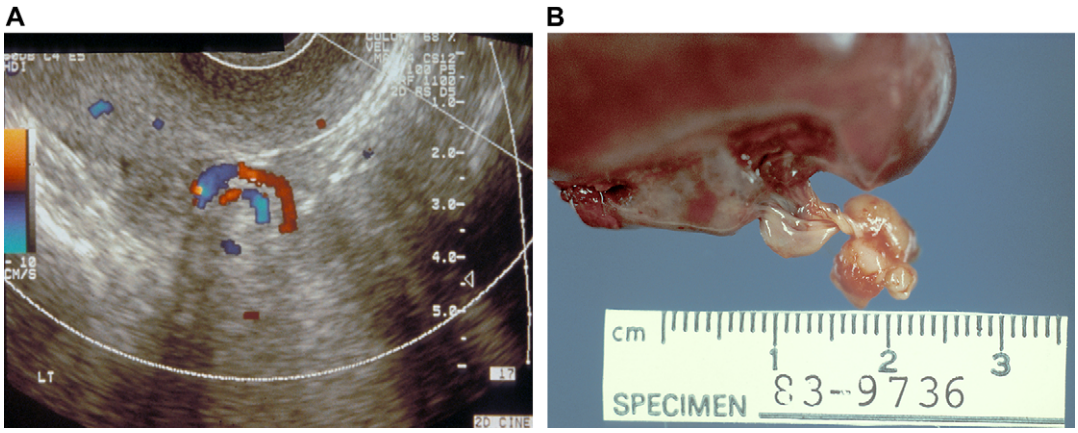

Fig. 9. The twisted vascular pedicle. (*A*) Color Doppler evaluation of the left adnexa representing a twisted vascular pedicle. (*B*) Surgical pathology specimen following oophorectomy, demonstrating the torsed pedicle seen sonographically.

The variety and discrepancy of Doppler findings associated with ovarian torsion in the literature may be linked to the completeness of obstruction of the vascular supply [42]. Venous thrombosis may cause symptoms before the development of arterial occlusion, explaining the more frequently demonstrated absence of venous Doppler signal (Fig. 11). Persistent Doppler arterial or venous flow or both may also be related to the dual blood supply to the ovary. To date, the authors have found no large-scale studies in the English literature evaluating the predictive value of Doppler flow in cases of ovarian torsion.

CT and MR imaging features

Although sonography is usually the initial examination of choice in the evaluation of pelvic pain, CT is being used more frequently in patients who have suspected appendicitis. Only a few reports in the literature concern CT findings of ovarian torsion [24,43–45]. Meyer and colleagues [24] referred to the appearance of a tortuous, low-density, retrovesical mass with an adjacent cystic ovary, which subsequently proved to represent hematosalpinx, a twisted fallopian tube, and incomplete ovarian torsion. In a case report, Gittleman and colleagues [45] described diagnostic findings identified on a contrast-enhanced CT: these included an enlarged ovary with small peripheral cystic structures and an associated large cyst that was believed to be the fulcrum for torsion. Furthermore, in a retrospective series by Rha and colleagues [43] of 25 patients who had the diagnosis of ovarian torsion, imaged using CT and MR imaging, the overall configuration of the twisted adnexa was described in more detail. The most common CT and MR imaging features included thickening of the fallopian tube that may present with a target-like appearance around an adnexal mass, smooth-walled thickening of a cystic adnexal mass exceeding 10 mm, and uterine deviation to the twisted side (Fig. 12). Findings that were less common, but were believed to be particular to hemorrhagic infarction, included hemorrhage within the thickened fallopian tube, hemorrhage within the twisted ovarian mass, andhemoperitoneum. A lack of contrast enhancement within the solid component or thickened walls of the twisted ovarian mass was also a finding suggestive of infarction. However, these findings have yet to be shown to be specific to ovarian torsion. CT may prove useful in the acute setting of right lower quadrant pain by facilitating the diagnosis of appendicitis as well as of ovarian torsion.

Whether MR imaging has a role in the diagnosis of ovarian torsion has not been established. Rha and colleagues [43] have shown similar diagnostic findings on MR and CT, as already discussed. MR findings have also been described by Ghossain and colleagues [46] in a review of 10 patients who underwent detorsion. These findings included enlargement and hyperintensity of the ovarian stroma, as well as tubal thickening. Further investigation of the use of this modality in the evaluation of pelvic pain, and more specifically ovarian torsion, is necessary before one can advocate its routine use, in view of its cost and limited availability.

Management

For many years, the standard treatment of torsion has involved oophorectomy rather than untwisting the torsed tubo-ovarian complex. However, over the past decade, clinical reports have supported a more conservative approach. The rationale for oophorectomy rested on uncertainties regarding the

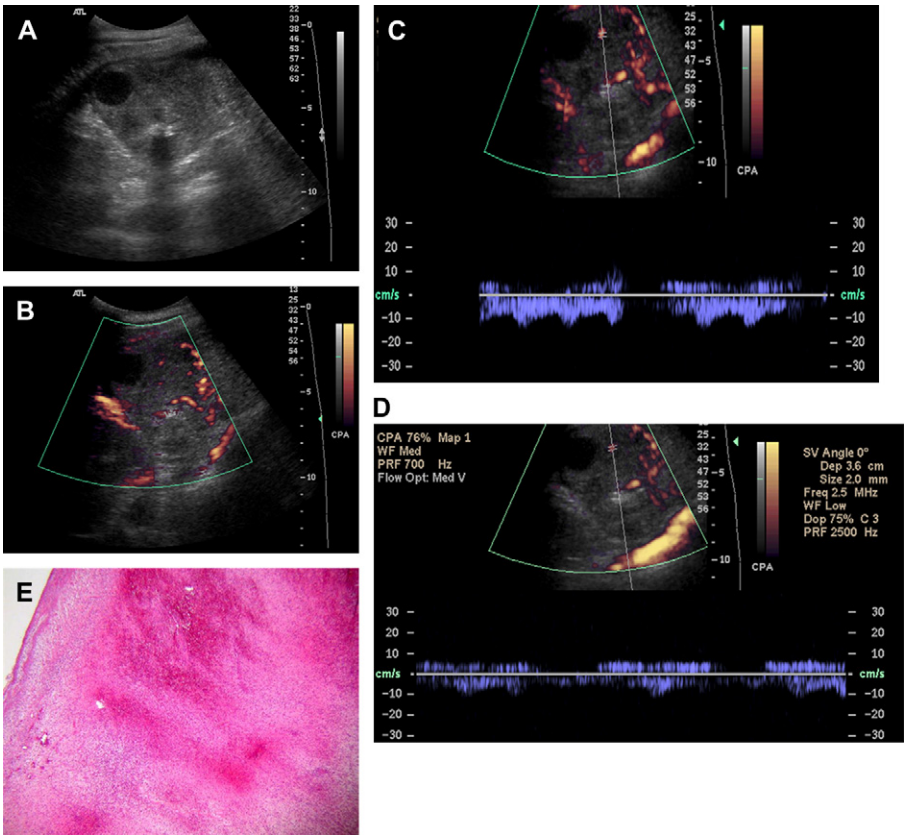

Fig. 10. Intraovarian arterial and venous Doppler signal seen in a pathology-proven infarcted, hemorrhagic ovary. Thirty-one-year-old postpartum woman with worsening abdominal pain. (*A*) Transvaginal sonogram of the right ovary in the sagittal plane demonstrates enlargement with a heterogeneous, hypoechoic parenchyma centrally. A focus of calcification is seen peripherally, despite the lack of evidence of tumor in the pathology specimen. (*B*) Power Doppler evaluation demonstrates an abundance of color Doppler signal within the ovary. Duplex Doppler evaluation showing arterial (*C*) and venous (*D*) signal. (*E*) Photomicrograph of the surgical pathology specimen. Apparent at low power is global ischemic necrosis of ovarian parenchyma, with no residual identifiable stroma or germ cells. Multifocal hemorrhage and profound edema involve the full extent of the ovary. (Hematoxylin-eosin, original magnification ×25.)

possibility of thromboembolism following detorsion or malignancy. Malignancies have been found to be seldom associated with ovarian torsion, and no cases of thromboembolus following detorsion have been reported in multiple series [47–51]. An initial necrotic, blue-black adnexal appearance intraoperatively may present a deceptive impression of irreversible damage, justifying the performance of an oophorectomy, but the patient may subsequently demonstrate viable ovarian tissue [14,16,52–54]. Detorsion, often with cystectomy or cyst aspiration, has been advocated as safe and beneficial, without significant postoperative complications [41,55]. Investigators have reported sonographic findings of Doppler arterial and venous flow and follicular development following conservative management [55,56]. In addition, a pelvic sonogram 6 weeks following initial surgery has been found helpful to exclude persistent cyst or tumor [52].

Recommendations

The authors now proceed to address what may be gleaned from reviewing the recent literature regarding the sonographic evaluation of the presence or absence of ovarian torsion. First, whether the patient is pre- or postpubertal is of utmost importance. A large cystic mass with debris has been shown to be fairly specific for torsion in neonates [26–29]. In older children and adolescents, a unilaterally enlarged ovary containing dilated peripheral follicular cysts is often described as characteristic of torsion [22,25,30]. These findings in the prepubertal age group, in

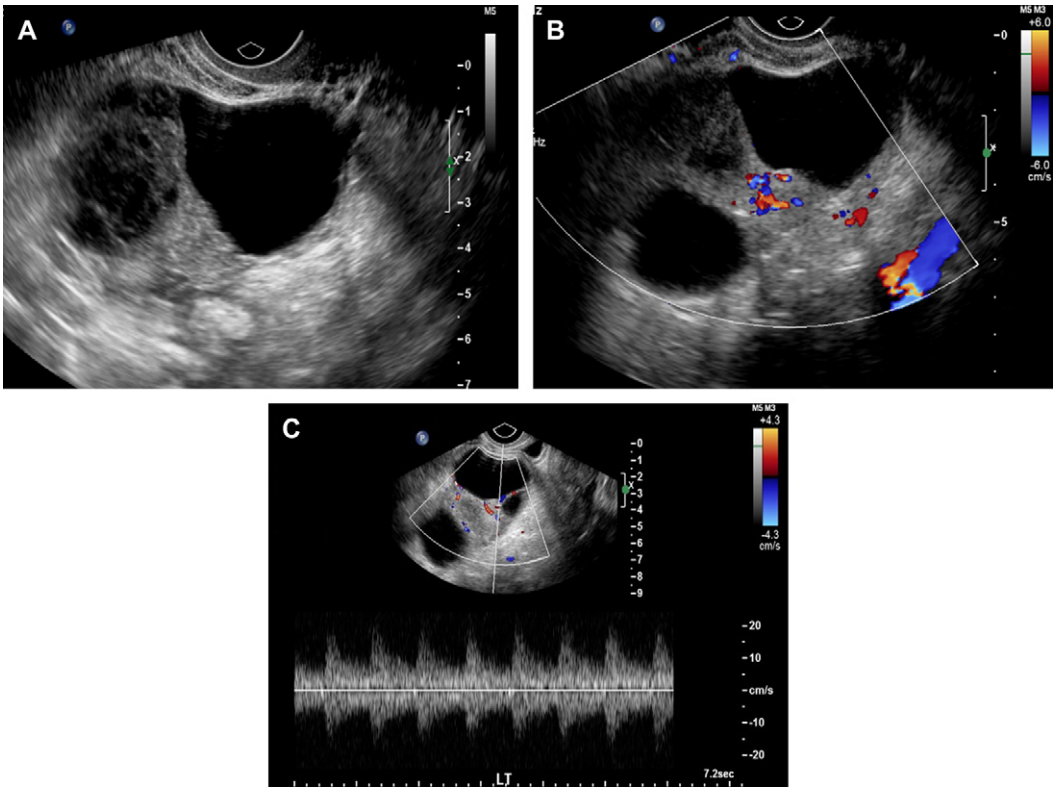

Fig. 11. Intraovarian arterial Doppler signal without evidence of venous signal. Thirty-one-year-old woman with surgically and pathologically proven hemorrhagic infarction of the left ovary containing a peripheral hemorrhagic cyst as well as a simple cyst. (*A*) Transvaginal sonogram of the left ovary in the sagittal plane, showing enlargement by a hemorrhagic as well as a simple functional cyst. (*B*) Color Doppler signal is seen centrally within the ovarian parenchyma. (*C*) Duplex Doppler evaluation of central vascularity reveals only arterial signal.

which follicular enlargement is not expected, may be specific for ovarian torsion.

Sonographic findings are much less specific in the postmenarchal age group. The enlarged, abnormal-appearing ovary appears to be a common denominator in most, if not all, cases of ovarian torsion. Evidence strongly points to the diagnosis in the presence of an enlarged ovary with absence of

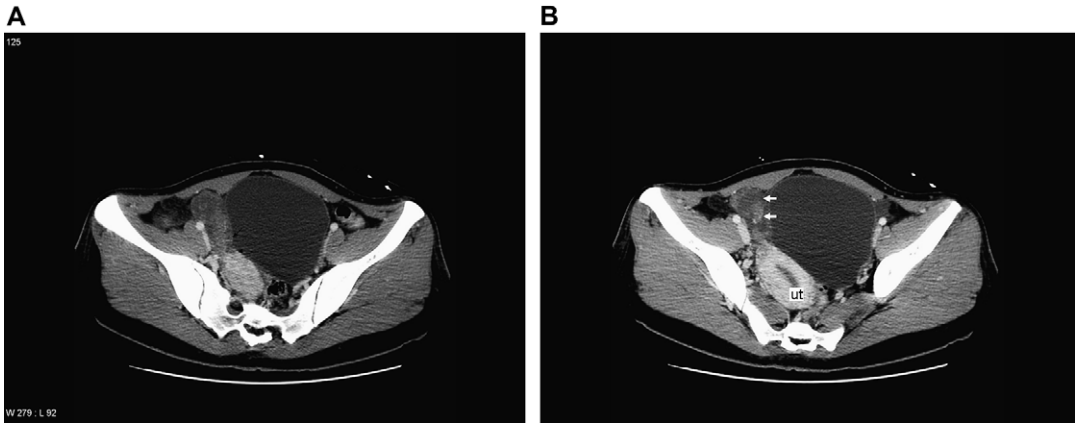

Fig. 12. CT of the pelvis in a patient who has pathology-proven ovarian torsion. Sonographic findings are shown in Fig. 8. (*A, B*) Thickening of the fallopian tube, with a target-like appearance around an adnexal mass (*arrows*), which proved to represent torsion of the pedicle ×4. (*B*) Demonstration of deviation of the uterus (ut) toward the twisted adnexa.

associated arterial and venous Doppler signal [34–36]. However, multiple case reports and series in the literature suggest the presence of both arterial and venous Doppler signal within the ovary or associated vascular pedicle in cases of ovarian torsion. Furthermore, these patients in whom vascularity is still present may be the very ones who would benefit from conservative surgery. Hence surgical exploration should not be delayed when clinical suspicion remains high in the setting of an enlarged ovary with Doppler flow.

Perhaps investigators should now turn their attention to research that would develop methods of determining the viability of the ovary. The demonstration of the twisted ovarian pedicle may be a promising avenue to explore, because its appearance has been shown to be characteristic of ovarian torsion in both the sonographic and CT literature, and the presence or absence of vascular flow within the pedicle may correlate with ovarian viability. Comparing the vascularity of the abnormal-appearing ovary with that of the normal contralateral side may prove helpful. Additionally, further investigation of the use of contrast-enhanced sonography may provide more accurate assessment of ovarian vascular flow and viability.

Summary

Although progress has been made with the advent of imaging modalities, the diagnosis of ovarian torsion remains a clinical and imaging enigma. Abdominal pain is the most reliable symptom of torsion but is nonspecific. Other frequent symptoms, such as fever, leukocytosis, and nausea and vomiting, are more variable in their presentation.

The use of pelvic sonography has enhanced our ability accurately to evaluate patients at risk for ovarian torsion. Sonography has been found to be useful in excluding other causes of acute abdominal pain. The most common grayscale characteristic of torsion is the enlarged ovary or ovarian complex; this is routinely seen by transvaginal and transabdominal sonography, although appearances may be nonspecific. The findings of torsion have also been described on CT and MR studies, but the specificity of these findings has not been confirmed by large clinical series. The addition of duplex and color Doppler imaging is most helpful in making the diagnosis when Doppler signal is absent. However, the presence of Doppler signal cannot eliminate the diagnosis.

Even so, surgery is often delayed based on misleading ultrasound findings. Consequently, one should maintain an appropriately high index of suspicion of ovarian torsion when evaluating patients who present with unilateral abdominal or pelvic pain that cannot be attributed to other causes, even when the sonographic findings are not strongly suggestive.

Acknowledgments

The authors wish to acknowledge the expert editorial assistance of Vera A. Merriweather and the photographic support of John Bobbitt.

References

[1] Hibbard LT. Adnexal torsion. Am J Obstet Gynecol 1985;152:456–61.
[2] Burnett LS. Gynecological causes of the acute abdomen. Surg Clin North Am 1988;68:385–98.
[3] Gardner E, Gray DJ, O'Rhahilly R. The pelvis. In: Grey D, O'Reilly R, editors. Anatomy: a regional study of human structure. 5th edition. Philadelphia: WB Saunders; 1986. p. 445.
[4] Gray DJ, Henry. Splanchnology: reproductive organs of the female. In: Williams PM, Warwick R, editors. Gray's anatomy. 36th edition. Edinburgh (UK): Churchill Livingston; 1980. p. 1423.
[5] Kokoska ER, Keller MS, Weber TR. Acute ovarian torsion in children. Am J Surg 2000;180(6): 462–5.
[6] Anders JF, Powell EC. Urgency of evaluation and outcome of acute ovarian torsion in pediatric patients. Arch Pediatr Adolesc Med 2005;159(6): 532–5.
[7] Sommerville M, Grimes DA, Koonings PP, et al. Ovarian neoplasms and risk of adnexal torsion. Am J Obstet Gynecol 1991;164:577–8.
[8] Cappell MS, Friedel D. Abdominal pain during pregnancy. Gastroenterol Clin North Am 2003; 32(1):1–58.
[9] Lee CH, Raman S, Sivanesaratnam V. Torsion of ovarian tumors: a clinicopathological study. Int J Gynaecol Obstet 1989;28:21–5.
[10] Davis AJ, Feins NR. Subsequent asynchronous torsion of normal adnexa in children. J Pediatr Surg 1990;25:687–9.
[11] Nissen ED, Kent RD, Nissen SE, et al. Unilateral tuboovarian autoamputation. J Reprod Med 1977;19:151–3.
[12] Kennedy LA, Pinckney LE, Currarino G, et al. Amputated calcified ovaries in children. Radiology 1981;141:83–6.
[13] Nichols DH, Julian PT. Torsion of the adnexa. Clin Obstet Gynecol 1985;28:375–80.
[14] Bayer AL, Wiskind AK. Adnexal torsion: can the adnexa be saved? Am J Obstet Gynecol 1994; 171(6):1506–10 [discussion: 1510–1].
[15] Kruger E, Heller DS. Adnexal torsion: a clinicopathologic review of 31 cases. J Reprod Med 1999;44(2):71–5.
[16] Celik A, Ergün O, Aldemir H, et al. Long-term results of conservative management of adnexal

torsion in children. J Pediatr Surg 2005;40(4): 704–8.
[17] Ward M, Frazier T. Torsion of the normal adnexa in childhood: case report. Pediatrics 1978;61: 573–4.
[18] Pryor RA, Wiczyk HP, O'Shea DL. Adnexal infarction after conservative management of torsion of a hyperstimulated ovary. Fertil Steril 1995;63(6): 1344–6.
[19] Beyth Y, Bar-on E. Tuboovarian autoamputation and infertility. Fertil Steril 1984;42(6): 932–4.
[20] Siegel MJ, Carel C, Surratt S. Ultrasonography of acute abdominal pain in children. JAMA 1991; 266:1087–9.
[21] Sivit CJ, Newman KD, Boenning DA, et al. Appendicitis: usefulness of US in diagnosis in a pediatric population. Radiology 1992;185: 549–52.
[22] Stark JE, Siegel MJ. Ovarian torsion in prepubertal and pubertal girls: sonographic findings. AJR Am J Roentgenol 1994;163(6):1479–82.
[23] Albayram F, Hampton U. Ovarian and adnexal torsion: spectrum of sonographic findings with pathologic correlation. J Ultrasound Med 2001; 20:1083–9.
[24] Meyer JS, Harmon CM, Harty MP, et al. Ovarian torsion: clinical and imaging presentation in children. J Pediatr Surg 1995;30(10):1433–6.
[25] Graif M, Itzchak Y. Sonographic evaluation of ovarian torsion in childhood and adolescence. AJR Am J Roentgenol 1988;150(3):647–9.
[26] Meizner I, Levy A, Katz M, et al. Fetal ovarian cysts: prenatal ultrasonographic detection and postnatal evaluation and treatment. Am J Obstet Gynecol 1991;164:874–8.
[27] Mordehai J, Mares AJ, Barki Y, et al. Torsion of uterine adnexa in neonates and children: a report of 20 cases. J Pediatr Surg 1991;26: 1195–9.
[28] Nussbaum AR, Sanders RC, Hartman DS, et al. Neonatal ovarian cysts: sonographic-pathologic correlation. Radiology 1988;168:817–21.
[29] Shere DM, Shah YG, Eggers PC, et al. Prenatal sonographic diagnosis and subsequent management of fetal adnexal torsion. J Ultrasound Med 1990;9:161–3.
[30] Graif M, Shalev J, Strauss S, et al. Torsion of the ovary: sonographic features. AJR Am J Roentgenol 1984;143:1331–4.
[31] Weed JC, Collins CG. Cystic degeneration of the ovaries: an experimental study. Surgery 1942;11: 292–8.
[32] Chervenak FA, Castadot MJ, Wiederman J, et al. Massive ovarian edema: review of world literature and report of two cases. Obstet Gynecol Surv 1980;35:677–84.
[33] Coleman BG. Transvaginal sonography of adnexal masses [review]. Radiol Clin North Am 1992;30:677–91.
[34] Ben-Ami M, Perlitz Y, Haddad S. The effectiveness of spectral and color Doppler in predicting ovarian torsion: a prospective study. Eur J Obstet Gynecol Reprod Biol 2002;104:64–6.
[35] Fleischer A, Stein S, Cullinan J, et al. Color Doppler sonography of adnexal torsion. J Ultrasound Med 1995;14:523–8.
[36] Lee EJ, Kwon HC, Joo HJ, et al. Diagnosis of ovarian torsion with color Doppler sonography: depiction of twisted vascular pedicle. J Ultrasound Med 1998;17:83–9.
[37] Tepper R, Zelel Y, Goldberg S, et al. Diagnostic value of transvaginal color Doppler flow in ovarian torsion. Eur J Obstet Gynecol Reprod Biol 1996;68:115–8.
[38] Hurh PJ, Meyer JS, Shaaban A. Ultrasound of a torsed ovary: characteristic gray scale appearance despite normal arterial and venous flow on Doppler. Pediatr Radiol 2002;32:586–8.
[39] Rosado WM Jr, Trambert MA, Gosink BB, et al. Adnexal torsion: diagnosis by using Doppler sonography. AJR Am J Roentgenol 1992;159: 1251–3.
[40] Shadinger LL, Andreotti RF, Kurian RL. Preoperative sonographic and clinical characteristics as a predictor of ovarian torsion [abstract]. Presented at the Radiological Society of North America meeting. Chicago, IL; December 1, 2006.
[41] Dolgin SE, Lublin M, Shlasko E. Maximizing ovarian salvage when treating idiopathic adnexal torsion. J Pediatr Surg 2000;35:624–6.
[42] Pena JE, Utberg D, Cooney N, et al. Usefulness of Doppler sonography in the diagnosis of ovarian torsion. Fertil Steril 2000;73: 1047–50.
[43] Rha SE, Byun JY, Jung SE, et al. CT and MR imaging features of adnexal torsion. Radiographics 2002;22(2):283–94.
[44] Bellah RD, Griscom NT. Torsion of normal uterine adnexa before menarch: CT appearance. AJR Am J Roentgenol 1989;152:123–4.
[45] Gittleman AM, Price AP, Goffner L, et al. Ovarian torsion: CT findings in a child. J Pediatr Surg 2004;39:1270–2.
[46] Ghossain MA, Hachem K, Buy JN, et al. Adnexal torsion: magnetic resonance findings in the viable adnexa with emphasis on stromal ovarian appearance. J Magn Reson Imaging 2004;20: 451–62.
[47] Breech LL, Hillard PJA. Adnexal torsion in pediatric and adolescent girls. Obstet Gynecol 2005; 17(5):483–9.
[48] Mage G, Canis M, Manhes H, et al. Laparoscopic management of adnexal torsion: a review of 35 cases. J Reprod Med 1989;34:520–4.
[49] McGovern PG, Noah R, Koenigsberg R, et al. Adnexal torsion and pulmonary embolism: case report and review of the literature. Obstet Gynecol Surv 1999;54:601–8.
[50] Wagaman R, Williams RS. Conservative therapy for adnexal torsion: a case report. J Reprod Med 1990;35:833–4.
[51] Oelsner G, Cohen SB, Soriano D, et al. Minimal surgery for the twisted ischaemic adnexa can

preserve ovarian function. Hum Reprod 2003;18: 2599–602.
[52] Oelsner G, Bider D, Goldenberg M, et al. Long-term follow-up of the twisted ischemic adnexa managed by detorsion. Fertil Steril 1993;60:976–9.
[53] Ben-Rafael Z, Bider D, Mashiach S. Laparoscopic unwinding of twisted ischemic hemorrhagic adnexum after *in vitro* fertilization. Fertil Steril 1990;53:569–71.
[54] Shalev E, Bustan M, Yarom I, et al. Recovery of ovarian function after laparoscopic detorsion. Hum Reprod 1995;10:2965–6.
[55] Shalev E, Peleg D. Laparoscopic treatment of adnexal torsion. Surg Gynecol Obstet 1993;176: 448–50.
[56] Aziz D, Davis V, Allen L, et al. Ovarian torsion in children: is oophorectomy necessary? J Pediatr Surg 2004;39:750–3.